STRUCTURAL, ELECTRONIC, AND MAGNETIC PROPERTIES OF COPPER (I) AND (II) OXIDES AT DIFFERENT MORPHOLOGIES: FIRST - PRINCIPLES STUDY

A THESIS SUBMITTED TO THE

CENTRAL DEPARTMENT OF PHYSICS

INSTITUTE OF SCIENCE AND TECHNOLOGY

TRIBHUVAN UNIVERSITY

NEPAL

FOR THE AWARD OF

DOCTOR OF PHILOSOPHY

IN PHYSICS

BY

TARANI PRASAD YADAV

MARCH 2022

STRUCTURAL, ELECTRONIC, AND MAGNETIC PROPERTIES OF COPPER (I) AND (II) OXIDES AT DIFFERENT MORPHOLOGIES: FIRST - PRINCIPLES STUDY

A THESIS SUBMITTED TO THE

CENTRAL DEPARTMENT OF PHYSICS

INSTITUTE OF SCIENCE AND TECHNOLOGY

TRIBHUVAN UNIVERSITY

NEPAL

FOR THE AWARD OF

DOCTOR OF PHILOSOPHY

IN PHYSICS

BY

TARANI PRASAD YADAV

MARCH 2022

DECLARATION

Thesis entitled "**Structural, Electronic and Magnetic Properties of Copper (I) and (II) Oxides at Different Morphologies: First-Principles Study**" is being submitted to the Central Department of Physics, Institute of Science and Technology (IOST), Tribhuvan University, Nepal for the award of the degree of Doctor of Philosophy (Ph. D.), is a research work carried out by me under the supervision of Associate Prof. Dr. Gopi Chandra Kaphle of Central Department of Physics, Tribhuvan University and co-supervised by Prof. Dr. Anurag Srivastava of Atal Bihari Vajpayee - Indian Institute of Information Technology and Management, Gwalior, Madhya Pradesh, India.

This research is original and has not been submitted earlier in part or full in this or any other form to any university or institute, here or elsewhere, for the award of any degree.

……

Tarani Prasad Yadav

THIS THESIS IS DEDICATED

TO

MY LATE MOTHER “PURANI YADAV”

AND

LATE FATHER “JAGANNATHA YADAV”

RECOMMENDATION

This is to recommend that **Mr. Tarani Prasad Yadav** has carried out research entitled "**Structural, Electronic and Magnetic Properties of Copper (I) and (II) Oxides at Different Morphologies: First-Principles Study**" for the award of Doctor of Philosophy (Ph. D.) in **Physics** under our supervision. To our knowledge, this work has not been submitted for any other degree.

He has fulfilled all the requirements laid down by the Institute of Science and Technology (IOST), Tribhuvan University, Kirtipur for the submission of the thesis for the award of a Ph. D. degree.

.....

Dr. Gopi Chandra Kaphle

Supervisor

Associate Professor

Central Department of Physics

Tribhuvan University,

Kirtipur, Kathmandu, Nepal.

.....

Dr. Anurag Srivastava

Co - Supervisor

Professor

Computational Nanoscience and Technology Lab

Atal Bihari Vajpayee - Indian Institute of Information Technology and Management, Gwalior, Madhya Pradesh, India

March 2022

LETTER OF APPROVAL

14 / 03 / 2022

On the recommendation of Associate **Prof. Dr. Gopi Chandra Kaphle** (Supervisor) and **Prof. Dr. Anurag Srivastava** (Co-Supervisor), this Ph. D. thesis submitted by **Mr. Tarani Prasad Yadav**, entitled "**Structural, Electronic and Magnetic Properties of Copper (I) and (II) Oxides at Different Morphologies: First-Principles Study**" is forwarded by the Central Department Research Committee (CDRC) to the Dean, IOST, TU.

……..

Dr. Om Prakash Niraula

Professor,

Head,

Central Department of Physics

Tribhuvan University

Kirtipur, Kathmandu

Nepal

ACKNOWLEDGMENTS

My first sincere gratitude goes to supervisor Associate Professor Dr. Gopi Chandra Kaphle from Central Department of Physics, Tribhuvan University (TU), Kirtipur, Kathmandu, Nepal, and co-supervisor Professor Dr. Anurag Srivastava from Computational Nanoscience and Technology Lab (CNTL), Atal Bihari Vajpayee - Indian Institute of Information Technology and Management (AVB-IIITM), Gwalior, MP, India, who have provided me the opportunity for the Ph. D. research work. At this moment, I would like to thank from my heart to both my supervisors who care for me like my parents and love me like my friends. During the research period, they shared various knowledge and research skills with the great patient which was an unforgettable moment for me and always keep encourage my enthusiasm for the research activity. I would like to thank Professor Dr. Binil Aryal, Dean of Institute of Science and Technology, TU, Professor Dr. Om Prakash Niraula, Head, Central Department of Physics (CDP), TU, Professor Dr. Narayan Prasad Adhikari, and the CDRC members for their valuable suggestions, support, and encouragement, during this thesis work.

All the professors, teaching and non-teaching staffs, and technicians of Central Department of Physics, Tribhuvan University, Kirtipur, Kathmandu, Nepal as well as Central Campus of Science and Technology, Mid-West University, Birendranagar, Surkhet, Nepal are acknowledged for their co-operation and support.

Thanks to Dr. Sukhbir Singh, Mr. Ravi Mehla, and Mr. Kumar Gaurav for helping me with computational simulation and lab works. Dr. Boddepalli Santhibhushan, Mrs. Monika Srivastava, Mrs. Sonal Agrawal, and Mr. Kirtesh Khare are acknowledged for their co-operation and help during my stay in the hostel of ABV-IIITM, Gwalior, MP, India. I am grateful to Mrs. Muna Kaphle and Dr. Reena Srivastava for inspiring me during this period of my thesis work in Nepal and India. I am also grateful to Associate Prof. Dr. Binay Kumar Das for his assistantship in the language and grammatical structures of the thesis. I would like to thank Mr. Shyam Prasad Shreshtha, CDP Book and Stationery Center, TU, Kirtipur for printing our thesis. I feel proud to have the opportunity to work with all of you.

Nepal Academy of Science and Technology (NAST), Nepal is greatly acknowledged for providing partial financial support through Ph. D. Fellowship - 2074 (2017 AD) for the study in Advanced Materials and Nanotechnology.

Last but not least, my deepest and most heartfelt gratitude to my beloved wife Lila Yadav, my daughters Indu Yadav, Bindu Yadav, Shikha Yadav, and sons Parash Yadav, Sudarshan Yadav, son-in-laws Er. Manik Lal Yadav and Pharmacist Sanjiba Kumar Yadav for their endless love and support because of which I have been down with energy and always motivated to do new things even outside the country.
My appreciation goes to all of you. Thank you all.

…….

(Tarani Prasad Yadav)

March 2022

ABSTRACT

We find different morphological structures of Copper (I) and (II) oxides (Cu_2O and CuO) which are suitable candidates for semiconductors, magnetic and spintronic devices, batteries, catalysts, supercapacitors etc. In the present work, we explore the extensive properties related to crystal structure, electronic band structures and density of states of nanoclusters of Cu_2O and CuO (0D), nanowires of Cu_2O (1D), nanotubes and nanoribbons of CuO (1D), nanosheets of CuO (2D), and bulks of Cu_2O and CuO (3D) respectively. We use the exchange-correlation functionals LSDA + U, SGGA + U, and meta-spin generalized gradient approximation (MSGGA), respectively under the density functional theory (DFT) approach implemented in Virtual Nanolab-Atomistix ToolKit (VNL-ATK).

Here, the XC- functional SGGA + U is used to study $(Cu_2O)_{n = 1, 2, 3}$ and $(CuO)_{m = 2, 4, 6}$ nanoclusters. The nanoclusters $(Cu_2O)_1$ show semiconducting and diamagnetic behaviors, whereas the $(Cu_2O)_2$ and $(Cu_2O)_3$ nanoclusters have magnetic moments per atom 0.33 μ_B and 0.22 μ_B with spin polarization 1 respectively, confirm the half-metallic and semiconducting ferromagnetic behaviors. The nanoclusters $(CuO)_2$, and $(CuO)_6$ of magnetic moments per atom 0.49 μ_B and 0.58 μ_B show semiconducting and ferromagnetic behaviors, respectively whereas $(CuO)_4$ of magnetic moment per atom 0.50 μ_B is a half-metal ferromagnetic nanocluster.

The Cu_2O nanowires of the diameter range 4-6 Å having magnetic moments per atom 0.36 μ_B, 0.03 μ_B and 0.02 μ_B respectively are ferromagnetic nanomaterials. We find the magnetic moment per atom of the nanowire decreases concerning an increase in its diameter which is resembling with previously reported data. Our calculation reveals that Cu_2O nanowires are suitable for sensor and solarcell applications.

The (2, 1) CuO chiral nanotube with magnetic moment per atom 0.36 μ_B, shows semiconducting behavior with an energy band gap of 2.2 eV, whereas the CuO chiral nanotubes of the chiralities (3, 1), (3, 2), (4, 1), (4, 2) with magnetic moments per atom 0.31 μ_B, 0.35 μ_B, 0.36 μ_B, and 0.37 μ_B respectively show the half-metal ferromagnetic behaviors. These results also follow the magnetic moment per atom increases with increasing in the chirality of CuO chiral nanotube. The magnitude of buckling of the optimized (4, 0), (6, 0), (8, 0), and (10, 0) CuO zigzag nanotubes decrease on increasing the diameter of the nanotube. The magnetic moment shows

decreasing trend as increasing the diameter up to a particular limit. The investigation also reveals that the diameter and number of atoms are directly proportional to the binding energy of CuO zigzag nanotubes. The analysis of electronic band structures and density of states of CuO nanoribbons confirm their metallic and ferromagnetic behaviors. The calculations show that the magnetic moments of CuO armchair nanoribbons are higher than that of the magnetic moments of CuO zigzag nanoribbons. The zigzag and armchair forms of CuO nanosheet show metallic behaviors and the computed magnetic moment per atom changes irregularly concerning their chiralities.

The bulk form of Cu_2O shows diamagnetic and the bulk of CuO shows ferromagnetic behaviors with p-type semiconductors whereas the ordering of isolate $4Cu^{2+}$ ions of bulk CuO behaves as antiferromagnetic materials. The measured band gaps with the exchange-correlation functionals LSDA + U, SGGA + U and MSGGA are 0.70 eV, 0.56 eV and 0.79 eV, respectively for bulk Cu_2O , whereas 2.42 eV, 2.22 eV, and 2.20 eV, respectively for bulk CuO. Present calculated results closely agree with the corresponding available experimental report for CuO (1.2 eV - 1.9 eV), and less value for Cu_2O (2 eV - 2.2 eV) bulk structures, respectively.

In short, the present investigation reports the prediction of crystallographic nanostructures in different morphologies along with their bulk structures and characterized them under DFT based first-principles study through VNL - ATK toolkit. In most of the cases, the present result agrees well with the available experimental as well as theoretical data.

LIST OF ACRONYMS AND ABBREVIATION

0D	Zero Dimension
1D	One Dimension
2D	Two Dimension
3D	Three Dimension
AAO	Aluminum Anodic Oxide
AD	Anno Domini
AES	Auger Electron Spectroscopy
AFM	Atomic Force Microscopy
ANR	Armchair Nanoribbon
ANS	Armchair Nanosheet
ANT	Armchair Nanotube
ASW	Augmented–Spherical - Wave
BCC	Body Centered Cubic
BE	Binding Energy
BIS	Bremsstrahlung Isochromatic Spectra
BOA	Born Oppenheimer Approximation
BS	Band Structure
BZ	Brillion Zone
CHNS	Copper Hydroxide Nano Strands
CMC	Carboxy Methyl Cellulose
CNR	Chiral Nanoribbon
CNS	Chiral Nanosheet
CNSs	colloidal nanocrystal clusters

CNT	Chiral Nanotube
CPU	Central Processing Unit
CTAB	Cetyl trimethyl ammonium bromide
DFT	Density Functional Theory
DOS	Density of States
EELS	Electron Energy Loss Spectroscopy
FCC	Face Centered Cubic
FE-SEM	Field - Emission Scanning Electron Microscopy
FTIR	Fourier Transforms Infrared Spectroscopy
GGA	Generalized Gradient Approximation
GS	Ground State
GW	Green function (G) and screened Coulomb interaction (W)
HDD	Hard Disc Drives
HFA	Hartree - Fock Approximation
HK	Hohenberg - Kohn
HOMO	Highest Occupied Molecular Orbitals
HRTEM	High-Resolution Transmission Electron Microscopy
HSE	Heyd - Scuseria - Ernzerhof
IC	Integrated Circuit
IMMS	Ion Mobility Mass Spectrometry
IPA	Iso Propyl Alcohol
ITO	Information Technology Outsourcing
K. E.	Kinetic Energy
KS	Kohn - Sham

L(S)DA	Local Spin Density Approximation
LAPW	Linearized Augmented Plane Wave
LCD	Liquid Crystal Display
LDA	Local Density Approximation
LED	Light - Emitting Diode Display
LESER	Light Amplification by Stimulated Emission of Radiation
LSDA	Local Spin Density Approximation
LSI	Large - Scale Integretion
LUMO	Lowest Unoccupied Molecular Orbital
MM	Magnetic Moment
MOCVD	Metal - Organic Chemical Vapor Deposition
MSGGA	Meta Spin Generalized Gradient Approximation
NEGF	Non-Equilibrium Green Function
NW	Nanowire
OPA - MBE	Oxygen Plasma-Assisted Molecular - Beam Epitaxy
P. E.	Potential Energy
PAM	Porous Alumina Membrane
PDOS	Projected Density of States
P^H	Potential of Hydrogen
PVDF	Poly Vinylidene Fluoride
PW	Perdew - Wang
PWA	Plane-Wave Approach
PZ	Perdew - Zunger
rPBE	review - Perdew - Burke - Ernzerhof

SAED	Selected Area Electron Diffraction
SC	Self - Consistent, Sodium Citrate
SEM	Scanning Electron Microscope
SGGA	Spin Generalized Gradient Approximation
SIBs	Sodium-Ion Batteries
SP	Spin Polarization
SSD	Solid State Drives
TEM	Transmission Electron Microscopy
TFT	Thomas Fermi Theory
TOAB	Tetra-Octyl Ammonium Bromide
U	Hubard potential
UPS	Ultraviolet Photoemission Spectra
VNL-ATK	Virtual Nanolab - Atomistix ToolKit
VWN	Vosko - Wilk - Nusair
XC	Exchange-Corelation Functionals
XPS	X-ray Photoelectron Spectrometer, X-ray Photoemission Spectra
XRD	X-Ray Diffraction
ZNR	Zigzag Nanoribbon
ZNS	Zigzag Nanosheet
ZNT	Zigzag Nanotub

LIST OF SYMBOLS

ρ	Density
$\hat{V}_{n,n}$	Repulsive potential operator between nuclei
$-\frac{\nabla^2}{2}$	Kinetic Energy Operator
$\hat{T}_e$	K. E. operators of electrons
$\hat{T}_n$	K. E. operators of nuclei
$\hat{V}_{e,e}$	Repulsive potential operator between electrons.
$\hat{V}_{n,e}$	Attractive potential operator between nuclei and electrons
E_F	Fermi Energy
E_X	Exchange energy due to Pauli exclusion principle, antisymmetry
E_{XC}	Exchange - Correlation energy
$\hat{h}$	Hamiltonian operator for an electron
V_{ext}	Multiplicative operator
ϵ	Eigenenergy of a moving electron,
μ_B	Bohr's Magneton
Φ	Electron wave function or orbital wave function
$\hat{H}$	Hamiltonian Operator
M_α	Mass of atomic nuclei
R_α	Position of atomic nuclei
Z_α	Charge of atomic nuclei
m_e	Mass of electron

r_i	Position of ith - electron
∇	Gradient Vector Operator
a, b, c	Lattice Constants
β, α, γ	Lattice Angles
C_p	Specific heat capacity
-e	Charge of electron
E_c	Correlation energy
E_g	Bandgap gap energy at room temperature
eV	Electron Volt
i, j	Partial numbers of M electrons
$\mathbf{s_i}$	Spin variable
T	Kinetic energy operator
U	Interaction energy operator
α, β	Partial numbers of N nuclei
μ	Chemical potential
σ	Pauli spin matrix
ψ	Wave function

LIST OF TABLES

Page No.

Table 1: The values of different parameters of unit cell of bulk Cu_2O **11**

Table 2: The values of different parameters of unit cell of bulk CuO **13**

Table 3: Exchange - corelation functionals **43**

Table 4: The computed values of different parameters of the nanoclusters $(Cu_2O)_{n = 1, 2, 3}$ and $(CuO)_{m = 2, 4, 6}$ **54**

Table 5: The computed values of different parameters of Cu_2O NWs **59**

Table 6: The chiralities of CuO CNTs with their diameters, BE / atom, MM / atom, and spin polarizations (SP) **64**

Table 7: Bond length, Binding energy, Diameter and Total energy of CuO ZNTs **68**

Table 8: The obtained values of different parameters of CuO ZNRs **75**

Table 9: The obtained values of different parameters of CuO ANRs **75**

Table 10: The width, binding energy, magnetic moment per atom, and spin polarization of CuO ZNSs with different chiralities **83**

Table 11: The width, binding energy, magnetic moment per atom, and spin polarization of CuO ANSs with different chiralities **83**

Table 12: Comparatively crystallographic properties of the Bulks Cu_2O and CuO **93**

LIST OF FIGURES

Page No.

Figure 1: The innovative applications of in the field of nanoscience and nanotechnology **1**

Figure 2(a, b): The atomic and electronic structures of oxygen and copper atoms **2**

Figure 3: The moleculer and electronic structures of Cu_2O **3**

Figure 4: The moleculer and electronic structures of CuO **3**

Figure 5: The unit cell of bulk Cu_2O **10**

Figure 6: The unit cell of bulk CuO **12**

Figure 7: The system of electrons and nuclei of atoms **28**

Figure 8: Electrons in a Helium atom **32**

Figure 9: Hohenberg - Kohn theorem **39**

Figure 10: Kohn - Sham theorem **40**

Figure 11(a, b): Brillouin zones with special high symmetry $k = b_1g_1 + b_2g_2 + b_3g_3$ points of cubic (a) Cu_2O, (b) monoclinic CuO **48**

Figure 12: Flow - chart of VNL - ATK **48**

Figure 13: Schematic diagram showing CuO nanosheet; zigzag, armchair and chiral forms of CuO NT **50**

Figure 14(a - f): The molecular structures of nanoclusters $(Cu_2O)_{n = 1, 2, 3}$ and $(CuO)_{m = 2, 4, 6}$ **53**

Figure 15(a, b): Total energy and bond length of Cu - O in Å vs total number of atoms **54**

Figure 16(a-c): The molecular energy spectrums of the nanoclusters $(Cu_2O)_{n = 1, 2, 3}$ **55**

Figure 16(d-f): The density of states of the nanoclusters $(Cu_2O)_{n = 1, 2, 3}$ **56**

Figure 17(a-c): The molecular energy spectrums of the nanoclusters $(CuO)_{n = 2, 4, 6}$ **57**

Figure 17(d-f): The density of states of the nanoclusters $(CuO)_{n = 2, 4, 6}$ **57**

Figure 18(a - c): The molecular structures of Cu_2O NWs of the diameters 4, 5, 6 **59**

Figure 19: BE / atom, MM / atom and spin polarization vs diameter of Cu_2O NWs **59**

Figure 20(a - c): Electronic band structures of Cu_2O NWs of different diameters (4–6 Å) **60**

Figure 21(a - c): DOS of Cu_2O NWs of different diameters (4 - 6 Å) **61**

Figure 22(a - e): The (n, m) CuO CNTs in molecular forms **62**

Figure 23(a - e): The (n, m) CuO CNTs in bulk forms **63**

Figure 24(a - e): The electronic band structures of (n, m) CuO CNTs **65**

Figure 25(a - e): The density of states of (n, m) CuO CNTs **66**

Figure 26(a): The graphs of (a) Diameter, no. of atoms, magnetic moment, and spin polarization vs chirality of (n, m) CuO CNT **67**

Figure 27(a - d): The initial nanostructures of CuO ZNTs **68**

Figure 28(a - d): The optimized nanostructures of CuO ZNTs **68**

Figure 29: Relation between binding energy and total number of atoms in CuO ZNTs **69**

Figure 30(a - d): Band structure of CuO ZNTs with majority and minority spins **70**

Figure 31(a - d): Spin - polarized density of states of CuO ZNTs **71**

Figure 32(a, b): Magnetic moment as a function of diameter and a function of electronic temperature of CuO ZNTs **73**

Figure 33: Bulk form of supercell of (3, 0) CuO ZNR **74**

Figure 34: Bulk form of super cell of (3, 3) CuO ANR **74**

Figure: 35: Binding energy as a function of the width of (n = 3 - 10, m = 0) CuO ZNRs and (n, m = n = 3 - 10) CuO ANRs **76**

Figure 36(a - h): Band structures with DOS profiles of (n = 3 - 10, m = 0) CuO ZNRs **78**

Figure 37(a - h): Band structures with DOS profiles of (n, m = n = 3 - 10) CuO ANRs **79**

Figure 38: Magnetic moment as a function of width of (n = 3 - 10, m = 0) CuO ZNRs and (n, m = n = 3 - 10) CuO ANRs **80**

Figure 39: Spin polarization as a function of width of (n = 3 - 10, m = 0) CuO ZNRs and (n, m = n = 3 - 10) CuO ANRs **80**

Figure 40: Supercell (1 × 3 × 4) of unit cell (1, 0) CuO ZNS **82**

Figure 41: Supercell with (1 × 2 × 6) of unit cell (1, 1) CuO ANS **82**

Figure 42: Binding energy per atom of CuO ZNS and CuO ANS as a function of width **84**

Figure 43(a - h): Band structures of the (n = 1 - 8, m = 0) CuO ZNSs with DOS profile, using SGGA **85**

Figure 44(a - h): Band structures of the (n = 1 - 8, m = 0) CuO ZNSs with DOS profile, using SGGA + U **87**

Figure 45(a - h): Band structures of the (n = 1 - 8, m = n) CuO ANSs with DOS profile, using SGGA **88**

Figure 46(a - h): Band structures of the (n = 1 - 8, m = n) CuO ANSs with DOS profile, using SGGA + U **89**

Figure 47: Magnetic moment of CuO ZNSs and CuO ANSs as a function of the width **90**

Figure 48: Spin polarization of CuO ZNSs and CuO ANSs as a function of the width **91**

Figure 49(a, b): The bulk configurations of (a) cuprous oxide (Cu_2O) and (b) cupric oxide (CuO) **92**

Figure 50(a - c): The electronic band structure with DOS of cuprous oxide (Cu_2O) **94**

Figure 51(a - d): The band structure with DOS of cupric oxide (CuO) **95**

Figure 52(a, b): The PDOS profiles of bulk (a) Cu_2O and (b) CuO 95

TABLE OF CONTENTS

Page No.

Declaration ..... **ii**

Recommendation ..... **iv**

Letter of approval ..... **v**

Acknowledgments ..... **vi**

Abstract ..... **viii**

List of acronyms and abbreviation ..... **x**

List of symbols ..... **x**

List of tables ..... **xvi**

List of figures ..... **xvii**

Table of contents ..... **xxii**

CHAPTER 1 ..... **1**

1. INTRODUCTION **1**

1.1 Introduction 1

1.2 Rationale of the Study 5

1.2.1 Zero - Dimensional Nanostructures 6

1.2.1.1 Nanoclusters of Cu_2O and CuO 6

1.2.2 One - Dimensional Nanostructures 7

1.2.2.1 Nanowire of Cu_2O 7

1.2.2.2 Nanotubes of CuO 7

1.2.2.3 Nanoribbons of CuO 8

1.2.3 Two - Dimensional Nanostructures of CuO 8

1.2.3.1 Nanosheets of CuO 8

1.2.4 Three - Dimensional Structures of Cu_2O and CuO 9

1.2.4.1 Bulk of Cu_2O 9

1.2.4.2 Bulk of CuO 11

1.3 Research Objectives.....14

1.4 Organization of study.....15

CHAPTER 2.....17

2. LITERATURE REVIEW.....17

2.1 Zero - Dimensional Nanostructures of Cu_2O and CuO.....17

2.1.1 Nanoclusters of Cu_2O and CuO.....17

2.2 One - Dimensional Nanostructures of Cu_2O and CuO.....19

2.2.1 Nanowires of CuO.....19

2.2.2 Nanotubes of CuO.....20

2.2.3 Nanoribbons of CuO.....22

2.3 Two - Dimensional Nanostructures of CuO.....23

2.3.1 Nanosheets of CuO.....23

2.4 Three - Dimensional Structures of Cu_2O and CuO.....24

2.4.1 Bulks of Cu_2O and CuO.....24

CHAPTER 3.....26

3. MATERIALS AND METHODS.....27

3.1 Theory.....27

3.1.1 General Cosideration.....27

3.1.2 Schrodinger wave equation.....28

3.1.3 Hartree Approximation.....31

3.1.4 Hartree - Fock Approximation.....33

3.1.5 Density Functional Theory (DFT).....36

3.1.5.1 Thomas Fermi (TF) Theory.....37

3.1.5.2 The Hohenberg - Kohn (H - K) Theorem.....38

3.1.5.3 The Self-Consistent Kohn - Sham Theorem.....40

3.1.5.4 Construction of Exchange - Correlation Functionals.....43

3.1.5.4.1 Local Density Approximation (LDA).....43

3.1.5.4.2 Generalized Gradient Approximation (GGA)……44
3.1.5.4.3 Meta - GGA Functional……44
3.1.5.4.4 L(S)DA / SGGA + U....45
3.2 Computational Details....47
3.3. Experimental Information....50
3.3.1. Nanoclusters of Cu_2O and CuO....50
3.3.2. Nanowires of Cu_2O....51
3.3.3. Nanotubes of CuO....51
3.3.4. Nanoribbons of CuO....51
3.3.5. Nanosheets of CuO....51
3.3.6. Bulks of Cu_2O and CuO....52
CHAPTER 4....53
4. RESULTS AND DISCUSSION....53
4.1 Zero - Dimensional Nanostructures of Cu_2O and CuO....53
4.1.1 Structural, Electronic, and Magnetic Properties of Nanoclusters of....53
4.1.1.1 Structural Property....53
4.1.1.2 Electronic Property....55
4.1.1.3 Magnetic Property....57
4.1.1.4 Discussion....58
4.2 One - Dimensional Nanostructures of Cu_2O and CuO....58
4.2.1 Structural, Electronic, and Magnetic Properties of Nanowires of Cu_2O 58
4.2.1.1 Structural Property....58
4.2.1.2 Electronic Property....60
4.2.1.3 Magnetic Property....61
4.2.1.4 Discussion....62
4.2.2 Structural, Electronic, and Magnetic Properties of Chiral CuO Nanotubes 62
4.2.2.1 Structural Property....62
4.2.2.2 Electronic Property....64

4.2.2.3 Magnetic Property 66
4.2.2.4 Discussion 67
4.2.3 Magnetic Moment of Zigzag CuO Nanotubes at Different Temperatures and Sizes 68
4.2.3.1 Structural Property 68
4.2.3.2 Electronic Property 69
4.2.3.3 Magnetic Property 72
4.2.3.4 Discussion 73
4.2.4 Structural, Electronic, and Magnetic Properties of Nanoribbons of CuO ... 73
4.2.4.1 Structural Property 73
4.2.4.2 Electronic Property 74
4.2.4.3 Magnetic Property 79
4.2.4.4 Discussion 81
4.3 Two - Dimensional Nanostructures of CuO 81
4.3.1 Structural, Electronic, and Magnetic Properties of Nanosheets of CuO 81
4.3.1.1 Structural Property 81
4.3.1.2 Electronic Property 84
4.3.1.3 Magnetic Property 90
4.3.1.4 Discussion 91
4.4 Three - Dimensional Structures of Cu_2O and CuO 92
4.4.1 Structural, Electronic, and Magnetic properties of bulks of Cu_2O and CuO 92
4.4.1.1 Structural Property 92
4.4.1.2 Electronic Property 93
4.4.1.3 Magnetic Property 95
4.4.1.4 Discussion 95

CHAPTER 5 ..... **97**

5. CONCLUSION AND RECOMMENDATIONS **97**

5.1 Conclusion 97

5.2 Recommendations 99

CHAPTER 6 ..... **99**

6. SUMMARY **100**

REFERENCES **104**

APPENDIX **121**

LIST OF PUBLICATIONS 121

LIST OF CONFERENCE PRESENTATIONS 122

CHAPTER 1

1. INTRODUCTION

1.1 Introduction

The application of nanotechnological devices is the only way to fulfill the demand of the present world and lead to future generation activities. Nowadays, the innovative applications of nanoscale devices cover almost all the sectors which directly or indirectly affect our daily lives like education, medicine, engineering, industry, energy harvesting as shown in Figure 1 (Karakasidis, *et al*., 2007; Khan, 2013; Tran, *et al*., 2014; Khan , *et al.*, 2017; & Nasrollahzadeh, *et al*., 2019).

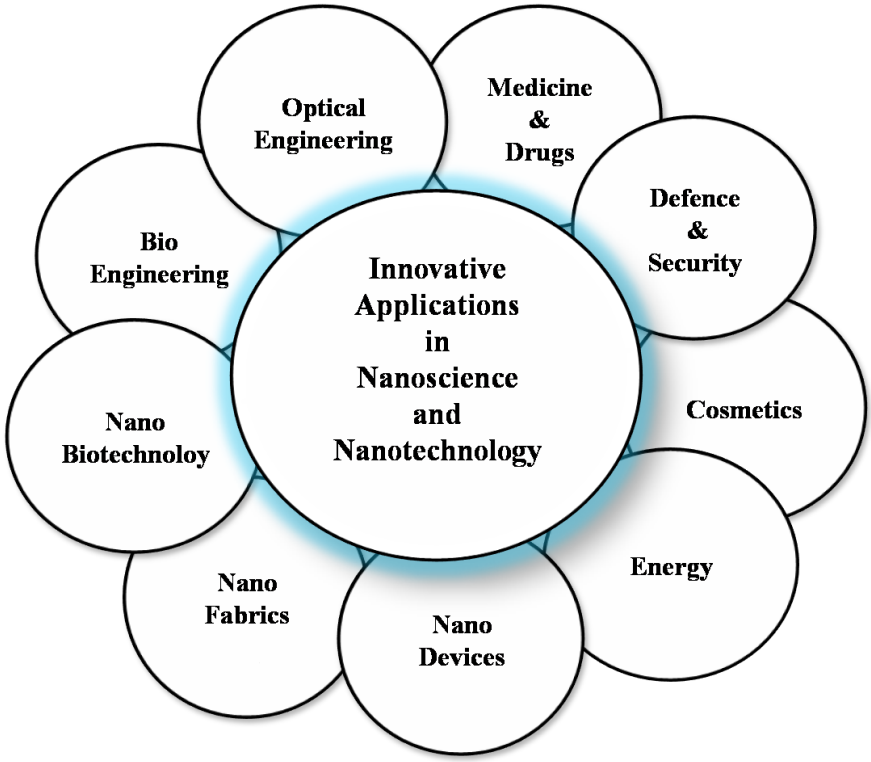

Figure 1: The innovative applications in the field of nanoscience and nanotechnology

Most nanotechnological devices are manufactured from the transition metal oxides which show peculiar properties when extending their dimension (D) from 0D to 3D via 1D and 2D, and vice versa. The increasing interest in the extended dimensions of transition metal oxide is due to their versatile properties, compared to their bulk counterparts, and applicable as promising materials in various fields of nanoscience

and nanotechnology. Copper oxides, which are mostly used as transition metal oxides, play a vital role in innovative applications. Cu_2O is commonly used as a semiconductor, a pigment, a fungicide, antifouling agent for marine paints, pink color in a positive Benedict's test etc. The hybrid Cu_2O - based heterogeneous nanostructures contribute a significant role in both fundamental study and multifunctional applications likes solar cell, photocatalyst, field emission, carbon monoxide oxidation, sensors, template, etc. (Barreca, *et al*., 2007; & Sun, 2015). Similarly, CuO is commonly used as a drycell, batteries, copper salts, wood preservatives, pigments in ceramics, diatary supliment in animals feed, disposal to safely dispose of hazardous materials and dioxins through oxidation. It is one of the top ten transition metal oxides used in the above mentioned applications, and also its one - dimensional structures like nanoribbon, nanotube, nanorod, and nanowire are being used in sensors (Choi & Jang, 2010).

Structural-wise, Copper (I) and (II) oxides (Cu_2O and CuO) originated from the copper and oxygen elements in a fixed empirical ratio through copper oxidation (Zhu, *et al*., 2006). Copper is the conducting and diamagnetic d-block solid element, whereas Oxygen is the insulating and paramagnetic p-block gaseous element. The atomic and orbital structures of both the oxygen and copper atoms are shown in Figure 2(a, b).

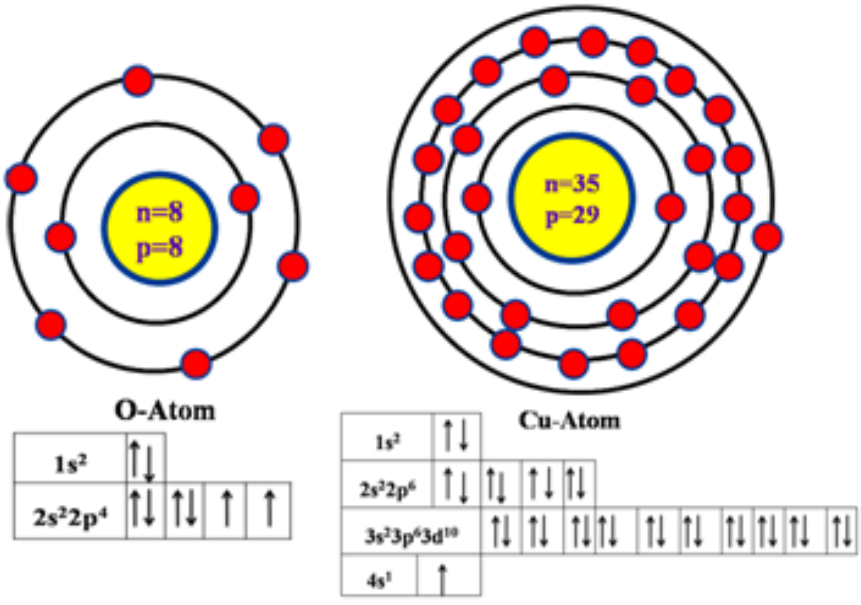

(a) (b)

Figure 2(a, b): The atomic and electronic structures of oxygen and copper atoms

The copper and oxygen ratios in Cu_2O and CuO are 2:1 and 1:1 respectively, which are found either in crystals or molecules in their stable forms. Their applications in the fields of optoelectronics and solar technology provide the research interest on them (Heinemann *et al.*, 2013, Devine, *et al.*, 2011). Copper oxides are non-toxic, chemically stable, low-cost materials having abundant resources and also, can be easily prepared in different shapes and sizes (morphologies) (Ghijsen, *et al.*, 1988; Zeng, 2007; Wang, *et al.*, 2016). The molecular and orbital structures of both the Cu_2O and CuO are respectively shown in Figures 3 and 4.

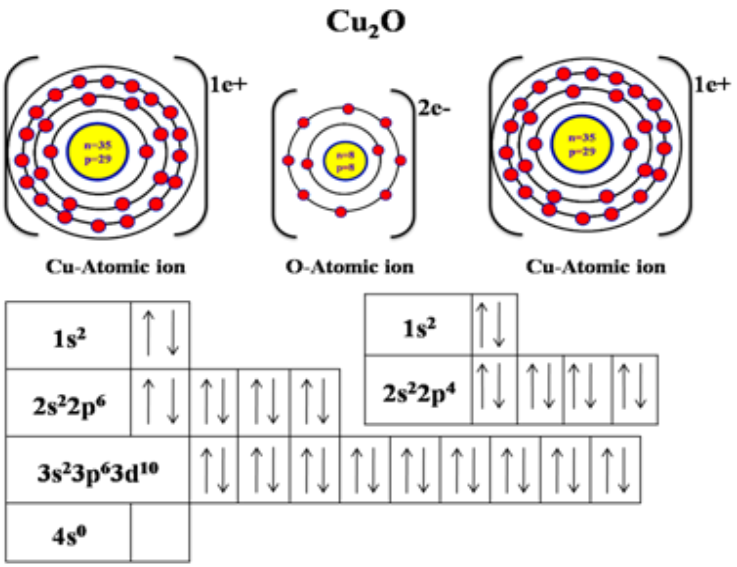

Figure 3: The molecular and electronic structures of Cu_2O

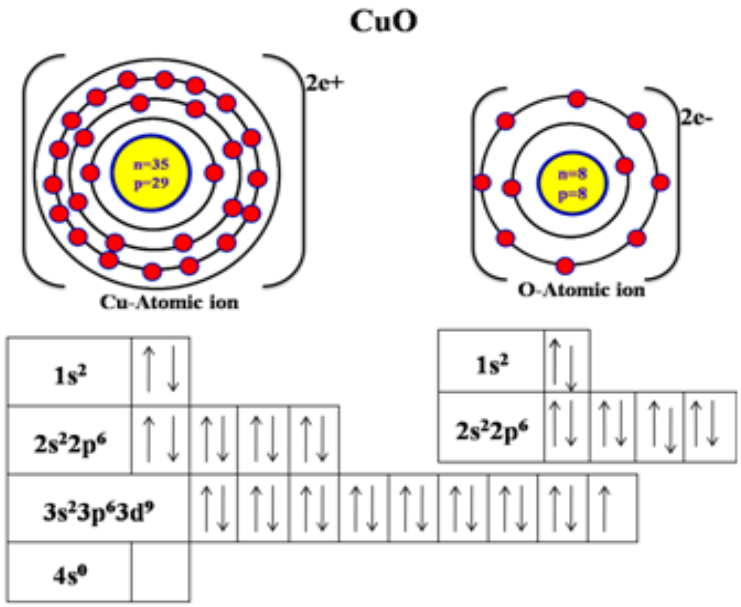

Figure 4: The molecular and electronic structures of CuO

Both copper oxides which have a broad range of application from conductor to insulator are introduced as prototype materials. Generally, copper oxides with different geometric and electronic structures exhibit semiconducting and sometimes metallic behaviors (Xiao, *et al*., 2007; Mojica, 2007; Abdu and Musa, 2009; Jin, *et al*., 2014; Pan, *et al*., 2018; & Linnera, *et al*., 2018). In the nanotechnological applications, these oxides are also employed in the manufacturing of optoelectronics, spintronics, solar energy transformation, supercapacitor, energetic materials, coating for surfaces protection against corrosion, etc (Li, *et al*., 2004; Yin, *et al*., 2005; Nolan & Elliott, 2006; Joseph, *et al*., 2010; Zhang, *et al*., 2014; & Rongxin, *et al*., 2021). For this cause, we focus our attention on theoretically, studying the structural, electronic, and magnetic properties of the different morphologies of both Cuprite and Tenorite like nanoclusters (0D), (Subramaniam, *et al*., 2015); nanowires (1D), (Wang, *et al*., 2003), nanotubes (1D), (Xu, *et al*., 2014), and nanoribbons (1D), (Xu, *et al*., 2014); nanosheets (2D) (Ang, *et al*., 2009); and bulks (3D) (Heinemann, *et al*., 2013, & Rongxin, *et al*., 2021). The main aim of the present study is their systematic study from nanocluster to bulk, to explore the new properties, and to resolve the reasons behind the applications.

The nanostructures of copper oxides have different properties due to the increasement in the ratio between surface and volume in comparison to the conventional forms and the quantum effects. The high surface - volume ratio leads to greater chemical reactivity and affects their strengths, and the quantum effect leads to determining the novel properties, and characteristics of copper oxide nanomaterials (Ching, *et al*. 1989; & Zhang, *et al*., 2014). In comparison to the structural characteristics like lattice symmetry and cell parameters, the bulk form of copper oxide is usually strong and stable in the crystallographic structure than the nanostructure at the different morphologies. The electronic property of the bulk oxide surface shows a long - range effect on the Madelung field, whereas it is not limited to the nanostructures of copper oxide. On the other hand, the interaction between Cu and O increases or decreases by the magnitude of bond length (Stefanovich & Truong, 1995; & Stefanovich & Truong, 1998).

Theoretically, the copper oxide reveals the redistribution of charges when extending from nanocluster to bulk structure. It must be relatively small for ionic solids, while significantly large for covalent ones. The degree of ionicity or covalence in copper -

oxygen bond depends on the size of structures (Espino, *et al*., 2002). The binding energy, electronic band structure, and density of states demonstrate various properties of copper oxides which are influenced by the sizes as well. If the average nanosize of copper oxides increases, then the magnitudes of the electronic band gap, conductivity, and chemical reactivity also change (Dar, *et al*., 2009). The surface property of metal oxides is also important to be analyzed because of their immense use in spintronics and optoelectronics fields of nanotechnology. According to surface property, the nature of 2D - surfaces depends on the typical structures of the bulk geometry and electronics. The properties of the surface are strongly modified for 2D - infinite surface in the case of nanostructure copper oxides (Torrance *et al*., 1988; Elesin, *et al*., 1996; Ma, *et al*., 2008; & Debbichi, *et al*., 2012). In addition, the atoms lying at the corners or edges of the nanostructure of copper oxide must be arranged in the specific geometrical shape and size and also corresponding occupied electronic states lie above the valence band of its bulk material which directly affects on the mentioned properties. Finally, the nanostructure is formed only when the bulk is limited to the nanoscale. (Koshy & George, 2015; Sachin, *et al*., 2016; & Stepniowski & Misiolek, 2018). To know above mentioned properties and interplay with electronic and magnetic related properties, we must have the idea of structural, electronic and magnetic properties of the material under study of the behaviors starting from nanocluster to bulk.

Here, we explore the various morphologies of both Cu_2O and CuO and deal with structural, electronic, and magnetic properties, their effects, and the innovative applications crossing our daily lives. For this, the nanostructures as nanoclusters, nanowires, and bulk of copper (I) oxide; and nanotubes, nanoribbons, nanosheets, and bulk of copper (II) oxide are designed and then they are simulated for their optimization and analyzation of the electronic and magnetic properties of the most stable structures which are performed through VNL - ATK tool under first - principles study.

1.2 Rationale of the Study

The justification of the present study for the use of different aspects is explained systematically as follows:

1.2.1 Zero - Dimensional Nanostructures

1.2.1.1 Nanoclusters of Cu_2O and CuO

Cu_2O and CuO are mostly stabled in their bulk phases and are categorized in general as the transition metal compounds and in particular as high - temperature superconductors. The causes of large specific surface to volume ratio and quantum confinement effects, the nanoclusters are more active and selective than that of the bulk (Ching, *et al*., 1989; & Zhang, *et al*., 2014). In the condensed phase, the chemical and physical properties of atomic or molecular species of the clusters Cu_2O_x (x = 1 - 4) were examined and observed that nanoclusters can play a vital role in the various environmental processes and in the synthesis of technological materials. (Wang, *et al*., 1996 - II; Lyubinetsky, *et al*., 2003; Ghodselahi, *et al*., 2008; Jadraque & Martin, 2008; Parra & Farrel, 2009; & Koshy & George, 2015). The structural and electronic properties of clusters Cu_nO_n (n = 1 - 8) were studied by using DFT and various basis sets which gave the best agreement with the experimental works. The clusters Cu_nO_n (n = 1 - 3) and Cu_nO_n (n = 4 - 8) were found as planar and nonplanar forms respectively. (Bae, *et al*., 2011; Chang, *et al*., 2012; Jin, *et al*., 2013; Musevi, *et al*., 2013; Sachin, *et al*., 2016; Du., *et al*., 2017). The colloidal nanocrystal clusters (CNCs) of CuO (60 nm) were prepared through a one - pot solvothermal synthetic method. In electrochemical reactions, it was shown that the surface of CuO nanoclusters act as a promoter for the reduction of O_2. The mesoporous SiO_2 coated CuO nanoclusters were found to be highly active and stable catalysts for olefin epoxidation (Massobrio, 2003; Qian, *et al*., & Chen, *et al*., 2011; 2012). After optimization, the point symmetry, total energy, DOS, ionization potential and electron affinity of the nanoclusters CuO and Cu_2O, were found (Subramaniam, *et al*., 2015; & Latif, *et al*., 2018).

We found the lack of the study of mentioned properties of nanoclusters like $(Cu_2O)_{n = 1, 2, 3}$ and $(CuO)_{n = 2, 4, 6}$. Hence, it is needed to optimize their structures and then analyze their various properties.

1.2.2 One - Dimensional Nanostructures

1.2.2.1 Nanowire of Cu_2O

The nanowires are the most important and the broad class of one - dimensional nanostructure at the foreground of nanoscience and nanotechnology. It is single - crystalline, highly anisotropic, and either insulating, semiconducting, or metallic. The Cu_2O nanowire shows ferromagnetic and metallic nature while Cu_2O bulk is a diamagnetic and p - type semiconductor of band gap 2.17 eV (Lieber & Wang, 2007; Singh, *et al*., 2007; Tan, *et al*., 2007; McAuley, *et al*., 2008; Hansen, *et al*., 2008; Shen, *et al*., 2010; Xu, *et al*., 2012; Zhou, *et al*., 2017; Khan, *et al*., 2017; & Sundar, *et al*., 2018). The diameter of a nanowire affects its structural stability and electronic and magnetic properties. The computational calculation confirms its metallic nature. The Cu_2O nanowire has been synthesized experimentally as well as computationally. With unique geometry and physical properties, the Cu_2O nanowires are promising materials for many novel applications: gas sensing, solar energy conversion, and magnetic storage media (Wang, *et al*., 2003; Zhang, *et al*., 2007; Xiao, *et al*., 2011; Lieber, 2011; Shi, *et al*., 2011; Ethiraj, *et al*., 2012; Back, *et al*., 2013; & Luo, *et al*., 2014).

The magnetism in these systems has not been studied much and hence, we need to focus on the calculation of magnetic moment per atom of Cu_2O nanowires of different diameters (4 - 6 Å) along with their structural and electronic properties.

1.2.2.2 Nanotubes of CuO

The other class of popular one - dimensional material is the nanotube. CuO nanotubes are manufactured through various methods, such as hydrothermal, thermal oxidation, anodic templating, etc. The copper oxide nanotubes have high potential applications in chemical and biological sensing, solar energy conversion, high - temperature superconductivity, and heterogeneous catalysis that have attracted researchers and scientists for further research works (Cao, *et al*., 2003; Malandrino, *et al*., 2004; Cho & Huh, 2008; Mu & He, 2011; Sun, *et al*., 2012; Xu, *et al*., 2014; Park, *et al*., 2015; Xiao, *et al*., 2015; & Zheng, *et al*., 2016). Computationally, they have been found in different chiralities as a zigzag (n, m = 0), and an armchair (n, m = n), which show the different structural, electronic, and magnetic behaviors. These types of CuO

nanotubes change their magnetic moments concerning temperature. Such CuO nanotubes are suitable for nanodiode, sensors, spintronic devices, etc (Lai, *et al*., 2010; Farrel & Parra, 2011; Hsuch, *et al*., 2011; Saini, *et al*., 2015; Paudel, *et al*., 2016; Muthaiyan, *et al*., 2018).

Hence, the study of binding energy per atom, electronic band structure, density of states, magnetic moment per atom, and spin polarization of the different chiralities (zigzag, armchair, and chiral) of CuO nanotubes can be of great importance.

1.2.2.3 Nanoribbons of CuO

The CuO nanoribbons, which have been synthesized through a wet chemical process, a facile organic - solution method and other experimental methods, are promising candidates for high - performance electrochemical capacitors, gas sensors, etc (Liu & Zeng, 2004; Gou, *et al*., 2008; Lo, *et al*., 2011; Yu, *et al*., 2012; Zhang, *et al*., 2013; Wang *et al*., 2018). An interesting fact about these nanostructures is that behave completely different at reduced dimensions. The variety of possible applications, that have motivated us to further computationally, optimize the zigzag, armchair, and chiral forms of CuO nanoribbon and analyze their mentioned properties. The binding energy per atom, magnetic moment per atom, and spin polarization have been computed as a marker for the required properties of the optimized zigzag ($3 \leq n \leq 10$, $m = 0$) and armchair ($3 \leq n \leq 10$, $m = n$) CuO nanoribbons.

1.2.3 Two - Dimensional Nanostructures of CuO

1.2.3.1 Nanosheets of CuO

CuO nanosheets were synthesized experimentally through hydrothermal process, surfactant - free, facile, low - temperature grow methods. The nanosheets are being used in different applications like a gas sensor for various flammable gases including ethanol, gasoline and nonflammable as H_2S, batteries, energy storage, photocatalysts, and non-enzymatic glucose sensors. Due to high-temperature superconductivity in copper oxide perovskites, the structural stability of nanosheets is of great interest to the scientific community (Ang, *et al*., 2009; Zhang, *et al*., 2010; Moura, *et al*., 2010; Jia, *et al*., 2010; Lu & Wang, 2011; Shahmiri, *et al*., 2013; Ibupoto, *et al*., 2013; Dubal, *et al*., 2013; Moser, *et al*., 2014; Maddinedi, *et al*., 2015; Demel, *et al*., 2015; Fan, *et al*., 2017; & He & Bae, 2018; Deng, *et al*., 2018). The variations in the

different properties at reduced 2D - CuO nanosheets as $(1 \leq n \leq 8, m = 0)$ zigzag and $(1 \leq n \leq 8,\ m = n)$ armchair forms of CuO nanosheet. These nanosheets are optimized and then analyzed for the calculations of their binding energy per atom, magnetic moment per atom and spin polarization which characterize their structural, electronic, and magnetic properties.

1.2.4 Three - Dimensional Structures of Cu_2O and CuO

1.2.4.1 Bulk of Cu_2O

Cu_2O (cuprous oxide) is known as cuprite which has come from "cuprum" in Latin word that means copper and is also called "ruby copper". Its major ores are found in the most places of the countries around the world. Besides pure copper, the one molecule of cuprite gives two copper atoms and one oxygen atom.

The cuprite is found in the different forms of crystal like cube, octahedral, dodecahedron and their combined forms in a mineral specimen (Huang, *et al*., 2012). It is seemed as red or deep red (almost black) color due to the internal reflections. It has been also found in the different forms of the chalcotrichite as long needle crystals having a admirable red color and a special sparkle which make them the popular display cabinet specimens.

Cuprous oxide having molecular formula Cu_2O, known as an inorganic compound is one of the principal oxide copper. The color of compound as the reddish mineral cuprite depends on the size of particles (He, *et al*., 2005; & Zoolfakar, *et al*., 2014). This inorganic compound is soluble in acid whereas insoluble in water. Cu_2O has been produced at a limited range of temperature and oxygen pressure by the oxidation of copper metal (Abdu & Musa, 2009; & Eivazihollagh, *et al*., 2018).

$4Cu + O_2 \rightarrow 2Cu_2O$

Cuprite crystal having two sublattices like a face centered cubic of Cu^{1+} ions and a body centered cubic of O^{2-} ions has been found in a simple cubic structure. In the cuprite crystal, copper is linearly coordinated by two neighboring oxygens, whereas oxygen is tetrahedrally co-ordinated by copper. The short bond length between Cu and O in Cu_2O is not compatible with the sum of any pair of the ionic radii for Cu^{1+} and O^{2-} for a metal. Cu_2O crystallizes in a cubical form of a lattice constant a (4.267

Å), space group (Pn3m) and number (225) consists of Cu^{1+} ions locating at the positions (1/4, 1/4, 1/4; 3/4, 3/4, 1/4; 3/4, 1/4, 3/4; 1/4, 3/4, 3/4) in the conventional fcc lattice and the O^{2-} ions locating at the positions (0, 0, 0; 1/2, 1/2, 1/2) in the conventional bcc lattice (Barreca, *et al*., 2009; Rasadujjaman, *et al*., 2012; Zemzemi & Alaya, 2015; Bhosale & Bhanage, 2016; & Du, *et al*., 2017). Cu_2O transition - metal oxide is prototypical material that shows quite peculiar characteristics. It is a non - toxic, abundant, and inexpensive p - type semiconductor. The cubic crystal Cu_2O consists of $4Cu^{1+}$ and $2O^{2-}$ ions and has lattice parameters (a) = 4.27Å, band gap (E_g) = 2.02 - 2.17 eV and net magnetic moment (μ) = 0 experimentally (Zhang, 2013; & Isseroff & Carter, 2013). The crystal structure of Cu_2O and the values of different parameters of a unit cell of bulk Cu_2O is shown in Figure 5 and Table 1 respectively.

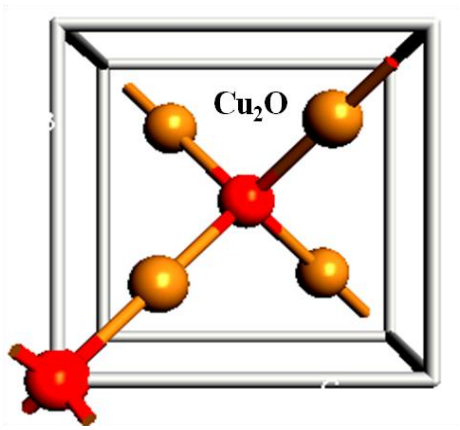

Figure 5: The unit cell of bulk Cu_2O

The Cu_2O is a promising material for industrial, engineering, and medical fields for its use in various applications such as photocatalytic, photovoltaic, perovskite solar cell, thermoelectric, and magnetic storage media. The nanosized Cu_2O has widely been used as a fungicide, and anti - fouling paint and has also great impact in various research fields including sensors, superconductors, electrochemistry, optics, and electronics (Badawy, *et al*., 2015; & Chatterjee & Pal, 2016). It is widely studied through theoretical, and experimental processes. The band gap of 0.99 eV vs 2.17 eV of Cu_2O in LDA + U with Heyd - Scuseria - Ernzerhof (HSE) hybrid functional was found (Wang Y. *et. al*., 2016).

Table 1: The values of different parameters of unit cell of bulk Cu_2O (Ghijsen, *et al*., 1988; & Wang, *et al*., 2016)

Space group and number	Pn3m, 225
Lattice Constants at RT (a, α, β, γ)	4.27Å, β = α = γ = 90
Cu - O	1.85Å (bond length)
O - O	3.68Å
Cu - Cu	3.02Å
Bandgap energy at RT (E_g)	2.17 eV
Valence band Hole mass	0.58 amu
Conduction band Electron mass	0.98 amu
Magnetic moment per atom (μ)	0
Relative permittivity	7.5
Density (ρ)	6.10 g / cm^3
Molecular mass (M)	143.092g / mol
Melting point	1235 ^{0}C

1.2.4.2 Bulk of CuO

The copper (II) oxide with molecular formula CuO in the black to brown color knowing as cupric oxide or tenorite is the another inorganic compound. It is obtained from the copper mining and also from the other copper - containing products and chemical compounds like copper (II) nitrate, copper (II) hydroxide, copper (II) carbonate etc. These compounds are used for the preparation of CuO in the laboratory for laboratory uses (Wang, *et al*., 2002; Bello, *et al*., 2014; Raj & Biju, 2017; Quirino, *et al*. 2018; & Cao, *et al*., 2018).

$2\ Cu(NO_3)_2 \rightarrow 2\ CuO + 4\ NO_2 + O_2$

$Cu(OH)_2\ (s) \rightarrow CuO\ (s) + H_2O$

$CuCO_3 \rightarrow CuO + CO_2$

The simple structure of the unit cell (monoclinic) of CuO lies in the space group (C2 / c) and number (15). The positions of Cu^{2+} and O^{2-} ions are found to be ± (1/4, 1/4, 0; 3/4, 1/4, 1/2) and ± (0, u, 1/4; 1/2, u + 1/2, 1/4) respectively. Where u is a parameter that describes the relative positions of O^{2-} ions along the lattice vector b. The experimental lattice parameters are a = 4.653 Å, b = 3.410 Å, c = 5.108 Å, u = -0.584, $\alpha = \gamma = 90$ and $\beta = 99.483^0$ (Wang, *et al*., 2002; & Cao, *et al*., 2018). The copper (II) oxide (CuO) is stable in its bulk phase. It is the transition metal compound in general and the superconductor at high - T in particular. The CuO is expected to have the essentially open Cu - 3d shell ($3d^9 4s^0$).

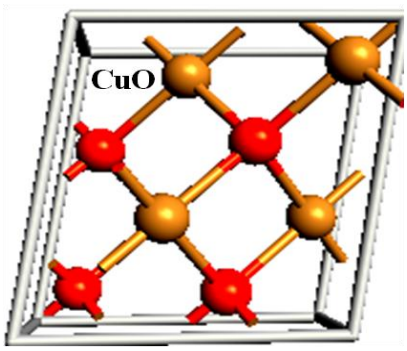

Figure 6: The unit cell of bulk CuO

The different dimensional shape and sizes of CuO play a significant roles and directly affect on its different mentioned properties in the nanoscale systems. In the experimental as well as theoretical study, it was seemed that the bulk CuO is the ferromagnetic p - type semiconductor with an energy band gap, E_g = 1.4 eV whereas the ordering of isolated $4Cu^{2+}$- ions in bulk CuO shows antiferromagnetic behavior. (Hagemman, *et al*., 1990; Grant, 2008; & Ekuma, *et al*., 2014). The structure of bulk CuO and its different parameters are shown in Figure 6 and Table 2 respectively. In this compound, the nanostructures of CuO are more active and selective in comparison to its bulk structure.

Table 2: The values of different parameters of a unit cell of bulk CuO (Tran & Nguyen, 2014; Wang *et al.* 2016)

Space group and number	C2 / c, 15
Lattice Constants at RT	a = 4.684Å, b = 3.423Å, c = 5.129Å, $\beta = 99.54^0$
Cu - O	1.95 Å (bond length)
O - O	2.62 Å
Cu - Cu	2.90 Å
Bandgap energy at RT (E_g)	1.2 - 1.9 eV
Valence band Hole mass	0.54 - 3.7 m_e
Magnetic susceptibility	$+238.9 \times 10^{-6}$ cm^3 / mol
Magnetic moment per atom (μ_T)	0.68 μ_B
Density	ρ = 6.32 g / cm^3
Molecular Mass	79.55 g / mol
Melting point	1134 ^{0}C
Boiling point	2,000 ^{0}C

The CuO transition - metal oxide is prototypical material that shows quite peculiar characteristics. It is a non-toxic, and inexpensive p - type semiconductor (Kliche & Popovic, 1990; Zaman, *et al*., 2012; Ekuma, *et al*., 2014; & Wanninayake, *et al*., 2015). The bulk structure of CuO is being broadly applied as a electrode material, a supercapacitor, hydrogen storage, and magnetic ceramics (Mao-hai, *et al*., 2010; Stucky, *et al*., 2014). CuO is widely studied through experimental and theoretical processes. Cao studied monoclinic and cubical structures of the bulk CuO in LDA and GGA and found monoclinic - CuO, showing metallic behavior, is more stable

than cubic - CuO structure. It has been reported that LDA and GGA potentials within DFT formalism fail to explain the bulk CuO as a p - type semiconductor (Cao H., *et al*. 2018). Wang found a band gap of 2.74 eV vs 1.57 eV of CuO in LDA + U with HSE hybrid functional (Wang, *et al.*, 2016). Heinemann investigated the magnetic moments 0.66 μ_B and 0.54 μ_B of CuO by using LDA + U and HSE06 respectively (Heinemann, *et al*., 2013).

These indicate that both the transition copper oxides Cu_2O and CuO are very important for general applications and still need to do a systematic study in different properties to gain insight into the following natures and applications points of view. The research gaps, which are going to be dealt with, are as follows,

I. There are few experimental and theoretical studies on the structural, electronic, and magnetic properties of the different morphologies of copper oxides.

II. There are the lacking of study on the changing of structural, electronic and magnetic phase or not in the proposed morphologies.

III. The structural models and properties of the mentioned morphologies need to be explored for the designations of semiconductor, magnetic, spintronics, and modern technological devices.

Due to these research gaps, we are motivated to optimize and analyze the different morphologies of the mentioned copper oxides to calculate the required physical quantities. The binding energy per atom, the energy band gap, the magnetic moment per atom, and spin polarization have to be calculated for their stability and other identifications. These parameters of the bulks and nanoclusters of both Cu_2O and CuO, the nanowires of Cu_2O, and the nanotubes, nanoribbons and nanosheets of CuO can be explored theoretically through exchange - correlation functionals like LSDA+U, SGGA+U, and MSGGA for bulks and SGGA+U for all other morphologies. It is because SGGA+U provides the accurate opening of band gaps for the reduced morphologies of strongly correlated systems.

1.3 Research Objectives

On the basis of motivations and previous work analysis (explain more detail in chapter 2), we have to fulfill the above mentioned research gaps by working on the structural, electronic, and magnetic properties of copper (I) and (II) oxides at different

morphologies through first - principles approach. The objectives of the present work are the followings:

General objective

To study the structural stability, electronic band structures, and density of states of different morphologies of Cu_2O and CuO individualy through the first - principles approach.

Specific objectives

i. To optimize the different morphologies (nanoclusters, nanowires, nanotubes, nanoribbons, and nanosheets and bulks) of copper oxides
ii. To analyze the structural evolution and calculate the binding energy of optimized structure for the structural stability of different morphologies.
iii. To analyze the electronic band structure and density of states for the electronic properties.
iv. To investigate the magnetic moment and spin polarization for the different systems and find the magnetic properties

1.4 Organization of study

This work deals with the different properties of the nanostructures of both copper (I) and (II) oxides like nanoclusters (0D), nanowires (1D), nanotubes (1D), nanoribbons (1D), nanosheets (2D) and bulks (3D).

The organization of the present study of the research work on "Structural, Electronic and Magnetic Properties of Copper (I) and Copper (II) Oxides at Different Morphologies: First - Principles Study", has been planned with six main chapters including 1. Introduction, 2. Literature review, 3. Materials and methods, 4. Results and discussion, 5. Conclusion and recommendations, 6. Summary. The references and appendix are also included after the summary.

All the chapters of our thesis are orderly arranged and expressed the research works in brief as follows:

Chapter 1: The brief introduction about copper (I) and (II) oxides and their applications, rationale, research gaps, and objectives of the research work are introduced in "Introduction".

Chapter 2: This chapter deals with the findings of former researchers related to the present work are briefly discussed and reviewed in literature review. This chapter is focused on the descriptions of various properties of Cu_2O and CuO nanostructures to their bulks, synthesis process, and their applications.

Chapter 3: In Materials and methods, the general considerations of theory and density functional theory are explained including computational details. The working procedure of VNL - ATK software used for the study of different morphologies of Cu_2O and CuO is also explained in brief.

Chapter 4: Results and discussion have been divided into four parts where the first, second, and third parts describe the structural, electronic, and magnetic properties respectively, whereas the fourth part consists of a discussion of the present results.

Chapter 5: Conclusion and recommendations chapter contains the main findings of the present work. Further, what can be done in the future is recommended as a further research possibility.

Chapter 6: Summary points out the remarkable findings of the present work in brief. These are key points that describe the whole ideas of our research works.

References and an Appendix have also been included in the last part of this thesis.

CHAPTER 2

2. LITERATURE REVIEW

The summaries of the various kinds of literature comprising the most significant and recently published reports related to the structural, electronic, and magnetic properties of Cu_2O and CuO at different morphologies have been provided in this chapter. The experimental basis of the theoretical study of the different morphologies of the copper oxides (nanoclusters, nanowires, nanotubes, nanoribbons, nanosheets, and bulks) have been reviewed. The modified strategies or approaches to deal with preparations, properties, and applications in different fields also have been studied. The reviews of the literature followed during the study of the present work have been described here briefly in the following sections .

2.1 Zero-Dimensional Nanostructures of Cu_2O and CuO

2.1.1 Nanoclusters of Cu_2O and CuO

The electronic structures of clusters Cu_2Ox (x = 1 - 4) were investigated through anion photoelectron spectroscopy (APS). The geometries of clusters including their electron affinity were found through density functional theory (DFT) as same as experimental observations. In the different oxidation states of clusters, the definitive structures of clusters were verified by the analyzation of their chemical bonding and electronic structures (Wang, *et al.,* 1996). The equilibrium structures of CuO_4 and CuO_5 nanoclusters were found by using both the density functional theory and plane - wave approach (PWA). The isomer containing $Cu(O_3)$ ozonide unit has higher energy than that of CuO_4 based on the $Cu(O_2)$ unit. The isomer with one O_3 motif has lower energy than that made of $Cu(O_2)$ unit in the different situations of CuO_5. The ozonide unit is formed by the hybridization of both Cu - 3d and O - 2p orbitals, and transforms into an O_3 chain which ensures the stability of the CuO_5 nanocluster. From the result, one can encounter an unconventional form of CuO bonding due to the O_3 group in the copper oxide nanoclusters (Massobrio & Pouillon, 2003). The single - phase nanoclusters of range 10 nm - 50 nm of Cu_2O were grown on the $SrTiO_3$ (100) substrates through the very narrow OPA - MBE growth parameter window. For experimental and theoretical predictions, the XPS and the AES spectrocopies were used to study the regions in the phase diagram for a small system. It was observed that the

Cu_2O nanocluster in a pure and single phase is much harder than of the bulk and other multicomponent materials. The relation between the data of composition of nanoclusters and the morphology was plotted with the help of atomic force microscopy (AFM) (Lyubinetsky, *et al.*, 2003). The constituents $Cu_nO_m^{+/0}$ and $Cu_nO_mH_1^{+/0}$ clusters of Cu_2O were observed through DFT calculation. The clusters $(Cu_2O)_n^+$ and $[(Cu_2O)_nCu]^+$ contain an even and odd number of copper atoms respectively. The structures of $Cu_nO_mH_2^{+/0}$ and $Cu_{2n}O_nH^{+/0}$ are hydrated and hydrogenated clusters respectively. In the experiment, they found H atom bounds to the divalent O in the even - numbered clusters $Cu_{2n}O_nH^+$ and also found the absence of the formation of odd - numbered clusters, $Cu_{2n+1}O_nH^+$ in the mass spectra due to the lack of the divalent O reactive site (Jadraque & Martin, 2008). The uniform CuO colloidal nanocrystal clusters (CNCs) were prepared through a one - pot solvothermal synthetic process. The CuO CNCs coated with mesoporous SiO_2 shells have been found to the highly active and stable catalysts in CuO nanocluster (CuO CNCs@meso - SiO_2). Its excellent activity and stability in olefin epoxidation reactions was experimentally observed through TEM and small angle x - ray diffracion. This process can help to make other catalytic systems with various dimensions and compositions (Chen, *et al.*, 2011). The structures and stabilities of copper oxide clusters, Cu_nO_n (n = 1 - 8) were found by using ab - initio simulations and calculations. The lowest energy of the structures of the neutral and charged copper oxide nonplanar clusters of range $n \geq 4$ through the primarily B3LYP / LANL2DZ model chemistry. The calculated atomization energy, ionization energy, electron affinity, and charge are functions of the number of Cu and O atoms. The clusters having n = 1 - 3 become planar whereas clusters having n > 3 nonplanar. The clusters having an even number of copper atoms exhibit less stable than that of an odd number of copper atoms due to less strain in the Cu - O - Cu bond angles (Bae G. T., *et al.*, 2011). The structural and electronic properties of CuO, CuO_2, and Cu_2O were studied through the B3LYP / 6 - 31G basis set under the density functional theory approach. The binding energy, molecular energy spectrums, HOMO - LUMO gap, ionization potential, electron affinity, point symmetry and also dipole moment of the nanoclusters were calculated. The high binding energies of CuO - 1 and CuO_2 - 1, Cu_2O - 1, and CuO - 2 were found. The dos profiles report the transition of electrons

due to the high value of the HOMO - LUMO gap and the availability of charges in energy intervals. The high ionization potential (IP) in CuO - 1, Cu_2O - 1, and Cu_2O - 3 clusters, whereas high electron affinities (EA) in Cu_2O clusters showed a metallic nature. (Subramanian, *et al.*, 2015). The stable compositions and structures of copper oxide cluster cations were studied through both the IMMS and DFT calculations. The cluster ions $Cu_nO_m^+$ (n : m = 2 : 1) increases monotonically in the mass spectrum and the collision cross sections with increasing of cluster size were observed. By comparing the CCSs obtained in both the IMMS experiments and DFT calculations, they assigned the stable compositions and structures to the optimized clusters (Latif, *et al.*, 2018).

2.2 One - Dimensional Nanostructures of Cu_2O and CuO

2.2.1 Nanowire of Cu_2O

A facile, solution - phase route was used to fabricate and characterise the large - scale of single - crystalline Cu_2O nanowire. The wire of controllable diameter is fabricated with high aspect ratio in the different morphologies. It was synthesized through the reduction of cupric acetate with o - anisidine, pyrrole under hydrothermal conditions. The current - voltage characteristics of both Cu_2O and Cu_2O / poly (2, 5 - dimethoxy aniline) core / shell nanowires are linear. The latter exhibited n - type characteristics and enhanced conductivity which are being used in electronic devices (Tan, *et al.*, 2007). The copper / cuprous oxide nanowire arrays were explored through the porous alumina membrane (PAM) templates. The growth of Cu_2O nanowires is increased through both oxygen diffusion and release of compressive stress under the template space limitation (Shen, *et al.*, 2010). The superstructures of Cu_2O nanowires in various regular polyhedral shapes were synthesized through hydrothermal routes. The reductant and the additive make the shape of the polyhedron Cu_2O nanowires. The shape of these nanowires in a batch reaction mode were controlled by the help of both the carboxylic acid-doped polymer chains and self - adjusting growth rate of the branched nanowires. The SEM and TEM studies demonstrate experimentally the polyhedral shape of Cu_2O nanowire (Shi, *et al.*, 2011). The Cu_2O nanowire arrays were fabricated by using the facile method. The nanowire of diameter 50 mm and length of 10 μm approximately was prepared on Cu substrate in the air at the optimal temperature of 400°C by simple heat treatment. The growth of the Cu_2O nanowires

was characterized by the electron microscopy. This method offers a great potential route for the manufacturing of Cu_2O nanowires on large scales. The based devices of Cu_2O nanowires are sensors and solar cells (Xu, et al., 2012). The hybrid p - Cu_2O with n - ZnO nanowires were used to fabricate an oxide p - n heterojunction device on the ITO / glass substrate for the study of the photovoltaic performance. The solar cells were prepared on the vertical arrangement of ZnO nanowires by the process of metal - organic chemical vapor deposition and electrodeposition of the p - type Cu_2O layer. The solar cells based on the Cu_2O / ZnO nanowire exhibits a higher conversion efficiency than the planar structure solar cell. (Baek, *et al*., 2013). The mechanism for the formation of Cu_2O and Cu nanowires in anodicaluminaoxide (AAO) template was explored through the electrodeposition process. The Potentiostate, XRD, SEM, etc were used to find the effects of potential and pH on the formation of these wires. The pure Cu_2O nanowires were electrodeposited at a lower voltage due to the formation of large - size critical Cu nuclei than the mixed Cu and Cu_2O nanowires. (Khan, *et al.*, 2016). The hierarchical CuO / Cu_2O @ $NiCo_2S_4$ nanowire arrays having ultra - high specific capacitance, a high rate, and excellent cycling stability, were constructed on copper foam.. The hybrid nanowires of Cu_2O and CuO works as a hierarchical scaffold for rapid ion diffusion and electron transport. The core of this hybrid nanowires and the shell of $NiCo_2S_4$ nanosheets work as the electroactive materials. The experimental results report the significance of optimal design and fabrication of nanowires including a simple method to build the 3D electrode for energy storage (Zhou, *et al.*, 2017).

2.2.2 Nanotubes of CuO

The nanotubes of Cu, Cu_2O and CuO were manufactured through the controllable synthetic route. Under the different reaction conditions, the Cu, Cu_2O, and CuO nanotubes were produced by using the same precursor $Cu(OH)_4^{2-}$ in the presence of Cetyl trimethyl ammonium bromide (CTAB). Their approaches manipulated the surfactant - inorganic aggregates in the solutions. It was found that the higher and the lower concentrations of $Cu(OH)_4^{2-}$ precursor generally leads to the rodlike formation and favors the tubular formation respectively. They invented the simple synthesis strategy for the synthesis of nanostructures of other metal oxides, such as Al_2O_3, ZnO, and SnO_2 (Cao, *et al.,* 2003). The CuO nanotubes were manufactured by the

templated metal - organic chemical vapor deposition (MOCVD) route. It is the first strategic technique to obtain the regularly packed nanotube array after the removal of the template. The other assessed MOCVD procedures with AAO have been also used to make the free - standing nanotube arrays of other oxide systems (Malandrino, *et al.*, 2004). The copper nanowire of length 50 μm as a template which produced the CuO nanotube of length 10 μm was made through the oxidation process at 400 ^{o}C in air. The tubular structures of CuO were prepared through the copper diffusion from the interior to the exterior of the nanowires before oxidation on or near the surface of nanowires. The powder x - ray diffraction (XRD) and the Cu Kα radiation were used for the analysis of the structures of CuO nanotubes. The morphologies of CuO nanotubes were observed through SEM) and HRTEM (Cho, et al., 2008). The CuO nanotubes were developed on the Cu / CuO / glass templates. Also, the porous structures were observed between CuO film and Cu layer after annealing. It was shown that both the mean length of nanotube and ickness of porous structure were monotonically increasing with respect to increase in the initial thickness of the copper film. The fabricated sensor measures a small current in the sealed test chamber containing injected isopropyl alcohol (IPA) at applied bias 5V. Furthermore, the sensors with the longer CuO nanotubes become more responsible for the measurement of current (Hsueh, et *al.*, 2011). The confined CuO nanotubes were made from the CuS nanowires embedded in AAO template by using an annealing – induced diffusion in the confined tube type space,. During the fabrication of the AAO template, they tuned their diameter and pore size by changing their electrochemical parameters. The CuO nanotubes are used in the applications of catalysis, electrochemistry, superconductivity, and super hydrophobic coating and also in sensor applications due to the large specific surface areas (Mu & He, 2011). The nanotubes array was synthesized directly on the Cu plate and improved the electrochemical performance of CuO nanotubes through the facile electrodeposition process. The prepared CuO nanotubes provide a large specific surface area for electrolyte access and the insertion of Li - ions and also adjust the volume change of CuO during cycling. The CuO nanotubes as an anode - electrodes exhibit good rate and cycling performances (Xiao, *et al.*, 2015). The CuO nanotubes were directly fabricated on the Cu substrate by the quantifying of the adhesion energy of CuO and $Cu(OH)_2$ through the nano scratch technique. In this reaction time, the adhension energy both components increases and also observed that CuO nanotubes exhibit higher

debonding behavior than that of $Cu(OH)_2$ nanotube (Saini, *et al.*, 2015). The structural stability, electronic band structure, and magnetic moment per atom of the zigzag and armchair forms of CuO nanotube were studied through the DFT under the ab - into the approach. The binding energy of both types of CuO nanotube increases with the diameter. These nanotubes also show the metallic and ferromagnetic behaviors. It is observed that the total magnetic moment decreases with the increasing diameter (Paudel, *et al.*, 2016). The electronic transport properties of Zinc-doped and undoped CuO armchair nanotubes, and both NH_3 - absorbed nanotubes were studied through the DFT - NEGF method. The adsorption effect of the ammonia (NH_3) molecules were observed on undoped and Zn - doped CuO nanotubes. The current and transmission values decrease in the Zn - doped CuO ANTs due to the 'd' orbital overlapping whereas increase in NH_3 - absorbed Zn – doped CuO ANTs. The increment in electric current confirms the adsorption of the NH_3 molecule on Zn - doped CuO nanotube (Muthaiyan, *et al.*, 2018).

2.2.3 Nanoribbons of CuO

The mesoscale organization of free - standing CuO nanoribbons spontaneously attached to rhombic crystal strips and then the nanoribbons self - assembled into dandelion - like architectures with hollow interiors. The constructed nanoribbons like rhombic CuO crystal strips and dandelion were observed by the SEM, TEM, and SAED. The crystal lattice fringes of d_{110} (2.7 ± 0.1 Å) and d_{200} (2.3 ± 0.1 Å) along the CuO nanoribbons in the rhombic crystalline building blocks were detected through HRTEM SI - 4 (Liu & Zeng, 2004). At the room temperature, the diluted solution of copper nitrate and ethanol amine synthesis nanostructures crystals like one dimensional copper hydroxide nano strands (CHNS), two dimensional $Cu_2(OH)_3NO_3$ nanoribbons, and three dimensional CuO nanowalnuts. The formation of blue $Cu_2(OH)_3NO_3$ nanoribbon - like precipitates were obsorved from the same precursor solution at 10 ^{0}C. which was further converted into CuO porous nanoribbon. The catalytic and electrochemical properties of this nanoribbon were also founded (Yu, *et al.*, 2012). The mesoporous CuO nanoribbons were synthesized by the facile and scaleable wet - chemical method at room temperature. The researchers used a soft templet like tetraoctyl ammonium bromide (TOAB) under ambient conditions. They investigated the structure and morphology of the as - synthesized CuO with the help

of XRD, and FTIR spectroscopy. The CuO nanoribbons having high specific surface area was confirmed by physical characteristics. The higher specific capacitance and the stable cycling performance capacitance of the as - synthesized CuO nanoribbons were found by electrochemical data analysis. The low - cost electrode of CuO nanoribbons are being used for high - performance electrochemical capacitors (Zhang, *et al.*, 2013). Both CuO nanoribbon and Ag - CuO nanoribbons were developed through a wet chemical methods. These are being used as ethanol gas sensor. Both sensors as CuO nanoribbon and Ag - CuO nanoribbon found fastly the ethanol gas at room temperature. These sensors are more excellent than other sensors due to the fast response time and low operating temperature. These materials are used to prepare the real - time monitoring ultrafast gas sensors (Wang, *et al.*, 2018).

2.3 Two - Dimensional Nanostructures of CuO

2.3.1 Nanosheets of CuO

The stable CuO nanosheet was synthesized through a mild hydrothermal process in the presence of CTAB and observed their primary gas sensing properties through XRD approach. Analysis confirms the single phase CuO nanosheets. The morphologies of CuO nanosheet were observed through FE - SEM and tested their gas sensing properties in the static state system. Experimentally synthesized uniform nanosheets of CuO, consisting of irregular plates of thickness 20 nm - 25 nm and length 100 nm - 200 nm, have gas sensing property. Furthermore, the CuO nanosheet gas sensors show a stable gas response and the same gas sensitivity trend as the tested gases (Jia, *et al.*, 2010). The CuO nanosheets were synthesized and developed for the sensitive and selective determination of H_2S gas with high recovery. Furthermore, the gas sensor demonstrates good reversibility and strong recovery ability in 9s. This sensor is also closely related to environmental pollution, climate change, and human health. It has opened up a new way for developing CuO nanosheets to determine H_2S gas sensors based on other two - dimensional like nanoplates, and nanodisks (Zhang, *et al.*, 2010). The CuO nanosheets were synthesized on the gold - coated glass substrate through the hydrothermal process. The structural property and the chemical composition of CuO nanosheets were observed through XRD and XPS technique respectively. The structural and chemical compositions were revealed as a highly dense, uniform, and good crystalline array. Furthermore, they are being used for the

development of the sensitive non - enzymatic glucose sensor which possesses the high sensitivity, wide glucose detection range, good selectivity, reproducibility, and stability (Ibupoto, *et al.*, 2013). The CuO nanosheets are easily synthesized through the controlled delamination of the layered copper hydroxide acetates. The hydroxide nanosheets during the transformation to CuO was preserved by this procedure. The thickness and lateral size of the nanosheets were found the corresponds three to four CuO_6 octahedral layers and about 5 nm respectively.. Due to the facile synthesis, nanostructures, nanosheet morphology, and use as CuO ink, the CuO dispersions are being used as the production of photocatalysts, sensors, and energy storage devices (Demel, *et al.*, 2015). The CuO nanosheets were prepared through the hydrothermal process which acted as the anode material for the sodium - ion batteries (SIBs). The CuO nanosheet electrode with a carboxymethyl cellulose (CMC) binder showed significantly more satisfactory electrochemical performance than the electrode containing polyvinylidene (PVDF). Furthermore, in practical applications, a SIB full cell consisting of CuO nanosheet anode and $Na_3V_2(PO_4)_3$ cathode has been assembled and tested (Fan, *et al.*, 2017). The CuO nanosheets were manufactured after mild heat treatment (300 $^{\circ}$C) and found as the improved crystallinity, the porous structure, manifesting superior Li - ion storage capability with high capacity, excellent rate, and cyclability. It was demonstrated the enhanced electrochemical performances for the synergy of porous nanosheet morphologies and the improved crystallinity (Deng, *et al*., 2018).

2.4 Three - Dimensional Structures of Cu_2O and CuO

2.4.1 Bulks Cu_2O and CuO

The former researchers investigated the electronic structure of the closed d shell Cu_2O nanostructure and observed the same result of the one - electron band structure calculation. They compared the electron spectra of Cu_2O using ASW method with the various experimental tools like XPS, UPS and BIS. They found a good agreement between the experimental and computational reports of the energy band gap. This kind of agreement is reasonable to expect for Cu_2O, which has an essentially full 3d shell (Ghijsen, *et al.*, 1988). The former investigators found the origin of the potential p - type transparent semiconducting property of Cu_2O with indirect energy band gap 1.5 eV and 3% concentration of Cu vacancy. The DFT + U description of a small

concentration of Cu vacancies is delocalized hole states with hole effective masses consistent (Nolan & Elliott, 2006). By applying both the functional LDA + U and the hybrid functional HSE06, the structural stability and electronic band structure of the bulk Cu_2O were observed, and also the semiconducting behavior as well as the direct energy band gap were found, which are in good agreement with the experiment value (Heinemann, *et al.,* 2013). The combined experimental and theoretical methods, the electronic structure, energy band gap, valence, and conduction band structures of Cu_2O were found by the help of optical absorption, photoemission, and electron energy loss spectroscopy (EELS), and compared with theoretical result from many - body GW calculation which provides a consistent electronic structure picture across band insulators (Wang *et al*., 2016).

In the other, self-consistent electronic structure and calculation of bulk CuO were observed by theoretical and experimental methods. The experimental x - ray and ultraviolet photoemission spectra (UPS) are good agreement with theoretically calculated electron spectra on account of the densities of occupied and unoccupied states of CuO by using the ASW method. Experimently, the bulk form of CuO with band gap 1.4 eV, is an antiferromagnetic semiconductor, whereas DFT calculation predict it as a non-magnetic metal (Ghijsen, *et al.,*1988). The different morphologies and characters of CuO were investigated and were explored through a facile hydrothermal process in the presence of sodium citrate (SC). The different CuO samples were founed like 1D nanorod, 2D flakelike and 3D branchlike with bandgap energies 2.36 eV, 1.60 eV, and 1.40 eV, respectively larger than Eg = 1.2 eV of bulk CuO (Xiao, *et al.,* 2007). The structural stability and electronic band structures of CuO were evaluated by using several approaches under DFT. The researchers used both the LDA + U and HSE06 hybrid functionals and investigated that CuO is the semiconductor of an indirect energy band gap 1 eV approximately (Heinemann, *et al.,* 2013). The growth mechanisms and fundamental properties together with applications of CuO presented a comprehensive review of its different research activities and synthesis techniques for producing different morphologies like 0D (nanoparticles), 1D (nanowire, nanorod, nanotube), 2D (nanodisc, nanoplate, nanoleave, nanosheet), and 3D (hierarchical nanostructures). The systemically and summarizing of the wide ranges of promising applications of CuO introduce its both physical and chemical properties. (Zhang Q. *et al.* 2014). The some peculiar properties of the nanostructures

of CuO which do not match with other transition metal oxides were observed and their potential applications were demonstrated (Tran & Nguyen, 2014). The electronic structures of CuO thin film were investigated through experimental and theoretical processes. Experimently, the energy band gap, valence and conduction band gap were determined by employing the optical absorption, photoemission, and EELSs and then compared with the theoretical results obtained from many - body GW calculations. The additional onsite potential for the Cu - d orbital energy, the indirect band gap (1.24 eV), and the direct band gap (1.46 eV) of bulk CuO were obtained (Wang, *et al.,* 2016). The electronic transport coefficient of the bulk CuO was investigated with the help of hybrid density functional theory. Both DFT and local Gaussian - type basis sets were used to find the band structures of both nonmagnetic and magnetic p - type metal oxides without empirical corrections. Also, the wave function and transport property were found by using the crystal code. This computational calculation is in good agreement with the experimental value of the Seebeck coefficient (Linnera J. *et al.,* 2018).

In short, above studies motivate and support us to work on the zero to higher dimensional structures to explore the structural, electronic and magnetic properties and possible use of these system in relevant fields. The research gaps need to be explored and have been already discussed in chapter 1. The method which we follow to calculate the related properties of materials is explain more detail in chapter 3.

CHAPTER 3

3. MATERIALS AND METHODS

3.1 Theory

3.1.1 General Consideration

Many - body problems mainly deal with two important points: Firstly, many electrons, many atoms, many molecules, and Secondly, the interaction among them with each other. The problems dealing with the effect of interacting behaviour among the number of bodies are said to be many - body problems. These problems are derived from the following facts:

(i) the real physical systems are composed of a set of interacting particles as nucleons in a nucleus interacting with nuclear forces, electrons in an atom, or metal interacting by Coulomb forces.

(ii) the calculation of physical properties of such systems as the energy levels of the atom, or magnetic susceptibility of the metal, interactions between particles play a very important role. So, the many - body problems deal fairly with general methods applicable to all many - body systems (Rodberg, 1957).

In condensed matter, the electric field that is generated by the atomic nuclei and their mutual interactions determines the motion of the electrons. The collection of arranged atomic nuclei identifies the symmetry and classification of electronic states. The strengths of the interactions among the electrons and the atomic nuclei distinguish valence and core electrons. The system of atoms, molecules, or clusters consists of α atomic nuclei and i electrons. M_α, Z_α, and R_α are the mass, charge, and position of atomic nuclei. m_e, e^-, and r_i are mass, charge, and position of ith electron respectively. Let $\mathbf{s_i}$ and σ are spin variables and Pauli spin matrix respectively (Bechstedt, 2014). They are expressed as:

$$s_i = \frac{\hbar}{2}\sigma \tag{3.1}$$

$$\sigma_x = \begin{pmatrix} 0 & 1 \\ 1 & 0 \end{pmatrix} \tag{3.2}$$

$$\sigma_y = \begin{pmatrix} 0 & -i \\ i & 0 \end{pmatrix} \quad (3.3)$$

and, $$\sigma_z = \begin{pmatrix} 1 & 0 \\ 0 & -1 \end{pmatrix} \quad (3.4)$$

Where $\sigma_x, \sigma_y,$ and σ_z are rectangular components of σ.

The particles possess momentum operators,

$$P_\alpha = -i\hbar\nabla_{R_\alpha}(\text{nucleus}) \quad (3.5)$$

and, $$P_i = -i\hbar\nabla_{r_i}(\text{electron}) \quad (3.6)$$

Where R_α and r_i are canonical position operators of αth nucleus and ith electron.

A system, in which all properties as structural, electronic, magnetic, transport, optical, thermal, mechanical, etc. are studied with neglecting the spins of nuclei, represents a quantum mechanical many - body system.

3.1.2 Schrodinger wave equation

The wave function (Ψ) or the probability amplitude is the amplitude of the wave associated with the microbody. It is the mathematical tool based on the first - principles study and applied in quantum mechanics for describing a physical system of electrons and nuclei of atoms as shown in Figure 7.

The first-principles study is free of adjustable parameters which treat electrons. The cost of the calculation limits system size and simulation time and does not depend on secondary data.

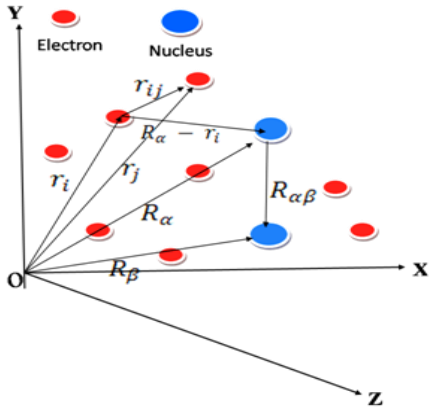

Figure 7: The system of electrons and nuclei of atoms

In 1926, Erwin Schrodinger proposed a wave equation used in quantum mechanics for the wave function of a particle and allowed the creation of a complete model for the atom, known as the Schrodinger wave equation. The solution of the time-independent and non - relativistic Schrodinger wave equation (Levada, *et al*., 2018) helps to find the position, momentum, and energy of the microsystem. The Schrodinger wave equation is expressed as:

$$\hat{H}_{n,e}\Psi_{n,e}(\{R_\alpha\},\{r_i\}) = E_{n,e}\,\Psi_{n,e}(\{R_\alpha\},\{r_i\}) \tag{3.7}$$

Where,

$$\hat{H}_{n,e} = \hat{T}_e + \hat{T}_n + \hat{V}_{n,n} + \hat{V}_{n,e} + \hat{V}_{e,e} \tag{3.8}$$

$$\hat{T}_e = -\sum_{i=1}^{M} \frac{\hbar^2}{2m_e}\nabla_i^2\,, \tag{3.9}$$

$$\hat{T}_n = -\sum_{\alpha=1}^{N} \frac{\hbar^2}{2M_n}\nabla_\alpha^2, \tag{3.10}$$

$$\hat{V}_{n,n} = \sum_{\alpha=1}^{N}\sum_{\beta>\alpha}^{N} \frac{Z_\alpha Z_\beta e^2}{R_{\alpha\beta}} \tag{3.11}$$

$$\hat{V}_{n,e} = -\sum_{i=1}^{M}\sum_{\alpha=1}^{N} \frac{Z_\alpha e^2}{|r_i - R_\alpha|} \tag{3.12}$$

and, $$\hat{V}_{e,e} = \sum_{i=1}^{M}\sum_{j>i}^{M} \frac{e^2}{r_{ij}} \tag{3.13}$$

$$\therefore \hat{H} = -\sum_{i=1}^{M} \frac{\hbar^2}{2m_e}\nabla_i^2 - \sum_{\alpha=1}^{N} \frac{\hbar^2}{2M_\alpha}\nabla_\alpha^2 + \sum_{\alpha=1}^{N}\sum_{\beta>\alpha}^{N} \frac{Z_\alpha Z_\beta e^2}{R_{\alpha\beta}} - \sum_{i=1}^{M}\sum_{\alpha=1}^{N} \frac{Z_\alpha e^2}{|r_i - R_\alpha|} + \sum_{i=1}^{M}\sum_{j>i}^{M} \frac{e^2}{r_{ij}} \tag{3.14}$$

Where, α and β represent numbers of N nuclei, and i and j represent numbers of M electrons in the system. $\hat{T}_e$ and $\hat{T}_n$ are the kinetic energies of electrons and nuclei.

$\hat{H}$ = Hamiltonian's energy operator

$\hat{V}_{e,e}$, = repulsive potential between electrons

$\hat{V}_{n,e}$= attractive potential between nuclei and electrons

and, $\hat{V}_{n,n}$ = repulsive potential between nuclei

The Hamiltonian consists of the sum of two kinetic energies; of electrons and nuclei and three of the potential energies; of electrons, nuclei, and interaction between both electrons and nuclei.

The last three potentials are, approximately, explained by Coulom potentials.

$$V(r_{ij}) = \frac{q}{4\pi\varepsilon_0|r_{ij}|} \tag{3.15}$$

Here, the permittivity of vacuum (ε_0) = 8.854188 × 10^{-12} As / Vm or farad/meter in SI units.

After knowing the value of V(r), the Schrödinger equation of many-body systems with a Hamiltonian operator predicting all types of properties can be solved.

In the theoretical method, certain approximations make it easy to solve the physical problems of a system. Atoms, molecules, clusters, or solids are systems composed of mutually interacting electrons and nuclei to one another. In the nuclei, each proton and each neutron are individually 1816 more massive than each electron. As a result, the nuclei have the least motion than that electrons and only show the time-averaged electronic potential.

Max Born and J. Robert Oppenheimer decouple and study the motion of electrons and nuclei in which the kinetic energy of nuclei is neglected as a first approximation in molecular physics. According to a crystallographic study, the atoms oscillate slightly and time - independently of their equilibrium positions. As a result, the total potential of nuclei remains constant which is neglected for the second approximation calculation (Born & Oppenheimer, 1927).

In mathematical terms, it counts the wave function of a molecule to be taken into electronic and nuclear components.

$$\psi_{total} = \psi_{electronic} \times \psi_{nuclear} \tag{3.16}$$

In the comparison of motion, the electron moves faster than the nucleus in its field. The motion of nuclei is assumed zero (i.e. zero kinetic energy) and the potential energy is taken to approximately constant. After neglecting K. E. and P. E. of nuclei, the electronic Hamiltonian becomes:

$$\hat{H}_{electronic} = \hat{T}_e + \hat{V}_{n,e} + \hat{V}_{e,e} = -\sum_{i=j}^{M} \frac{\hbar^2}{2m_e} \nabla_i^2 - \sum_{i=1}^{M} \sum_{\alpha=1}^{N} \frac{Z_\alpha e^2}{|r_i - R_\alpha|} + \sum_{i=1}^{M} \sum_{j>i}^{M} \frac{e^2}{r_{ij}}$$

(3.17)

From equations (3.8) and (3.17), the Hamiltonian-Schrodinger equation is expressed as

$$(\hat{H}_{electronic})\Psi_{n,e} = (\hat{T}_e + \hat{V}_{n,e} + \hat{V}_{e,e})\Psi_{n,e} \quad (3.18)$$

The solution of the equation (3.18) in the terms of electronic energy and electronic wave function becomes,

$$\hat{H}_{electronic}\Psi_{electronic} = E_{total}\Psi_{electronic} \quad (3.19)$$

Where,

$$E_{total} = E_{electrons} + E_{nuclei} \quad (3.20)$$

$E_{nuclei} = \sum_{\alpha=1}^{N} \sum_{\beta>\alpha}^{N} \frac{Z_\alpha Z_\beta e^2}{R_{\alpha\beta}}$ = total energy of constant nuclear repulsion (3.21)

$E_{electronic} = -\sum_{i=j}^{M} \frac{\hbar^2}{2m_e} \nabla_i^2$ = total energy of electrons (3.22)

Applying the Hamiltonian operator for solving the Schrodinger equations of a helium atom, the quantum states of electronic motion of one or two electrons can be obtained easily however not for more than two distinct electrons interact. The state of electronic motion is not solved analytically for the systems consist of three or more distinct particles. For this, the Hartree approximation is needed to apply for the solution of the Schrodinger equation of the system of large numbers of microbodies as atoms, molecules, etc.

3.1.3 Hartree Approximation

In 1928 AD, Hartree proposed an approximation to solve the equations related to the many - body problem consisting of multiple - electrons in the atom based on fundamental physical principles, known as Hartree Approximation (Echenique & Alonso, 2007).

According to Hartree, the electronic motion of a helium atom as shown in Figure 8 with Hamiltonian operator is expressed as follows

$$\hat{H} = -\frac{\hbar^2 \nabla_1^2}{2m_e} - \frac{\hbar^2 \nabla_2^2}{2m_e} + V_{ne}(r_1) + V_{ne}(r_2) + V_{ee}(r_1.r_2) \quad (3.23)$$

Where, $\hat{H}$ = Hamiltonian operator, r_n = the position vector of nth electron

∇_n = the gradient vector operator for nth electron, $-\frac{\hbar^2\nabla^2}{2m_e}$ = kinetic energy operator

$V_{ne}(r)$ = nuclear - electron electrostatic interaction potential

$V_{ee}(r_1.r_2)$ = two - electrons electrostatic interaction potential

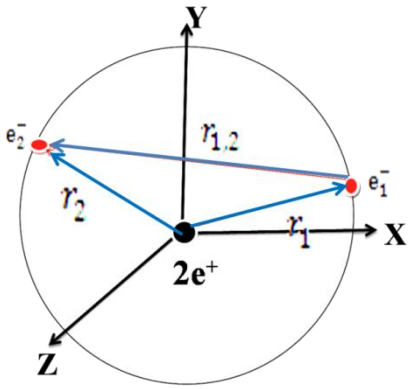

Figure 8: Electrons in a Helium atom

In Figure 8, two electrons of individual charge e^- and position vectors r_1 and r_2 move around the nucleus of charge $2e^+$ at the center under electrostatic interaction potentials V_{ne} and V_{ee} with kinetic energy $-\frac{\hbar^2\nabla^2}{2m_e}$ each.

Where, e, $\hbar$, $\frac{1}{4\pi\epsilon_0}$ are electron charge, reduced Plank constant and Coulomb force constant respectively.

According to Hartree, each electron moves in the average of interaction electrostatic potential as an effective potential (V_{eff}) with surrounding electrons. The Hamiltonian operator is divided into two parts for two electrons of the Helium atom in this approximation as below:

$$\therefore \hat{H} = \left[-\frac{\hbar^2\nabla_1^2}{2m_e} + V_{ne}(r_1) + V_{eff}(r_1)\right] + \left[-\frac{\hbar^2\nabla_2^2}{2m_e} + V_{ne}(r_2) + V_{eff}(r_2)\right]$$

$$\hat{H} = \hat{h}(r_1) + \hat{h}(r_2) \qquad (3.24)$$

Where, $\hat{h}(r_1)$ and $\hat{h}(r_2)$ are Hamiltonian operators for two electrons e_1^- and e_2^- respectively.

Generally, in the Hamiltonian operator, the wavefunction $\psi(r_1, r_2, \dots, r_n)$ is the product of the electronic motion wavefunctions or orbital wavefunctions $\phi_1(r_1), \phi_2(r_2), \dots, \dots, \phi_n(r_n)$ of n electrons $e_1^-, e_2^-, \dots, \dots, e_n^-$ respectively.

Let an electron system is approximately expressed by the status of one group of independent electrons. The wavefunction of this system is expressed as:

$$\therefore \psi(r_1, r_2, \dots, \dots, r_n) = \phi_1(r_1)\phi_2(r_2) \dots \dots \dots \phi_n(r_n) \quad (3.25)$$

The total energy becomes in the Hamiltonian form,

$$\therefore \hat{H}\psi(r_1, r_2, \dots, \dots, r_n) = E\psi(r_1, r_2, \dots, \dots, r_n) \quad (3.26)$$

In this case, the expectation value (E) is given as

$$\therefore E = \frac{\int d^3r_1 d^3r_2 \psi^*(r_1, r_2)\hat{H}\psi(r_1, r_2)}{\int d^3r_1 d^3r_2 \psi^*(r_1, r_2)\psi(r_1, r_2)} = \frac{\sum_{i=1}^{2} \int d^3r_i \phi_i^*(r_i)\hat{h}(r_i)\phi_i(r_i)}{\sum_{i=1}^{2} \int d^3r_i \phi_i^*(r_i)\phi_i(r_i)} \quad (3.27)$$

According to variational method, the Schrödinger equation of ith electron wavefunction $\{\phi_i\}$, is represented as:

$$\therefore \hat{h}_i \phi_i(r_i) = \epsilon_i \phi_i(r_i) \quad (3.28)$$

Where, ϵ_i = the eigenenergy of ith moving electron,

ϕ_i = ith electron wave function or orbital wave function

The total eigen energy (ϵ) is equal to the sum of the orbital energies of electrons in the different motions.

For helium atom,

$$\hat{H}\psi = (\epsilon_1 + \epsilon_2)\phi_1\phi_2 = \epsilon\psi \quad (3.29)$$

It is the Hartree method.

From equation (3.26), the effective potential for orbital wavefunction is derived as

$$V_{eff}(r_i) = \sum_j \int d^3r_j \frac{|\phi_j(r_j)|^2}{|r_i - r_j|} \quad (3.30)$$

Here, the Hartree method is suitable for the theory using the effective potential of a single atom in which the motion of each electron is free from this effective potential. Hartree approximation does not consider the antisymmetric orbital wave and does not calculate the exchange-correlation potential. So, Hartree - Fock approximation is needed for further study of the many-body problem in solid - states and molecular physics.

3.1.4 Hartree - Fock Approximation

In molecular theory, the approximate solution of Schrodinger wave equations through the slater determinant made up of one spin - orbital per electron is Hartree - Fock molecular theory. Fock used the slater determinant to Hartree method for solving the

many - body problem consisting of more distinct particles as electrons. According to H - F Approximation (Echenique & Alonso, 2007), the closed - shell systems consist of N sub - orbitals containing two electrons each defined as functions of the spatial and spin coordinates. The electronic (orbital) motion always has antisymmetric orbital wavefunction and can be expressed in Slater determinant as follows:

$$\phi(r_1, \dots, r_i, \dots, r_j, \dots, r_N) = -\phi(r_1, \dots, r_j, \dots, r_i, \dots, r_N) \tag{3.31}$$

and

$$\psi_{(r_1, r_2, \dots\dots, r_N)} = \frac{1}{\sqrt{N!}} \begin{vmatrix} \phi_1(r_1) & \phi_1(r_2) & \dots\dots & \dots\dots & \phi_1(r_N) \\ \phi_2(r_1) & \phi_2(r_2) & \dots\dots & \dots\dots & \phi_2(r_N) \\ \dots\dots & \dots\dots & \dots\dots & \dots\dots & \dots\dots \\ \dots\dots & \dots\dots & \dots\dots & \dots\dots & \dots\dots \\ \phi_N(r_1) & \phi_N(r_2) & \dots\dots & \dots\dots & \phi_N(r_N) \end{vmatrix} \tag{3.32}$$

where $\psi\{r\} = \psi\{r_1, r_2 \dots\dots, r_n\}$, different spin orbitals in columns and different electrons in rows

The wave function of the system can be expressed as

$$\therefore \psi(r_1, r_2, \dots, \dots, r_n) = \phi_1(r_1)\phi_2(r_2) \dots\dots\dots \phi_n(r_n) \tag{3.33}$$

The total energy will be of the form,

$$\therefore H\psi(r_1, r_2, \dots, \dots, r_n) = E\, \phi_1(r_1)\phi_2(r_2) \dots\dots\dots \phi_n(r_n) \tag{3.34}$$

$$\begin{aligned} E &= \langle \phi^* | \hat{H} | \phi \rangle \\ &= \int d^3r_1 \int d^3r_2 \dots\dots \int d^3r_n \, (\phi_1{}^* \phi_2{}^* \dots\dots \phi_n{}^* H\, \phi_1 \phi_2 \dots\dots \phi_n) \\ &= \sum_{i=1}^{n} \int d^3r \phi_i^*(r) \left[-\frac{\hbar^2 \nabla_i^2}{2m_e} + V_{ext}(r) \right] \phi_i(r) + \\ &\quad \sum_{i,i \neq j} \int d^3(r) \int d^3(r') \phi_i^*(r) \phi_i(r) \frac{e^2}{|r - r'|} \phi_j^*(r') \phi_j(r') \end{aligned} \tag{3.35}$$

The orbital or electron wave function $\phi_i(r)$ can be obtained by the minimization of the total energy subjected to the normalization condition,

$$I = \int \phi_i^* \phi_i \, dr = 1 \tag{3.36}$$

By variation method, the orbital wave function $\phi_i(r)$ and total energy E satisfy,

$$\delta \frac{\langle \phi^* | H | \phi \rangle}{\langle \phi^* | \phi \rangle} = 0 \tag{3.37}$$

$$\delta(E - \lambda I) = 0 \tag{3.38}$$

$$\int d^3(r)\,\delta\phi_i^*(r)\left\{\begin{matrix}\left(-\frac{\hbar^2\nabla_i^2}{2m_e}+V_{ext}\right)\phi_i+\\ \left(\int d^3r'\frac{e^2}{(|r-r'|)}\right)\sum_{i\neq j}\phi_i^*(r')\,\phi_i(r')\phi_i-\lambda\phi_i\end{matrix}\right\}$$

$$+\int d^3(r)\,\delta\phi_i(r)\left\{\left(-\frac{\hbar^2\nabla_i^2}{2m_e}+V_{ext}\right)\phi_i^*+\left(\int d^3r'\frac{e^2}{(|r-r'|)}\right)\sum_{i\neq j}\phi_j^*(r')\,\phi_i^*(r')\phi_i^*-\lambda\phi_i^*\right\}=0$$

(3.39)

From equation (3.39), We can get Hamiltonian form of $\phi_i(r)$

$$\because\left(-\frac{\hbar^2\nabla_i^2}{2m_e}+V_{ext}\right)\phi_i+\left(\int d^3r'\frac{e^2}{(|r-r'|)}\right)\sum_{i\neq j}\phi_i^*(r')\,\phi_i(r')\phi_i-\lambda\phi_i=0$$

$$\left(-\frac{\hbar^2\nabla_i^2}{2m_e}+V_{ext}\right)\phi_i+\left(\int d^3r'\frac{e^2}{(|r-r'|)}\right)\sum_{i\neq j}\phi_i^*(r')\,\phi_i(r')\phi_i=\lambda\phi_i$$

$$\left(-\frac{\hbar^2\nabla_i^2}{2m_e}+V_{ext}+V_{sc}\right)\phi_i=\epsilon_i\phi_i\ (i=1,2,\ldots\ldots n,\ \lambda\to\epsilon_i)$$

$$\hat{F}\phi_i=\epsilon_i\phi_i \qquad (3.40)$$

It is Hartree – Fock equation and $\hat{F}$ is the Fock operator. It can be solved self - consistently.

Where, $V_{sc}=V_H$

$$=\left(\int d^3r'\frac{e^2}{(|r-r'|)}\right)\sum_{i\neq j}\phi_i^*(r')\,\phi_i(r')$$

$$=\int d^3r'\frac{e^2}{(|r-r'|)}n_i(r')n_i(r')$$

$$=\sum_{j\neq i}\left|\phi_j^*(r')\right|^2 \qquad (3.41)$$

Now, Hamiltonian in the form of orbital or electron wavefunction $\phi_i(r)$ can be expressed as,

$$\left[-\frac{\hbar^2\nabla_i^2}{2m_e}+V_{ext}\right]+\int d^3r'\frac{e^2}{(|r-r'|)}\sum_{j\neq i}\phi_j^*(r')\phi_j(r')\,\phi_i$$

$$-\sum_{j\neq i}\phi_j^*(r')\phi_i(r')\phi_j(r)\,\delta_{s_i s_j}=\epsilon_i\phi_i(r)$$

$$\left[-\frac{\hbar^2\nabla_i^2}{2m_e}+V_{ext}+V_H+V_x\right]\phi_i(r)=\epsilon_i\phi_i(r)$$

$$\left[-\frac{\hbar^2\nabla_i^2}{2m_e} + V_{ext} + V_{sc}\right]\phi_i(r) = \epsilon_i\phi_i(r) \tag{3.42}$$

Where,

$$V_{sc} = V_H + V_x \tag{3.43}$$

$$V_H = \int d^3r' \frac{e^2}{(|r-r'|)}\sum_{j\neq i}\phi_j^*(r')\phi_j(r')\,\phi_i \tag{3.44}$$

and the exchange potential can be expressed as

$$V_x = -\sum_{j\neq i}\phi_j^*(r')\phi_i(r')\phi_j(r)\,\delta_{s_i s_j} \tag{3.45}$$

It is shown that the total electron energy is not equal to the summation of two orbitals energies due to the double - counting of electron - electron interaction. The total energy is obtained by the addition of nucleus - nucleus repulsion energy to total electron energy.

The total energy is expressed as:

$$E_{total} = E + \sum_{\alpha\neq\beta}\frac{Z_\alpha Z_\beta}{R_{\alpha\beta}} \tag{3.46}$$

The self - consistent field method can solve the nonlinear Hartree – Fock equation. V_x is non - local and related to the interaction between all electrons in the system. Hence, it is difficult to calculate in practice. The Hartree - Fock approach for many - body systems as molecules is very difficult to solve even computationally. Further, H - F calculation also can not consider electron correlation. Due to the high computational cost for calculation, it is restricted to small systems. To remove the above descripancies, we need to go further advanced approach. Here, in this work we follow "Density Functional Theory (DFT)" where density plays a main role for the electronic calculation applicable for every level of calculations. The brief description of DFT is given in following section.

3.1.5 Density Functional Theory (DFT)

In the early 20th century, Thomas - Fermi, and Hartree - Fock's methods were more in practice than Density Functional Theory (DFT). In the previous chapter, we are familiar with the way to deal with the electronic Schrodinger equation approximately through Hartree and Hartree - Fock methods on the base of the many - body wave

functions. The wave functions determine the energy as well as all related physical properties like structural, electronic, magnetic, electrical, optical, and others. But it is complex because it depends on 3N spatial variables together with the spin variables. Where N is the electronic number in the system. The wave function is not used to describe the materials but the electron density is used. So, the density functional theory (Burke, 2012) is required to investigate the electronic structure of many - body systems as atoms, molecules, and the condensed phases at the ground state. DFT can describe the ground state properties and the particle's applications based on approximations including exchange - correlation potential (E_{XC}) (Perdew, *et al*., 1996 - I). Where E_{XC} expresses the effect of the Pauli exclusion principle and the Coulomb potential without counting the pure electrostatic interaction of the electrons.

DFT contains mainly two theories as : (i) the nonrelativistic theory and (ii) the relativistic theory. The nonrelativistic theory logically discusses the central ideas and constructions of DFT with related mathematical aspects and the relativistic theory discusses the realistic quantum field theory. The density functional theory also consists of several versions: (i) theory with particle densities and spin - independent external potentials. (ii) theory with spin - up and spin - down densities and external potentials. (iii) theory with spin - density matrices and general doubly indexed spin - dependent potentials.

Hence, it is concluded that the alternate ab-initio approach based Hartree - Fock method for dealing with time - independent and nonrelativistic Schrodinger equation $H|\psi\rangle = E|\psi\rangle$ of individual electron wavefunctions in a system is a density functional theory (DFT). The DFT overcomes this problem through the terms of the density $\rho(r)$in Hohenberg - Kohn (H - K) and the orbital function $\phi_i(r)$ in Kohn - Sham (K - S) formulations. (Bretonnet, 2017).

3.1.5.1 Thomas Fermi (TF) Theory

Thomas - Fermi (TF) theory (Jerome, *et al*., 1987) based on electron density distribution was used to roughly compute electronic energy of only interacting electrons moving in an external potential but not predicated on the chemical binding. TF theory established an implicit relation between the external potential $V_{ext}(r)$ and the density distribution $\rho(r)$ as follows:

$$\rho(r) = \gamma[\mu - V_{eff}(r)]^{\frac{3}{2}} \quad (3.47)$$

Where, $\gamma = \frac{1}{3\pi^2}\left(\frac{2m}{\hbar^2}\right)^{\frac{3}{2}}$ and μ = chemical potential

The equation (3.47) is based on the physical equation $\rho = \gamma\,[\mu - V]^{\frac{3}{2}}$ for the density of a uniform, non - interacting, degenerate electrons gas at constant external pressure.

$$V_{eff}(r) = V_{ext}(r) + \int \frac{\rho(r')}{|r - r'|} dr' \quad (3.48)$$

Where $\int \frac{\rho(r')}{|r - r'|} dr'$ = electronic potential or Hartree potential V_H

TF theory was a rough solution of the many - electrons Schrodinger equation. It was unable to predicate their relation and the role of groundstate density $\rho(r)$ for the determination of the system (Rocco, *et al*., 2016).

3.1.5.2 The Hohenberg - Kohn (H - K) Theorem

Two basic theoretical results were discovered by P. Hohenberg and W. Kohn (Hohenberg & Kohn, 1964) "Inhomogeneous Electron Gas."

Theorem (I): The potential V(r) or the total energy E(r) is a unique function of the electron density $\rho(r)$.

Thus, $V(r) \Rightarrow \psi_i(r) \Rightarrow \rho(r) \Rightarrow V(r)$ (3.49)

Where, $\psi_i(r)$ = the non - degenerate ith wave function

$$\rho(r) = \sum_1^N |\psi(r)|^2 \quad (3.50)$$

We can determine $E(\rho)$, is variational. In the ground state, the total energy is minimized, $E(\rho_{GS})$ can be obtained in a system by using electron density.

Theorem (II): The total energy, $E(\rho)$ at the ground states is always less than that energy at the other states.

Thus, $E(\rho) \geq E(\rho_{GS})$ (3.51)

Hohenberg - Kohn theorem can be represented as shown in Figure 9

$$\begin{array}{ccc} V_{ext}(r) & \overset{HK}{\Leftarrow} & \rho_{GS}(r) \\ \downarrow & & \uparrow \\ \psi_i(r) & \rightarrow & \psi_{GS}(r) \end{array}$$

Figure 9: Hohenberg - Kohn theorem

Proof:

Let ψ_0 be a non - degenerate ground state (eigen function) of N electrons in the potential $V_{ext}(r)$ and its corresponding to the non - degenerate density $\rho_0(r)$ and the non - degenerate ground state energy E_0.

Then:

$$E_0 = \langle\psi_0|H|\psi_0\rangle = \int V_{ext}(r)\,\rho_0(r)dr + \langle\psi_0|T+U|\psi_0\rangle \quad (3.52)$$

Where, H = the total Hamiltonian corresponding to V_{ext}

V_{ext} = a multiplicative operator concerning ψ_0

T = kinetic energy operator and

U = interaction energy operator

Now, let us consider $V'_{ext}(r)$ to be a second external potential $\neq V_r + \text{constant}$ and ψ'_0 to be the corresponding ground state or eigen function $\neq e^{i\theta}\psi_0$, which gives rise to the same non - degenerate density $\rho_0(r)$. Then,

$$E'_0 = \int V'_{ext}(r)\,\rho_0(r)dr + \langle\psi_0{}'|T+U|\psi_0{}'\rangle \quad (3.53)$$

As $\psi_0$is non - degenerate, the variational principle (Rayleigh - Ritz minimal principle) is expressed as the following inequality:

$$E_0 < \langle\psi'_0|H|\psi'_0\rangle = \int V_{ext}(r)\,\rho_0(r)dr + \langle\psi'_0|(T+U)\psi'_0\rangle$$

$$= E'_0 + \int[V_{ext}(r) - V'_{ext}(r)]\rho_0(r)dr \quad (3.54)$$

Similarly,

$$E'_0 \leq \langle\psi_0|H'|\psi_0\rangle = E_0 + \int[V'_{ext}(r) - V_{ext}(r)]\rho_0(r)dr \quad (3.55)$$

Where ≤ is used for a simply ground state ψ_0' not for non - degeneracy. The sum of equations 3.52 and 3.53 leads to the contradiction:

$$E_0 + E_0' < E_0 + E_0' \tag{3.56}$$

Equation 3.55 shows the potential $V_{ext}'(r)$ having the same $\rho_0(r)$ but not equal to $V_{ext}(r) + \text{constant}$, is incorrect.

Here, $\rho_0(r)$ finds out N and $V_{ext}(r)$ for the electronic system. So, $\rho_0(r)$, indirectly, finds all properties of the system derived from the solution of the Schrodinger equation.

$$E_0[\rho_0(\vec{r})] = T[\rho_0(\vec{r})] + V_{ee}[\rho_0(\vec{r})] + \int d\vec{r}\, V_{ext}(\vec{r})\rho_0(\vec{r})dr \tag{3.57}$$

3.1.5.3 The Self - Consistent Kohn - Sham Theorem

Kohan & Sham (1965) proposed a single particle orbital function (ϕ) to make the K - S equation for the treatment of the kinetic and interaction energy terms.

$$V_{KS}(r) \Leftrightarrow \rho(r) \Leftrightarrow \psi \Leftrightarrow \phi_{i=1..N} \Leftrightarrow V_{KS}(r) \tag{3.58}$$

Kohn - Sham theorem can be represented as shown in Figure 10.

$$\begin{array}{ccc} \rho_{GS}(r) & \overset{KS_{GS}}{\Longrightarrow} & V_{KS}(r) \\ \uparrow & & \downarrow \\ \psi_{GS}(r) & \leftarrow & \varphi_{i=1,\ldots,I} \end{array}$$

Figure 10: Kohn - Sham theorem

The total energy consists of following terms:

$$E(\rho) = T(\rho) + U(\rho) + V(\rho) = T_s\{\varphi_i(\rho)\} + U_H(\rho) + E_{xc}(\rho) + V(\rho) \tag{3.59}$$

The kinetic energy consists of the K. E. of non - interacting particles and remaining particles of density (ρ):

$$T(\rho) = T_s(\rho) + T_c(\rho) \tag{3.60}$$

Here, s and c denote single - particle and correlation respectively.

U and U_H are interaction energy and classical electrostatic interaction or Hartree energy respectively.

Here, E_{xc} is a correction of the approximation raised by exchange (X) and correlation (C) effects.

Hence,

E_{XC} = correction K - S approximation

$$= (T - T_S) + (U - U_H) = T_C + (U - U_H) \quad (3.61)$$

$E_{XC} = E_X$ {exchange energy due to Pauili exclusion principle (Fan & Malozovski, 2023) antisymmetry} + E_C (correlation energy)

The corelation K. E. (Tc) of non-interacting particles in term of wavefunctions:

$$T_s(\rho) = -\frac{\hbar^2}{2m}\sum_i^N \int \phi_i^*(r)\nabla^2\phi_i(r)d^3r \quad (3.62)$$

Where, $T_s(\rho)$ = the expectation value of the K. E. operator $\hat{T}$ with the Slater determinant arising from the density ρ. A determinate wavefunction must describe all consequences of antisymmetrization (i.e. exchange energy) and

$T_C = T - T_S$ = the pure correlation effect. (Kohan & Sham, 1965) (3.63)

Hartree energy (U_H) is the classical electrostatic interaction energy that gives the mean-field result. U_H is expressed in term of density as follow:

$$U_H = \frac{q^2}{2}\int d^3r \int d^3r' \frac{\rho(r)\rho(r')}{|r-r'|} \quad (3.64)$$

The exchange energy term (E_X) arises due to interaction potential which may be expressed in terms of single-particle orbitals as in equation (3.60).

$$E_x\left[\{\phi_j(\rho)\}\right] = \frac{q^2}{2}\int d^3r \int d^3r' \frac{\phi_j^*(r)\phi_k^*(r')\phi_j(r')\phi_k(r)}{|r-r'|} \quad (3.65)$$

The energy of the exchanging particle j is located at r with other particle k located at r'. The electrons with like spins tend to avoid each other and electrons with unlike

spins tend to attract each other which may produce an exchange hole. It also helps to correct the Hartree energy or potential term $U_{H.}$

The difference between full ground - state energies obtained from the correct many - body wavefunction and the Hartree - Fock or Kohn - Sham Slater determinant may give the correlation energy (E_C). It is raised due to the mutual avoidance of the interaction electrons which are added to the obtained lowering energy in a real system.

The interaction energy operator ($\hat{U}$) may be expressed in two terms the density operators $\hat{\rho}$ and the delta function subtracts out the interaction of a charge with itself.

$$\hat{U} = \sum_{i<j} \frac{q^2}{|r-r'|} = \frac{q^2}{2} \int d^3r \int d^3r' \frac{\hat{\rho}(r)\hat{\rho}(r') - \rho(r)\delta(r-r')}{|r-r'|} \tag{3.66}$$

The E_C is the energy lowering that is created due to quantum fluctuations. There may be two causes for the quantum fluctuations (i) The electrons with unlike spins try to coordinate their movement for minimizing their Colombian energy. (ii) The change in magnitude of K. E. due to the difference between non - interacting and interacting kinetic energies.

The total energy at the groundstate is found through the minimization of total energy (E) with respect to the density (ρ),

$$\frac{\delta E[\rho]}{\delta \rho(r)} = 0 \tag{3.67}$$

$$\frac{\delta E[\rho]}{\delta \rho(r)} = \frac{\delta T_s[\rho]}{\delta \rho(r)} + \frac{\delta V[\rho]}{\delta \rho(r)} + \frac{\delta U_H[\rho]}{\delta \rho(r)} + \frac{\delta E_{XC}[\rho]}{\delta \rho(r)} = \frac{\delta T_s[\rho]}{\delta \rho(r)} + V(r) + V_H(r) + V_{xc} = 0 \tag{3.68}$$

Where, $\frac{\delta V[\rho]}{\delta \rho(r)} = V(r)$ (3.69)

$V(r)$ is the external potential produced by the fixed nuclei, the lattice, or a truly external field or all.

$\frac{\delta U_H}{\delta \rho}$ and $\frac{E_{XC}}{\delta \rho}$ are Hartree potential and exchange - correlation potential respectively.

For this system, the minimization condition is:

$$\frac{\delta E_s[\rho]}{\delta \rho(r)} = \frac{\delta T_s[\rho]}{\delta \rho(r)} + \frac{\delta V_s[\rho]}{\delta \rho(r)} = \frac{\delta T_s[\rho]}{\delta \rho(r)} + v_s(r) = 0 \tag{3.70}$$

The density - solving Euler equation (3.70) is $\rho_s(r)$.

Comparing equations (3.69) and (3.70), both minimized equations have

the same solutions as

$$\rho_s(r) = \rho(r), \text{ if } V_s(r) = V(r) + V_H(r) + V_{XC}(r) \quad (3.71)$$

Where, $V_{XC}(r) = V_X(r) + V_C(r)$

Hence, It can be calculated that the density of an interacting many - body system in potential V(r) is the same as the equation of a non - interacting single - body system in potential V(r).

$$\left[-\frac{\hbar^2}{2m}\nabla^2 + V_s(r)\right]\phi_i(r) = \epsilon_i\phi_i(r) \quad (3.72)$$

The density $\rho(r)$ may be calculated in terms of orbital functions,

$$\rho(r) = \rho_s(r) = \sum_i^N f_i|\phi_i(r)|^2 \quad (3.73)$$

where, f_i = occupation of ith orbital.

Equations (3.70) and (3.71) are also equivalence of the Kohn - Sham equation.

3.1.5.4 Construction of Exchange - Correlation Functionals

The listed exchange-correlation functionals in Table 3 can be used in density functional simulations. The non - local nature of the exchange - correlation functional is also introduced in one form or another.

Table 3: Exchange - correlation functionals

Dependencies	Family
Coulomb d - d or f electrons interaction	LDA/GGA + U or LSDA / SGGA + U
$\nabla^2\rho, \tau$	Meta - GGA or MSGGA
$\lvert\nabla\rho\rvert$	GGA or SGGA
P	LDA or LSDA

3.1.5.4.1 Local Density Approximation (LDA)

LDA is the exchange - correlation functional which can compute the value of E_{xc} from the density (ρ) of a uniform electron gas at every position in space (i.e. local value of ρ) in any DFT. LDA with parametrization Perdew - Zunger (PZ) is suitable to deal with the structure, elastic moduli, and relative phase stability of many materials but it is not so accurate for the binding energy and detail of the energy surface away from equilibrium geometries as transition states. The local spin density approximation (LSDA) (Stojanovic, 2020) is employed for molecular calculation. Each volume element $d\bar{r}$ centered in $\bar{r}$ contributes to E_{XC} as the part of a homogeneous electron gas with density $\rho = \rho(\bar{r})$

$$E_{XC}^{LDA}[\rho] = \int \rho(\vec{r})\, \epsilon_{XC}[\rho(\vec{r})]\, d\bar{r} \tag{3.74}$$

$$V_{XC}^{LDA}(\vec{r}) = \frac{\delta E_{XC}[\rho]}{\delta \rho(\bar{r})} = \epsilon_{XC}[\rho(\vec{r})] + \rho(\bar{r}) \frac{d\epsilon_{XC}(\rho)}{d\rho}\Big|_{\rho = \rho(\bar{r})} \tag{3.75}$$

It is difficult to calculate $\epsilon_{XC}(\rho) = \epsilon_X(\rho) + \epsilon_C(\rho)$ through LDA.

$$\epsilon_X = -\frac{3}{4}\left(\frac{3}{\pi}\right)^{\frac{1}{3}} \rho^{\frac{1}{3}} \text{ (from the Hartree - Fock approximation)} \tag{3.76}$$

ϵ_C = combination of Quantum Monte Carlo calculation for low ρ and results from many - body theory (Gell - Mann and Brueckner for high ρ) (Entwistle, *et al.*, 2016).

3.1.5.4.2 Generalized Gradient Approximation (GGA)

In a molecular system, the nonuniform electron density in space raised serious limitations for energies in LDA. These limitations were improved by making them depend on the generalized gradient of the density (GGA). The GGA improves the LDA's excellent description of bond - lengths with typical errors.

The GGA functional in the typical form is expressed as

$$E_{XC}^{GGA}(\rho) = \int \rho(r), \epsilon_{xc}[\rho(r), \nabla\rho(r)]\, d^3r \tag{3.77}$$

The GGA functional depending on boh the local value and the local gradient of the electron density is a large family of semi - local approximations for the exchange - correlation energy. The most commonly used variants in GGA functional are

parametrized by revised - Perdew - Burke - Ernzerhoff, (i.e. parametrization rPBE) (Perdew, *et al*., 1996).

3.1.5.4.3 Meta-GGA Functional

The TB09 meta - GGA (MGGA) is a higher - level approximation that computes more accurate values of energy band gaps of both semiconductor and insulator than ordinary LDA and GGA. It is also applied in systems involving both metal and semiconductors / insulators. The meta - GGA functional reduces typical errors in the excellent description of bond lengths in GGA. It depends on the semi - local information in the Laplacian of the spin density or of the local kinetic energy density and also on the Kohn - Sham kinetic - energy density τ (r).
The typical form of meta - GGA is expressed as,

$$E_{xc}(\rho) = \int \rho\,(r), \epsilon_{xc}[\rho(r), \nabla\rho(r), \tau(r)]\, d^3r \qquad (3.78)$$

$$\tau(r) = \frac{\hbar^2}{2m}\sum_i |\nabla\phi_i(r)|^2 \qquad (3.79)$$

The exchange - correlation energy is expressed as $E_{XC}\,[\rho(r), \nabla\rho(r), \tau(r)]$.

The XC- functional MGGA finds the accurate band gap of a semiconductor which is comparable to the calculated value with hybrid functional (GW) having a significantly higher computational cost (Zahariev, *et al*., 2013).

3.1.5.4.4 L(S)DA / SGGA + U

The two interests of the various limitations in the local approximations used for the exchange - correlation energy are the following.

(a) Self - interaction: The electron is formally allowed to interact with itself. This can prevent electrons from localizing properly.

(b) Excited states: The LDA and GGA description of conduction band energy levels is often poor, so the energy band gap is often too low (Quantum ATK, 2019).

The mean - field Hubbard correction denoted as XC + U, DFT + U, LDA + U or GGA + U is semi - empirical correction. It attempts to improve on these limitations of the local exchange - correlation functional by adding an extra mean - field Hubbard

term (U) (Quantum ATK, 2019). The LDA and GGA can not predict the transition metal oxides to be semiconductors or Mott insulators due to the localized d electrons in the orbitals. However, the self - interaction correction (SIC), Hartree - Fock, GW, and LSDA / SGGA + U incorporate the strong electron - electron correlation between d electrons and f electrons. In the LSDA / SGGA + U method, the electrons are localized d or f electrons for which an orbital - dependent term $\frac{1}{2}\, U \sum_{i \neq j} n_i\, n_j$ should be used to describe Coulomb d or f interaction, where n_i are d or f orbital occupancy. The total energy is given as

$$E_{tot}^{LSDA/SGGA+U} = E_{LSDA\,/\,SGGA} + \frac{1}{2}\, U \sum_{i \neq j} n_i\, n_j - \frac{1}{2}\, U\, N\, (N - 1) \qquad (3.80)$$

The orbital energy (ε_i) is derivative of equation (3.80) with respect to orbital occupations n_j

$$\varepsilon_i = \frac{\partial E^{LSDA/SGGA+U}}{\partial n_i}$$

$$= \varepsilon_i^{LSDA\,/\,SGGA} + U \sum_{j \neq i} n_j - \frac{U(N-1)}{2} - \frac{UN}{2}$$

$$= \varepsilon_i^{LSDA/\,SGGA} + U(N - n_i) - UN + \frac{U}{2}$$

$$\varepsilon_i = \varepsilon_i^{LSDA\,/\,SGGA} + U\left(\frac{1}{2} - n_i\right) \qquad (3.81)$$

The orbital energy shifts with $-\frac{U}{2}$ for occupied orbital $n_i = 1$ and with $+\frac{U}{2}$ for occupied orbital $n_i = 0$.

The orbital dependent potential is expressed as

$$V_i(r) = V_{LSDA\,/\,SGGA} + U\,(\tfrac{1}{2} - n_i\,) \qquad (3.82)$$

The Hubbard potential U is included for higher order many - body terms or to be automatized for the calculation of effective interactions.

In this chapter - 3, we have illustrated the theoretical foundations of the Schrodinger Equation, Born - Oppenheimer Approximation (BOA), Hartree Approximation, Hartree - Fock Approximation (HFA), Density Functional Theory (DFT), Thomas

Fermi Theorem (TFT), The Hohenberg - Kohn Theorem (HKT), Kohn - Sham Theory (KST), Local Density Approximation (LDA), Generalized Gradient Approximation (GGA), Meta - GGA and L(S)DA / GGA + U, their corrective approach, prerogatives, limits, historical construction, and recent refinements. It has been described that the strong evidence of how these approaches can represent a useful framework to capture some effects of electronic exchange correlations. It has been also described how relatively minor extensions to their formulations can significantly improve the quantitative predictivity, quality, and numerical efficiency of computational approaches which can capture the physics of correlated systems (Tolba, S. A., *et al*., 2018; Kirchner - Hall, N. E., 2020). We detail the computational shoftwere, which are used to deal with our research works, in sub - section 3.2.

3.2 Computational Details

A powerful set of modeling tools Atomistix ToolKit (ATK) have been applied to investigate a variety of nanoscale systems starting from nanocluster to bulk systems. It is equally implemented for sensing devices and two - probe systems on Virtual Nanolab (VNL) (Soler, *et al*., 2002).

The Atomistic ToolKit (ATK) software device which is based on Density Functional Theory (DFT) is used to deals with stable structure calculations and electronic properties. In general, we use a basic exchange - correlation plus Hubbard potential (XC + U) functionals, like Local Spin Density Approximation (LSDA) and Spin Generalized Gradient Approximation (SGGA) with additional Hubbard coulomb Potential (U), and Meta - Spin Generalized Gradient Approximation (MSGGA) with suitable parameterizations Perdew - Zungger (PZ), revised - Perdew - Burke - Ernzerhof (rPBE) and TB09LDA for simulation perpose.

The script generator has been operated for the optimization of the different morphologies of Cu_2O and CuO through the job manager then we analyze the results. We adjust the various parameters to compute the binding energy per atom, electronic band structures, density of states profiles, energy band gap, the magnetic moment per atom, and spin polarization. Different K - point sampling are used for both Brillouin zone integration and linear combination of atomic orbitals (LCAO) for valence electrons are adjusted for different morphologies. In general, we used $(1 \times 1 \times 7)$, (1

× 7 × 7) , and (7 × 7 × 7) K - points sampling for one dimentional, two dimentional and for three dimensional material samples, respectively.

We choose the LCAOs for eigenfunctions, the basic set double - zeta - polarized for pseudopotentials, the Brillouin zone routes Γ for nanoclusters; Γ, Z for nanowires; nanotubes; nanoribbons; nanosheets; Γ, X, M, Γ, R, X, R, M for cubic bulk Cu_2O in Figure 11(a) and Γ, Y, C, Z, E, A, , Γ, B, , Z, Γ for monoclinic bulk CuO in Figure 11(b).

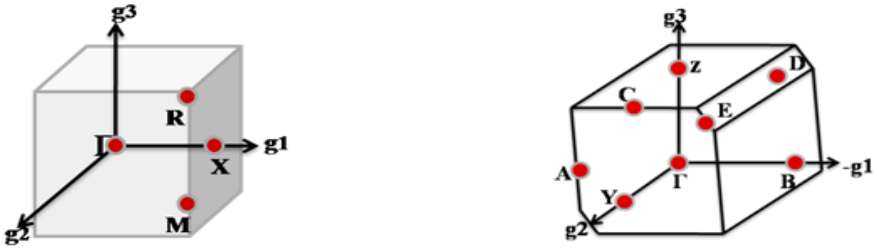

(a) (b)

Figure 11(a, b): Brillouin zones with special high symmetry k = $b_1g_1 + b_2g_2 + b_3g_3$ points of (a) cubic Cu_2O, (b) monoclinic CuO

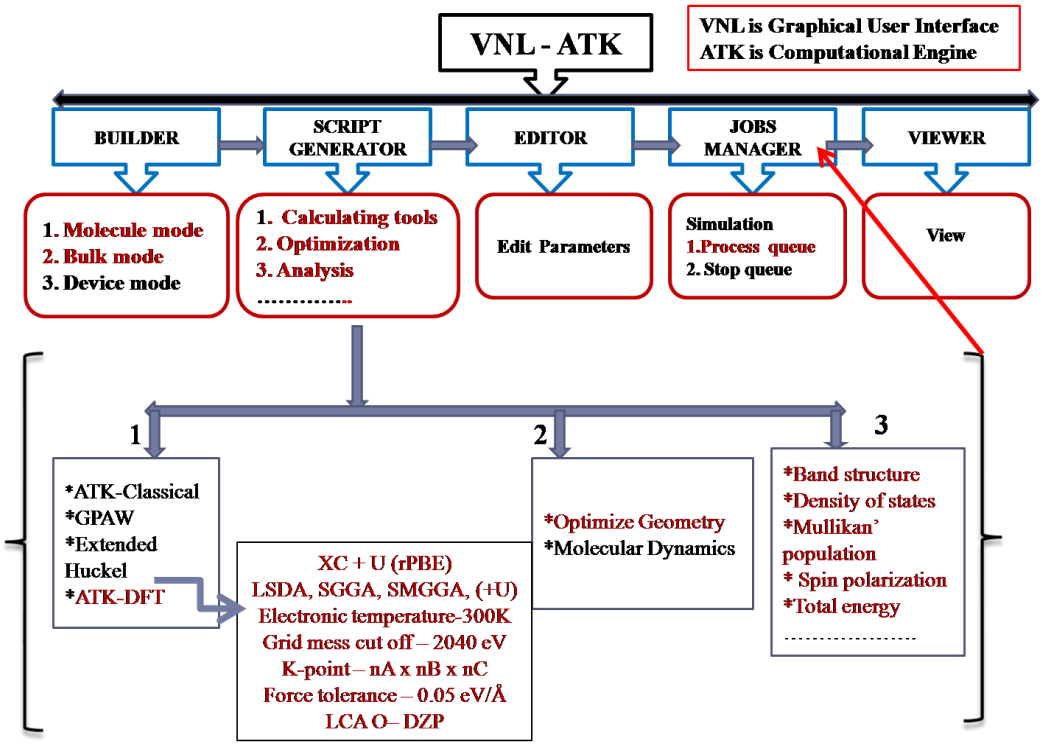

Figure 12: Flow - chart of VNL - ATK

The corresponding optimization geometry has been set at electron temperature 300 K, grid mesh cut off 2040 eV (75 Hartree), charge 0, spin - polarized. force tolerance 0.05 eV / Å, stress tolerance 0.05 GPa, the maximum number of steps 200, and maximum step size 0.2 Å, respectively (Quantum ATK, 2019). The flow chart of virtual nanolab (VNL - ATK) is shown in Figure 12.

By knowing the values of different parameters like total energy (E_T), the energy of Cu - ion (E_{Cu}), the energy of O - ion (E_O), numbers (N) of Cu^{+2} and (M) of O^{-2} ions, energy densities of up - spin or majority ($\rho\uparrow$), down - spin or minority ($\rho\downarrow$) and spin dipole moment of an electron or Bohr's magneton (μ_B), the binding energy per atom (E_b) (Parra, & Farrell, 2009; & Paudel, *et al.* 2016), the magnetic moment per atom (μ_{total}) (Choy, *et al*., 1999; Givovannetti, *et al*, 2011; Jones, *et al*., 2014; Wang, *et al*., 2017; Han, *et al*., 2019, & Miao, *et al*., 2019), spin polarization (SP) (Cherepkov, *et al*., 1981; Chalsani, *et al*., 2007; Tusche, *et al*., 2013; Kohashi, *et al*., 2018), and the chiral vector ($\vec{r}$) (Sun, B., 2010; & Paudel, *et al*., 2016) can be measured by using the following physical equations:

$$E_b = \frac{[N \times E_{Cu} + M \times E_O - E_{Cu_2O}]}{M + N} \tag{3.83}$$

$\mu_{atom} = \frac{\mu}{atom}$, where μ = magnetic moment of a system

$$= [N\uparrow - N\downarrow]\mu_B$$

$$= [\{\sum_0^{E_F}(\rho\uparrow - \rho\downarrow)\}/\text{atom}]\,\mu_B \tag{3.84}$$

$$\text{and, } P = \frac{[\rho\uparrow(E_F) - \rho\downarrow(E_F)]}{[\rho\uparrow(E_F) + \rho\downarrow(E_F)]} \tag{3.85}$$

$$\mu_B = \frac{e\hbar}{2m_e} = 9.27 \times 10^{-24}\ \text{A-m}^2$$

where, Ampere - square meter (A-m^2) is spin dipole moment of an electron or Bohr's magneton, $N\uparrow$ and $N\downarrow$ are the number of electrons per atom in majority (spin - up) and minority (spin - down) states respectively. $\rho\uparrow(E_F)$ and $\rho\downarrow(E_F)$ are density of states at Fermi level.

$$\vec{r} = n\vec{a} + m\vec{b} \tag{3.86}$$

Where $\vec{r}$, $\vec{a}$, and $\vec{b}$ are the chiral vector and two rectangular components or unit vectors of $\vec{r}$ along two directions in the plane lattice of a crystal as shown in Figure 13. n and m are indices of two vectors $\vec{a}$ and $\vec{b}$ respectively (Chatzichristos, *et al.*, 2022). We study theoretically the mentioned morphologies which have been, experimentally, described and published in the various papers. These published experimental papers are, briefly introduced in sub - section 3.3.

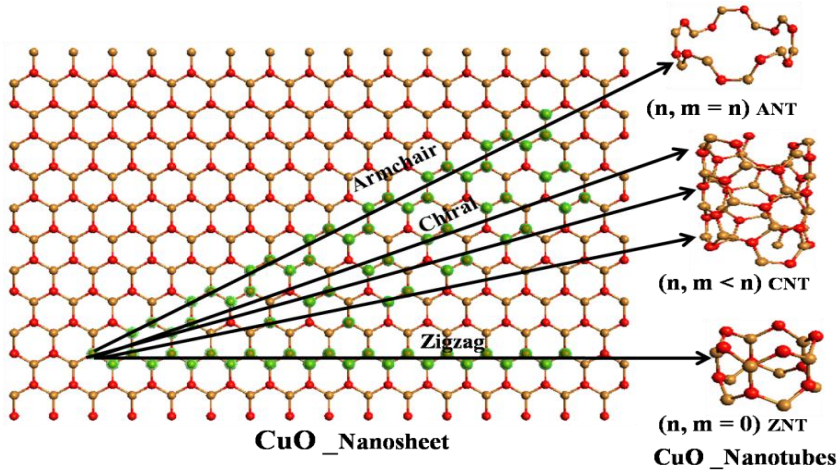

Figure 13: Schematic diagram showing CuO nanosheet, zigzag, armchair and chiral CuO NTs

3.3 Experimental Information

Many researchers have, experimentally, investigated the different morphologies like nanoclusters, nanowires, nanotubes, nanoribbons, nanosheets, and bulks of Cu_2O and CuO.

3.3.1 Nanoclusters of Cu_2O and CuO

The uniform CuO colloidal nanocrystal clusters (CNCs) with sizes of approximately 60 nanometers were prepared through a one - pot solvothermal synthetic method (Chen, 2011). The selective formation of the single - phase nanoclusters of Cu_2O in the size range of 10 nm - 50 nm on $SrTiO_3$ (100) substrates was found in a very narrow oxygen plasma - assisted molecular - beam epitaxy growth parameter window (Lyubinetsky, *et al.*, 2003).

3.3.2 Nanowires of Cu_2O

The Cu_2O nanowire arrays from the oxidation of the synthesized Cu metal nanowire arrays were prepared through a porous alumina membrane (PAM) template with a high aspect ratio, and uniform pore size of 120 nm - 140 nm, and ordered pore arrangement (Shen, *et al.,* 2010). The formation of pure Cu_2O nanowires at - 0.3V with pH 8.2 and - 0.5V with pH 9.0 in pores of anodic alumina oxide (AAO) templates was investigated by using larger Cu critical clusters (Khan, *et al.,* 2017).

3.3.3 Nanotubes of CuO

The free - Standing Copper (II) Oxide Nanotube Arrays were prepared through an MOCVD Template Process (Malandrino, *et al.,* 2004). Through the nano scratch technique, CuO and $Cu(OH)_2$ nanotubes were directly grown on a Cu substrate and found the energy of both increased with the reaction time. Also, they found a higher debonding energy in CuO nanotubes than in $Cu(OH)_2$ nanotubes (Saini, *et al.,* 2015).

3.3.4 Nanoribbons of CuO

The mesoporous ribbon - like CuO were synthesized through a facile and scaleable wet - chemical method, accompanied by tetraoctyl ammonium bromide (TOAB) as a soft template under ambient condition (Zhang, *et al*., 2013). The nanoribbons approximately 50 nm thin were prepared by dissolving CuCl in ethylene glycol before raising the solution temperature to 150°C in air through the developed facile organic - solution method (Lo, *et al.,* 2011).

3.3.5 Nanosheets of CuO

In the hydrothermal process, the oxidation of commercial copper (Cu) substrates fabricated the CuO nanosheets at 150°C (Zhi - Ang, *et al.,* 2009). As the controlled delamination of layered copper hydroxide acetate followed by the in situ solvothermal transformations of hydroxide to oxide, the CuO nanosheets were formed (Demel, *et al.,* 2017). In the same way, Cu_2O and CuO thin films were deposited on glass and silicon substrates at room temperature by reactive pulsed - DC magnetron sputtering in an argon and oxygen atmosphere (Wang, *et al.,* 2016).

3.3.6 Bulks of Cu_2O and CuO

The bulk of Cu_2O was prepared by using thermal oxidation, electrodeposition, and sputtering methods. $4Cu + O_2 \rightarrow 2Cu_2O$, the unwanted CuO is removed using the solution of $FeCl_3$, HCl, and NaCl (Abdu & Musa, 2009). The CuO nanostructures were prepared by a typical solution method concerning the following steps: preparing the precursor solution, modification of nanoproducts with additives or surfactants, heat treatment, and washing and drying process (Tran & Nguyen, 2014).
Copper salt + Alkaline hydroxide $\rightarrow Cu(OH)_2$+ Salt of alkaline metal $Cu(OH)_2 \rightarrow CuO + H_2O$

From the above mentioned experimental research works, we came to know that the different morphologies of Cu_2O and CuO can be synthesized and need to explain their structural evolution, electronic and magnetic properties systematically. Because of these properties, the nanosystems have wide range of applications. Keeping in mind, this research works are mainly focused on the computational works which have not been included in the previous research but have been experimentally synthesized. The overall results with discussion are presented in the incoming chapter 4.

CHAPTER 4

4. RESULTS AND DISCUSSION

4.1 Zero - Dimensional Nanostructures of Cu_2O and CuO

4.1.1 Structural, Electronic, and Magnetic Properties of Nanoclusters of Cu_2O and CuO

4.1.1.1 Structural Property

We have optimized and analyzed the various molecular structures of nanoclusters $(Cu_2O)_{n = 1, 2, 3}$ and $(CuO)_{m = 2, 4, 6}$ as shown in Figures 14(a - f), where the yellow and red color spheres represent the copper and oxygen atoms respectively. The nanoclusters $(Cu_2O)_{n = 1, 2, 3}$ contain atoms 3, 6, 9, and the nanoclusters $(CuO)_{m = 2, 4, 6}$ contain atoms 4, 8, 12, respectively. The binding energy of unit cell as well as per atom of both types of nanoclusters are calculated by using the equation (3.83). Our computational result revealed that the total energy of system increases with increasing the number of atoms. It is also observed that the nanoclusters having more molecules are more stable than those having fewer atoms indicating that nanoclusters tend to reach towads the bulk properties, as listed in Table 4 and also illustrated in Figure 15(a). In both cases, the bond length between Cu and O increases by increasing the number of atoms as shown in Figure 15(b), which affects on their electronic and magnetic properties.

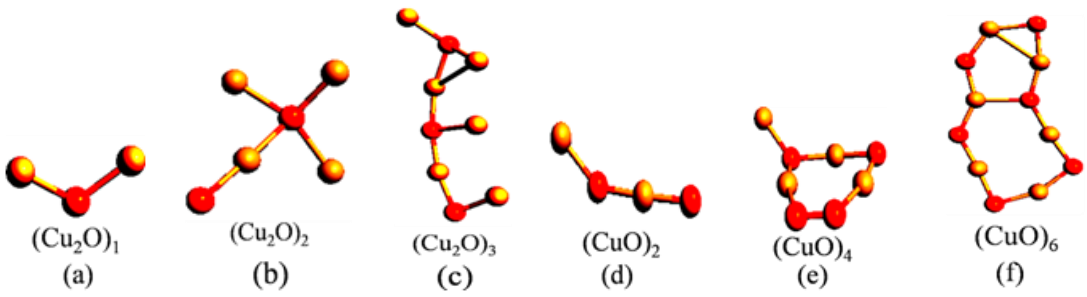

Figure 14(a - f): The molecular structures of nanoclusters $(Cu_2O)_{n = 1, 2, 3}$ and $(CuO)_{m = 2, 4, 6}$

Table 4: The computed values of different parameters of the nanoclusters $(Cu_2O)_{n = 1, 2, 3}$ and $(CuO)_{m = 2,4, 6}$ (Yadav, *et al*, 2020)

Nano-Clusters (NCs)	Total Atoms	Total Energy (eV)	Binding Energy/ Atom (eV)	Bond Lengths (Cu-O)	Band Gap (eV)	HUMO - LUMO (eV)	MM/unit cell (μ_T)	MM/atom (μ_B)	Spin Polarization	Natures
$(Cu_2O)_1$	3	2892.65	1.38	1.79	1.00	1.40	0	0	indefinable	Dia, Semi-conductor
$(Cu_2O)_2$	6	5785.94	1.58	1.82	0	0.28	2	0.33	1	Ferro, Half-metal
$(Cu_2O)_3$	9	8682.47	1.82	1.88	0.20	0.56	1.32	0.22	indefinable	Ferro, Semi-conductor
$(CuO)_2$	4	3325.89	1.30	1.81	0.80	1.20	0.98	0.49	indefinable	Ferro Semi-conductor
$(CuO)_4$	8	6656.35	1.55	1.85	0	0.40	4	0.50	1	Ferro Half-metal
$(CuO)_6$	12	9985.65	1.57	1.90	0.1	0.60	3.48	0.58	indefinable	Ferro Semi-Conductor

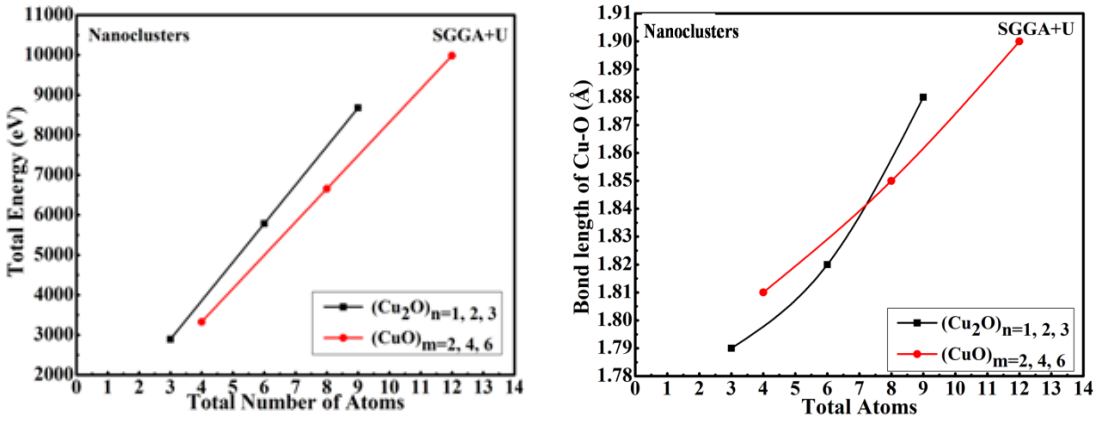

(a) **(b)**

Figures 15(a, b): Total energy and bond length of Cu - O in Å vs total number of atoms

4.1.1.2 Electronic Property

Here, we have found the molecular energy spectrums (MES) and DOS profiles of both types of nanoclusters $(Cu_2O)_{n = 1, 2, 3}$ in Figures 16(a - c) and Figure 16(d - f); and $(CuO)_{m = 2, 4, 6}$ in Figure 17(a-c) and Figure 17(d-f), respectively. The MES and DOS profiles provide the electronic behaviors of $(Cu_2O)_1$, $(Cu_2O)_3$, $(CuO)_2$, and $(CuO)_6$ as semiconductors and $(Cu_2O)_2$ and $(CuO)_4$ as half-metals (Groot, *et al.*, 1983). The MES gives the information related to HUMO - LUMO gap of the sytems. It does not clearly shows the electronic properties, so we use DOS to distinguish proper properties of the given nanoclusters. Overall computational results listing in Table 4 indicate that the molecular forms of the both nanoclusters $(Cu_2O)_2$ and $(CuO)_4$ have different properties than that of the bulk counterpart. Experimentally, both bulk Cu_2O and CuO are semiconductors with band gaps of 2.17 eV and 1.4 eV, respectively (Ghijsen, *et al.*, 1988; & Barreca, *et al.*, 2007).

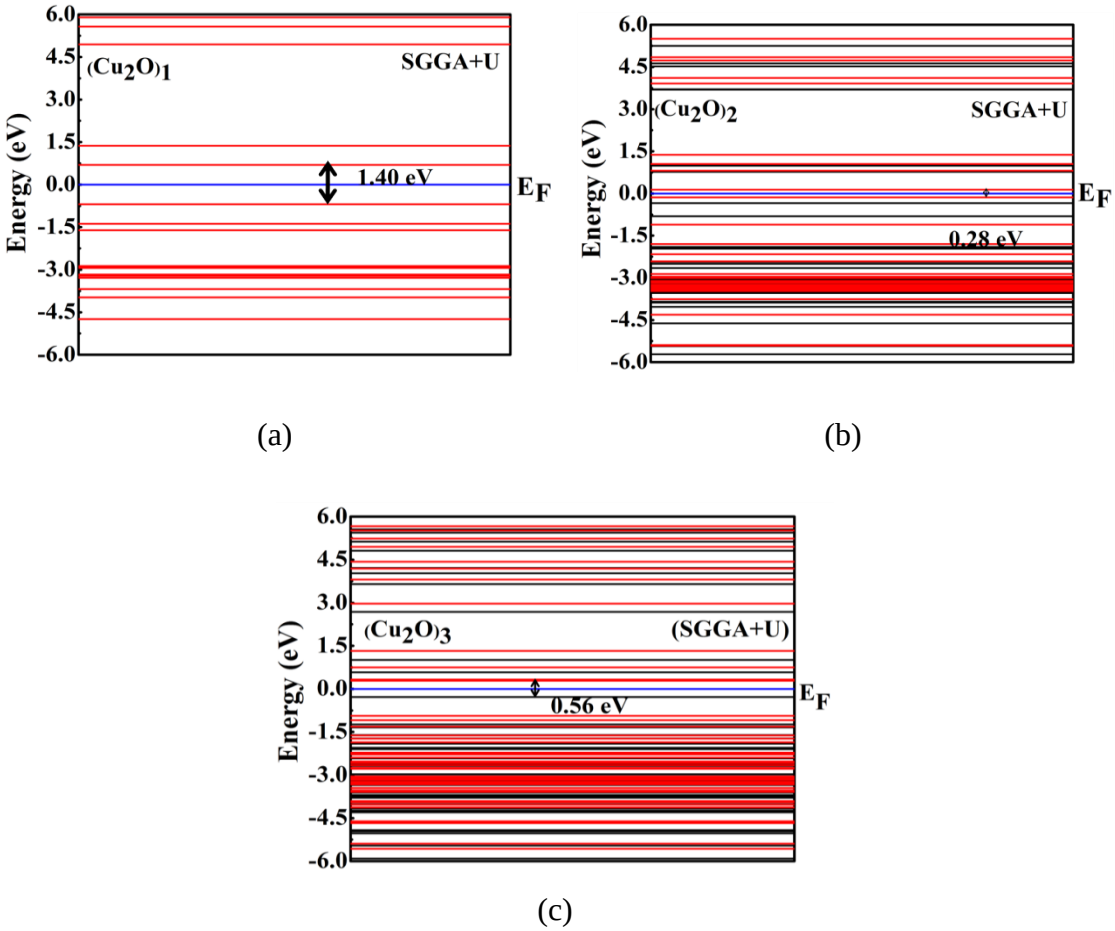

Figure 16(a-c): The molecular energy spectrums of the nanoclusters $(Cu_2O)_{n = 1, 2, 3}$

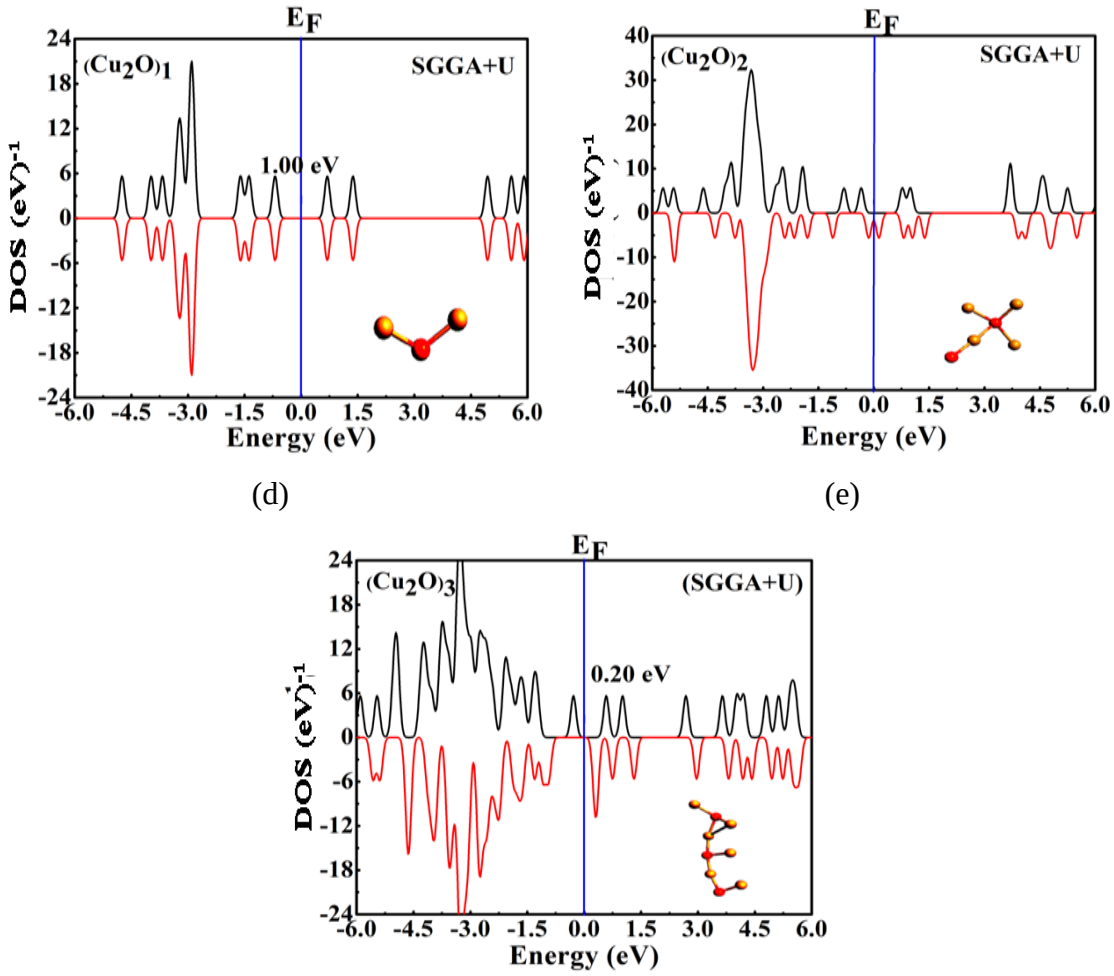

Figure 16(d-f): The density of states of the nanoclusters $(Cu_2O)_{n=1,2,3}$

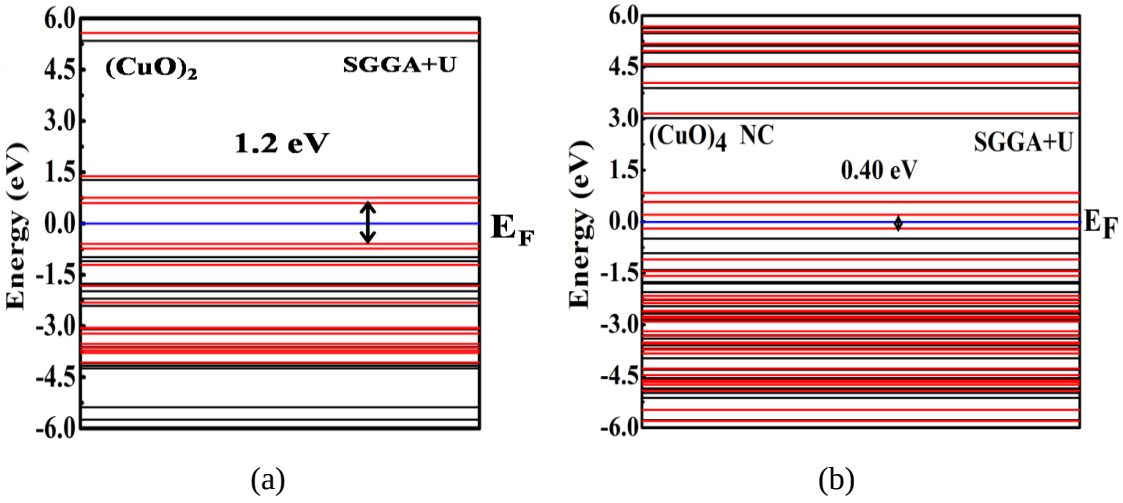

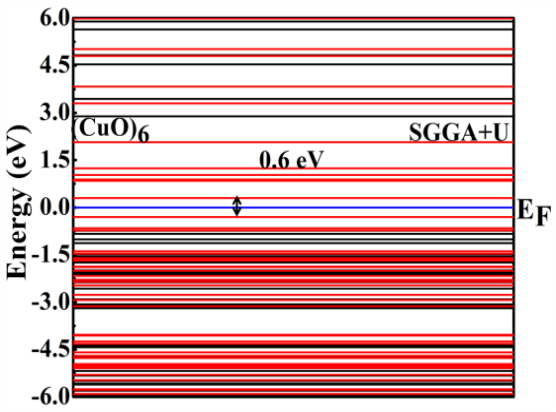

(c)

Figure 17(a-c): The molecular energy spectrums of the nanoclusters $(CuO)_{n = 2, 4, 6}$

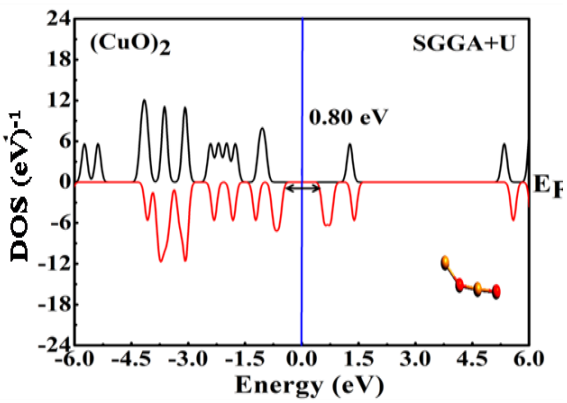

(d)

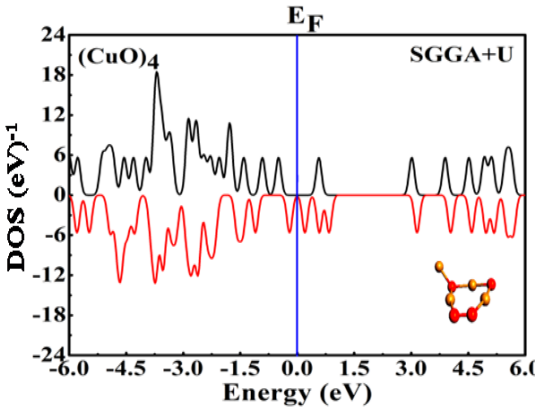

(e)

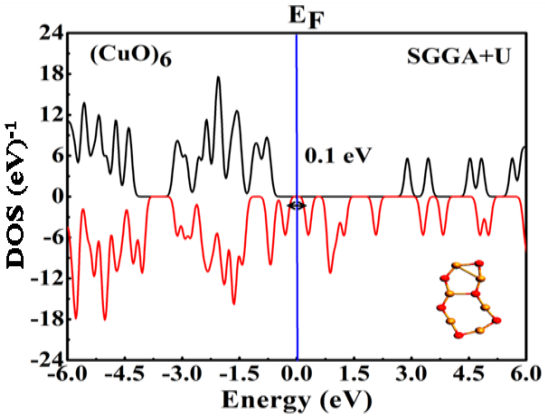

(f)

Figure 17(d-f): The density of states of the nanoclusters $(CuO)_{n = 2, 4, 6}$

4.1.1.3 Magnetic Property

We investigated the magnetic moments of unit cell, MM per atom and also the spin polarization of the various nanoclusters as listed in Table 4. The magnetic properties of the nanoclusters are studied through these concepts. From the DOS plot and spin orientation, only $(Cu_2O)_1$ nanocluster shows diamagnetic behavior whereas all others $(Cu_2O)_2$, $(Cu_2O)_3$, $(CuO)_2$, $(CuO)_4$, and $(CuO)_6$ nanoclusters are found to be ferromagnetic materials. From the calculation, their magnetic moments are 0.33 μ_B, 0.22 μ_B, 0.49 μ_B, 0.50 μ_B, and 0.58 μ_B respectively. The spin polarization of $(Cu_2O)_2$ and $(CuO)_4$ is individually 1 that represents half - metal ferromagnetic natures whereas other nanoclusters behave as metal. Here, the total magnetic moments of the unit cells of $(Cu_2O)_2$ and $(CuO)_4$ are 2 μ_B and 4 μ_B respectively.

4.1.1.4 Discussion

The $(Cu_2O)_1$ nanocluster shows the semiconducting and diamagnetic behaviors, whereas all others $(Cu_2O)_2$, $(Cu_2O)_3$ $(CuO)_2$, $(CuO)_4$, and $(CuO)_6$ show the ferromagnetic behaviors. The computed values of the total magnetic moments of the half - metallic ferromagnets $(Cu_2O)_2$ and $(CuO)_4$ nanoclusters are $2\mu_B$ and $4\mu_B$ respectively and their spin polarizations 1 individually. The total energy and the bond length of Cu - O increase concerning the number of atoms. The stability of a nanocluster having more number of atoms is stronger than that of less number ones.

4.2 One - Dimensional Nanostructures of Cu_2O and CuO

4.2.1 Structural, Electronic, and Magnetic Properties of Nanowires of Cu_2O

4.2.1.1 Structural Property

We selected 3 nanowires of different diameters like 4, 5 and 6 Å respectively and optimized them as shown in Figure 18(a - c). Their structural stabilities, electronic and magnetic behaviors have been explored through the analysis of binding energy per atom, electronic band structure, and density of states respectively. The binding energy per atom of Cu_2O nanowire of the different diameters has been calculated as dipicted in Table 5. The binding energy/atom of the nanowire of diameter 4 Å is 2.08 eV, which is observed to be more stable than the others as shown in Figure 19.

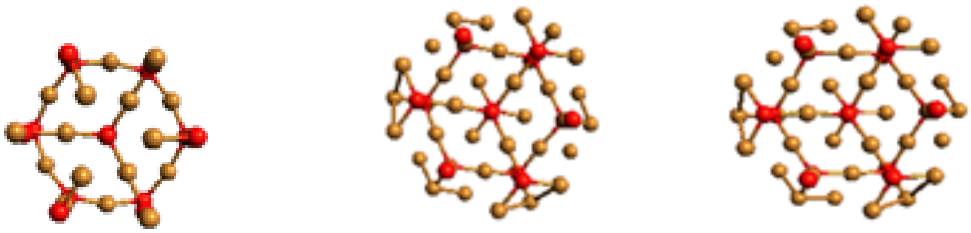

(a) (b) (c)

Figure 18(a - c): The molecular structure of Cu_2O NWs of the diameters 4, 5, 6

Table 5: The computed values of different parameters of Cu_2O NWs

Diameter (Å)	BE / atom (eV)	MM/unit cell (μ_T)	MM/atom (μ_B)	Spin Polarization
4	2.08	8	0.36	1
5	1.46	1.02	0.03	0.14
6	1.48	0.68	0.02	0.08

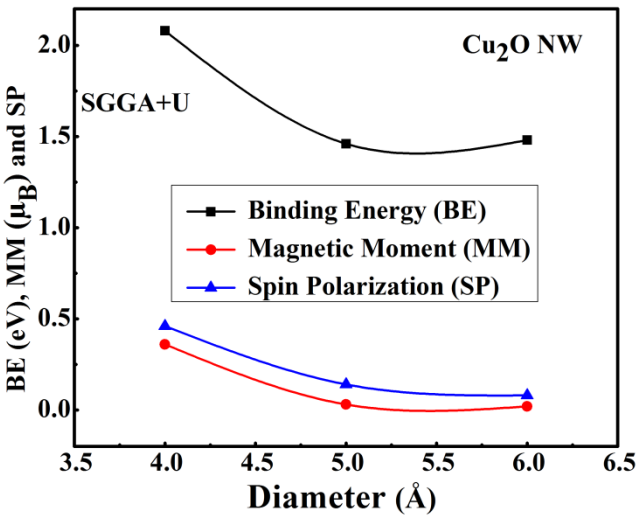

Figure 19: BE/atom, MM/atom, and spin polarization vs diameter of Cu_2O NWs

4.2.1.2 Electronic Property

We analysed the electronic band structures (EBS) and density of states (DOS) of the Cu_2O nanowire of different diameters (4 - 6 Å) with the majority and minority of electronic densities through SGGA + U as shown in Figure 20(a - c) and Figure 21(a - c), respectively. Here, the black and red lines indicate the majority and minority components respectively. The EBS and DOS plots report that the Cu_2O nanowire (d = 4 Å) is half - metal while others are full - metals, which are resemble available literatures (Zhou, *et al*., 2017).

.

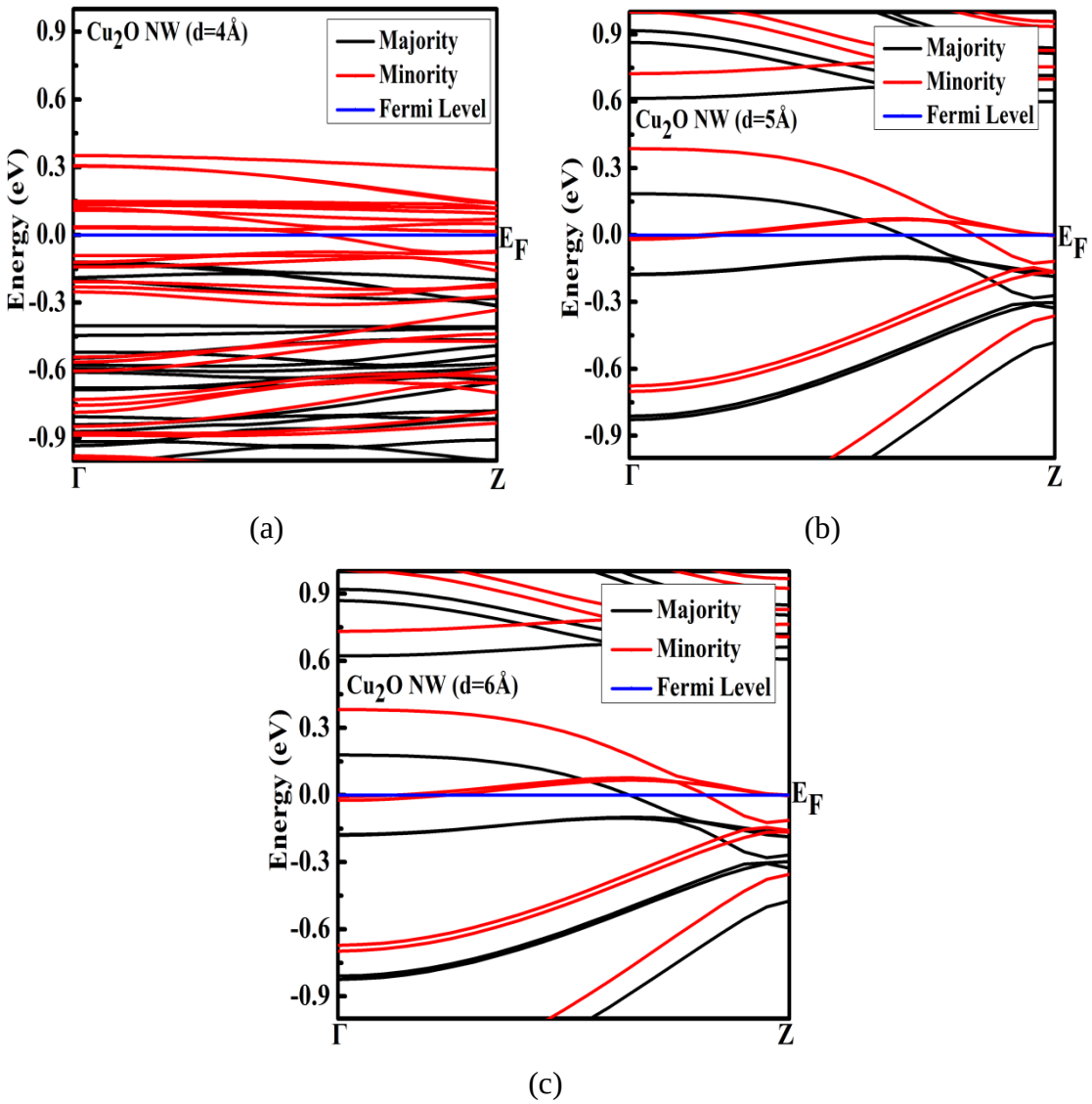

Figure 20(a - c): Electronic band structure of Cu_2O NWs of different diameters (4 - 6Å)

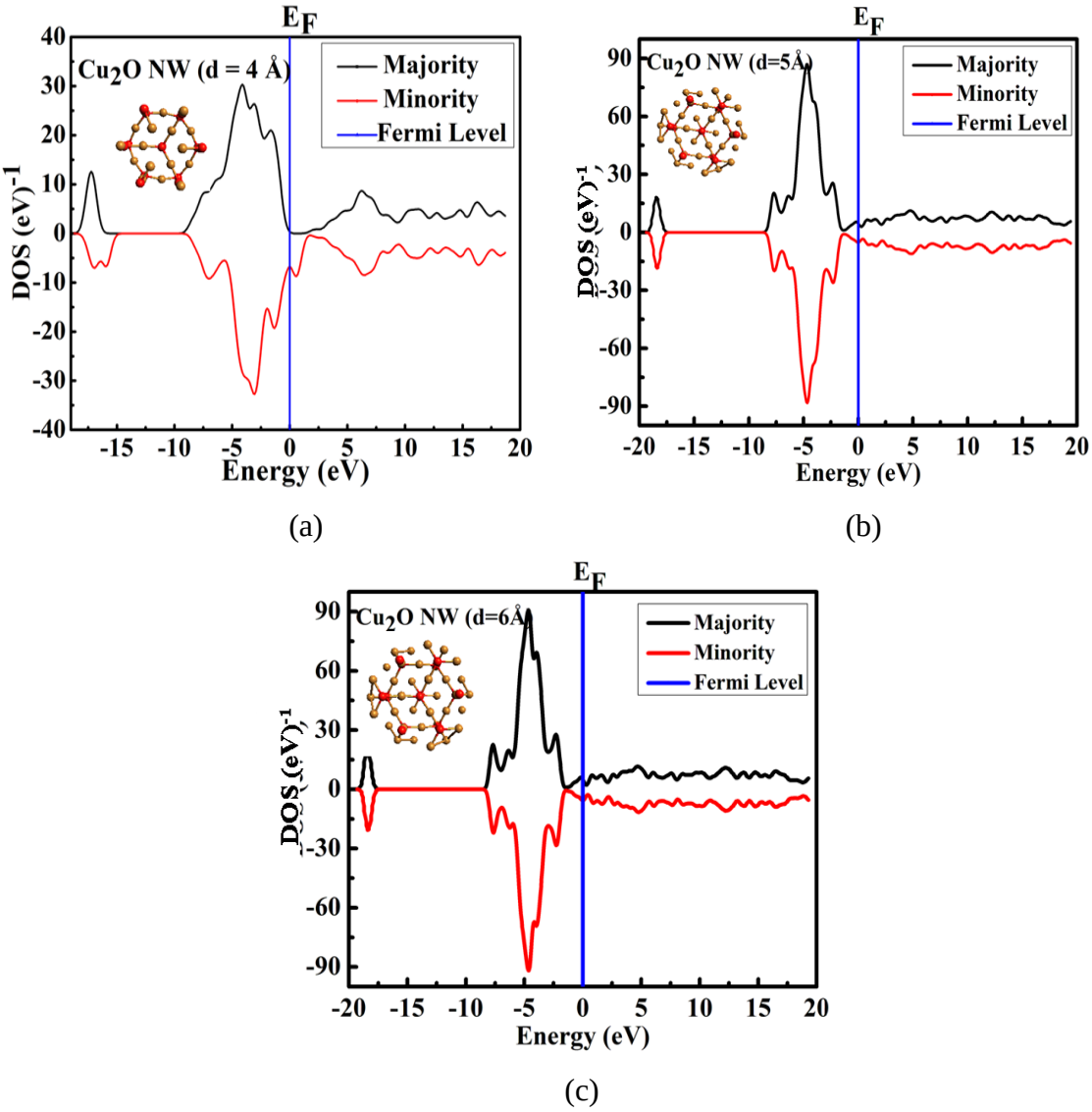

Figure 21(a - c): DOS of Cu_2O NWs of different diameters (4 - 6 Å)

4.2.1.3 Magnetic Property

We analysed the magnetic behaviors from the calculations of the magnetic moment of unit cell, magnetic moment per atom (MM/atom) and spin polarization (SP) at the Fermi level. Their computational values have been tabulated in Table 5. Calculations show that the total magnetic moment of the unit cell of Cu_2O nanowire directly depends on the individual magnetic moment of Cu and O atoms. The strong interaction makes their magnetic moment decrease and affects the total magnetic moment. The variations of the MM/atom, SP, and BE/atom regarding the diameter (4 - 6 Å) of the Cu_2O nanowire are shown in Figure 19. The variation of magnetic moment with diameter depends upon the hybridization between Cu - $3d^{10}4s^1$ and O - $2p^4$ states, and the contribution of the oxygen atom (O) at the Fermi level. The total

magnetic moment of unt cell of a stable Cu_2O nanowire of diameter 4 Å is 8 μ_B which reports it is ferromagnetic half metal with unit spin polarization and other structures are approximately diamagnetic in nature.

4.2.1.4 Discussion

The Cu_2O nanowire with a diameter of 4 Å is found to be more stable than other nanowires. The magnetic moment per atom, spin polarization, and binding energy vary with its diameter of range from 4 Å to 6 Å. The calculated total magnetic moment of a Cu_2O nanowire of diameter 4 Å is 8 μ_B greater than other nanowires revealing that it is a half - metallic and ferromagnetic nanomaterial.

4.2.2 Structural, Electronic, and Magnetic Properties of Chiral CuO Nanotubes

4.2.2.1 Structural Property

The chiral CuO nanotubes of chiralities (2, 1), (3, 1), (3, 2), (4, 1), and (4, 2) consist of 28, 52, 76, 28, and 56 atoms, respectively with different views (cross-sectional and side view) are shown in Figure 22(a - e) and Figure 23(a - e), respectively. The yellow and red color spheres indicate the copper and oxygen atoms respectively. The computed value of binding energy per atom of the different nanotubes are listed in Table 6. From the calculation, it is observed that the (2, 1) CuO nanotube has a binding energy per atom of 2.63 eV which shows it as a more stable structure than other (3, 1), (4, 1), and (4, 2) CuO nanotubes. The structural stability of the different chiralities of CuO nanotubes depends on the binding energy at electronic temperature 300K. Over the systems, the stability order is (2, 1) $>$ (4, 2) $>$ (3, 2) $>$ (4, 1) $>$ (3, 1).

(2, 1) CuO NT (3, 1) CuO NT (3, 2) CuO NT (4, 1) CuO NT (4, 2) CuO NT

(a) (b) (c) (d) (e)

Figure 22(a - e): The (n, m) CuO CNTs in molecular forms

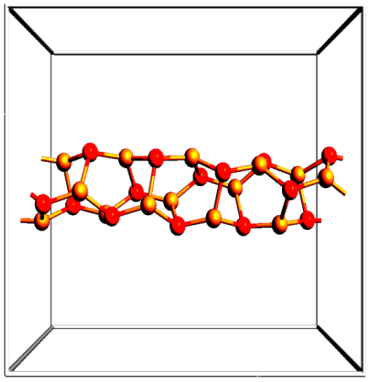

(2, 1) CuO CNT

(a)

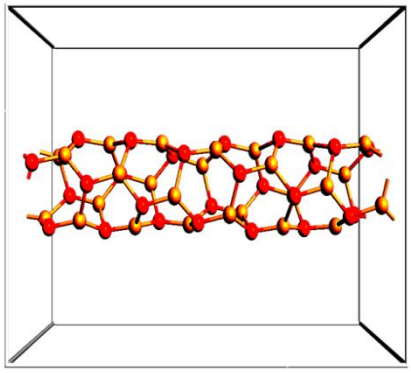

(3, 1) CuO CNT

(b)

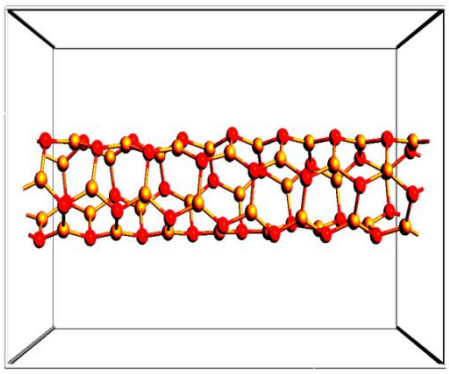

(3, 2) CuO CNT

(c)

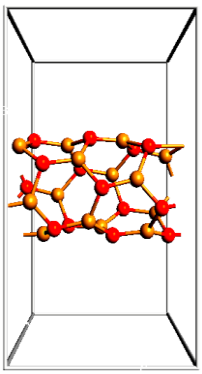

(4, 1) CuO CNT

(d)

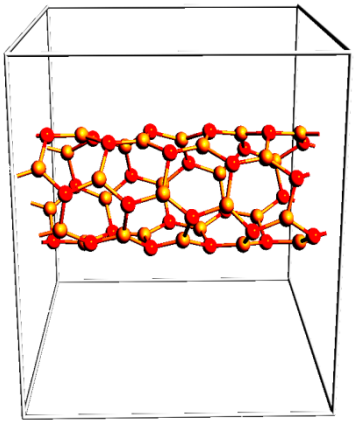

(4, 2) CuO CNT

(e)

Figure 23(a - e): The (n, m) CuO CNTs in bulk forms

Table 6: The chiralities of CuO CNTs with their diameters, BE / atom, MM / atom, and spin polarization (SP)

Chirality (n, m)	Diameter (Å)	BE/atom (eV)	MM / unit cell (μ_B)	MM / atom (μ_B)	Spin Polarization	Remarks For chiral (n > m)
(2, 1)	2.80	2.63	5.07	0.36	Indefinable	Semiconductor, Ferro,
(3, 1)	3.84	2.38	8	0.31	1	Half metal, Ferro
(3, 2)	4.62	2.51	13	0.35	1	Half metal, Ferro
(4, 1)	4.77	2.47	5	0.36	1	Half metal, Ferro
(4, 2)	5.57	2.56	10	0.37	1	Half metal, Ferro

4.2.2.2 Electronic Property

The electronic band structures and density of states (DOS) profiles of the chiral CuO nanotube of chiralities (2, 1), (3, 1), (3, 2), (4, 1), and (4, 2), are depicted in Figure 24(a - e) and Figure 25(a - e) respectively. The black and red lines indicate energy (E) vs wave vector (K) plot of up and down spin channels. From the Figures, (2, 1) CuO nanotube shows semiconducting nature with an energy bandgap of 2.2 eV whereas (3, 1), (3, 2), (4, 1), and (4, 2) CuO nanotubes show half-metallic behaviors.

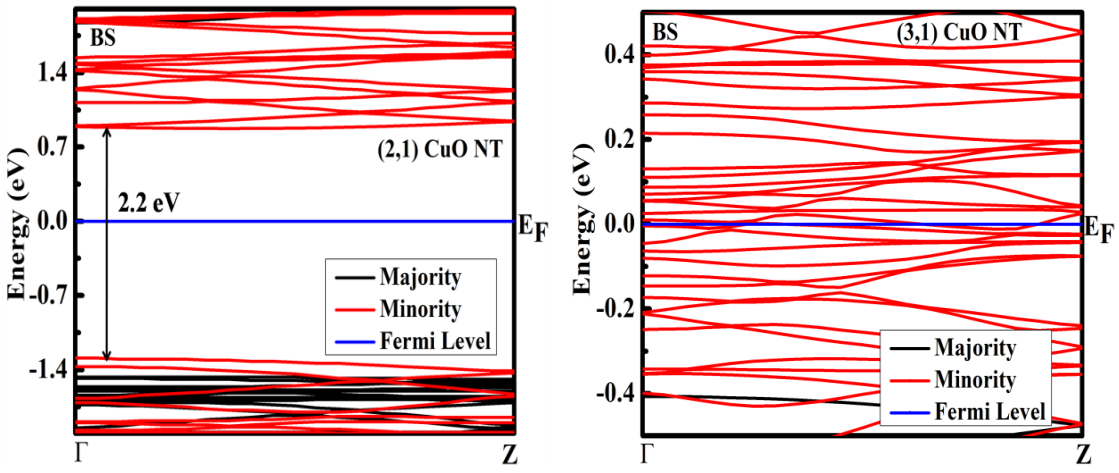

(a) (b)

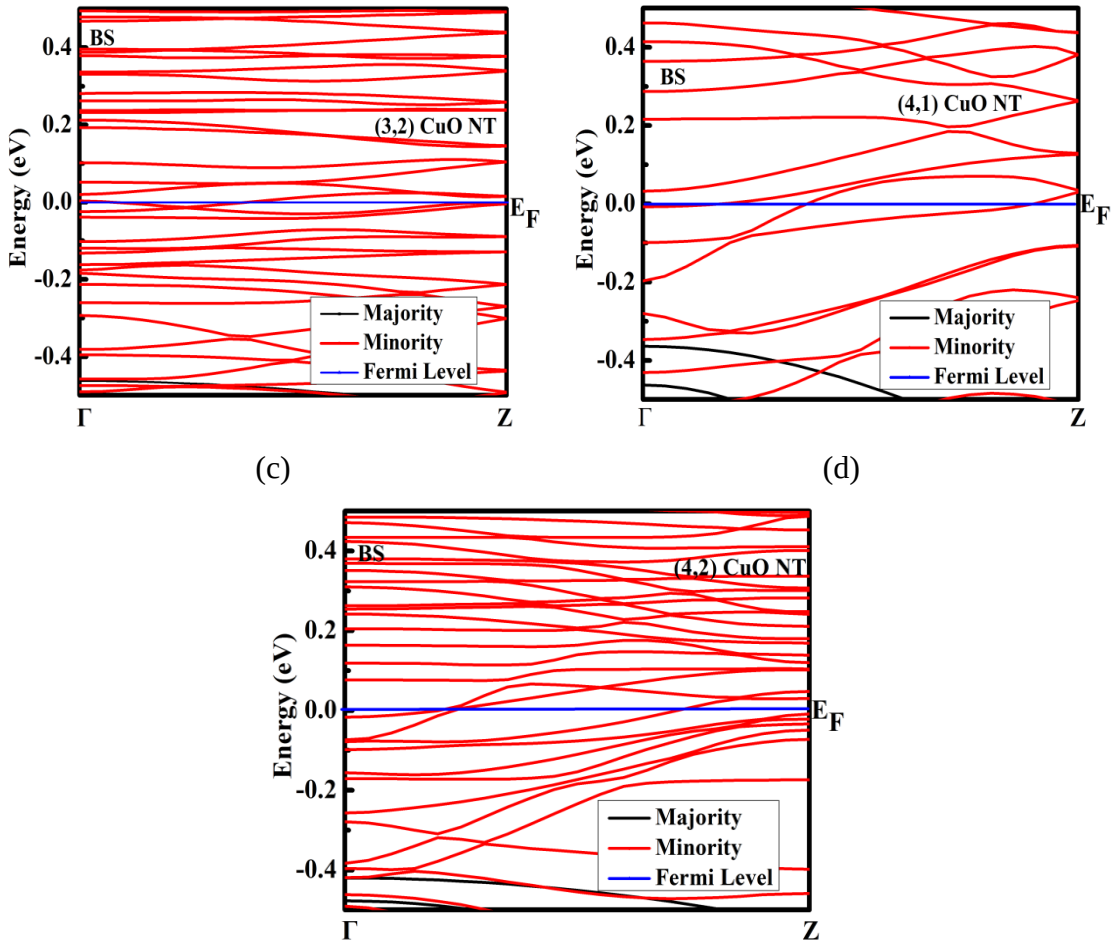

Figure 24(a - e): The electronic band structures of (n, m) CuO CNTs

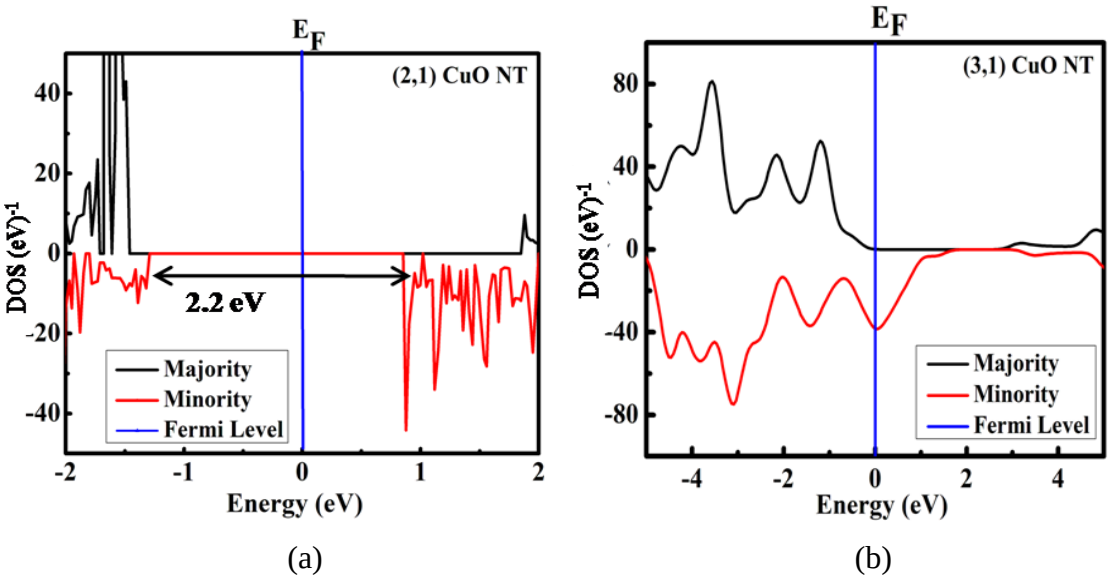

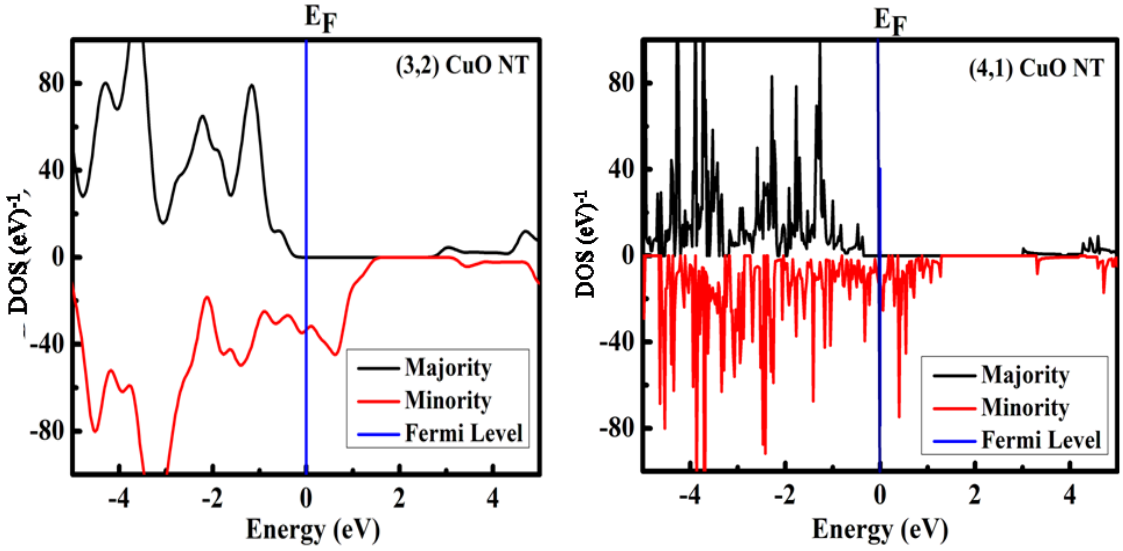

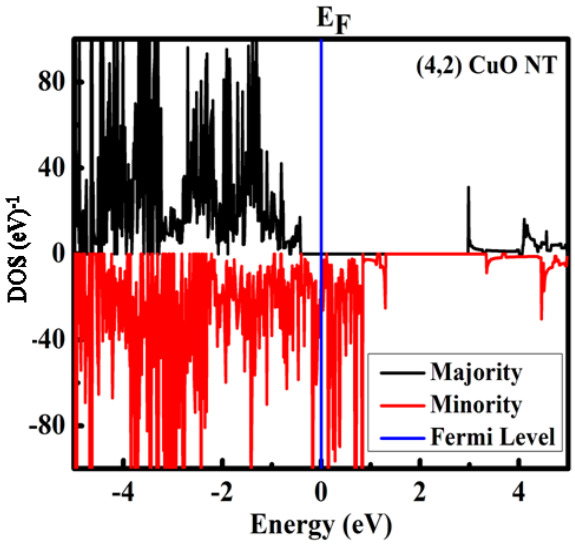

(e)

Figure 25(a - e): The density of states \of (n, m) CuO CNTs

This result reveals that the (2, 1) CuO nanotube is useful for the nanodiode whereas the (3, 1), (3, 2), (4, 1), and (4, 2) CuO nanotubes are useful for the applications of high-frequency devices. The energy bandgap of (2, 1) nanotube is close to the energy band gap of bulk CuO (1.4 eV - 1.9 eV).

4.2.2.3 Magnetic Property

The electronic band structures and the DOS profiles show that the chiral CuO nanotube of the chiralities (3, 1), (3, 2), (4, 1), and (4, 2) all have metallic natures with varying magnetic moments. The calculated values of magnetic moment per atom and spin polarization of the CuO are listed in Table 6. The magnetic moments of chiral

CuO nanotubes depend on the spin dipole moments of electrons of both isolated atoms Cu and O separately, and their interaction. From the calculations, we found that the magnetic moment per atom decreases with increasing the diameter or chirality of the chiral CuO nanotube, The increasing order is found for the the binding energy. Based on spin polarization, the chiral CuO nanotube of chiralities (3, 1), (3, 2), (4, 1), and (4, 2) are half - metallic (Groot, *et al*., 1983) in nature, while the chiral CuO nanotube of chirality (2, 1) is ferromagnetic with magnetic moment 0.36 μ_B and semiconductor having a band gap of 2.3 eV at the Fermi level. The total MM of unit cell also confirms their half - metallic natures. The characteristics curves of the magnetic moment per atom and spin polarization concerning the width and chirality of (n, m ≠ n) CuO nanotubes are depicted in Figure 26(a).

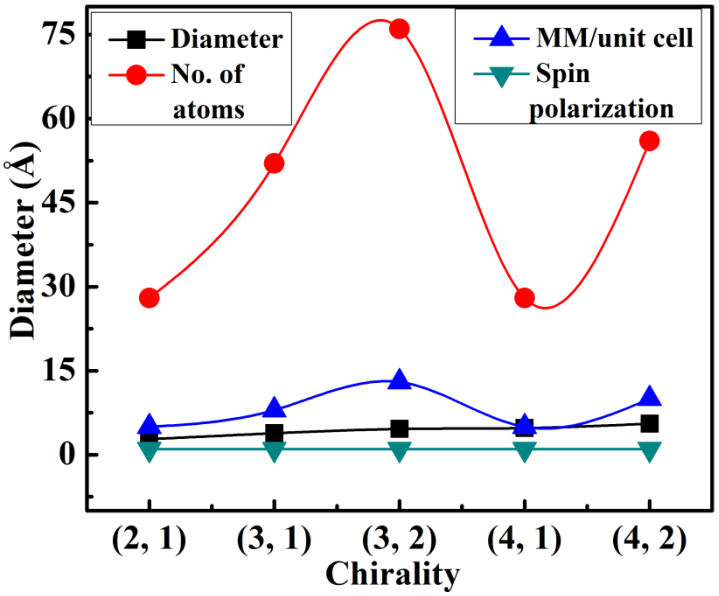

Figure 26 : The graphs of Diameter, no. of atoms, magnetic moment, and spin polarization vs chirality of (n, m) CuO_CNT

4.2.2.4 Discussion

We have found the optimized structures of the chiral CuO nanotubes with different diameters. The chiral (2, 1) CuO nanotube with magnetic moment 0.36μ_B shows the semiconducting behavior, while the chiral CuO nanotubes of chiralities (3, 1), (3, 2), (4, 1), and (4, 2) have magnetic moments of 0.31 μ_B, 0.35 μ_B, 0.36 μ_B, and 0.37 μ_B respectively, indicating that they bear the half - metal ferromagnetic behaviors. The

calculation shows that the magnetic moment per atom decreases with increasing the diameter of the chiral (n, m) CuO nanotube. Based on the above characteristics, we predict that the CuO nanotubes of different diameters are suitable candidates for nanodiode, sensor, and spintronic devices.

4.2.3 Magnetic Moment of Zigzag CuO Nanotubes at Different Temperatures and Sizes

4.2.3.1 Structural Property

We calculated the binding energies and magnetic moments of some optimized (n, 0) zigzag CuO nanotubes at different temperatures. The binding energies, bond lengths of the different diameters of CuO nanotubes with total energies of different chiralities have been listed in Table 7.

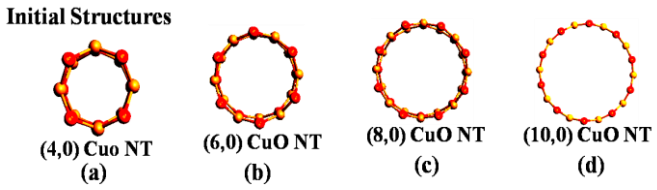

Figure 27(a - d): The initial nanostructures of CuO ZNTs

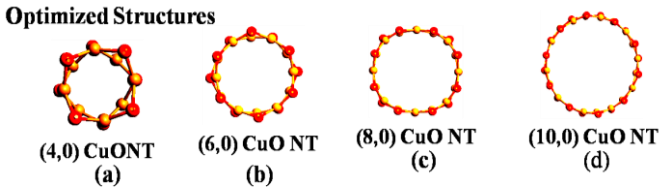

Figures 28(a - d): The optimized nanostructures of CuO ZNTs

Table 7: Bond length, Binding energy, Diameter, and Total energy of CuO ZNTs

Chirality (n, 0)	No.of atom (N)	Bond length (Å)	Diameter (Å)	Binding energy / atom E_b(eV)	Total energy E_T(eV)
(4, 0)	16	1.95	4.30	4.73	-13328.95
(6, 0)	24	1.90	6.29	4.81	-19995.52
(8, 0)	32	1.90	8.39	4.84	-26661.54
(10, 0)	40	1.90	10.46	4.85	-33326.89

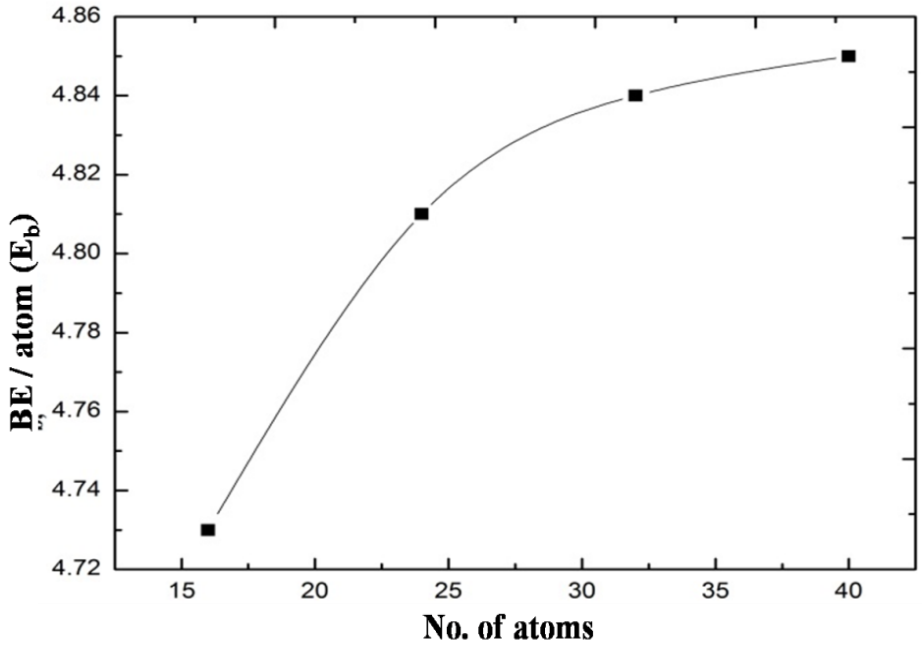

Figure 29: Relation between binding energy and total number of atoms in CuO ZNTs

From the calculation, It is seen that the (4, 0) CuO NT has a larger bond length than others and found that the number of atoms and diameter is directly proportional to the binding energy. The initial and optimized nanostructures of different chiralities as (4, 0), (6, 0), (8, 0), and (4, 0) of zigzag CuO NTs are shown in Figure 27(a - d) and Figure 28(a - d) respectively. The copper and oxygen atoms are represented by the yellow and red - colored spheres respectively. They are electropositive and electronegative atoms, respectively. The binding energy per atom increases concerning the number of atoms as shown in Figure 29.

4.2.3.2 Electronic Property

The electronic band structures of zigzag (n, 0) CuO nanotubes with up and down spins of electronic energy density were investigated at the Fermi energy level as shown in Figure 30(a - d). The zigzag (4, 0), (6, 0), (8, 0), and (10, 0) CuO nanotubes show the metallic nature due to the hybridization between Cu - 3d and O - 2p states at the Fermi level. The Cu - $3d^9 4s^2$ loses 2 electrons from the d - orbital, and the O - $2p^4$ gains these two electrons due to which one sub - orbital (d_x^2 - $_y^2$) of 3d must be partially filled, resulting in metallic behavior. This result is following some computational and experimental values of other nanostructures of CuO analyzed at different diameters (Poudel *et al*., 2016).

The total density of states and partial DOS of Cu - 4s, Cu - 3d, and O - 2p states of zigzag CuO through the spin polarization - based DFT are shown in Figure 31(a - d). The Peak values of density of states near the Fermi level in the valance and conduction bands are formed due to the hybridizations of Cu - 3d and O - 2p states, and Cu - 4s states, respectively. The finite contribution of the O atom to the density of states at the Fermi level shows these nanotubes behave as metal. The spectral distributions in a zigzag (n, 0) CuO have a large range, which provides evidence of strong electron - electron interaction and Coulomb interaction (U).

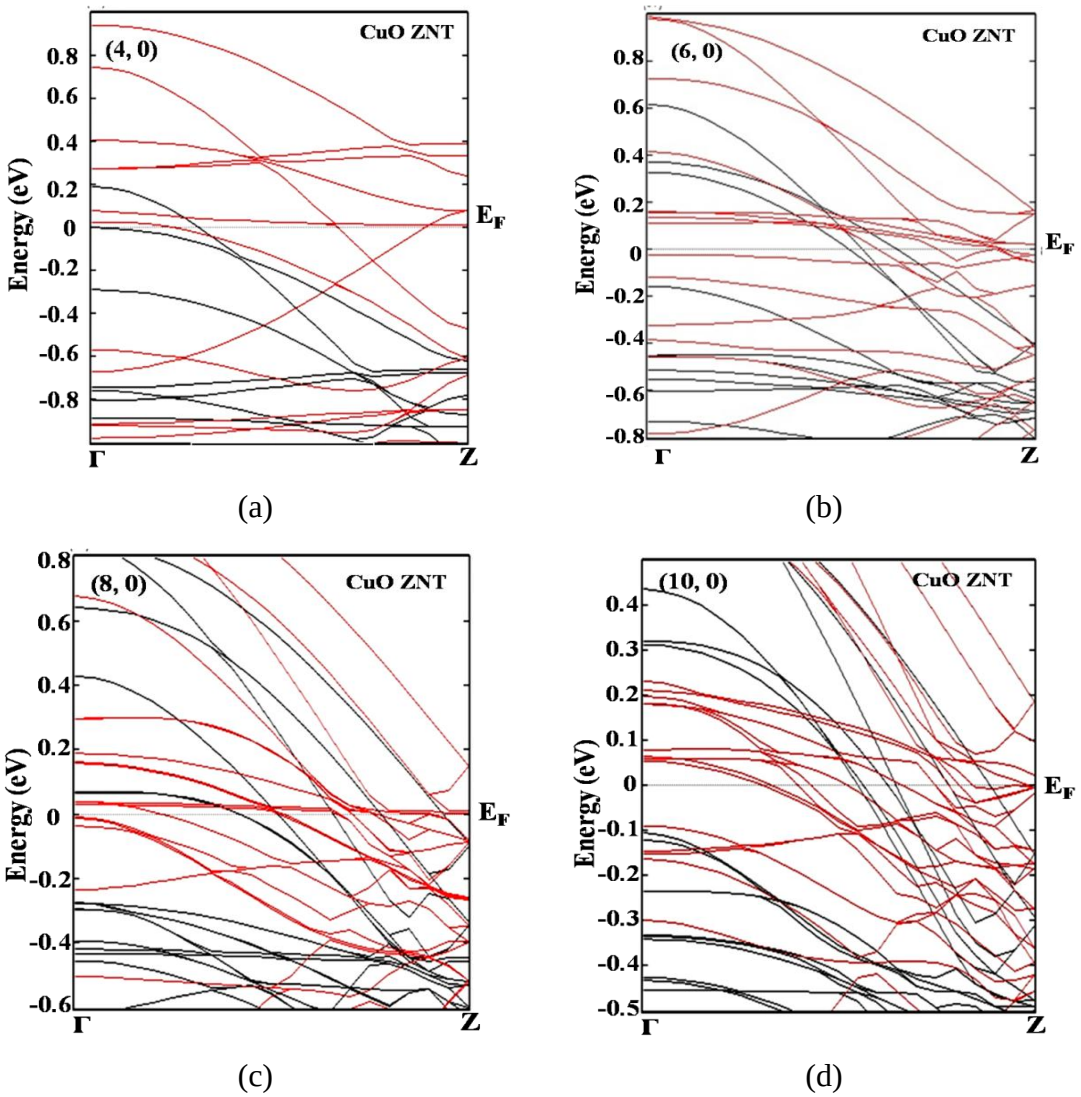

Figure 30(a - d): Band structure of CuO ZNTs with the majority and minority spins

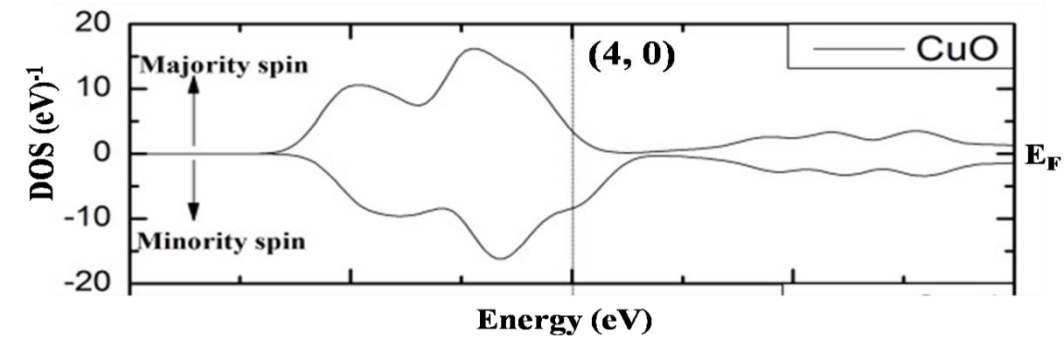

(a)

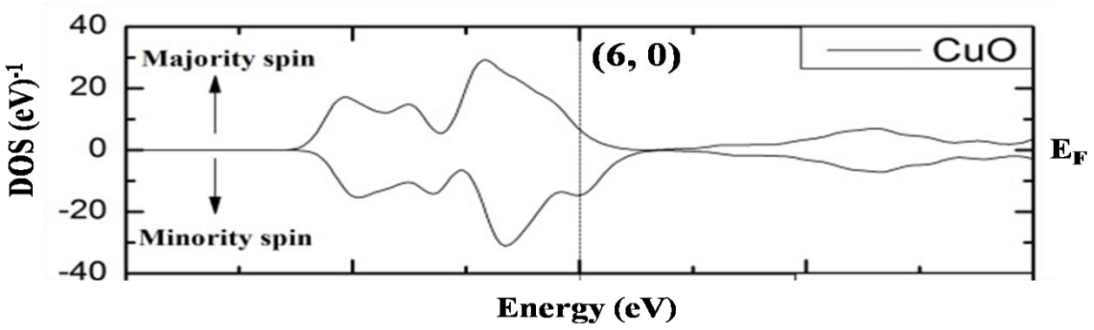

(b)

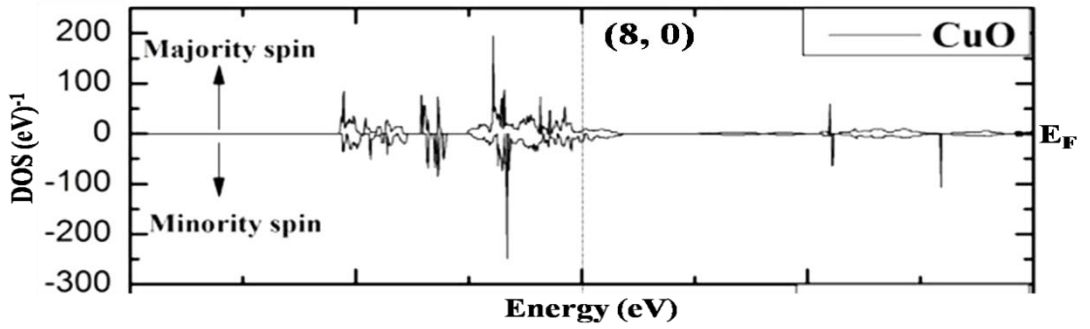

(c)

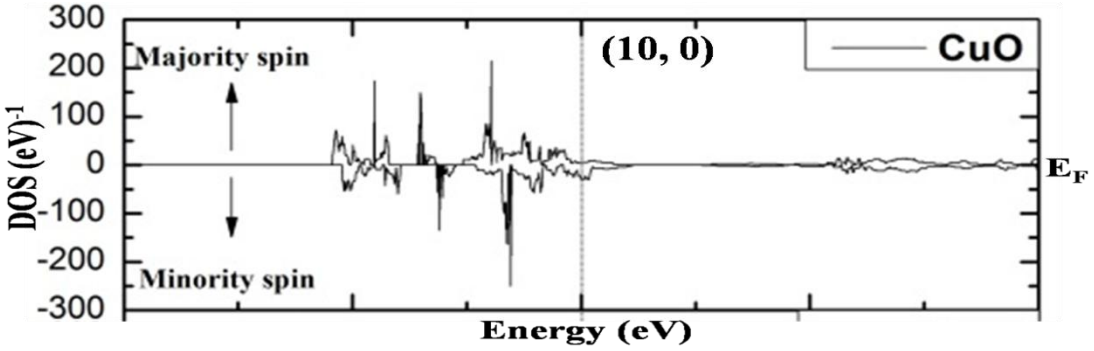

(d)

Figure 31(a - d): Spin-polarized Density of states of CuO ZNTs

4.2.3.3 Magnetic Property

Magnetic moments of (4, 0), (6, 0), (8, 0), and (10, 0) CuO ZNTs are 0.45 μ_B, 0.31 μ_B, 0.19 μ_B, and 0.23 μ_B, respectively whereas the magnetic moments for CuO bulk, Cu atom and O atom are 0.68 μ_B and, 0.70 μ_B, and 0.14 μ_B respectively. These values are a resemblance to the experimental values of Cu (0.70 μ_B) and O (0.14 μ_B), respectively (Wang, *et al*., 2003). The exchange splitting of the Cu - 3d and O - 2p states electrons provide a magnetic moment to CuO ZNTs. The fluctuation in the magnetic moment on increasing the diameter is due to the number of electrons present in the Cu - 3d state. The magnetic moment per electron (μ_B) is directly linked to the number of unpaired electrons and the magnetic properties of unpaired electrons that arise from electron spin and electron orbital motion. Magnetic moment decreases with an increment of diameter until we reached (10, 0), then the magnetic moment increases with the diameter as shown in Figure 32(a). Furthermore, we have analyzed magnetic moments with different temperatures. We found that magnetic moment has a high value at room temperature then it decreases at higher temperatures. However, (8, 0) NT magnetic moment increases with temperature as shown in Figure 32(b). Calculations reveal that the maximum magnetic moment is obtained for (4, 0) nanotube with a diameter of 4.30 Å and the minimum for (8, 0) nanotube with a diameter of 8.39 Å.

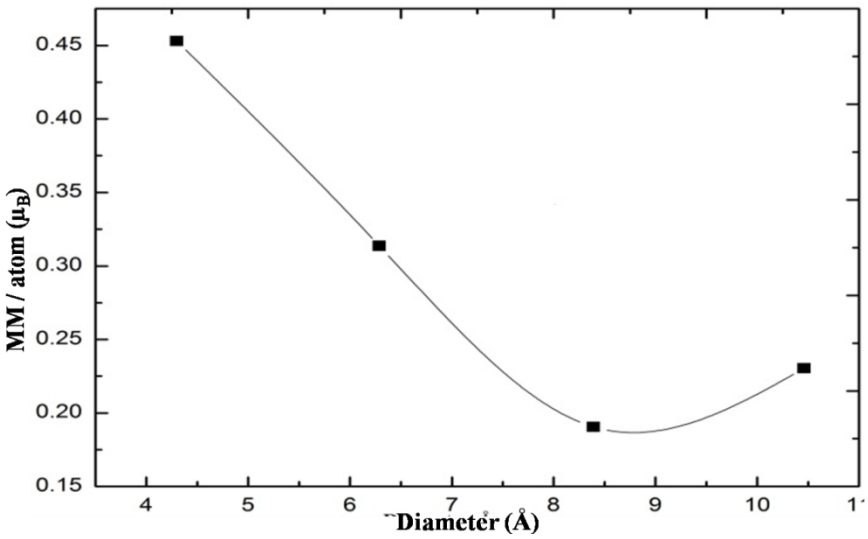

(a)

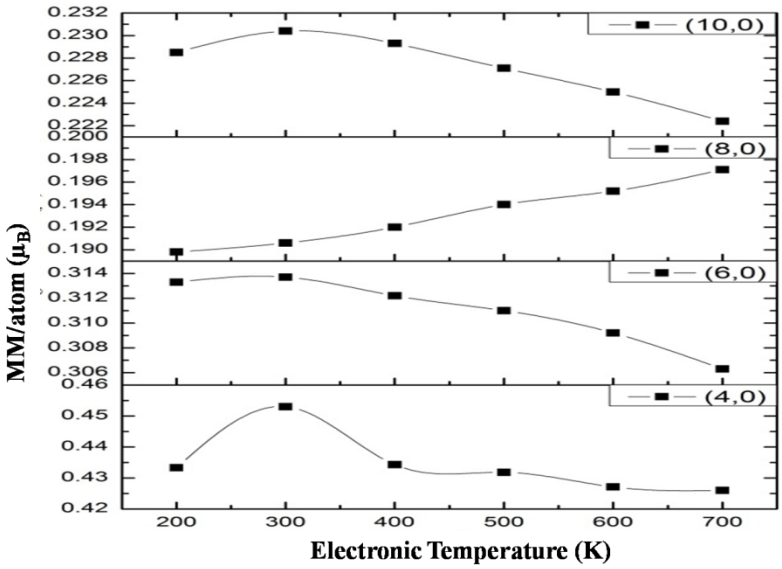

(b)

Figure 32(a, b): Magnetic moment as a function of diameter and a function of the electronic temperature of CuO ZNTs

4.2.3.4 Discussion

The structural, electronic, and magnetic properties of the optimized (4, 0), (6, 0), (8, 0), and (10, 0) zigzag CuO nanotubes were analyzed using the density functional theory based ATK - VNL tool. The magnitude of buckling decreases with the increasing diameter of the nanotube. The diameter of the nanotube and the number of atoms are directly proportional to the binding energy of the CuO ZNT. They show metallic nature due to the hybridization of the Cu - 3p state and O - 2p state. Magnetic moments change concerning the different diameters and electronic temperatures. The highest value of the magnetic moment, . 0.45 μ_B is observed for (4, 0) at 300 K. The magnetic moments for (4, 0), (6, 0), and (10, 0) nanotubes decrease whereas increases for (8, 0) nanotube. These nanotubes show remarkable magnetic moments, indicating that these are potential candidates for spintronic devices, memory devices, and magnetic sensors.

4.2.4 Structural, Electronic, and Magnetic Properties of Nanoribbons of CuO

4.2.4.1 Structural Property

We built up computationally the (n = 3 - 10, m = 0) zigzag and (n = 3 - 10, m = n) armchair forms of CuO nanoribbon for their optimization and then analyzed their

structural stabilities through their binding energies respectively. The supercells (1 × 1 × 6) with (3, 0) and (1 × 1 × 6) with (3, 3) of the armchair and zigzag nanoribbons have been shown in Figure 33 and Figure 34, respectively. All the calculated data using equations (3.83), (3.84) (3.85), and (3.86) have been listed in Table 8. and Table 9, respectively.The length of the supercell of nanoribbon increases along the C direction at constant A and B directions. The width as well as number of atoms of the nanoribbon increases with respect to increase of its chirality. The binding energy per atom of both types of the nanoribbons randombly varies with the width as depicted in Figure 35.

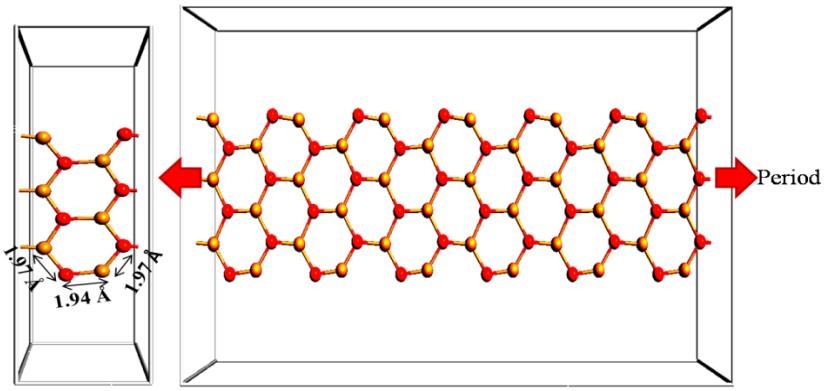

Figure 33: Bulk form of (1×1×6) supercell of (3,0) CuO ZNR

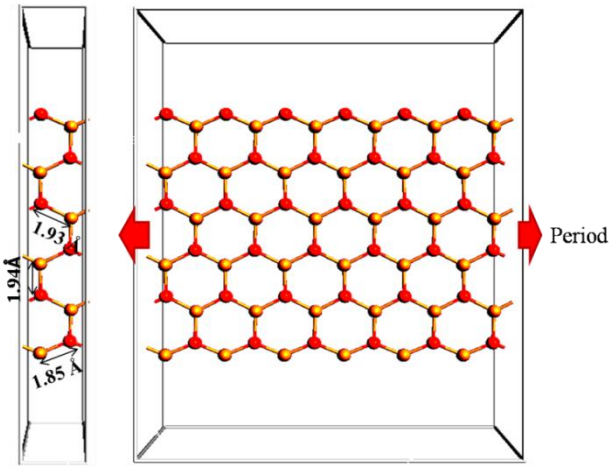

Figure 34: Bulk form of (1×1×6) supercell of (3,3) CuO ZNR

Table 8: The obtained values of different parameters of (n = 3 - 10, m = 0) CuO ZNRs (Yadav, et al., 2021)

Chirality (n, 0)	Width (Å)	BE/atom (eV)	MM/atom (μ_B)	Spin Polarization	Remarks
(3, 0)	8.14	-2.39	0.44	1	HMF*
(4, 0)	11.36	-2.42	0.28	1	HMF
(5, 0)	14.49	-3.09	0.19	0.41	FMF*
(6, 0)	17.93	-3.10	0.27	0.29	FMF
(7, 0)	21.21	-2.54	0.41	0.77	FMF
(8, 0)	24.75	-2.46	0.61	0.88	FMF
(9, 0)	28.70	-2.41	0.23	0.37	FMF
(10, 0)	32.09	-2.47	0.41	0.55	FMF

Table 9: The obtained values of different parameters of (n, m = n = 10) CuO ANRs (Yadav, et al., 2021)

Chirality (n, m = n)	Width (Å)	BE/atom (eV)	MM/atom (μ_B)	Spin Polarization	Remarks
(3, 3)	14.83	-2.44	0.71	1	HMF
(4, 4)	20.51	-3.33	0.51	0.62	FMF
(5, 5)	26.60	-2.47	0.39	1	HMF
(6, 6)	32.34	-3.13	0.25	0.26	FMF
(7, 7)	38.05	-3.16	0.84	0.70	FMF
(8, 8)	43.87	-2.51	0.71	1	HMF
(9, 9)	50.41	-2.36	0.53	0.56	FMF
(10, 10)	55.61	-3.17	0.47	0.50	FMF

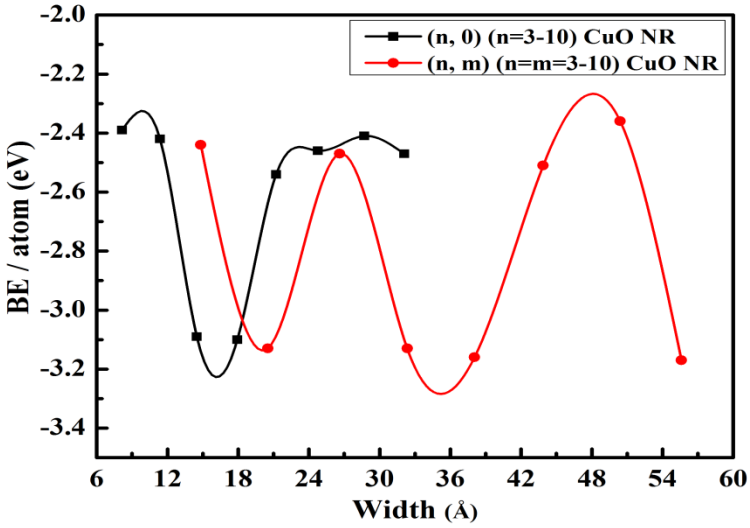

Figure 35: Binding energy as a function of width of (n = 3 – 10, m = 0) CuO ZNRs and (n, m = n = 3 - 10) CuO ANRs.

4.2.4.2 Electronic Property

The stable geometries were found for the study of electronic property. The electronic band structure and DOS profiles were used to distinguish conductor (metal), semiconductor, half - metal, and insulator (nonmetal). The present calculation reveals that CuO nanoribbons possess half - metallic and full metallic nature depending upon the chiralities in contrast to the bulk (Heinemann*et al.*, 2013; & Wang*et al.*, 2016). The plots of electronic band structures of both the zigzag and armchair forms of CuO NRs including their density of states profiles are shown in Figure 36(a - h) and Figure 37(a - h), respectively. The black and red colors individualy represent the majority and minority of electronic energy density of states, respectively. The electronic band structures and the density of states specify their metallic natures. Our calculation reveals that the nanoribbons are extended towards the bulk then CuO converts from conductor to semiconductor. Both type of CuO nanoribbons exhibit the metallic property due to the finite contribution of the oxygen atom (O) and the hybridization of both Cu - 3d and O - 2p states. Their hybridization states produce the peak value of DOS in the valance band whereas the Cu - 4s state produces the peak value of DOS in the conduction band at Fermi level.

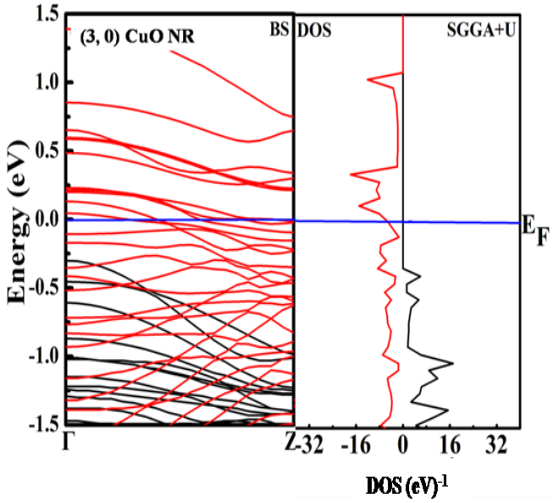
(3, 0) CuO NR
BS
DOS
SGGA+U
Energy (eV)
1.5
1.0
0.5
0.0
-0.5
-1.0
-1.5
E_F
Γ
Z
-32
-16
0
16
32
DOS (eV)^-1

(a)

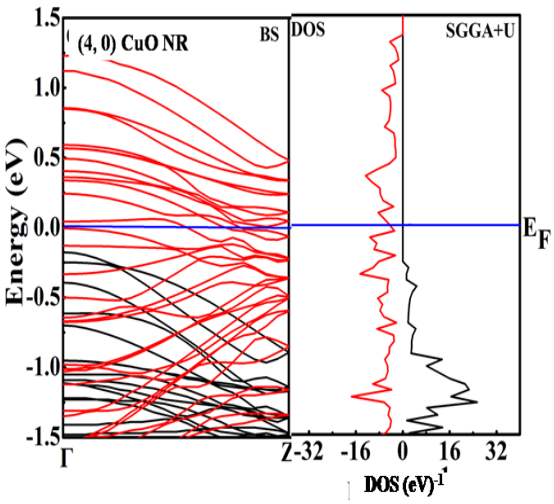
(4, 0) CuO NR
BS
DOS
SGGA+U
Energy (eV)
1.5
1.0
0.5
0.0
-0.5
-1.0
-1.5
E_F
Γ
Z
-32
-16
0
16
32
DOS (eV)^-1

(b)

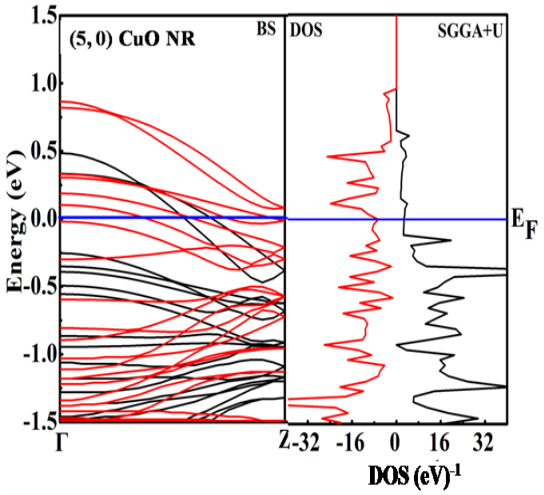
(5, 0) CuO NR
BS
DOS
SGGA+U
Energy (eV)
1.5
1.0
0.5
0.0
-0.5
-1.0
-1.5
E_F
Γ
Z
-32
-16
0
16
32
DOS (eV)^-1

(c)

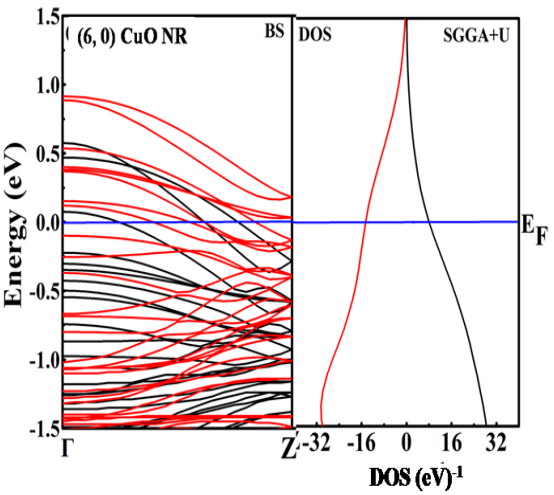
(6, 0) CuO NR
BS
DOS
SGGA+U
Energy (eV)
1.5
1.0
0.5
0.0
-0.5
-1.0
-1.5
E_F
Γ
Z
-32
-16
0
16
32
DOS (eV)^-1

(d)

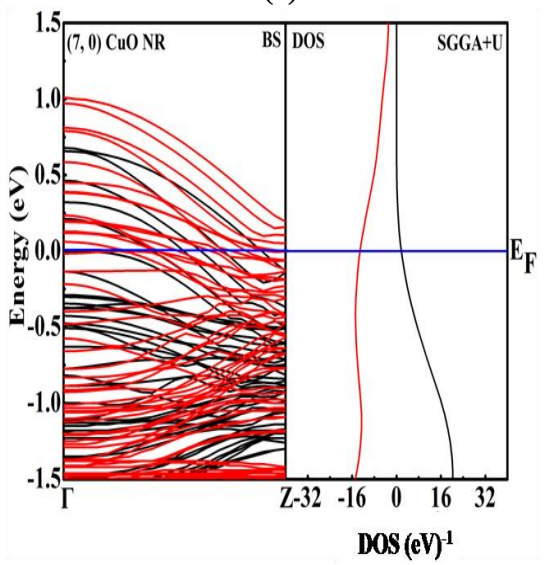
(7, 0) CuO NR
BS
DOS
SGGA+U
Energy (eV)
1.5
1.0
0.5
0.0
-0.5
-1.0
-1.5
E_F
Γ
Z
-32
-16
0
16
32
DOS (eV)^-1

(e)

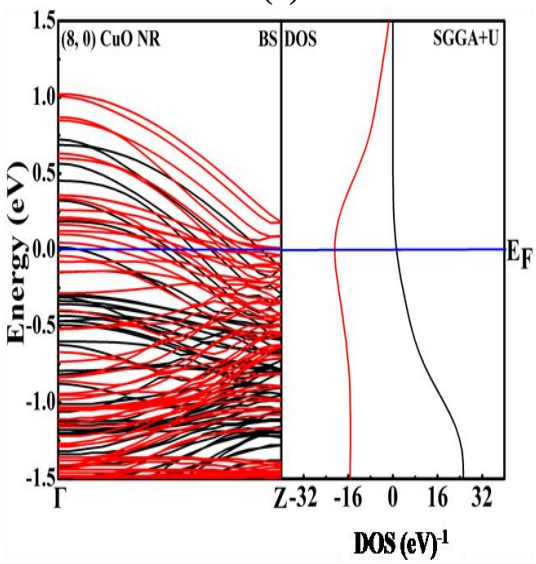
(8, 0) CuO NR
BS
DOS
SGGA+U
Energy (eV)
1.5
1.0
0.5
0.0
-0.5
-1.0
-1.5
E_F
Γ
Z
-32
-16
0
16
32
DOS (eV)^-1

(f)

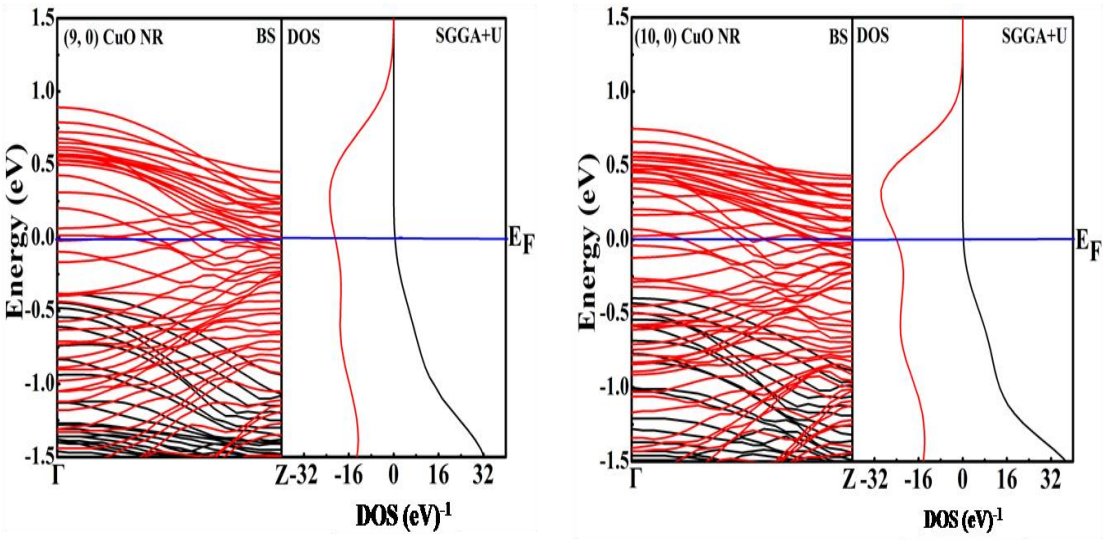

(g) (h)

Figure 36(a - h): Band structures with DOS profiles of (n = 3 – 10, m = 0) CuO ZNRs

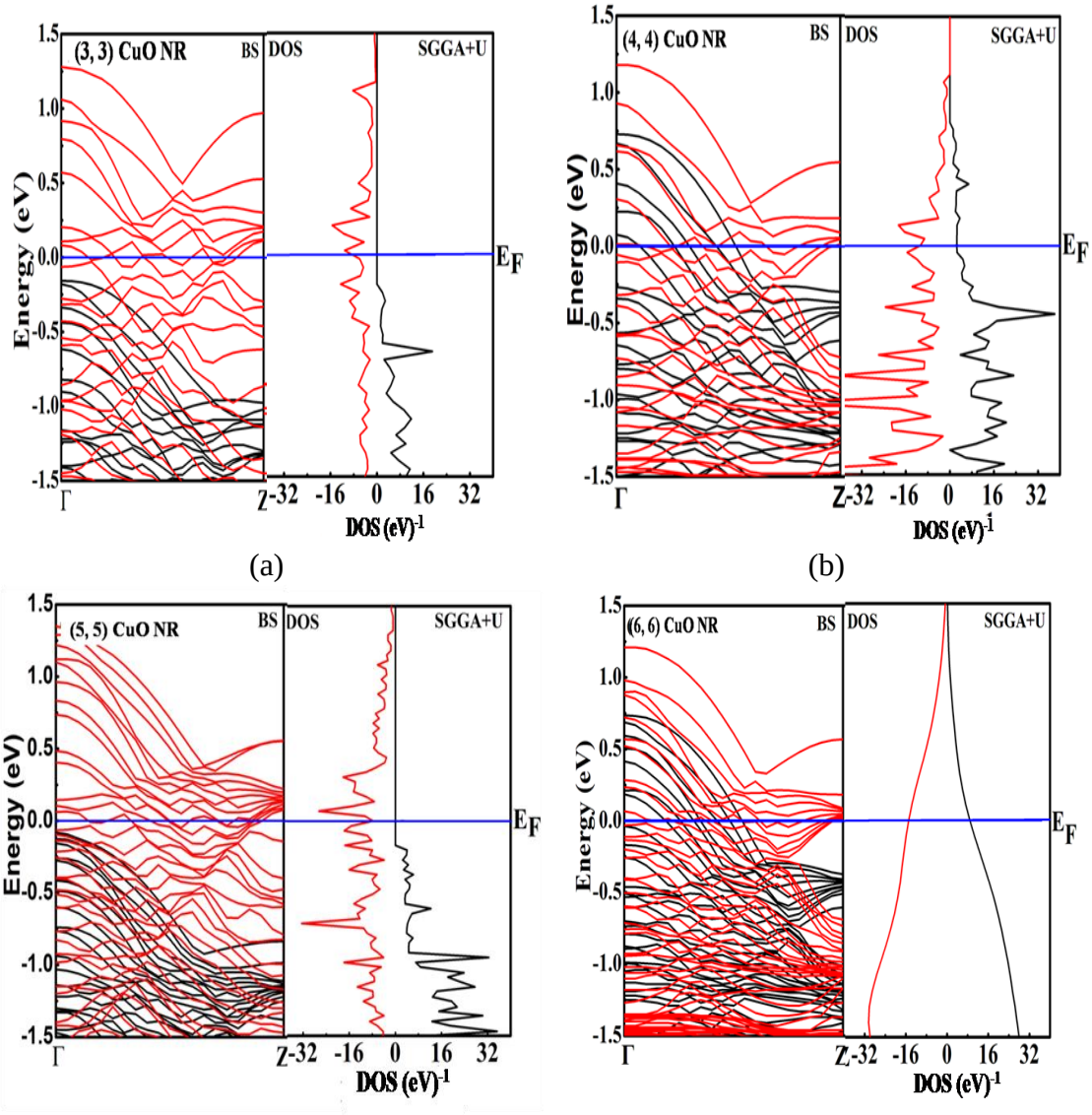

(a) (b)

(c) (d)

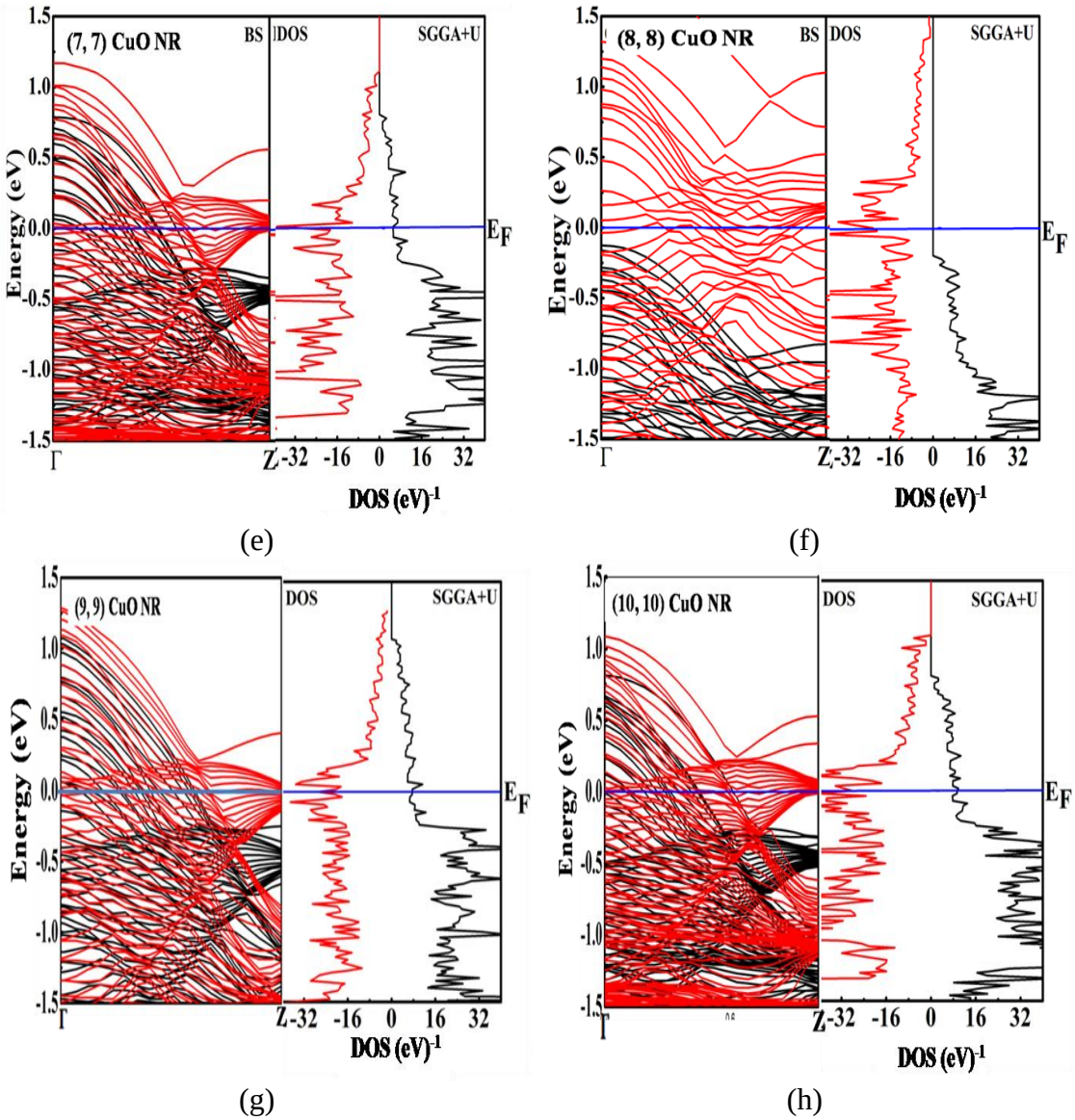

Figure 37(a - h): Band structures with DOS profiles of (n, m = n = 3 - 10) CuO ANRs

4.2.4.3 Magnetic Property

Both the electronic band structures and the density of states have confirmed the metallic natures of both zigzag and armchair forms of CuO nanoribbon. The magnetic moment per atom varies with the width of both CuO nanoribbons in Figure 38. The variation of magnetic moment ranges from 0.19 μ_B - 0.61 μ_B in zigzag and between 0.24 μ_B - 0.97 μ_B in armchair forms of CuO nanoribbon at the Fermi level. The net magnetic moment arises mainly due to the exchange splitting of Cu - 3d and O - 2p states. Total magnetic moment depends upon the magnetic moment of individual atoms Cu and O atoms following Hund's rule (Sanjeev, *et al.*, 2008; & Medel, *et al.*, 2011). The fluctuation of magnetic moment in different widths of CuO nanoribbon is

due to change in bond length of Cu and O. It is found that the magnitude of magnetic moment of armchair nanoribbon is more than that of zigzag nanoribbon of CuO in every case. The variation of spin polarizations of both zigzag and armchair CuO nanoribbons with width are either greater than 0 or equal to or less than 1, tabulated in Table 8 and Table 9 respectively and also depicted in Figure 39.

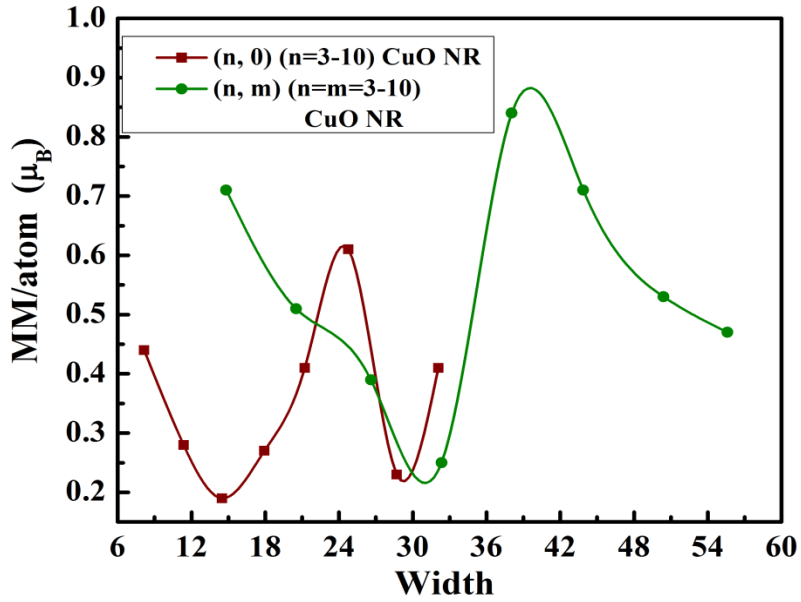

Figure 38: Magnetic moment as a function of width of (n = 3 - 10, m = 0) ZNRs and (n, m = n = 3 - 10) CuO ANRs

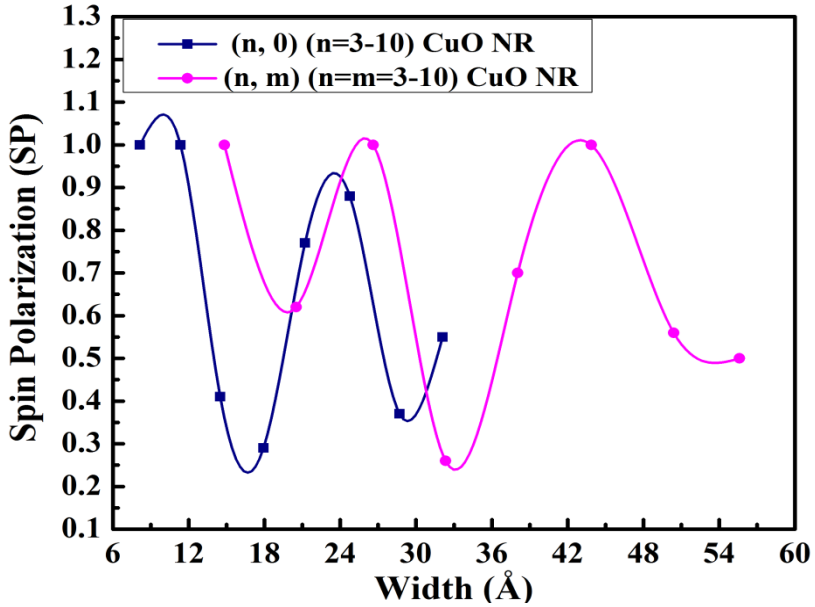

Figure 39: Spin polarization as a function of width of (n = 3 -10, m = 0) CuO ZNRs and (n, m = n = 3 - 10) CuO ANRs

The spin polarization distinguishes the half - metal (Groot, et al., 1983) and full - metal ferromagnetism in the cases of both zigzag and armchair forms of CuO nanoribbon. The observation confirms that the half - metal $(SP = 1)$ and full - metal $(0 < SP \leq 1)$ ferromagnetic natures of both CuO nanoribbons.

4.2.4.4 Discussion

The exchange - correlation functional SGGA + U under ATK - DFT approach was used to calculate the binding energy per atom, magnetic moments per atom, and spin polarization of CuO nanoribbons. The binding energy per atom varies between - 3.16 eV and - 2.18 eV concerning the width of nanoribbons. The magnetic moment varies between 0.19 μ_B and 0.61 μ_B in zigzag and, 0.24 μ_B between 0.97 μ_B in armchair forms, respectively. Comparatively, the magnetic moment of armchair is greater than that of CuO zigzag nanoribbon. The spin polarization is greater than 0 and equal to or less than 1, representing the half or full metal ferromagnetic CuO nanoribbon. The property of nanoribbon reports the suitable candidate for high - frequency devices, memory devices, sensors, etc (Gou, *et al.*, 2008).

4.3 Two - Dimensional Nanostructures of CuO

4.3.1 Structural, Electronic, and Magnetic Properties of Nanosheets of CuO

4.3.1.1 Structural Property

The different nanostructures of the zigzag and armchair forms of CuO nanosheet were modeled. The structural stability was confirmed through binding energy per atom of optimized confirmers. The optimized (1 × 3 × 4) supercell of (1, 0) zigzag and supercell (1 × 2 × 6) of (1, 1) armchair forms of CuO nanosheet are shown in Figure 40 and Figure 41, respectively. The calculated parameters of both types of CuO nanosheets with the help of equation (3.83) are listed in Table 10 and Table 11, respectively. The periods of supercell of CuO nanosheet increasing along B and C at constant C direction is the function of the area. The binding energy of the mentioned CuO zigzag nanosheet varies from - 2.57 eV to - 2.52 eV in SGGA + U and from - 29.28 eV to - 3.88 eV in SGGA indicating that SSGA fails to calculate the structural stability in some cases to general explanations. Similarly, the binding energy varies from - 3.20 eV to - 2.50 eV in SGGA + U and from - 3.16 eV to - 3.04 eV in SGGA

for armchair. The variation of binding energy is mainly due to the variation of bond length of Cu - O. The variation of binding energy with width is depicted in Figure 42. Also, the present calculation shows that the CuO zigzag nanosheet is more stable at higher (9, 0) chirality, whereas the CuO armchair nanosheet shows more stability at (3, 3) chirality in SGGA. The binding energy per atom remains fixed at around - 3 eV for both cases in SGGA + U calculation. The comparative analysis through SGGA + U confirms that the (7, 7) and (8, 8) CuO armchair nanosheets have relatively higher stability than their zigzag counterparts.

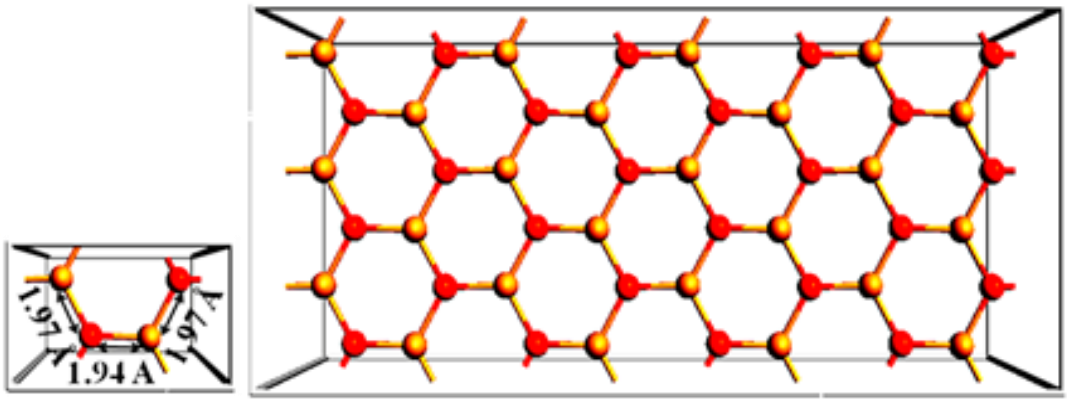

Figure 40: Supercell (1 × 3 × 4) of unit cell (1, 0) CuO ZNS

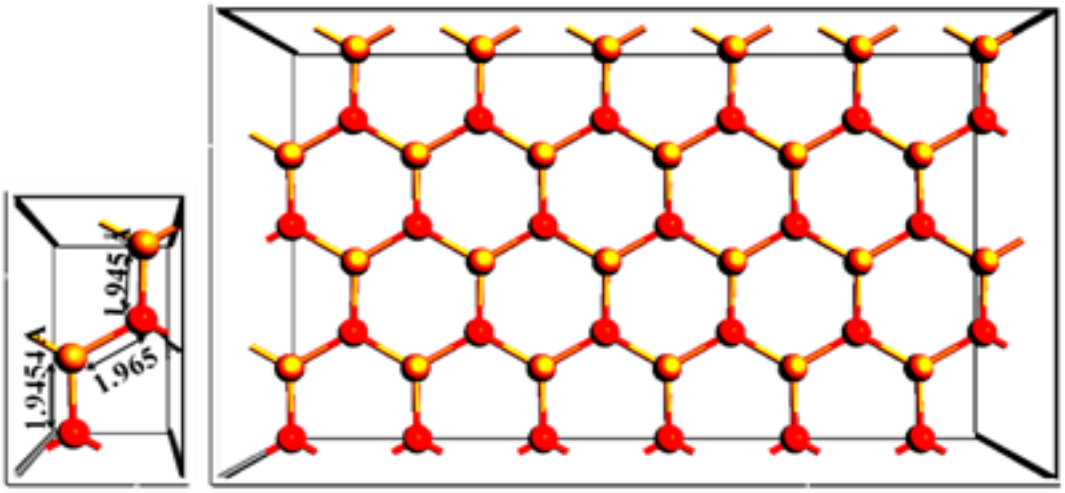

Figure 41: Supercell (1 × 2 × 6) of unit cell (1, 1) CuO ANS

Table 10: The width, binding energy, magnetic moment per atom, and spin polarization of CuO ZNSs with different chiralities (Yadav, *et al*., 2020)

S.N.	Zigzag Nanosheet of CuO	Widths (Å)	Binding/atom (eV)		Magnetic/atom (μ_B)		Spin Polarization	
			SGGA	SGGA + U	SGGA	SGGA + U	SGGA	SGGA + U
1	(1, 0)	1.97	- 3.89	- 2.57	0.71	0.76	0.61	1
2	(2, 0)	5.18	- 3.88	- 2.57	0.93	0.72	0.70	1
3	(3, 0)	8.52	- 3.89	- 2.56	0.66	0.69	0.58	1
4	(4, 0)	11.88	- 3.88	- 2.56	0.97	0.70	0.63	1
5	(5, 0)	15.25	- 3.88	- 2.56	0.93	0.76	0.61	1
6	(6, 0)	18.62	-25.81	- 2.56	1.19	0.73	0.69	1
7	(7, 0)	21.99	-22.42	- 2.55	0.72	0.76	0.58	1
8	(8, 0)	25.37	-29.28	- 2.52	0.90	0.68	0.64	1

Table 11: The width, binding energy, magnetic moment per atom, and spin polarization of CuO ANSs with different chiralities (Yadav, *et al*., 2020)

S.N.	Armchair nanosheet of CuO	Widths (Å)	BE/atom (eV)		MM/atom (μ_B)		Spin Polarization	
			SGGA	SGGA + U	SGGA	SGGA + U	SGGA	SGGA + U
1	(1, 1)	5.15	- 3.04	- 2.58	0.71	0.62	0.61	1
2	(2, 2)	10.84	- 3.08	- 2.50	0.59	0.71	0.59	1
3	(3, 3)	16.63	- 3.16	- 2.50	0.63	0.72	0.58	1
4	(4, 4)	22.46	- 3.11	- 2.50	1.53	0.69	0.75	1
5	(5, 5)	28.29	- 3.14	- 3.20	0.69	0.73	0.61	0.62
6	(6, 6)	34.14	- 3.09	- 2.50	0.70	0.65	0.61	1
7	(7, 7)	39.98	- 3.10	- 3.20	0.63	1.28	0.58	0.75
8	(8, 8)	45.83	- 3.09	- 3.20	1.21	0.74	0.72	1

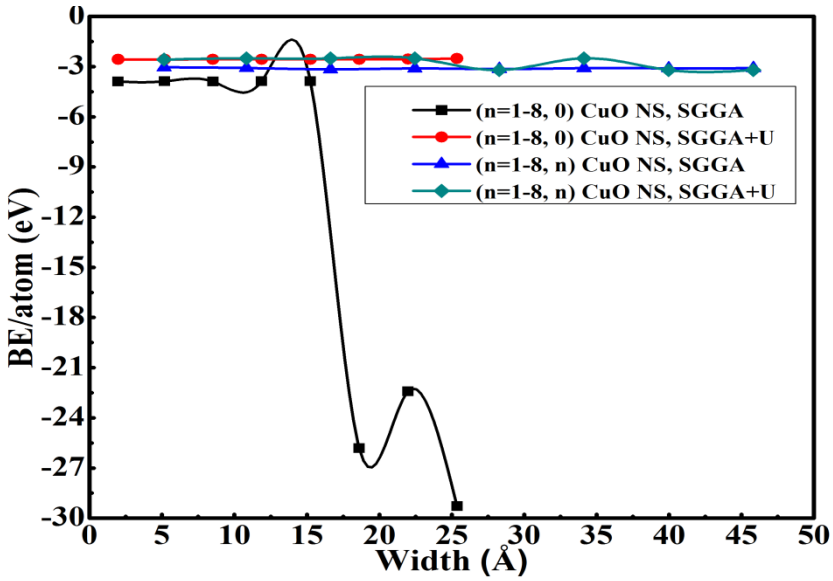

Figure 42: Binding energy per atom of CuO ZNS and CuO ANS as a function of width

4.3.1.2 Electronic Property

The electronic band structures and density of states of (n = 1 - 8, 0) CuO ZNSs have been investigated by using the SGGA and SGGA + U functionals, as shown in Figure 43(a - h) and Figure 44(a - h), respectively. In the same way, the electronic band structures and density of states of (n = 1 - 8, n) CuO ANSs have been found as shown in Figure 45(a - h) and Figure 46(a - h), respectively. The black and the red lines indicate the majority and the minority of electron energy density, respectively. Both CuO nanosheets show metallic behaviors due to the hybridization between Cu($3d^{10}4s^1$) and O($2p^4$) states and also the finite contribution of the O atom at the Fermi level (Paudel, et al., 2016). The density of states (DOS) have been also analyzed for the CuO nanosheets of the different chiralities near the Fermi level. The high and low peaks of DOS in the valance band and conduction band are due to the combined effect of Cu - 3d and O - 2p, and Cu - 4s states respectively.

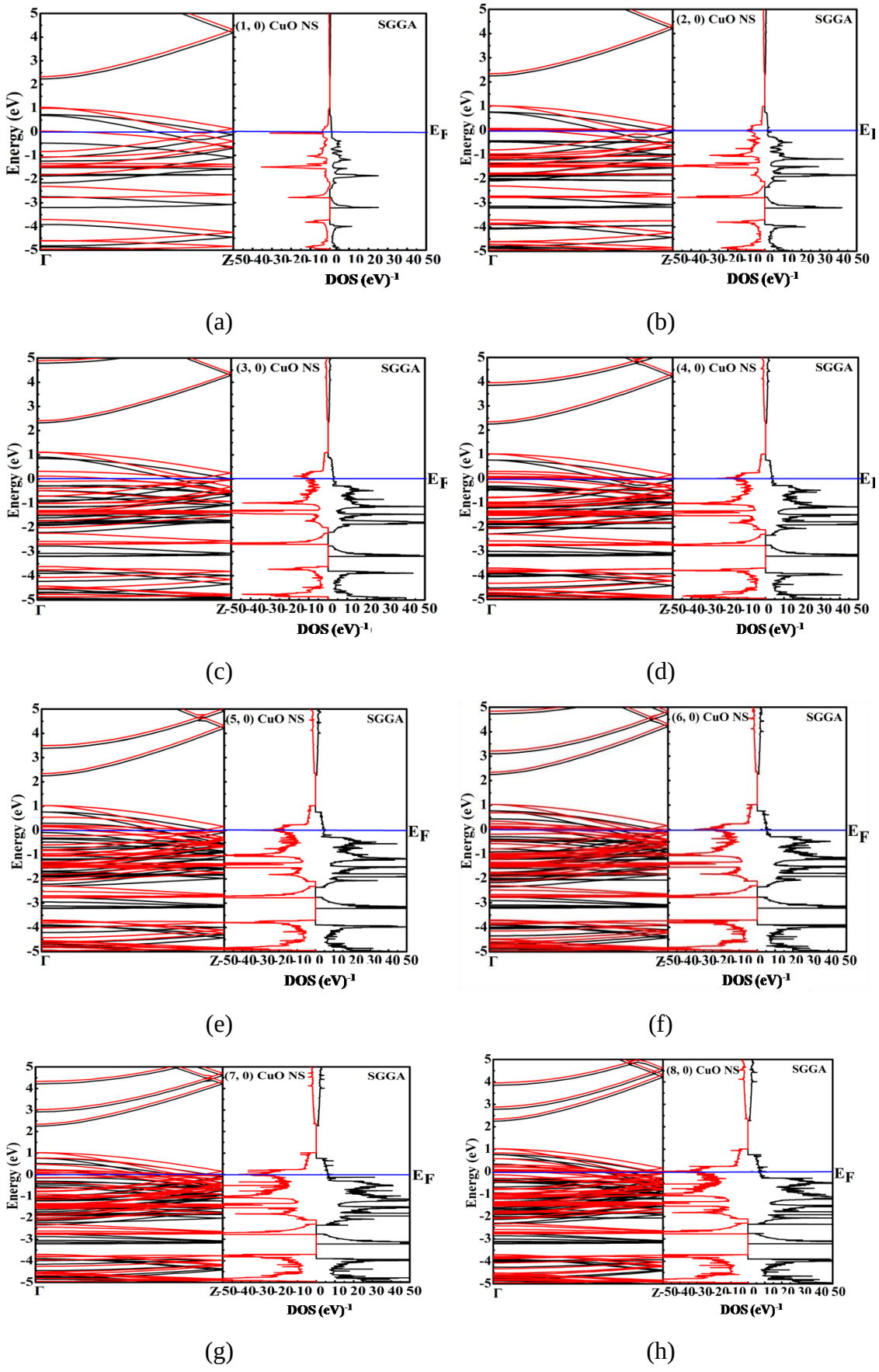

Figure 43(a - h): Band structures of the (n = 1 - 8, m = 0) CuO ZNSs with DOS profile, using SGGA

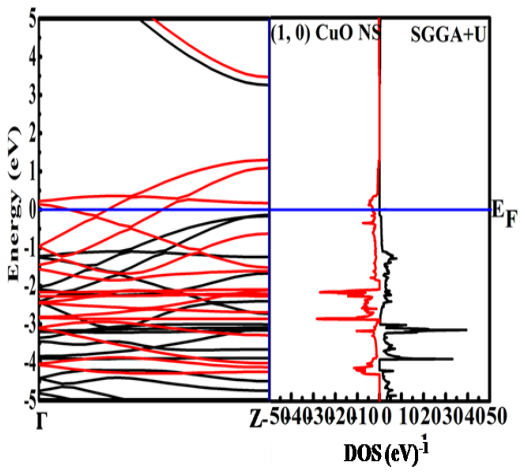
(1, 0) CuO NS
SGGA+U
Energy (eV)
E_F
Γ
Z
DOS (eV)^-1

(a)

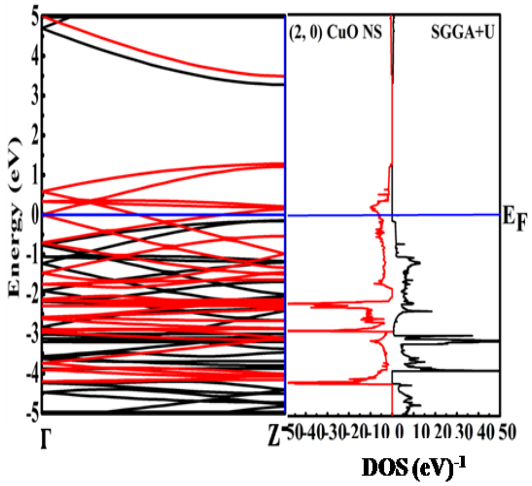
(2, 0) CuO NS
SGGA+U
Energy (eV)
E_F
Γ
Z
DOS (eV)^-1

(b)

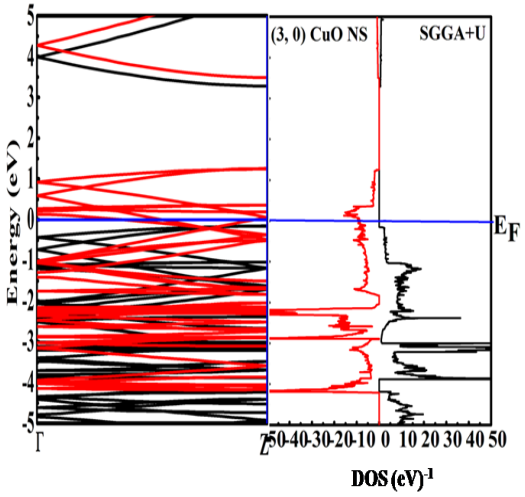
(3, 0) CuO NS
SGGA+U
Energy (eV)
E_F
Γ
Z
DOS (eV)^-1

(c)

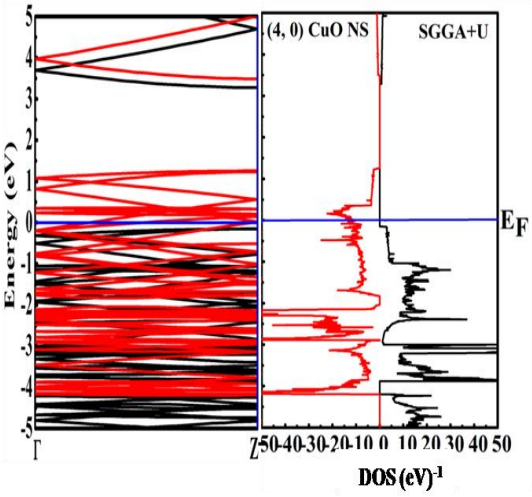
(4, 0) CuO NS
SGGA+U
Energy (eV)
E_F
Γ
Z
DOS (eV)^-1

(d)

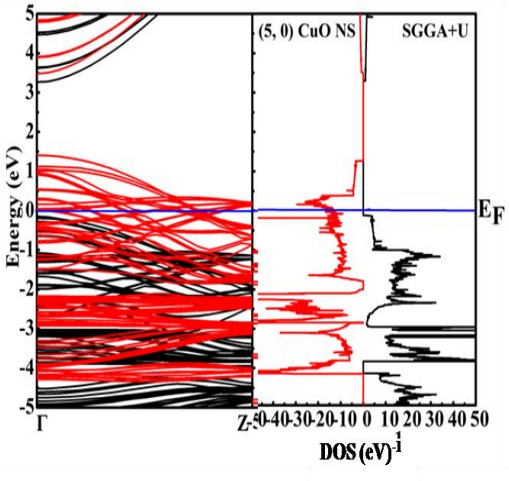
(5, 0) CuO NS
SGGA+U
Energy (eV)
E_F
Γ
Z
DOS (eV)^-1

(e)

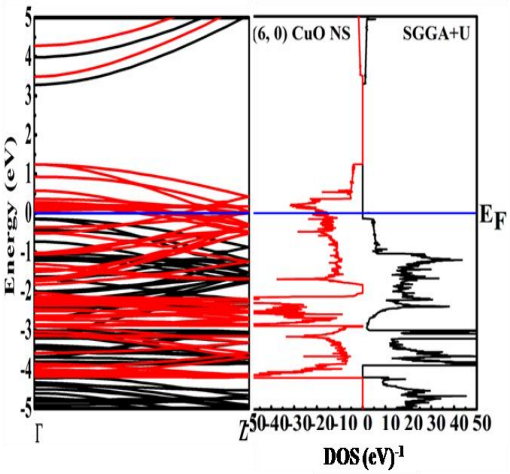
(6, 0) CuO NS
SGGA+U
Energy (eV)
E_F
Γ
Z
DOS (eV)^-1

(f)

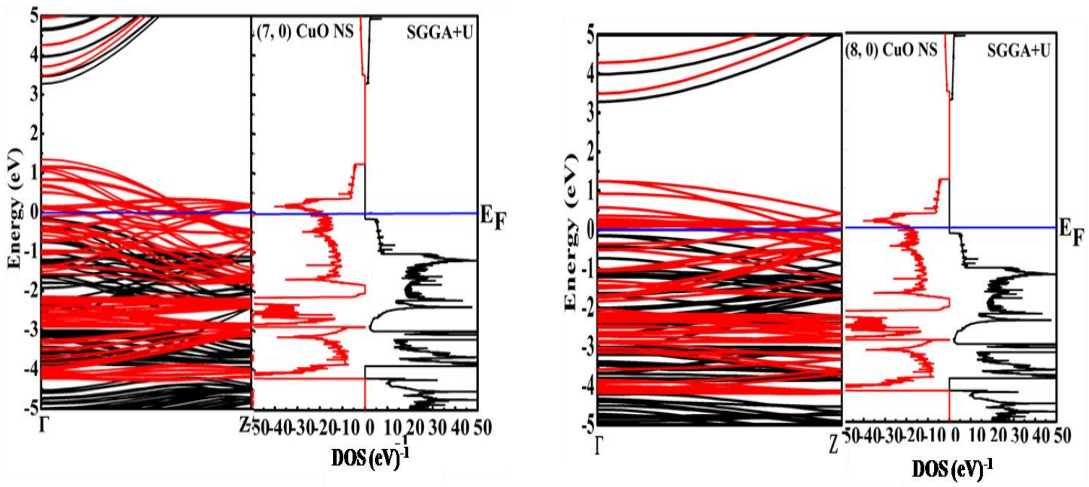

(g) (h)

Figure 44(a - h): Band structures of the (n = 1 - 8, m = 0) CuO ZNSs with DOS profile, using SGGA + U

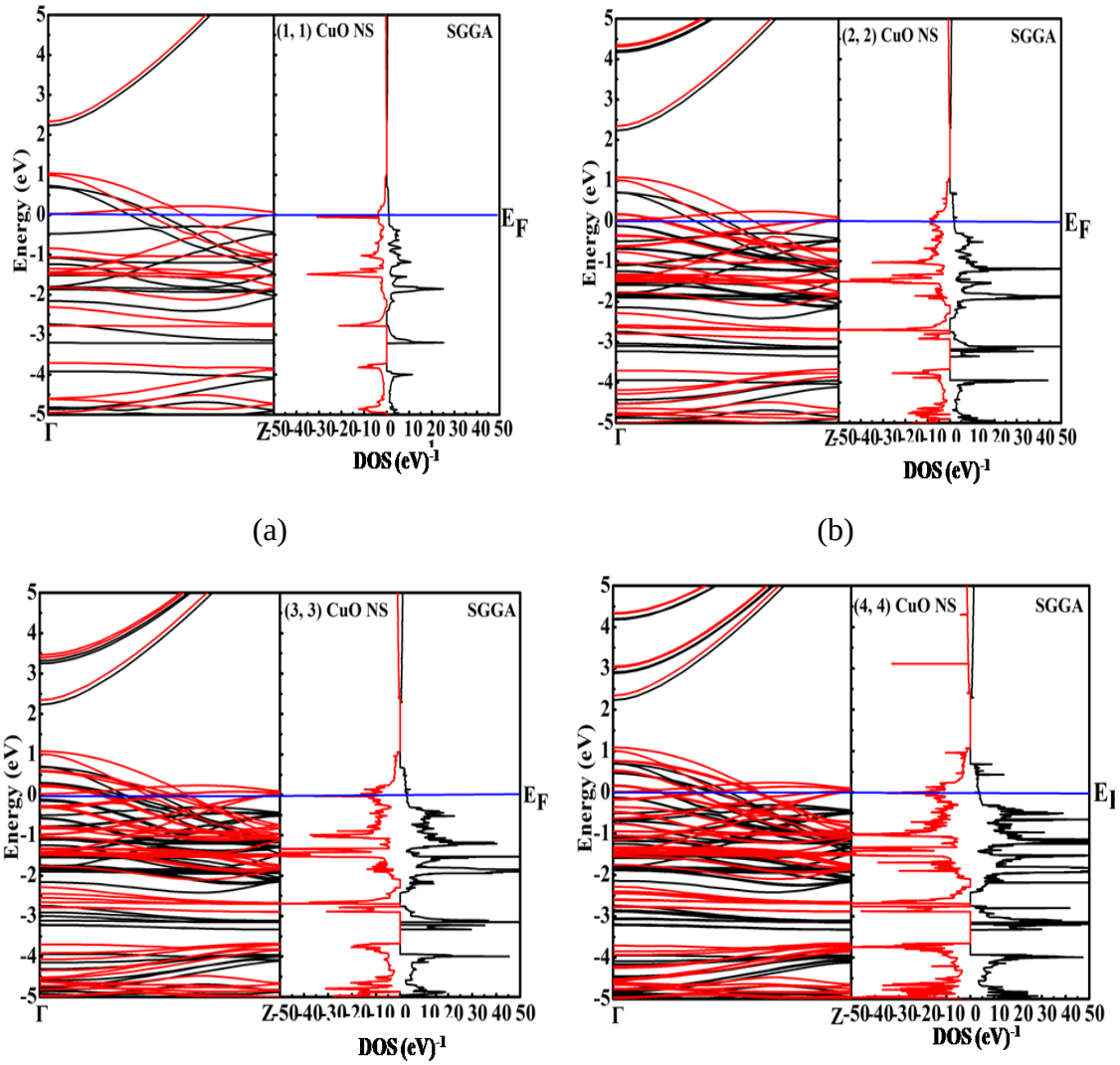

(a) (b)

(c) (d)

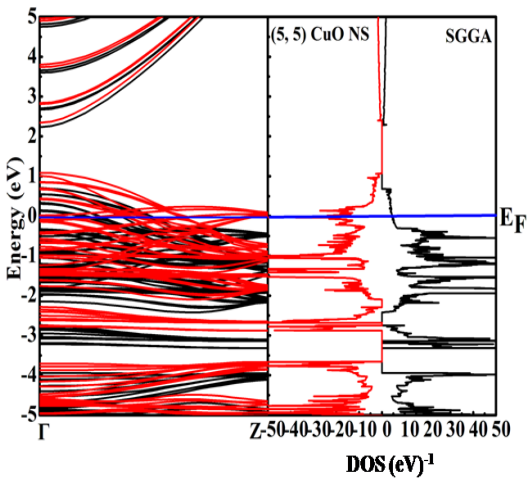

(e)

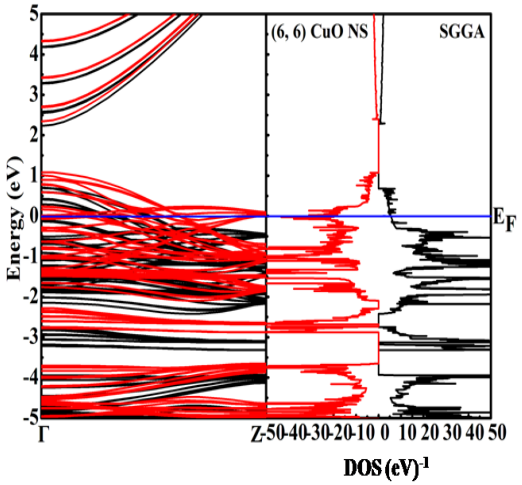

(f)

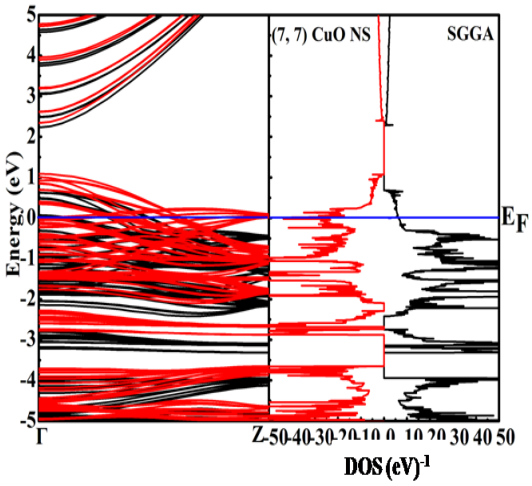

(g)

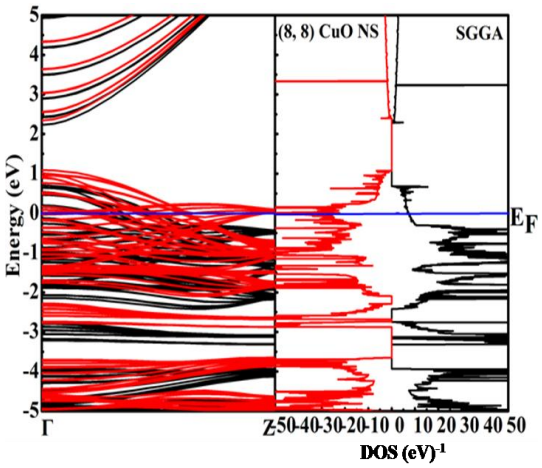

(h)

Figure 45(a - h): Band structures of the (n = 1 - 8, m = n) CuO ANSs with DOS profile, using SGGA

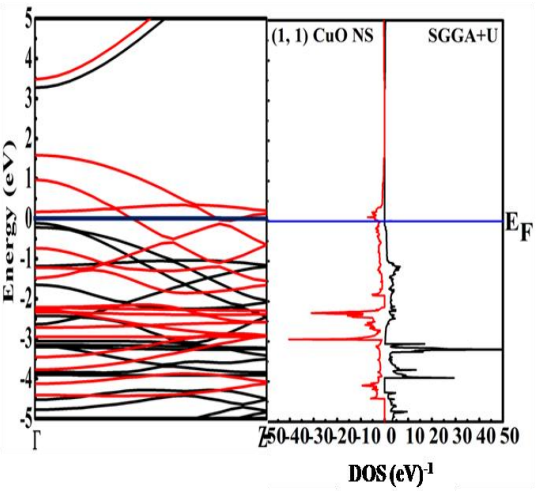

(a)

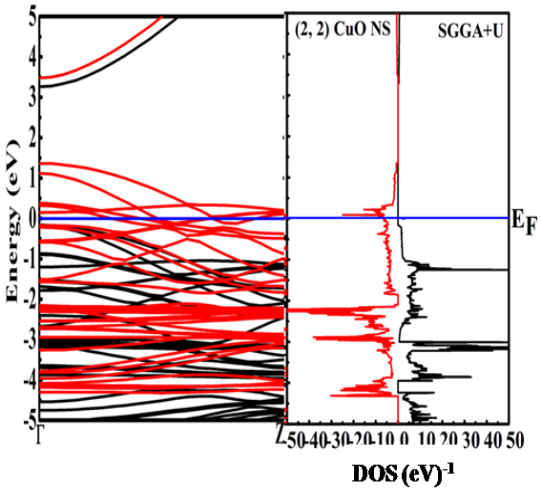

(b)

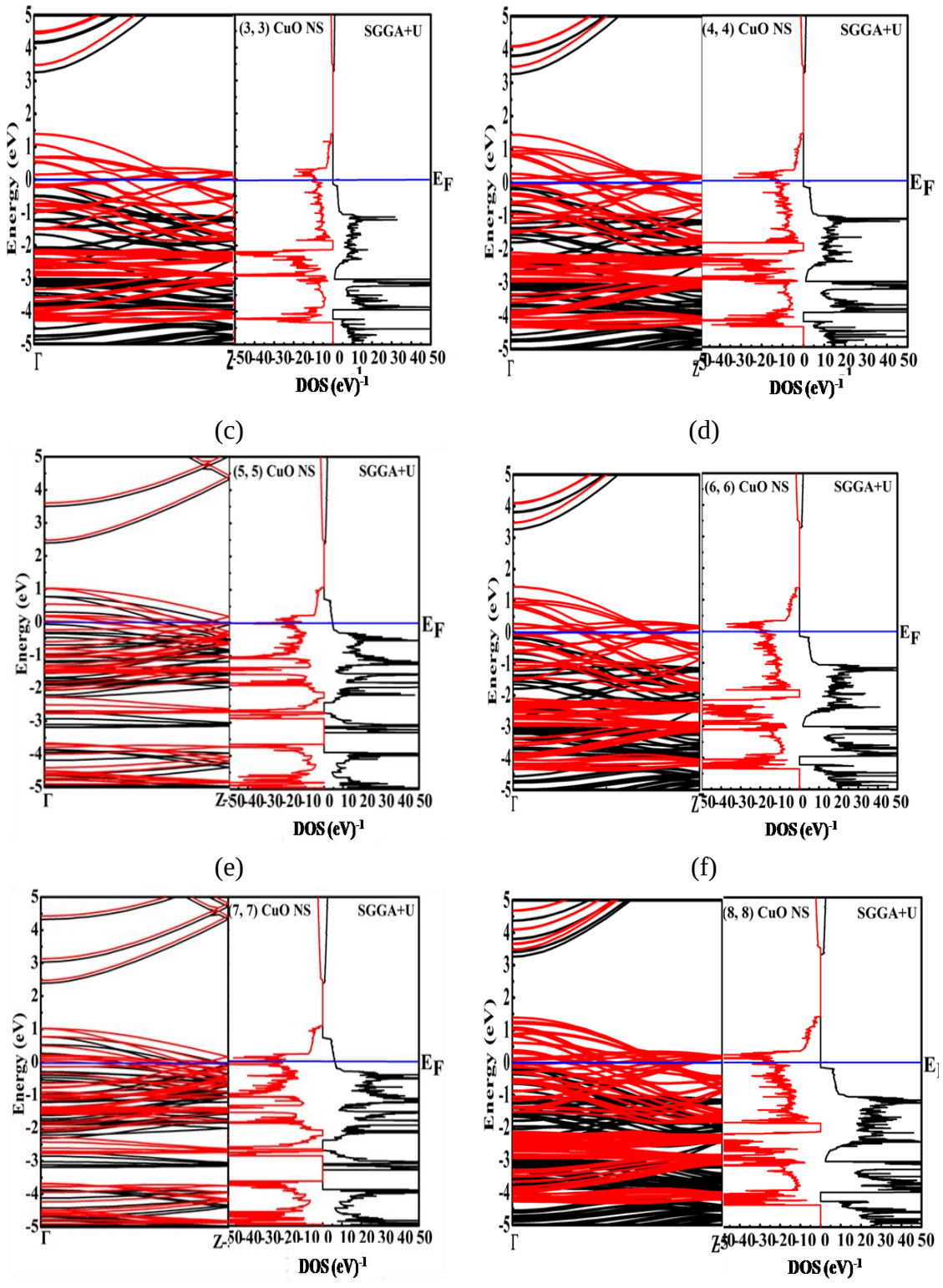

Figure 46(a - h): Band structures of the (n = 1 - 8, m = n) CuO ANSs with DOS profile, using SGGA + U

4.3.1.3 Magnetic Property

The electronic band structures and density of states, predict the metallic nature of the zigzag and armchair forms of CuO nanosheet. The calculated values of magnetic moments per atom and spin polarizations for the different chiralities of these nanosheets have been given in Table 10 and Table 11, respectively. The magnitude of the given magnetic moment and the spin polarization change with the width of both CuO nanosheets have been shown in Figure 47 and Figure 48, respectively. The highest value of magnetic moments for zigzag (6, 0) and armchair (4, 4) CuO nanosheets in SGGA are 1.19 μ_B and 1.53 μ_B, respectively, whereas the highest magnetic moments of zigzag (5, 0) and armchair (7, 7) of CuO nanosheets in SGGA + U are 0.76 μ_B and 1.28 μ_B respectively. Both types of nanosheets confirm the ferromagnetic nature, these are due to the exchange splitting of Cu - 3d and O - 2p states. The variation in the magnetic moment concerning the width of zigzag and armchair forms of CuO nanosheet is due to the variation in the bond length of Cu - O.

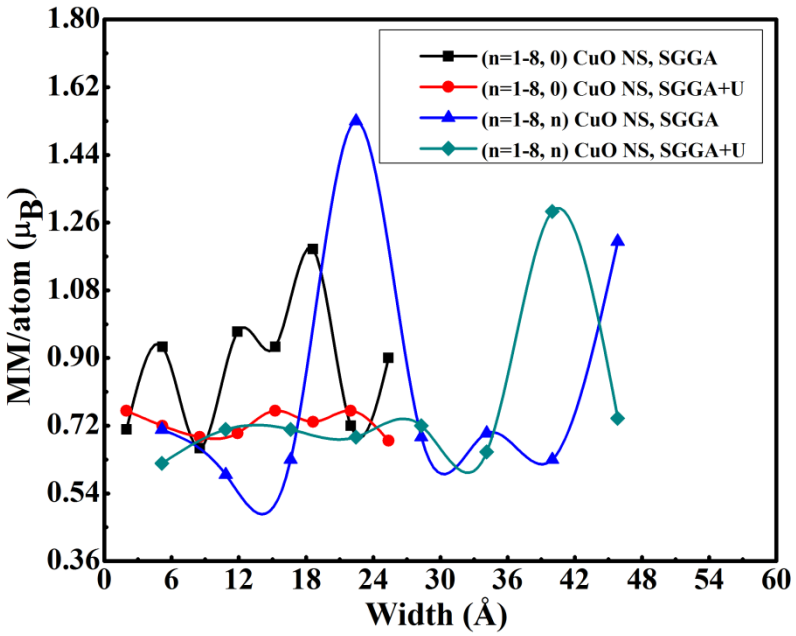

Figure 47: Magnetic moment of CuO ZNSs and CuO ANSs as a function of the width

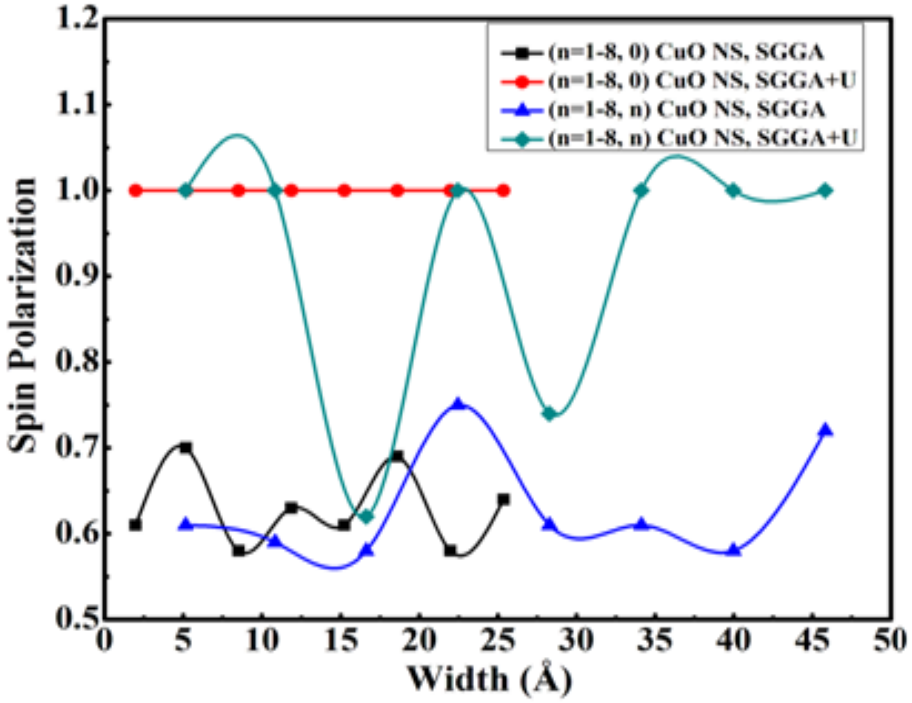

Figure 48: Spin polarization of CuO ZNSs and CuO ANSs as a function of the width

4.3.1.4 Discussion

The exchange - correlation functionals SGGA and SGGA + U were applied to optimize the structures of the zigzag and armchair forms of CuO nanosheet under DFT based ab - initio approach. The analysis of binding energies confirms the structural stabilities of CuO nanosheets. The electronic band structures and the density of states including spin - up and spin - down, show the metallic ferromagnetic natures. The CuO nanosheets show the outstanding magnetic moment and spin polarization at particular chirality. These are suitable candidates for gas sensors, batteries, energy storage devices as well as magnetic storage media (Ang, *et al*., 2009).

4.4 Three - Dimensional Structures of Cu_2O and CuO

4.4.1 Structural, Electronic, and Magnetic properties of bulks of Cu_2O and CuO

4.4.1.1 Structural Property

Bulks Cu_2O and CuO, were optimized and analyzed by using DFT through the VNL - ATK code under "First - Principles Study". The yellow and red colored spheres are copper and oxygen atoms in the crystal structures of bulks, respectively as shown in Figure 49(a, b). The computational values of lattice parameters (a, b, c, α, β and γ) and the minimum binding energies with their experimental values of both copper oxides have been reported in Table 12. These crystallographic parameters have been investigated through the exchange - correlation functionals LSDA + U, SGGA + U, and MSGGA using equation (3.83). The calculations show that the bulk Cu_2O is the most stable conformer obtained under the MSGGA with binding energy - 2.9525 eV and interatomic Cu - O distance 1.89 Å (cell volumes 83.58 $Å^3$). Similarly, the LSDA + U gives the most stable structure of bulk CuO with binding energy -3.10581 eV and interatomic Cu - O distance of 1.98 Å (Cell volume 74.76 $Å^3$). These parameters closely agreed with experimental values (Ghijsen, et al., 1988).

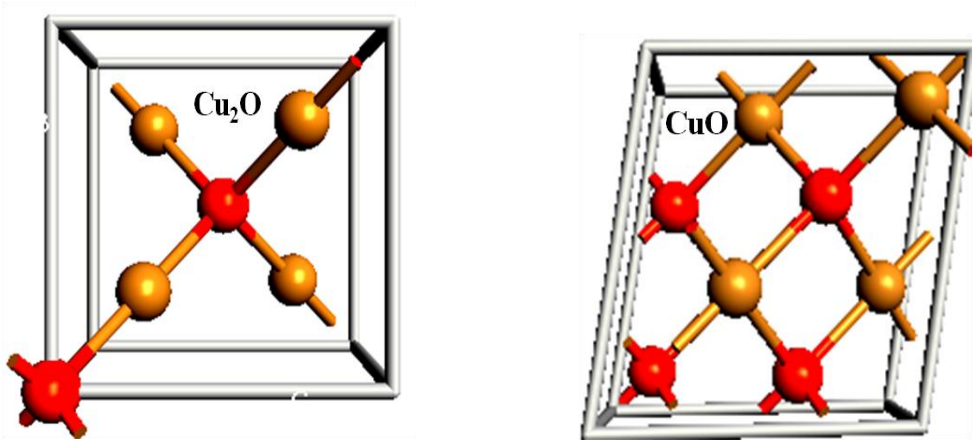

(a) (b)

Figure 49(a, b): The bulk configurations of (a) Cuprous Oxide (Cu_2O) and (b) Cupric Oxide (CuO)

Table 12: Comparative crystallographic properties of Bulks Cu_2O and CuO (Ghijsen, *et al*., 1988; Tran *et al*., 2014; & Wang, *et al*., 2016)

Physical quantity	Cu_2O (Pn3m, 225) Cubic				CuO (C2/c, 15) Monoclinic			
	Theoretical values			Experimental Values	Theoretical values			Experimental values
	LSDA +U*	SGGA +U*	SMGGA		LSDA +U**	SGGA +U**	SMGGA	
Lattice parameters								
a (Å}	4.27	4.56	4.37	4.25	4.81	4.65	4.78	4.67
b (Å}	4.27	4.56	4.37	4.25	3.19	3.41	3.25	3.42
c (Å}	4.27	4.56	4.37	4.25	5.03	5.11	5.19	5.13
α (°)	90	90	90	90	90	90	90	90
β (°)	90	90	90	90	104.81	99.54	99.21	99.59
γ (°)	90	90	90	90	90	90	90	90
Interatomic distances								
Cu - O	1.85	1.97	1.89	1.84	1.98	1.93	1.95	1.95
O - O	3.70	3.95	3.79	3.68	2.89	2.89	2.89	2.62
Cu - Cu	3.02	3.22	3.09	3.01	2.98	3.07	3.06	2.90
Cell volume (Å³)	77.83	94.71	83.58	76.49	74.76	79.88	79.52	81.17
Number of atoms in Cell	6	6	6	6	8	8	8	8
Binding energy/atom	-2.57	-2.95	-2.95	-	-3.11	-2.65	-2.19	-
Bandgap (eV)	0.70	0.56	0.79	2.0 - 2.2	2.42	2.22	2.20	1.2 - 1.9
Magnetic moment (μ_B)		0		0		0.80		0.68

Where, U^* = 7 eV and U^{**} = 7.5 eV

4.4.1.2 Electronic Property

The electronic band structures and DOS profiles of bulk Cu_2O have been found as a semiconductor with a band gap ranging from 0.56 eV to 0.79 eV. These values are less than the experimental result (2 eV - 2.17 eV) (Ghijsen, *et al*., 1988; & Heinemann, *et al*., 2013) as shown in Figure 50(a-c). Similarly, the bulk CuO shows semiconducting nature with band gap ranging from 2.2 eV to 2.42 eV. These are

slightly overestimated than the experimental result (1.2 eV - 1.9 eV) as shown in Figure 51(a-c). From the calculation, it is seen that the TB09 meta-GGA (MSGGA), a higher level approximation, provides more accurate values of electronic bandgaps 0.79 eV of Cu_2O and 2.20 eV of CuO at the Fermi level than both the LSDA + U and SGGA + U. Here, the MSGGA is more preferred for the calculation of bandgap at Fermi level.

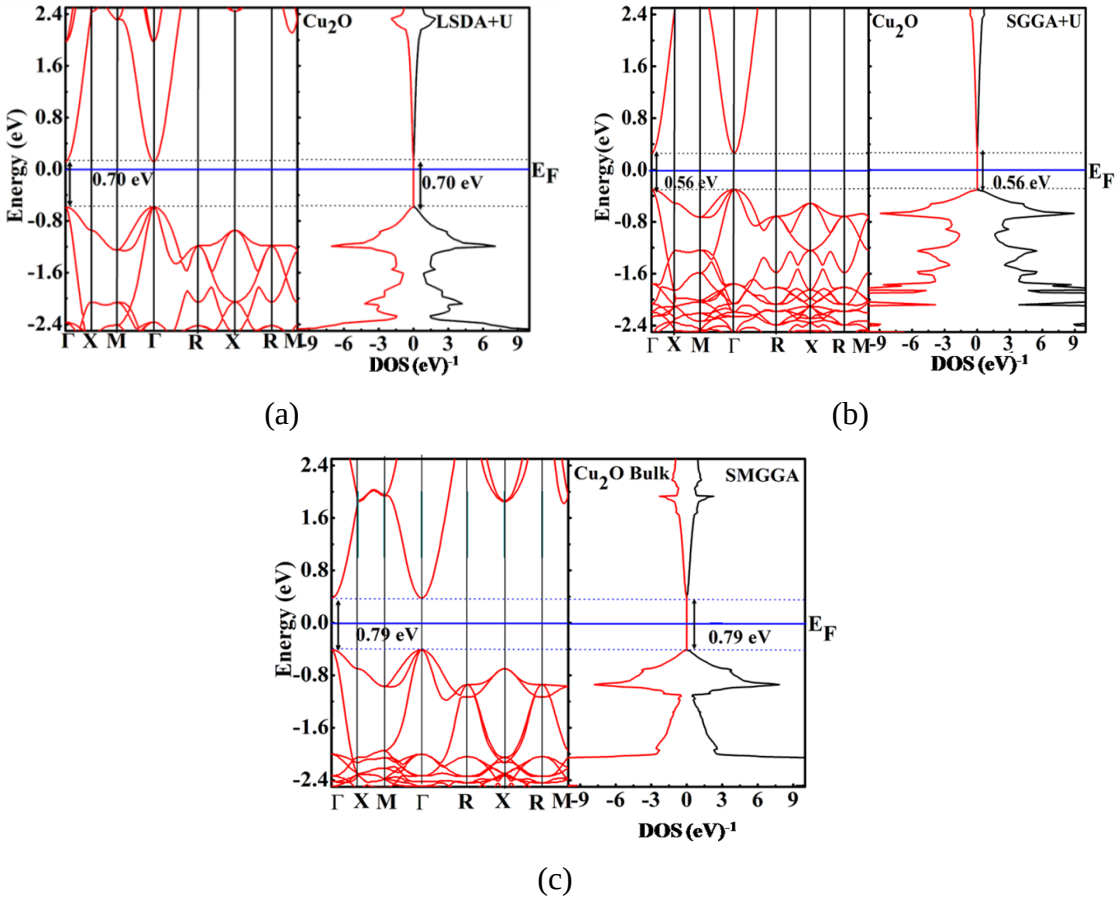

Figure 50(a-c): The electronic band structure with DOS of Cuprous Oxide (Cu_2O)

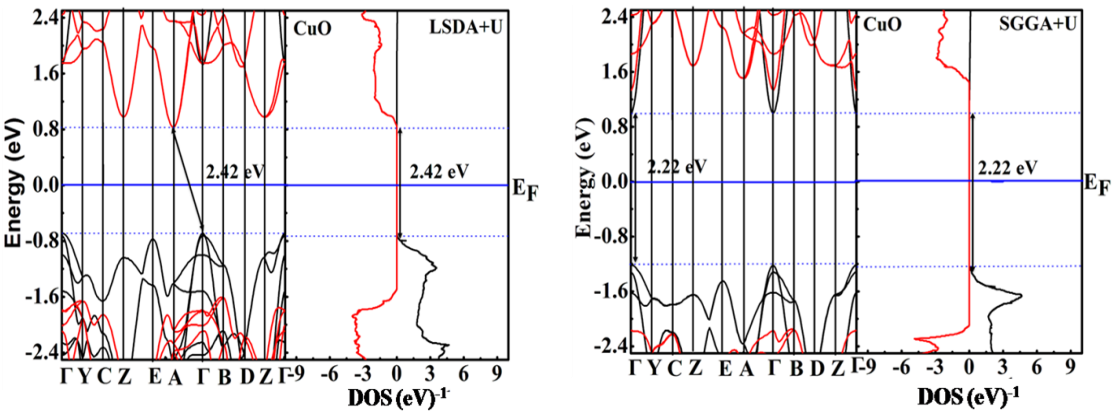

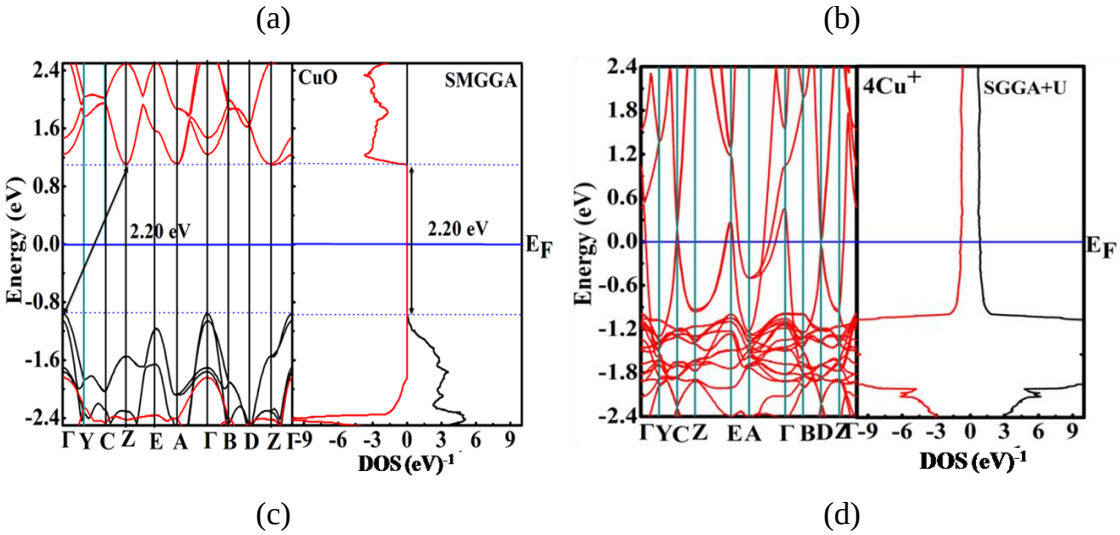

Figure 51(a - d): The band structure with DOS of cupric oxide (CuO)

4.4.1.3 Magnetic Property

From the DOS and PDOS plots, the bulk structures of Cu_2O and CuO show diamagnetic and antiferromagnetic nature respectively. The equal magnitudes of the up and down spins in Cu_2O cancel each other and show zero magnetic moments, whereas CuO is ferromagnetic with a magnetic moment per atom of 0.80 μ_B estimated through the Mulliken Population report.

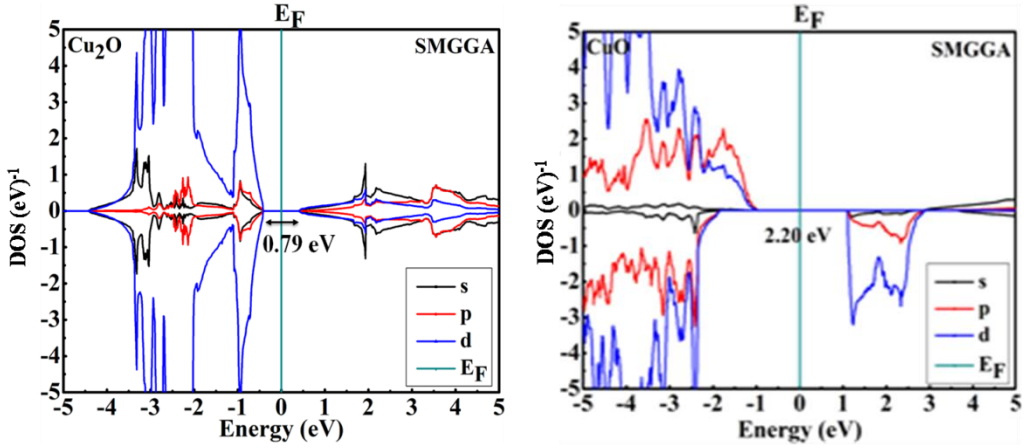

Figure 52(a, b): The PDOS profiles of bulk (a) Cu_2O and (b) CuO

The experimental and theoretical results are 0.68 μ_B and; 0.66 μ_B and 0.54 μ_B respectively (Ghijsen, *et al.*, 1988; & Heinemann, *et al.*, 2013). However, if we closely observed the nature of Cu^{2+} ions in CuO, we found there is antiferromagnetic ordering shown in Figure 51(d). The main cause of the ferromagnetic property of CuO

is due to unpair electron in $d_{x^2-y^2}$ orbital on $4Cu^{2+}$ ions. AFM ordering of $4Cu^{2+}$ ions in the unit cell of CuO is dominated by AFM nature. The magnetic moment so obtained are mainly due to the hybridization of $Cu(4d^{10}3s^1)$ and $O(2p^4)$ which provides the antiferromagnet at the ground state (Sha, *et al.*, 2021). The computational PDOS profiles of both copper oxides, shown in Figure 52(a, b)., also reports theoretical and experimental results of their magnetic behaviors.

4.4.1.4 Discussion

The functionals LSDA + U, SGGA + U, and MSGGA based on first - principles were applied for the study of Cu_2O and CuO. We have observed the p - type semiconducting diamagnetic nature in Cu_2O and the p - type semiconducting antiferromagnetic nature in CuO. The band gap of Cu_2O is of range 0.56 eV - 0.79 eV, less than that of experimental value 2 eV - 2.17 eV whereas the band gap of CuO is of range 2.20 eV - 2.42 eV approximately its experimental value 1.2 eV - 1.9 eV. The binding energies of Cu_2O and CuO are -2.95 eV and -2.19 eV, respectively. The bulks Cu_2O and CuO are used as potential candidates for photocell, storage media, gas sensors, and electronic devices (Tran, *et al*., 2014; & Sha, *et al*., 2021).

CHAPTER 5

5. CONCLUSION AND RECOMMENDATIONS

5.1 Conclusion

The present work focuses on the study of structural, electronic, and magnetic properties of the different morphologies of copper (I) and (II) oxides (Cu_2O and CuO) starting from nanostructure to bulk such as 0D, 1D, 2D and 3D systems. We perform the ab - initio calculations through DFT - based VNL - ATK tool with the different exchange - correlation functionals such as LSDA + U, SGGA + U and MSGGA for bulks, and SGGA + U for all other morphologies becase SGGA + U underestimates the band gap and is strong correlated to the systems. The final results are obtained from the calculation of the optimized nanostructures and from the analysis of electronic band structure and density of states. The overall conclusion obtained from the study is subdivided into four parts like conclusion for (a) 0D (b) 1D, (c) 2D and finally (d) 3D systems, separately as follows,

In the 0D system, we have focused on the structural stability of the nanoclusters like $(Cu_2O)_1$, $(Cu_2O)_3$, $(CuO)_2$, and $(CuO)_6$. Out of them, $(Cu_2O)_2$ and $(CuO)_4$ are obtained to be more stable. Both are semiconductors in nature, however, the $(Cu_2O)_1$ shows diamagnetic behavior, and others $(Cu_2O)_2$, $(Cu_2O)_3$, $(CuO)_2$, $(CuO)_4$, and $(CuO)_6$ show metallic with ferromagnetic behavior, respectively. The nanoclusters $(Cu_2O)_2$ and $(CuO)_4$ having magnetic moments per unit cell 2 μ_B and 4 μ_B respectively with unit spin polarizations are half - metals. The total maximum energy also increases concerning the increasing number of atoms. The nanoclusters can play a key role in various environmental processes, in the synthesis of technological materials, and also contribute to health hazards associated with airborne fine particles.

In the 1D system, Cu_2O nanowires of diameters 5 and 6 Å are full metallic in nature whereas the nanowire of diameter 4 Å having binding energy of 2.08 eV / atom and total magnetic moment 8 μ_B is most stable half - metallic ferromagnet. Magnetic moment varies with the diameter and all the nanowires are found to be with ferromagnetic properties. In particular, the magnetic moment per atom of the nanowire of diameter 4Å is 0.36 μ_B . Due to their unique geometry and physical property, the Cu_2O nanowires can be used for many novel applications such as gas sensing, solar energy conversion, and magnetic storage media. Similarly, in the case

of CuO chiral nanotubes (CNTs), the (2, 1) CuO nanotube with magnetic moment 0.36 μ_B shows the semiconducting behavior while the CuO CNTs of chiralities (3, 1), (3, 2), (4, 1), (4, 2) with magnetic moments per unit cell 8 μ_B , 13 μ_B, 5 μ_B, and 10 μ_B respectively, show half - metal ferromagnetic behaviors. The magnetic moment per atom varies with varing chirality of (n = 2, 3, 4, m = 1, 2) CuO CNT. The structural stability shows that (2, 1) CuO CNT with binding energy 2.63 eV / atom has stronger stability than others. The CuO nanotubes, popular 1D nanomaterials, having high potential can be used for chemical and biological sensing, solar energy conversion, high - temperature superconductivity, heterogeneous catalysis, etc. Furthermore, the investigation of CuO nanoribbons (NRs) indicates that they are metallic or half - metallic depending on the chiralities but all the nanoribbons are found as ferromagnetic natures. In case of CuO ZNRs, the range of magnetic moments per atom of (n = 3 - 10, m = 0) CuO ZNRs have been found between 0.19 μ_B - 0.61 μ_B , whereas the magnetic moments of (n = 3 - 10, m = n) CuO ANRs between 0.24 μ_B - 0.97 μ_B . The magnetic moments per atom of CuO ANRs are higher than those of CuO ZNRs. The spin polarization, in both cases, is greater than 0 and equal to or less than 1, confirm the half or full metal ferromagnetic nature of nanoribbons. The binding energy per atom varies between 2.18 eV and 3.16 eV concerning with the width, confirms the stability of selected nanostructures. The CuO nanoribbons, promising candidates, can be used for high - performance electrochemical capacitors, and gas sensors.

In the 2D system, the zigzag and armchair forms of CuO nanosheets show metallic and ferromagnetic behaviors. The magnetic moment per atom of CuO ZNS varies irregularly between 0.66 μ_B and 1.19 μ_B, whereas for CuO ANS, between 0.59 μ_B and 1.53 μ_B. The addition of the mean - field Hubbard correction (U) changes these variations from 0.68 μ_B to 0.76 μ_B in ZNSs and from 0.62 μ_B to 1.28 μ_B in ANSs, respectively. The spin polarization greater than 0 and equal or less than 1 identify the half and full - metal ferromagnetic nanomaterials respectively. The CuO nanosheets are also 2 - dimensional high potential candidates for gas sensing of various flammable gases like ethanol, gasoline, acetone, H_2S, batteries, novel energy storage devices, photocatalysts, non - enzymatic glucose sensors.

Finally, in the 3D system, the different exchange - correlation functionals as LSDA + U, SGGA + U, and MSGGA have been used for the study of both the bulks

Cu_2O and CuO. The calculations have confirmed the diamagnetic (MM / atom = 0) and the ferromagnetic (MM / atom = 0.80 μ_B) behaviors for both the p - type semiconductors Cu_2O and CuO respectively whereas the order of isolated $4Cu^{2+}$ ions in the unit cell shows antiferromagnetic behavior. we have measured the band gaps of Cu_2O as 0.70 eV, 0.56 eV, and 0.79 eV respectively which underestimate the experimental result of 2 eV - 2.2 eV for Cu_2O. Similarly, they have obtained the band gaps of CuO as 2.42 eV, 2.22 eV, and 2.20 eV, respectively which approximately, agrees with the experimental value of 1.2 eV - 1.9 eV for CuO. Our investigations reveal that all the materials start from nanoclusters to bulks are the potential candidates for the applications of semiconductor devices, magnetic devices, spintronics devices and so on.

Present result supports that bulk of Cu_2O is a suitable candidate for various applications like photocatalytic, photovoltaic, perovskite solar cell, thermoelectric, fungicide, and anti-fouling paints. Similarly, the bulk of CuO is the vital candidate for the applications of gas sensors, electrode materials, magnetic ceramics, hydrogen storage materials, solar cells, and photocatalysis.

In particular, the crystallographic or molecular structures have been predicted with an accuracy approaching that of the computation structural techniques. Rather a good accuracy of ATK - DFT calculations makes them suitable for the prediction of the other properties, especially in situations when the experimental approach may be difficult or impossible.

5.2 Recommendations

The nanostructures of Copper oxides demonstrate excellent structural, electronic, and magnetic properties and exhibit promising candidates for wide fields of application. They may show other peculiar properties which will be new and interesting problems. Hence, they are recommended for further study of

- Further study on optical, electrical, thermal, mechanical related properties
- Comprehensive theoretical and experimental study
- Possible applications in photoelectronics, sensors, and others
- Applications in green energy and future generation technologies

CHAPTER 6

6. SUMMARY

Finally, the overall findings, investigations, and predictions from the present study copper (I) and (II) oxides (Cu_2O and CuO) are summarized as follows,

1. We have studied the structural, electronic, and magnetic properties of nanoclusters (0D); nanowires, nanotubes, and nanoribbons (1D), nanosheets (2D) of both Cu_2O and CuO through SGGA + U and their bulks through LSDA + U, SGGA + U, and MSGGA under the first principles study.
2. **In the 0D system**, we have observed the structural stability of the nanoclusters $(Cu_2O)_1$, $(Cu_2O)_2$, $(Cu_2O)_3$, $(CuO)_2$, $(CuO)_4$, and $(CuO)_6$. Out of them $(Cu_2O)_2$, and $(Cu_2O)_3$ are found to be more stable in accordance with their binding energy. The $(Cu_2O)_1$ shows diamagnetic and semiconducting behaviors whereas all others $(Cu_2O)_2$, $(Cu_2O)_3$, $(CuO)_2$, $(CuO)_4$, and $(CuO)_6$ show ferromagnetic behaviors, respectively. The magnetic moments of the nanoclusters $(Cu_2O)_2$ and $(CuO)_4$ are 0.33 μ_B and 0.50 μ_B respectively with spin polarization 1. The total maximum energy increases concerning an increase in the number of atoms. The nanoclusters can be applied in environmental processes, in a synthesis of technological materials, and health hazards.
3. **In the 1D system**, Cu_2O nanowires having diameters 5 and 6 Å are full metal in which the nanowire of diameter 4 Å having half metallic nature is most stable with binding energy 2.08 eV/atom. Its magnetic moment decreses with the increasing diameter of the ferromagnetic nanowires. In particular, the magnetic moment per atom of the nanowire of diameter 4Å is 0.36 μ_B. It can be used in applications as gas sensing, solar energy conversion, and magnetic storage media.

   In the case of CuO chiral nanotubes, the (2, 1) CuO nanotube having magnetic moment 0.36 μ_B is the semiconductor whereas the (3, 1), (3, 2), (4, 1), (4, 2) CuO nanotubes are with magnetic moments per atom 0.31 μ_B, 0.35 μ_B, 0.36 μ_B, and 0.37 μ_B show half - metal ferromagnetic behaviors. The magnetic moment per atom is varies with the varing diameter of (n = 2, 3, 4, m = 1, 2)

CuO chiral nanotubes. The structural stability shows that the (2, 1) CuO chiral nanotube with binding energy 2.63 eV / atom has stronger stability than other nanotubes. The CuO nanotubes are being used for chemical and biological sensing, solar energy conversion, high - temperature superconductivity, and so on.

Furthermore, the investigation of CuO nanoribbons indicates that they are ferromagnetic full or half - metal depending on their chiralities. In the case of CuO zigzag nanoribbons, magnetic moments per atom ranges from 0.19 μ_B - 0.61 μ_B whereas the value of magnetic moments ranges from 0.24 μ_B - 0.97 μ_B in the CuO armchair nanoribbons. The magnetic moment per atom of CuO ANR is higher than that of the magnetic moment per atom of CuO ZNR. The spin polarization, in both cases, is greater than 0 and equal to or less than 1, confirming the half or full metal ferromagnetic nature of nanoribbons. The binding energy per atom varies between 2.18 eV and 3.16 eV for the width, confirming the stability of the nanoribbons. They can be used for high - performance electrochemical capacitors, and gas sensors.

4. **In the 2D system**, the zigzag and armchair forms of CuO nanosheets show metallic and ferromagnetic behaviors. The magnetic moment per atom of CuO zigzag nanosheet varies irregularly between 0.66 μ_B and 1.19 μ_B, whereas for CuO armchair nanosheet, between 0.59 μ_B and 1.53 μ_B. The addition of the mean - field Hubbard correction (U) changes this variation from 0.68 μ_B to 0.76 μ_B in zigzag and from 0.62 μ_B to 1.28 μ_B in armchair nanosheets, respectively. The computed spin polarization as unity or less than unity identifies the ferromagnetism in these nanomaterials. The CuO nanosheets could be used for gas sensing of various flammable gases like ethanol, gasoline, acetone, H_2S, batteries, novel energy storage devices, photocatalysts, and non - enzymatic glucose sensors.
5. **In the 3D system**, the different exchange - correlation functions are implemented for the study of both the bulks Cu_2O and CuO. The calculations have confirmed the diamagnetic and the ferromagnetic behaviors of both the p - type semiconductors Cu_2O and CuO respectively whereas the resultant ordering of isolated $4Cu^{2+}$ ions in the unit cell of CuO reports antiferromagnetic behavior. The measured band gaps of Cu_2O through

LSDA + U, SGGA + U and SMGGA functionals are 0.70 eV, 0.56 eV and 0.79 eV respectively contradict with experimental result 2 eV - 2.2 eV whereas the energy band gaps of CuO are 2.42 eV, 2.22 eV, and 2.20 eV, respectively agree with the experimental result 1.2 eV - 1.9 eV. The bulks Cu_2O and CuO are being used in various applications like photocatalytic, photovoltaic, perovskite solar cell, thermoelectric, fungicide, anti - fouling paints, electronics, gas sensors, electrode materials, magnetic ceramics, hydrogen storage materials, solar cell, photocatalysis.

6. The explored properties of different morphologies of copper oxides reveal that all the materials starting from nanocluster to bulk are potential candidates for the applications like semiconductor devices, magnetic devices, spintronic devices, photocell, sensors, solar energy conversion, telephones, high-frequency devices, electrodes, energy storage devices, catalyst, etc. In particular, the crystallographic or molecular structures have been predicted with an accuracy approaching that of the computation structural techniques. Rather a good accuracy of ATK - DFT calculations makes them suitable for the prediction of the other properties, especially in situations when the experimental approach may be difficult or impossible.
7. In short, the nanostructures as well as bulks of copper oxide can be used for sensors, supercapacitors, electrodes for lithium - Ion batteries, photocatalyst, and solar energy conversion, field emission display instead of CRT, and paint protect from corrosion.

REFERENCES

Abdu, Y. & Musa, A. O. (2009). Copper (I) Oxide (Cu_2O) based solar cells - A Review, *Journal of Pure and Applied Sciences*, **2**(2): 8 – 12

Ang, J. Z., Tao, C. J., Jun, W., Fu, Z. R., De, Y., Fei, Z., & Xun, Y. P. (2009). CuO Nanosheets Synthesized by Hydrothermal Process, *Chinese Physics Letters***,** **26**(8): 086202 - 086204

Badawy, S. M., El - Khashab, R. A., & Nayl, A. A., (2015). Synthesis, Characterization and Catalytic Activity of Cu / Cu_2O Nanoparticles Prepared in Aqueous Medium, *Bulletin of Chemical Reaction Engineering & Catalysis*, **10**(2): 169 - 174

Bae, G. T., Dellinger, B., & Hall, R. W. (2011). Density Functional Calculation of the Structure and Electronic Properties of Cu_nO_n (n = 1 - 8) Clusters, *The Journal of Physical Chemistry A*., **115**(11): 2087 - 2095

Baek, S. K., Lee, K. R., & Cho, H. K. (2013). Oxide p - n Heterojunction of Cu_2O / ZnO Nanowires and Their Photovoltaic Performance, *Journal of Nanomaterials*, **7**: 1 – 7

Barreca, D., Fornasiero, P., Gasparotto, A., Gombac, V., Maccato, C., Montini, T., & Tondello, E. (2009). The Potential of Supported Cu_2O and CuO Nanosystems in Photocatalytic H_2 Production, *Chem Sus Chem: Chemistry & Sustainability Energy & Materials*, **2**(3): 230 - 233

Barreca, D., Gasparotto, A., & Tondello, E. (2007). CVD Cu_2O and CuO Nanosystems Characterized by XPS, *Surface Science Spectra*, **14**(1): 41 - 51

Bechstedt, F. (2014). Born - Oppenheimer Approximation. Many-Body Approach to Electronic Excitations, *Springer Series in Solid-State Sciences*, **181**: 3 - 11

Bhosale, M. A., Bhanage, B. M. (2016). A simple approach for the sonochemical synthesis of Cu_2O nanoparticles with high catalytic properties, *Advanced Powder Technology*, **27**: 238 - 244

Born, M. & oppenheimer, J. R. (1927). Quantum theory of the molecules. *Annalen der Physik*, **84**: 457 - 484

Bretonnet, J. L. (2017). Basics of the density functional theory, *AIMS Materials Science*, **4**(6): 1372 - 1405

Burke, K. (2012). Perspective on density functional theory, *The Journal of Chemical Physics,* **136**(15): 150901- 1509010

Cao, H., Zhou, Z., Yu, J., Zhou, X. (2018). DFT study on structural, electronic, and optical properties of cubic and monoclinic CuO, *Journal of Computational Electronics*, **17**(1): 21 - 28

Cao, M., Hu, C., Wang, Y., Guo, Y., Guo, C. & Wang, E. (2003). A controllable synthetic route to Cu, Cu_2O, and CuO nanotubes and Nanorods, *Chemical Communications*, **15**: 1884 - 1885

Chalsani, P., Upadhyay, S. K., Ozatay, O., & Buhrman, R. A. (2007). Andreev reflection measurements of spin polarization, *APS, Physica Review B*, **75**(9): 094417 - 094433

Chang, Y. N., Zhang, M., Xia L., Zhang, J., & Xing, G. (2012). The Toxic Effects and Mechanisms of CuO and ZnO Nanoparticles, *Materials*, **5**(12): 2850 - 2871

Chatterjee, S., & Pal, A. J. (2016). Introducing Cu_2O Thin Films as a Hole - Transport Layer in Efficient Planar Perovskite Solar Cell Structures, *The Journal of Physical Chemistry C*, **120**(3): 1428 - 1437

Chen, C., Qu, J., Cao, C., Niuab, F. & Song, W. (2011). CuO nanoclusters coated with mesoporous SiO_2 as highly active and stable catalysts for olefin epoxidation, *Journal of Materials Chemistry*, **21**(15): 5774 - 5779

Cherepkov, N. A. (1981). Theory of spin polarisation phenomena in molecular photoionization processes, *J. Phys. B: Atomic and Molecular Physics,* **14**(13): 2165 - 2177

Ching, W. Y., Xu, Y. N., & Wong, K. W. (1989). Ground - state and optical properties of Cu & O and CuO crystals, *Physical Review B,* **40**(11): 7684 - 7695

Chatzichristos, A., & Jamal Hassan, J (2022) Current Understanding of Water Properties inside Carbon Nanotubes, *Nanomaterials*, **12**(174): 1 - 41

Cho, Y. S. & Huh, Y. D. (2008). CuO Nanotubes Synthesized by the Thermal Oxidation of Cu Nanowires, *Bulletin of the Korean Chemical Society*, **29**(12): 2525 - 2527

Choi K. J. & Jang H. W. (2010). One - Dimensional Oxide Nanostructures as Gas Sensing Materials: Review and Issues, *Sensors*, **10**(4): 4083 - 4099

Choy, T. S., Chen, J., & Hershfield, S. (1999). Correlation between spin polarization and magnetic moment in ferromagnetic alloys, *Journal of Applied Physics*, **86**(1): 562 - 564

Dar, M. A., Ahsanulhaq, Q., Kim, Y. S., Sohn, J. M., Kim, W. B., & Shin, H. S. (2009). Versatile synthesis of rectangular - shaped nanobot-like CuO nanostructures by hydrothermal method; structural properties and growth mechanism, *Applied Surface Science*, **255**: 6279 - 6284

Debbichi, L., Marco - de - Lucas, M. C., Pierson, J. F., & Krüger, P. (2012). Vibrational Properties of CuO and Cu_4O_3 from First-Principles Calculations, and Raman and Infrared Spectroscopy, *The Journal of Physical Chemistry C*, **116**: 10232 - 10237

Demel, J., Zhigunov, A., Jirka, I., Klementova, M., Lang, K. (2015). Facile synthesis of CuO nanosheets via the controlled delamination of layered copper hydroxide acetate, *Journal of Colloid and Interface Science*, **452**: 174 - 179

Deng Z., Ma, Z., Li, Y., Li, Y., Chen, L., Yang X., Wang H. E. & Su, B. L. (2018). Boosting Lithium-Ion Storage Capability in CuO Nanosheets via Synergistic Engineering of Defects and Pores, *Frontiers in Chemistry*, **6**: 428 - 436

Devine, B., Shan, T. R., Cheng, Y. T., McGaughey, A. J. H., Lee, M., Phillpot, S. R., & Sinnott, S. B. (2011). Atomistic simulations of copper oxidation and Cu/Cu_2O interfaces using charge - optimized many - body potentials, *Physical Review B*, **84**(12): 125308 - 125324

Du, B. D., Phu, D. V., Quoc, L. A., & Hien N. Q. (2017). Synthesis and Investigation of Antimicrobial Activity of Cu_2O Nanoparticles / Zeolite, *Journal of Nanoparticles*, **6**: 7056864 - 7056870

Dubal, D. P., Gund, G. S., Holze, R., Lokhande, C. D. (2013). Mild chemical strategy to grow micro - roses and micro - woolen like arranged CuO nanosheets for high - performance supercapacitors, *Journal of Power Sources*, **242**: 687 - 698

Echenique, P., & Alonso, J. L. (2007). A mathematical and computational review of Hartree – Fock SCF methods in quantum chemistry, *Molecular Physics*, **105**(23 - 24): 3057 - 3098

Eivazihollagh, A., Norgren, M., Dahlström, C. & Edlund H. (2018). Controlled Synthesis of Cu and Cu_2O NPs and Incorporation of Octahedral Cu_2O NPs in Cellulose II Films, *Nanomaterials*, **8**(4): 238 - 248

Ekuma, C. E., Anisimov, V. I., Moreno, J., & Jarrell, M. (2014). Electronic structure and spectra of CuO, *The European Physical Journal B*, **87**(1): 1 - 6

Elesin, V. F., Openov, L. A., & Kholmovskii, E. G. (1996). Calculation of electronic and magnetic properties of CuO, sheets using a modified mean - field approximation, *Journal of Experimental and Theoretical Physics C / C of Zhurnal Eksperimental'noi I Teoreticheskoi Fiziki*, **82**: 309 - 320

Entwistle, M. T., Hodgson, M. J. P., Wetherell, J., Longstaff, B., Ramsden, J. D., & Godby, R. W. (2016). Local density approximations from finite systems, *Physical Review B*, **94**(94): 205134 - 205145

Espino, J. P., Morales, J., Barranco, A., Caballero, A., Holgado, J. P., & Elipe, A. R. G. (2002). Interface Effects for Cu, CuO, and Cu_2O deposited on SiO_2 and ZrO_2. XPS Determination of the Valence State of Copper in Cu / SiO_2 and Cu / ZrO_2 Catalysts, *The Journal of Physical Chemistry B*, **106**(27): 6921 - 6929

Ethiraj, A. S., & Kang, D. J. (2012). Synthesis and characterization of CuO nanowires by a simple wet chemical method, *Nanoscale Research Letters*, **7**(1): 1 - 5

Fan, J. D., Malozovsky, Y. M. (2013). Pauli Exclusion Principle, *International Journal of Modern Physics B*, **27**(15): 1362024 - 1362032

Fan, M., Yu, H., & Chen, Y. (2017). High-capacity sodium - ion battery anodes based on CuO nanosheets and carboxymethyl cellulose binder, *Materials Technology*, **32**(10): 598 - 605

Farrell, H. H., & Parra, R. D. (2011). Oxide nanotube analogs: CuO nanobarrels, *Journal of Vacuum Science & Technology B, Nanotechnology and Microelectronics: Materials, Processing, Measurement, and Phenomena*, **29**(6): 061806 – 061810

.Ghijsen, J., Tjeng, H., Elp, J. V., Eskes, H., Westerink, J., Sawatzky, G. A., & Czyzyk, M. T. (1988). Electronic structure of Cu_2O and CuO, *Physical Review B*, **38(**16): 11322 - 11330

Ghodselahi, T., Vesaghi, M. A., Shafiekhani, A., Baghizadeh, A., & Lameii, M. (2008). XPS study of the Cu@Cu_2O core-shell nanoparticles, *Applied Surface Science*, **255**(5): 2730 - 2734

Giovannetti, G., Kumar, S., Stroppa, A., Brink, J. V. D., Picozzi, S., & Lorenzana, J. (2011). High - Tc Ferroelectricity Emerging from Magnetic Degeneracy in Cupric Oxide, *Physical Review Letters*, **106**(2): 026401 - 026404

Gou, X., Wang, G., Yang, J., Park, J., & Wexler, D. (2008). Chemical synthesis, characterization, and gas sensing performance of copper oxide nanoribbons, *Journal of Materials Chemistry*, **18**(9): 965 - 969

Grant, P. M. (2008). Electronic properties of rocksalt copper monoxide: A proxy structure for high - temperature superconductivity, In *Journal of Physics: Conference Series*, **129**(1): 012042 - 012050

Groot, R. A. D., Mueller, F. M., Engen, P. G. V., and Buschow, K. H. J. (1983). New Class of Materials: Half - Metallic Ferromagnets, *Physical Review Letters*, **50**(25): 2024 - 2027

Hagemman, H., Bill, H., Sadowski W., Walker, E., and Francois, M. (1990). Raman Spectra of Single Crystal CuO, *Solid State Communications*, **73**(6): 447 - 451

Han, X., Mi, W., & Wang, X. (2019). Spin polarization and magnetic properties at the C60 / Fe4N(001) interface, *Journal of Materials Chemistry C*, **7**(27): 8325 - 8334

Hansen, B. J., Lu, G., & Chen, J. (2008). Direct Oxidation Growth of CuO Nanowires from Copper - Containing Substrates, *Journal of Nanomaterials*, **2008**: 1-7

He, P., Shen, X., & Gao, H. (2005). Size - controlled preparation of Cu_2O octahedron nanocrystals and studies on their optical absorption, *Journal of Colloid and Interface Science*, **284**(2): 510 - 515

He, X., & Bae, J. (2018). Facile Synthesis of Amorphous CuO Nanosheets on Nickel Foam by Utilizing ZnO Nanowires for High - Performance Supercapacitors, *Journal of Electronic Materials*, **47**(9): 5468 - 5476

Heinemann, M., Eifert, B., & Heiliger, C. (2013). Band structure and phase stability of the copper oxides Cu_2O, CuO, and Cu_4O_3, *Physical Review B*, **87**(11): 115111 - 115115

Hohenberg, P. & Kohn, W. (1964). Inhomogeneous Electron Gas, *Physical Review*, **136**(3B): B864 – B871

Hsueh, H. T., Chang, S. J., Hung, F. Y., Weng, W. Y., Chang, S. P., Hsueh, T. J., Hsu, C. L., & Dai, B. T. (2011). Isopropyl Alcohol Sensors of CuO Nanotubes by Thermal Oxidation of Copper Films on Glass, *IEEE Sensors Journal*, **11**(12): 3276 - 3282

Huang, W. C., Lyu L. M., Yang, Y. C., & Huang, M. H. (2011). Synthesis of Cu_2O Nanocrystals from Cubic to Rhombic Dodecahedral Structures and Their Comparative Photocatalytic Activity, *Journal of the American Chemical Society*, **134**(2): 1261-1267

Ibupoto, Z. H., Khun, K., Beni, V., Liu, X. & Willander, M. (2013). Synthesis of Novel CuO Nanosheets and Their Non-Enzymatic Glucose Sensing Applications, *Sensors*, **13**(6): 7926 - 7938

Isseroff, L. Y., & Carter, E. A. (2013). Electronic Structure of Pure and Doped Cuprous Oxide with Copper Vacancies: Suppression of Trap States, *Chemistry of Materials*, **25**(3): 253 - 265

Jadraque, M., & Martin, M. (2008). DFT calculations of $Cu_nO_m^{0/+}$ clusters: Evidence for Cu_2O building block, *Chemical Physics Letters*, **456**: 51 - 54

Jerome, A., Goldstein, & Gisele Ruiz Rieder, G.R. (1987). A rigorous modified Thomas - Fermi theory for atomic systems, *Journal of Mathematical Physics*, **28**(5): 1198 - 1202

Jia, X., Fan, H. & Yang, W. (2010). Hydrothermal Synthesis and Primary Gas Sensing Properties of CuO Nanosheets, *Journal of Dispersion Science and Technology*, **31**(7): 866 - 869

Jin, Q., Fujishima, M., Iwaszuk, A., Nolan, M., & Tada, H. (2013). Loading Effect in Copper (II) Oxide Cluster - Surface - Modified Titanium (IV) Oxide on Visible - and UV - Light Activities, *The Journal of Physical Chemistry C*, **117**(45): 23848 - 23857

Jin, S., Zhu, X., & Qian, Y. (2014). Copper Oxide Hierarchical Microspheres Grown on Copper Foil and Their Enhanced Performance as Anodes for Li - ion Batteries, *International Journal of Electrochemical Science*, **9**: 2859 - 2866

Jones, S. P. P., Gaw, S. M., Doig, K. I., Prabhakaran, D., Wheeler, E. M. H., Boothroyd, A. T. & Hughes, J. L. (2014). High - temperature electromagnons in the magnetically induced multiferroic cupric oxide driven by inter sublattice exchange, *Nature Communications*, **5**(1): 1 - 7

Joseph, D. P., Venkateswaran, C., & Vennila, R. S. (2010). Critical Analysis on the Structural and Magnetic Properties of Bulk and Nanocrystalline Cu – Fe - O, *Advances in Materials Science and Engineering*, **2010**: 1 - 14

Karakasidis, T. E., & Charitidis, C. A. (2007). Multiscale modeling in nanomaterials science, *Materials Science and Engineering: C*, **27**(5 - 8): 1082 - 1089

Khan, B. S., Saeed, A., Hayat, S. S., Mukhtar, A., Mehmood, T. (2017). The mechanism for the Formation of Cuprous Oxide Nanowires in AAO template by Electrodeposition, *International Journal of Electrochemical Science*, **12**: 890 - 897

Khan, F. H. (2013). Chemical Hazards of Nanoparticles to Human and Environment (A Review), *Oriental Journal of Chemistry.*, **29**(4): 1399 - 1408

Kirchner-Hall, N. E.; Zhao, W.; Xiong, Y.; Timrov, I.; Dabo, I., (2021). Extensive Benchmarking of DFT + U Calculations for Predicting Band Gaps. *Applied Science*, **11**(5): 2395 - 2416

Kliche, G., Popovic, Z. V. (1990). Far - infrared Spectroscopic investigations on CuO, *Physical Review B*, **42**(16): 10060 - 10066

Kohashi, T. (2018). Magnetization Analysis by Spin-Polarized Scanning Electron Microscopy, *Scanning*, **2018**: 1 - 6

Kohn, W. & Sham, L. J. (1965). Self-Consistent Equations Including Exchange and Correlation Effects, *Physical Review*, **140**(4A): A1133 – A1138

Koshy, J. & George, K. C.(2015). Annealing effects on the crystallite size and band gap of CuO nanoparticles, *International Journal of Nanoscience and Nanotechnology*, **6**(1): 1 - 8

Lai, M., Mubeen, S., Chartuprayoon, N., Mulchandani, A., Deshusses, M. A. & Myung, N. V. (2010). Synthesis of Sn doped CuO nanotubes from the core - shell Cu / SnO_2 nanowires by the Kirkendall effect, *Nanotechnology*, **21**(29): 295601 - 295606

Latif, M. A., Wu, J. W. J., Moriyama, R., Nakano, M., Ohshimo, K., & Misaizu F. (2018). Stable Compositions and Structures of Copper Oxide Cluster Cations $Cu_nO_m^+$ (n = 2 - 8) Studied by Ion Mobility Mass Spectrometry, *American Chemical Society Omega*, **3**(12): 18705 - 18713

Levada, C. L., et al. (2018). Review of the Schrödinger Wave Equation, *IOSR Journal of Applied Chemistry*, **11**(4): 1 - 7

Li, S., Zhang, H., Ji, Y. & Yang, D. (2004). CuO nanodendrites synthesized by a novel hydrothermal route, *Nanotechnology*, **15**(12): 1428 - 1432

Lieber, C. M., & Wang, Z. L. (2007). Functional Nanowires, *Materials Research Society Bulletin*, **32**(2): 99 - 108

Lieber, C. M. (2011). Semiconductor nanowires: A platform for nanoscience and nanotechnology, *Materials Research Society Bulletin*, **36**(12): 1052 - 1063

Linnera, J., Sansone, G., Maschio, L., & Karttunen A. J. (2018). Thermoelectric Properties of p - type Cu_2O, CuO, and NiO from Hybrid Density Functional Theory, *The Journal of Physical Chemistry C*, **122**(27): 15180 - 15189

Liu, B. & Zeng, H. C., (2004). Mesoscale Organization of CuO Nanoribbons: Formation of"Dandelions", *Journal of the American Chemical Society*, **126**(26): 8124 - 8125

Lo, K. J., Liao, H. Y., Cheng, H. W., Lin, W. C., Yu, B. Y., Shyue, J. J., & Chang, C. C. (2011). Polyol synthesis of polycrystalline cuprous oxide nanoribbons and their growth chemistry, *Journal of the American Chemical Society*, **126**(26): 8124 - 8125

Lu, L. Q. & Wang, Y. (2011). Sheet - like and fusiform CuO nanostructures were grown on graphene by rapid microwave heating for high Li - ion storage capacities, *Journal of Materials Chemistry*, **21**(44): 17916 - 17921

Luo, L. B., Wang, X. H., Xie, C., Li, Z. J., Lu, R., Yang, X. B. and Lu, J. (2014). One - dimensional CuO nanowire: synthesis, electrical, and optoelectronic devices application, Nanoscale Research Letters, **9**(1): 1 - 8

Lyubinetsky, I., Thevuthasan, S., Mc Cready, D. E., & Baer, D. R. (2003). Formation of single - phase oxide nanoclusters: Cu_2O on $SrTiO_3$. 100, *Journal of Applied Physics*, **94**(12): 7926 - 7928

Ma, L., Lin, Y., Wang, Y., Li, J., Wang, E., Qiu M., & Yu Y. (2008). Aligned 2 - D Nanosheet Cu_2O Film: Oriented Deposition on Cu Foil and Its Photoelectrochemical Property, *The Journal of Physical Chemistry C*, **112**(48): 18916 - 18922

Maddinedi, S. B., Mandal, B. K., Pappu, G., Anna, K. K., Ghosh, A. R. & Reddy, P. S. (2015). Synthesis of CuO nanosheets and its applications towards catalysis and antimicrobial activity, *Journal of the Indian Chemical Society*, **92**: 1 - 6

Malandrino, G., Finocchiaro, S. T., Nigro, R. L., Bongiorno, C., Spinella, C., & Fragala, I. L. (2004). Free - Standing Copper (II) Oxide Nanotube Arrays through an MOCVD Template Process, *Chemistry of materials*, **16**(26): 5559 - 5561

Mao - hai, Y., You - gen, T., Li, Z., Hai - hua, Y., & Jian - hui, Y. (2010). Photocatalytic activity of CuO towards HER in catalyst from oxalic acid solution under simulated sunlight irradiation, *Transactions of Nonferrous Metals Society of China*, **20**(10): 1944 - 1949

Massobrio, C. (2003). Structural properties of CuO_4 and CuO_5 clusters: A density functional study, *The Journal of chemical physics*, **119**(16): 8305 - 8310

McAuley, C. B., Du, Y., Wildgoose, G. G., Compton, R. G. (2008). The use of copper (II) oxide nanorod bundles for the non-enzymatic voltammetric sensing of carbohydrates and hydrogen peroxide, *Sensors and actuators B: Chemical*, **135**(1): 230 - 235

Medel, V. M., Reveles, J. U., Khanna, S. N., Chauhan, V., Sen, P., & Castleman, A. W. (2011). Hund's rule in superatoms with transition metal impurities, *Proceedings of the National Academy of Sciences*, **108**(25): 10062 - 10066

Miao, L., Basak, R., Ran, S., Xu, Y., Kotta, E., He, H., Denlinger, J. D., Chuang, Y. D., Zhao, Y., Xu, Z., Lynn, J. W., Jeffries, J. R., Saha, S. R., Giannakis, I., Aynajian, P., Kang, C. J., Wang Y., Kotliar, G., Butch, N. P., & Wray, L. A. (2019). High-temperature singlet-based magnetism from Hund's rule correlations, *Nature communications*, **10**(1): 1 - 8

Mojica, E. R. E. (2007). Copper Oxide as Mediator for the Amperometric Determination of Hydrogen Peroxide, *Philippine Journal of Science*, **136**(1): 25 - 32

Moser, S., Moreschini, L., Yang, H. Y., Innocenti, D., Fuchs, F., Hansen, N. H., Chang, Y. J., Kim, K. S., Walter, A. L., Bostwick, A., Rotenberg, E., Mila, F., & Grioni, M. (2014). Angle - Resolved Photoemission Spectroscopy of Tetragonal CuO: Evidence for Intralayer Coupling Between Cupratelike Sublattices, *Physical Review Letters*, **113**(18): 187001 - 187005

Moura, A. P., Cavalcante, L. S., Sczancoski, J. C., Stroppa, D. G., Paris, E. C., Ramirez, A. J., Varela, J. A., Longo, E. (2010). Structure and growth mechanism of CuO plates obtained by microwave - hydrothermal without surfactants, *Advanced Powder Technology*, **21**(2): 197 - 202

Mu, C., & He, J. (2011). Confined conversion of CuS nanowires to CuO nanotubes by annealing - induced diffusion in nanochannels, *Nanoscale Research Letters*, **6**(1): 1 - 6

Musevi, S. J., Aslani, A., & Salimi, H. (2013). H_2 Sensing Characterization of Pd - Doped CuO Nanoparticles; Synthesized by Solvothermal method, *Journal of Nanotechnology & Advance Materials*, **1**(1): 1 - 8

Muthaiyan, L., Sriram, S. & Balamurugan, D. (2018). The Electronic Transport Properties of CuO and Zn Doped CuO Nanotubes, *International Journal of Nanoelectronics & Materials*, **11**(1): 33 - 42

Nasrollahzadeh, M., Sajadi, S. M., Sajjadi, M., & Issaabadi, Z. (2019). Applications of Nanotechnology in Daily Life. *Interface Science and Technology*, **28**: 113 - 143

Nolan, M. & Elliott, S. D., (2006). The p-type conduction mechanism in Cu_2O: a first-principles study, *Physical Chemistry Chemical Physics*, **8**(45): 5350 - 5358

Pan, L., Kim, J. H., Mayer, M. T., Son, M. K., Ummadisingu, A., Lee, J. S., Hagfeldt, A., Luo, J., & Grätzel, M. (2018). Boosting the performance of Cu_2O photocathodes for unassisted solar water splitting devices, *Nature Catalysis*, **1**(6): 412 - 420

Park, S., Kim, S., Park, & S., Lee, C. (2015). Facile synthesis of CuO nanotubes and their formation mechanism, *Materials Letters*, **138**: 110 - 112

Parra, R. D., & Farrell, H. H. (2009). Binding Energy of Metal Oxide Nanoparticles. *The Journal of Physical Chemistry C*, **113**(12): 4786 - 4791

Paudel, S., Dandeliya, S., Chaurasiya, R., Srivastava, A., & Kaphle, G. C. (2016). Magnetism in zigzag & armchair CuO nanotubes: Ab - initio study, *Journal of Magnetism and Magnetic Materials*, **406**: 8 - 14

Paudel, S., Yadav, T. P., Srivastava, A. & Kaphle, G. C. (2018). Magnetic Moment of Zigzag CuO Nanotubes at Different Temperature and Size: Ab - Initio Study, *Journal of Magnetism and Magnetic Materials*, **6**(1): 1 - 5

Perdew, J. P., Burke, K. & Wang, Y. (1996 - I). Generalized gradient approximation for the exchange-correlation hole of a many-electron system, *APS, Physical Review. B*, **54**(23): 16533 - 16540

Perdew, J. P., Burke, K., Ernzerhof, M. (1996). Generalized Gradient Approximation Made Simple, *Physical Review Letters*, **77**(18): 3865 - 3868

Qian, Y., Ye F., Xu, J., Le, Z. G. (2012). Synthesis of Cuprous Oxide (Cu_2O) Nanoparticles / Graphene Composite with an Excellent Electrocatalytic

Activity Towards Glucose, *International Journal of Electrochemical Science*, **7**(10): 10063 - 10073

Quantum ATK Atomic-Scale Modeling for Semiconductor & Materials. https://www.synopsys.com/silicon/quantumatk.html. Accessed 18 Dec 2019

Quirino, M. R., Lucena, G. L., Medeiros, J. A., Santos, I. M. G. D., Oliveira, & M. J. C. D. (2018). CuO Rapid Synthesis with Different Morphologies by the Microwave Hydrothermal Method, *Materials Research,* **21**(6): e20180227 - e20180235

Raj, A. S. A., & Biju, V.(2017). Nanostructured CuO: Facile synthesis, optical absorption, and defect dependent electrical conductivity, *Materials Science in Semiconductor Processing*, **68**: 38 - 47

Rasadujjaman, M., Shahjahan, M., Khan, M. K. R. & Rahman, M. M. (2012). Deposition and Characterization of p - Cu_2O Thin Films, *Journal of Science and Technology*, **20**(6): 1 - 7

Rocco, H. O. D., Lanzini, F. & Aguiar, J. C. (2016). Thomas – Fermi approach to density functional theory: binding energy for atomic systems, *European Journal of Physics*, **37**(6): 065402 - 065417

Rodberg, S. L. (1957). The many-body problem and the Brueckner approximation, *Annals of Physics*, **2**(3): 199 - 225

Saini, K., Kumar, R. M., Lahiri, D., & Lahiri, I. (2015). Quantifying bonding strength of CuO nanotubes with the substrate using the nano - scratch technique, *Nanotechnology,* **26**(30): 305701 - 305708

Sajeev, Y., Sindelka, M., & Moiseyev, N. (2008). Hund's multiplicity rule: From atoms to quantum dots, *The Journal of Chemical Physics*, **128**(6): 061101 - 061105

Sawant, S. S., Bhagwat, A. D., & Mahajan, C. M. (2016). Synthesis of Cuprous Oxide (Cu_2O) Nanoparticles - a Review, *Journal of Nano and Electronic Physics*, **8**(1): 01035 - 01039

Sha, R., Liu, Q., Wang, M., Liu, M., Peng, Y., Zhang, Z., Zou, A., Xu, Y., Jiang, X., and Qiu, Z. (2021). Spin transport in different oxide phases of copper, *Physical Review B,* **103**(2): 024432 - 024436

Shahmiri, M., Ibrahim, N. A., Zainuddin, N., Asim, N., Bakhtyar, B., Zaharim, A., Sopian, K. (2013). Effect of pH on the Synthesis of CuO Nanosheets by Quick Precipitation Method, *WSEAS Transactions on Environment and Development*, **9**(2): 137 - 145

Shen, Y. M., Shih, Y. T., Wang, S. C., Nayak, P. K., Huang, J. L. (2010). Characterization of ordered Cu_2O nanowire arrays prepared by heat-treated Cu / PAM composite, *Thin Solid Films*, **519**(5): 1687 - 1692

Shi, J., Li, J., Huang, X., & Tan, Y. (2011). Synthesis and Enhanced Photocatalytic Activity of Regularly Shaped Cu_2O Nanowire Polyhedra, *Nano Research*, **4**(5): 448 - 459

Singh, D. P., Neti, N. R., Sinha, A. S. K., & Srivastava, O. N. (2007). Growth of Different Nanostructures of Cu_2O (Nanothreads, Nanowires, and Nanocubes) by Simple Electrolysis Based Oxidation of Copper, *The Journal of Physical Chemistry C*, **111**(4): 1638 - 1645

Soler, J. M., Artacho, E., Gale, J. D., Garcıa, A., Junquera, J., Ordejon, P. & Portal D. S. (2002). The SIESTA method for ab - initio order - N materials Simulation, *Journal of Physics: Condensed Matter*, **14**(11): 2745 - 2779

Stefanovich, E. V. & Truong, T. N. (1995). Correlation between the Madelung field and the reactivity of the MgO low - coordinated surface sites, *The Journal of Chemical Physics*, **102**(12): 5071 - 5076

Stefanovich, E. V., & Truong, T. N. (1998). A Simple Method for Incorporating Madelung Field Effects into ab Initio Embedded Cluster Calculations of Crystals and Macromolecules, *The Journal of Physical Chemistry B*, **102**(16): 3018 - 3022

Stepniowski, W. J., & Misiolek, W. Z. (2018). Review of Fabrication Methods, Physical Properties, and Applications of Nanostructured Copper Oxides Formed via Electrochemical Oxidation, *Nanomaterials*, **8**(6): 379 - 397

Stojanovic, B. (2020). Local Density Approximation of Spherically Symmetric Atomic Ground States, *Matrika*, **7**: 1 - 16

Stucky, A., Ubaldini, A., Levallois, J., Tran, Marel, M. K., D. V. & Giannini, E. (2014). Shining light on CuO for exploring high - Tc multiferroics, In *Journal of Physics: Conference Series*, **566**(1): 012012 - 012017

Subramanian, S., Valantina, R., & Ramanathan C. (2015). Structural and Electronic Properties of CuO, CuO_2 and Cu_2O Nanoclusters - a DFT Approach, *Materials Science,* **21**(2): 173 - 178

Sun, B. (2010). Formulation of 2D Graphene Deformation Based on Chiral - Tube Base Vectors, *Journal of Nanomaterials*, **2010**: 402591 - 402597

Sun, S. (2015). Recent advances in hybrid Cu_2O - based heterogeneous nanostructures, *Nanoscale*, **7**(25): 10850 - 10882

Sun, Y., Ma, L., Zhou, B., & Gao, P. (2012). $Cu(OH)_2$ and CuO nanotube networks from hexaoxacyclooctadecane - like posnjakite microplates: Synthesis and electrochemical hydrogen storage, *International Journal of Hydrogen Energy*, **37**(3): 2336 - 2343

Sundar, S., Venkatachalam, G., & Kwon, S. J. (2018). Biosynthesis of Copper Oxide (CuO) Nanowires and Their Use for the Electrochemical Sensing of Dopamine, *Nanomaterials*, **8**: 823 - 839.

Tan, Y., Xue, X., Peng, Q., Zhao, H., Wang, T., & Li, Y., (2007). Controllable Fabrication and Electrical Performance of Single - Crystalline Cu_2O Nanowires with High Aspect Ratios, *Nano Letters*, **7**(12): 3723 - 3728

Tolba, S. A., Gameel, K., M., & Ali, B., A., Hossam A. (2018). Almossalami and Nageh K. Allam, The DFT + U: Approaches, Accuracy, and Applications, *Energy Materials Laboratory*, **2018:** 3 - 30

Torrance, J. B., Tokura, Y., Laplaca, S. J., Huang, T. C., Savoy, R. J., & Nazzal, A. I. (1988). New Class of High T_c Structures: Intergrowth of Multiple Copper Oxide Perovskite - Like Layers with Double sheets of BiO, *Solid State Communications*, **66**(7): 703 - 706

Tran, T. H., & Nguyen, V. T. (2014). Copper Oxide Nanomaterials Prepared by Solution Methods, Some Properties, and Potential Applications: A Brief Review, *International Scholarly Research Notices*, **2014**: 1 - 14

Tusche, C., Ellguth, M., Krasyuk, A., Winkelmann, A., Kutnyakhov, D., Lushchyk, P., Medjanik, K., Sch¨onhense, G., & Kirschner, J. (2013). Quantitative spin polarization analysis in photoelectron emission microscopy with an imaging spin filter, *Ultramicroscopy*, **130**: 70 - 76

Valeev, E. F. & Sherrill, C. D. (2003). The diagonal Born – Oppenheimer correction beyond the Hartree - Fock approximation, *The Journal of Chemical Physics*, **118**(9): 3921 - 3927

Wang, G., Yan, P, Wei, L., & Deng, Z. (2017). The Magnetic Memory Effect of Ferromagnetic Materials in the Process of Stress - Magnetism Coupling, *Advances in Materials Science and Engineering*, **2017**: 1284560 - 1284567

Wang, H., Xu, J. Z., Zhu, J. J., Chen, H. Y. (2002). Preparation of CuO nanoparticles by microwave irradiation, *Journal of Crystal Growth*, **244**(1): 88 - 94

Wang, L. S., Wu, H., & Desai, S. R. (1996 - II). Electronic structure of small copper oxide clusters: From Cu_2O to Cu_2O_4, *Physical Review B*, **53**(12): 8028 - 8031

Wang, W., Varghese, O. K., Ruan, C., Paulose, M., & Grimes, C. A. (2003). Synthesis of CuO and Cu_2O crystalline nanowires using $Cu(OH)_2$ nanowire templates, *Journal of Materials Research*, **18**(12): 2756 - 2759

Wang, Y., Lany, S., Ghanbaja, J., Fagot - Revurat, Y., Chen, Y. P., Soldera, F., Horwat, D., Mucklich, F., & Pierson, J. F. (2016). Electronic structures of Cu_2O, Cu_4O_3, and CuO: A joint experimental and theoretical study, *Physical Review B*, **94**(24): 245418 - 245427

Wang, Z., Li, F., Wang, H., Wang, A., & Wu, S. (2018). An enhanced ultra-fast responding ethanol gas sensor based on Ag functionalized CuO nanoribbons at room - temperature. *Journal of Materials Science: Materials in Electronics*, **29**(19): 16654 - 16659

Wang, Z., P. V., Saxena, S. K., & Lazor, P. (2002). X - ray diffraction and Raman spectroscopic study of nanocrystalline CuO under pressures, *Solid State Communications*, **2**: 275 - 279

Wanninayake, A. P., Gunashekar, S., Li, S., Church, B. C. & Zahra, N. A. (2015). Performance enhancement of polymer solar cells using copper oxide nano parts, *Semiconductor Science and Technology*, **30**(6): 064004 - 064010

Xiao, A., Zhou, S., Zuo, C., Zhuan, Y., & Ding, X. (2015). Improved electrochemical performances of CuO nanotube array prepared via electrodeposition as anode for lithium - ion battery, *Materials Research Bulletin*, **70**: 795 - 798

Xiao, G., Gao, P., Wang, L., Chen, Y., Wang, Y., & Zhang, G. (2011). Ultrasonochemical - Assisted Synthesis of CuO Nanorods with High Hydrogen Storage Ability, *Journal of Nanomaterials.*, **2011**: 439162 - 439167

Xiao, H. M., Fu, S. Y., Zhu, L. P., Li, Y. Q., & Yang, G. (2007). Controlled Synthesis and Characterization of CuO Nanostructures through a Facile Hydrothermal Route in the Presence of Sodium Citrate, The *European Journal of Inorganic Chemistry*, **2007**: 1966 - 1971

Xu, L., Yang, Q., Liu, X., Liu, J., & Sun, X. (2014). One - dimensional copper oxide nanotube arrays: biosensors for glucose detection, *Royal Society of Chemistry Advances*, **4**(3): 1449 - 1455

Xu, Z., Bi, Z., Shen, C. (2012). Facile fabrication of Cu_2O nanowire arrays on Cu substrates, *Central European Journal of Engineering*, **2**(3): 364 - 368

Yadav, T. P., Srivastava, A., & Kaphle, G. C. (2020). DFT Analysis of Ferromagnetism in Zigzag and Armchair CuO Nanosheets, *Physics of the Solid State*, **62**(8): 1361 - 1369

Yadav, T. P., Srivastava, A., & Kaphle, G. C., (2020). Computational Study of the Structural, Electronic and Magnetic Properties of Nanoclusters of Cu_2O and CuO: Ab - Initio Approach, *Journal of Nepal Physical Society*, **6**(1): 68 - 72

Yadav, T. P., Srivastava, A., & Kaphle, G. C. (2021). Magnetism in Zigzag and Armchair CuO Nanoribbons: Ab - Initio Analysis, *Physics of the Solid State*, **63**(2): 279 - 285

Yin M., Wu, C. K., Lou, Y., Burda, C., Koberstein, J. T., Zhu, Y., & O'Brien, S. (2005). Copper Oxide Nanocrystals, *Journal of the American Chemical Society*, **127**(26): 9506 - 9511

Yu, Q., Huang, H., Chen, R., Wang, P., Yang, H., Gao, M., Peng, X. & Ye, Z. (2012). Synthesis of CuO nanowalnuts and nanoribbons from aqueous solution and their catalytic and electrochemical properties, *Nanoscale,* **4**: 2613 - 2620

Zahariev, F., Leang, S. S., & Gordona, M. S. (2013). Functional derivatives of meta-generalized gradient approximation (meta - GGA) type exchange-correlation density functional, *The Journal of Chemical Physics*, **138**(24): 244108 - 244118

Zaman, S., Zainelabdin, A., Amin, G., Nur, O., & Willander, M. (2012). The efficient catalytic effect of CuO nanostructures on the degradation of organic dyes, *Physics and Chemistry of Solids,***11**(73): 1320 - 1325

Zemzemi, M., Alaya, S. (2015). First Principles Study of the Structural and Electronic Properties of the ZnO/Cu_2O Heterojunction, *Materials Sciences and Applications*, **6**(07): 661 - 675

Zeng, H. C. (2007). Oriented attachment: a versatile approach for the construction of nanomaterials, *International Journal of Nanotechnology*, **4**(4): 329 - 346

Zhang D. (2013). Synergetic effects of Cu_2O photocatalyst with titania and enhanced photoactivity under visible irradiation, *Acta Chimica Slovaca*, **6**(1): 141 - 149

Zhang, F., Zhu, A., Luo, Y., Tian, Y., Yang, J., & Qin, Y. (2010). CuO Nanosheets for Sensitive and Selective Determination of H_2S with High Recovery Ability, *The Journal of Physical Chemistry C*, **114**(45): 19214 - 19219

Zhang, K., Rossi, C., Tenailleau, C., Alphonse, P. & Ching, J. Y. C. (2007). Synthesis of the large - area and aligned copper oxide nanowires from the copper thin film on the silicon substrate, *Nanotechnology*, **18** (27): 275607 - 275614

Zhang, Q., Zhang, K., Xu, D., Yang, G., Huang, H., Nie F., Liu C., & Yang S. (2014). CuO nanostructures: Synthesis, characterization, growth mechanisms, fundamental properties, and applications, *Progress in Materials Science*, **60**: 208 - 337

Zhang, Y. X., Huang, M., Kuang, M., Liu, C. P., Tan, J. L., Dong, M., Yuan, Y., Zhao, X. L., & Wen, Z. (2013). Facile Synthesis of Mesoporous CuO Nanoribbons for Electrochemical Capacitors Applications, *International Journal of Electrochemical Science*, **8**: 1366 - 1381

Zheng, X., Su, Y., Chen, Y., Wan, R., Li, M., Huang, H. & Li, X. (2016). Carbon nanotubes affect the toxicity of CuO nanoparticles to denitrification in marine sediments by altering the cellular internalization of nanoparticles, *Scientific Reports*, **6**(27748): 1 - 8

Zhou, L., He, Y., Jia, C., Pavlinek, V., Saha, P. & Cheng, Q. (2017). Construction of Hierarchical CuO / Cu2O@NiCo2S4 Nanowire Arrays on Copper Foam for High-Performance Supercapacitor Electrodes, *Nanomaterials*, **7**: 273 - 284

Zhu, Y., Mimura, K., lim, J. W., Isshiki, M., & Jiang, Q. (2006). Brief Review of Oxidation Kinetics of Copper at 350°C to 1050°C, *Metallurgical and Materials Transactions A*, **37**: 1231 - 1237

Zoolfakar, A. S., Rani, R. A., Morfa, A. J., O'Mullaned, A. P. & zadeh, K. K. (2014). Nanostructured copper oxide semiconductors: a perspective on materials, synthesis methods, and applications, *Journal of Materials Chemistry C*, **2**(27): 5247 - 5270

APPENDIX

LIST OF PUBLICATIONS

1. Yadav, T. P., Srivastava, A., & Kaphle, G. C. (2021) Magnetism in Zigzag and Armchair CuO Nanoribbons: Ab - Initio Analysis, *JPSS*, **63**(2), 270 – 285.
2. Upadhyay, O. P., Adhikari, P. R., Yadav, T. P., Kaphle, G. C., and Srivastava, A. (2021) Half - Metallic and Magnetic Properties for Cu_2O Nanowire: Ab-initio Study, *Materials Today Proceedings*, **47**(18), 6526 – 6535.
3. Yadav, T. P., Srivastava, A., and Kaphle, G. C. (2020) DFT Analysis of Ferromagnetism in Zigzag and Armchair CuO Nanosheets, JPSS, **62**(8), 1361 – 1369.
4. Yadav, T. P., Kaphle, G. C., and Srivastava, A. (2020) Computational Study of the Structural, Electronic and Magnetic Properties of Nanoclusters of Cu_2O and CuO: Ab-Initio Approach, JNPS 6 (1), 68 - 72.
5. Paudel, S., Yadav, T. P., Srivastava, A., and Kaphle, G.C. (2018) Magnetic Moment of Zigzag CuO Nanotubes at Different Temperature and Size: Ab-initio study, *J Mat Sci Nanotechol* **6**(1), 102 – 106.

ISSN 1063-7834, Physics of the Solid State, 2021, Vol. 63, No. 2, pp. 279–285. © Pleiades Publishing, Ltd., 2021.

MAGNETISM

Magnetism in Zigzag and Armchair CuO Nanoribbons: Ab-Initio Analysis

T. P. Yadav[a, b, c], A. Srivastava[b, *], and G. C. Kaphle[a]

[a] *Central Department of Physics, Tribhuvan University, Kirtipur, Kathamandu, Nepal*

[b] *Advance Materials Research Group, CNTLab, Atal Bihari Vajpayee—Indian Institute of Information Technology and Management, Gwalior, India*

[c] *Central Campus of Science and Technology, Mid-Western University, Surkhet, Nepal*

** e-mail: profanurag@gmailcom*

Received October 10, 2020; revised October 10, 2020; accepted October 16, 2020

Abstract—The present work reports the magnetism analysis of zigzag and armchair forms of CuO nanoribbons by using density functional theory (DFT)-based ab initio approach. The structural stability has been confirmed through the binding energy calculation. The electronic and magnetic properties have been analyzed as a function of varied width of CuO nanoribbons, interesting information for variety of applications. The metallic and ferromagnetic behaviors of CuO nanoribbons are observed, whereas its bulk counterpart shows a p-type semiconducting and antiferromagnetic nature. The computed magnetic moments for the zigzag and armchair forms of CuO nanoribbon are in the ranges of 0.19–0.61 μ_B and 0.24–0.97 μ_B, respectively. The computed spin polarizations confirms the half or full metallic ferromagnetic nature of these nanoribbons.

Keywords: CuO, nanoribbon, DFT + U, magnetic moment, ferromagnetism, spin polarization, band structure

DOI: 10.1134/S1063783421020256

1. INTRODUCTION

In the modern age of science and technology, the nanostructures [1] have attracted the significant attention of scientific and industrial groups, due to their unique behaviors at the reduced dimensions, especially copper(II) oxide (CuO). Various prospective applications are in chemical, photochemical, electrochemical fields and as catalyst for removing the dye during purification of water, glass for solar energy conversion [2–5]. Experimental findings have confirmed that the CuO in its bulk form is a semiconducting material with a band gap in the range of 1.2–1.9 eV, having high electron communication features, high stability antimicrobial activity [6–8], etc., black brown in color and insoluble in water. In comparison to the other transition metal oxides having rock-salt structures, CuO has monoclinic structure showing peculiar structural, electronic, and magnetic properties at its different morphologies. Same as other transition metal oxides, it has antiferromagnetic ground state at 213 and 231 K, however, paramagnetic at high temperature, which may lead to superconductivity in copper oxide perovskites and novel magnetic property [9, 10]. Recently, Markus Heinemann et al. (2013) and Y. Wang et al. (2016) used local density approximation LDA + U (where U = 7.5 eV) and demonstrated that the bulk CuO is a p-type semiconductor with energy band gap roughly lying between 1–2 eV [11, 12]. Yu Xin Zhang et al. (2013) demonstrated that the electrochemical data analysis of nanoribbon of width range 2 to 50 nm has a higher specific capacitance of 137 F per gram and gives a stable performance of about 12% capacitance loss after 500 cycles. This shows that the low-cost CuO nanoribbons are promising candidate for high-performance electrochemical capacitors. Hence, it is worth analyzing the zigzag and armchair forms of CuO nanoribbons and others [13–18] computationally, to understand the fundamental science associated with the proposed one-dimensional morphologies of CuO. The well-known fact is that the materials behave completely differently at reduced dimension, like increment in relative surface area and new quantum effects, and the variety of possible application of CuO has prompted us to further analyze its possible one-dimension morphologies in form of nanoribbons, especially the magnetism in these.

In the present report, the binding energy, magnetic moment, and spin polarization have been calcutated as a marker for the electronic and magnetic properties of the optimized (n = 3–10, m = 0) zigzag and (n = 3–10, m = n) armchair CuO nanoribbons by using the exchange correlation as spin generalized-gradient

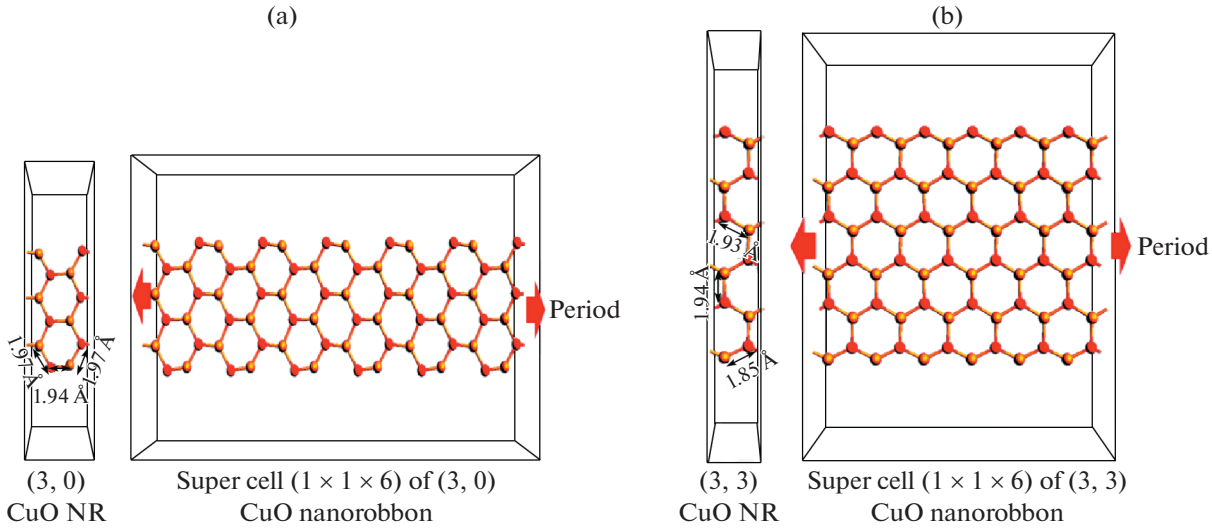

Fig. 1. Bulk forms of super cells of the (a) zigzag (3, 0) and (b) armchair (3, 3) of CuO nanoribbons.

approximation with additional Hubbard potential, i.e., SGGA + *U*. Where the integers *n* and *m* are the number of unit vectors along two directions in the crystal lattice of nanoribbon. The remaining steps are orderly organized as computational details, results and discussion, and conclusion.

2. COMPUTATIONAL DETAILS

In the present computational investigation, the density functional theory DFT + *U* calculator has been used, which is based on the methodology, models, algorithms developed in academic code TransSIESTA called TransSIESTA-C and McDCal employing localized basis sets as developed in SIESTA.

The super cells of order (1 × 1 × 6) of the optimized (3, 0) zigzag and (3, 3) armchair CuO nanoribbons in the bulk forms have been modeled and shown in Figs. 1a and 1b.

The geometries of ($n = 3–10, 0$) zigzag and ($n = 3–10, m = n$) armchair CuO nanoribbons have been optimized using total energy minimization approach, where the spin generalized gradient approximation including Hubbard potential (SGGA + *U*) with exchange correlation functional, having revised Perdew–Burke–Ernzerhof (rPBE) type parameterization, has been applied. The linear combination of atomic orbitals (LCAOs) with double zeta-polarizations (DZP) basis set is used to explain the valence electrons. The required parameters as *U* of 7.5 eV, mesh cutoff of 75 Hartree, and *k*-point sampling of 1 × 1 × 7 for Brillouin zone integration, have been selected for the computation of various properties of zigzag and armchair morphologies of CuO nanoribbons [19–22].

3. RESULTS AND DISCUSSION

The optimized geometries of CuO nanoribbons have been tested for their structural stability as a function of its varying width. Further, the electronic property depending on the electronic band and density of states (DoS) has been investigated to understand the magnetic behavior through the spin polarization of the zigzag and armchair forms of CuO nanoribbon.

3.1. Structural Stability and Electronic Properties

To analyse the structural stabilities of the ($n = 3–10, 0$) zigzag and ($n = 3–10, m = n$) armchair CuO nanoribbons (NRs), the binding energies of the nanostructures have been computed using Eq. (1) and listed in Tables 1 and 2, along with other parameters like magnetic moments and spin polarizations (H.M.F#. = half-metal ferromagnetic materials, F.M.F#. = full-metal ferromagnetic materials).

The size of super cell increases in periodic *C* direction with length variation at constant *A* and *B* directions as shown Figs. 1a and 1b, where the number of atoms per nanoribbon and its width depend on the chirality of the CuO nanoribbon.

$$E_b = \left[\frac{[E_T - (NE_{Cu}) - (ME_O)]}{N + M}\right], \quad (1)$$

where E_T, E_{Cu}, and E_O are total energy of CuO nanoribbon, energy of the isolated Cu and O atoms, respectively. *N* and *M* are numbers of the atoms of Cu in yellow and O in red color, respectively [23, 24] (the colors can be seen online).

The variation of binding energy per atom of zigzag as well as armchair nanoribbon has been plotted as a function of its width, depicted in Fig. 2.

Table 1. The obtained values of chirality, width, binding energy, magnetic moment and spin polarization of zigzag CuO nanoribbons

Chirality (n, 0)	Width, Å	Binding energy per atom, eV	μ_{total}	Spin polarization	Remarks
(3, 0)	8.14	–2.39	0.44	1	H.M.F#.
(4, 0)	11.36	–2.42	0.28	1	H.M.F.
(5, 0)	14.49	–3.09	0.19	0.41	F.M.F#.
(6, 0)	17.93	–3.10	0.27	0.29	F.M.F.
(7, 0)	21.21	–2.54	0.41	0.77	F.M.F.
(8, 0)	24.75	–2.46	0.61	0.88	F.M.F.
(9, 0)	28.70	–2.41	0.23	0.37	F.M.F.
(10, 0)	32.09	–2.47	0.41	0.55	F.M.F.

Table 2. The obtained values of chirality, width, binding energy, magnetic moment and spin polarization of armchair CuO nanoribbons

Chirality (n, n)	Width, Å	Binding energy per atom, eV	μ_{total}	Spin polarization	Remarks
(3, 3)	14.83	–2.44	0.71	1	H.M.F.
(4, 4)	20.51	–3.13	0.51	0.62	F.M.F.
(5, 5)	26.60	–2.47	0.39	1	H.M.F.
(6, 6)	32.34	–3.13	0.25	0.26	F.M.F.
(7, 7)	38.05	–3.16	0.84	0.70	F.M.F.
(8, 8)	43.87	–2.51	0.71	1	H.M.F.
(9, 9)	50.41	–2.36	0.53	0.56	F.M.F.
(10, 10)	55.61	–3.17	0.47	0.50	F.M.F.

The zigzag nanoribbon of chiralities (5, 0) and (6, 0) are relatively showing better stability than the others reported here. Similarly, the armchair nanoribbon of chiralities (4, 3), (6, 6) and (7, 7) are much stable than others.

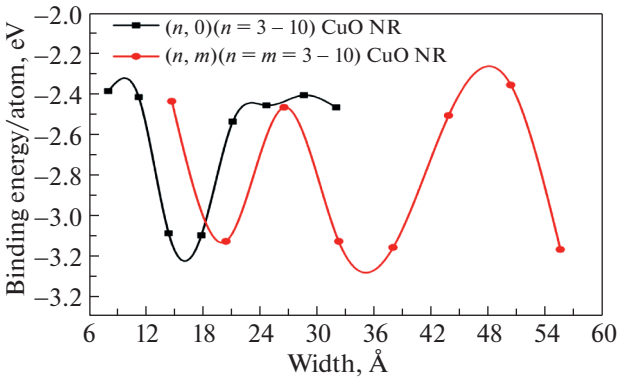

Fig. 2. Binding energy as a function of width of zigzag (n, 0) (n = 3–10) and armchair (n, m) (n = m = 3–10) CuO nanoribbons.

Further, the stable geometries have been investigated for their electronic properties, which further identify their nature as a metal on the basis of their band structure and DOS profile. Markus Heinemann et al. and Y. Wang et al. confirmed the importance of Hubbard potential U, without which the prediction of experimentally observed semiconducting nature of bulk CuO simply by using LDA was not possible, and demonstrated that the bulk CuO is a p-type semiconductor with energy band gap roughly ranging from 1–2 eV. The present study also confirms the importance of Hubbard potential (U = 7.5 eV) [10, 11] along with SGGA in analyzing electronic and magnetic properties of bulk CuO as well as its nanoribbons. The present investigation confirms that the bulk CuO is a semiconducting with approximate energy band gap of 2.02 eV.

The band structures with DOS profiles of zigzag and armchair CuO NRs are shown in Figs. 3a–3h and Figs. 4a–4h, respectively.

The spin up and spin down are the majority and minority of electronic density of states respectively. The computed band structures with DoS profiles con-

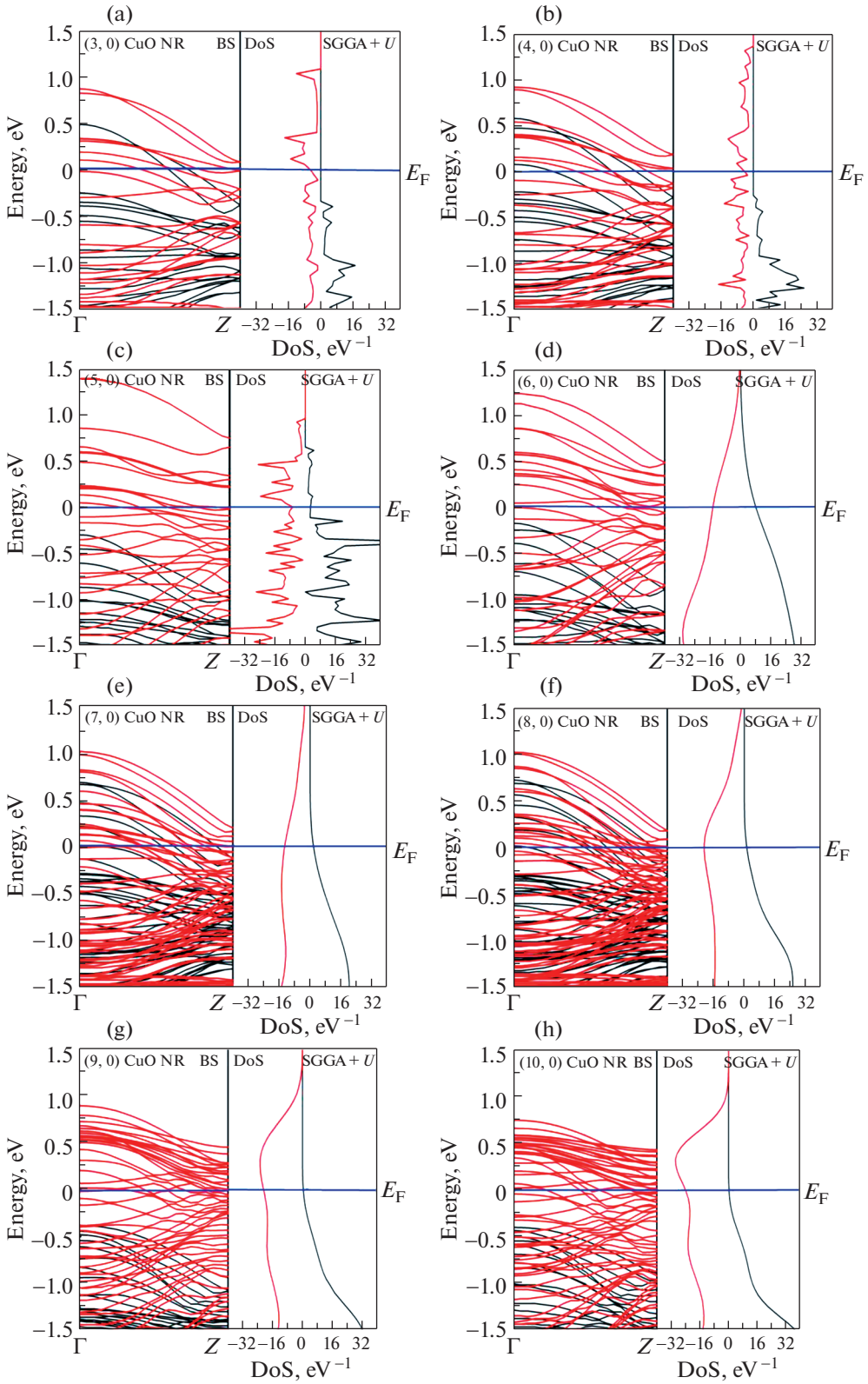

Fig. 3. Band structures with DOS profiles of zigzag (n, 0) (n = 3–10) CuO nanoribbons.

firm the metallic natures for both the morphologies of CuO nanoribbons, portraying a complete transformation from its bulk counterpart, which exhibits a p-type semiconducting behavior having a narrow band gap in range of 1.2–1.9 eV. The hybridization of Cu-3d and O-2p states may produce the peak value of DoS in

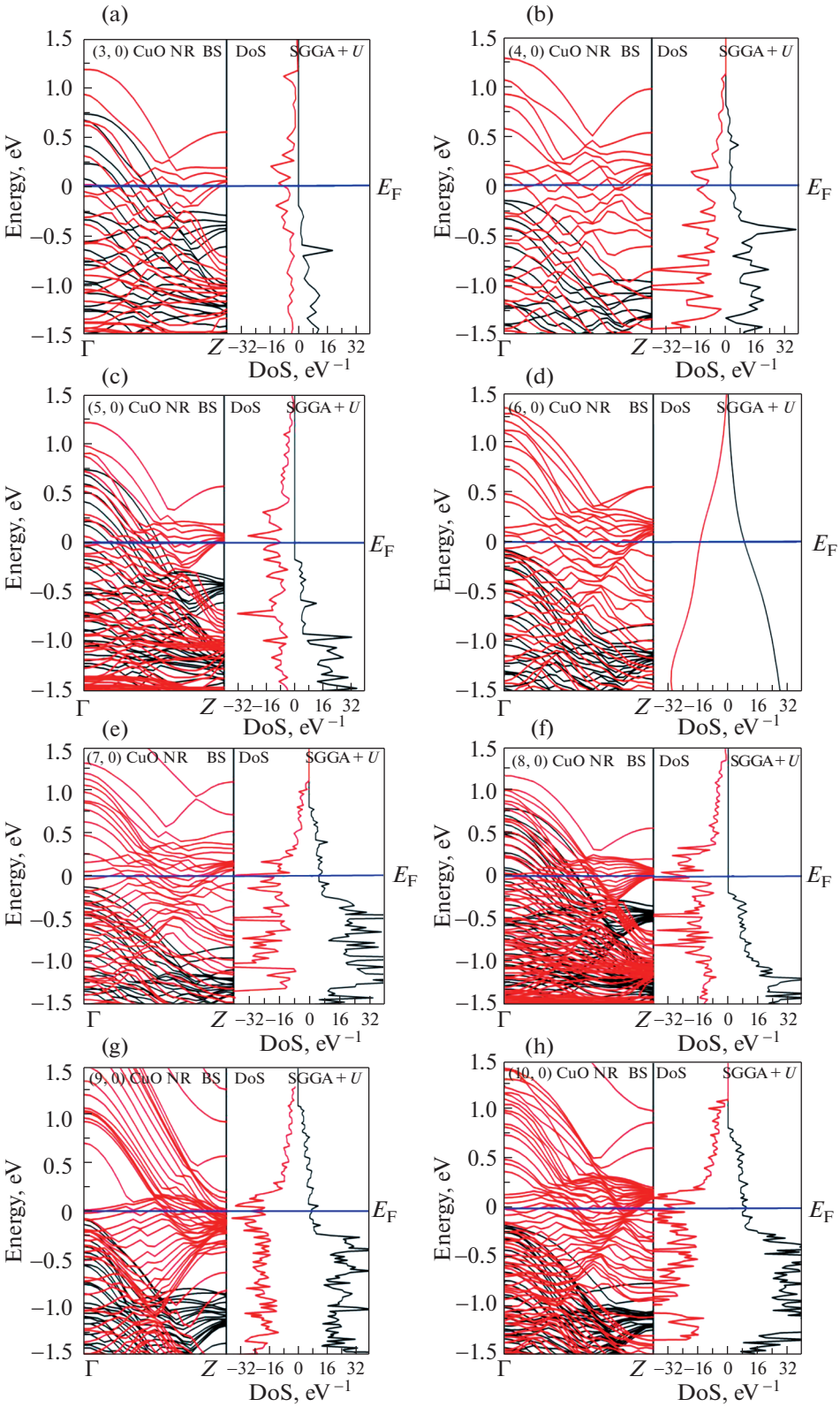

Fig. 4. Band structures with DOS profiles of armchair (n, m) ($n = m = 3–10$) CuO nanoribbons.

valence band, while only Cu-4*s* state may produce the peak value of DoS in conduction band near the Fermi level. The zigzag and armchair CuO nanoribbons have metallic nature due to finite contribution of oxygen atom (O) together with the hybridization of both Cu-3*d* and O-2*p* states [25].

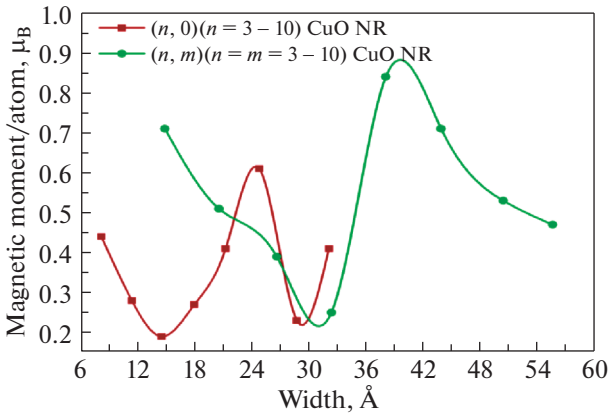

Fig. 5. Magnetic moment as a function of width of zigzag (n, 0) (n = 3–10) and armchair (n, n) (n = 3–10) CuO nanoribbons.

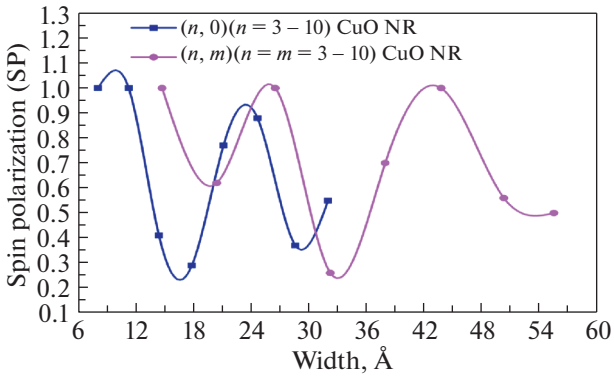

Fig. 6. Spin polarization as a function of width of zigzag (n, 0) (n = 3–10) and armchair (n, m) (n = m = 3–10) CuO nanoribbons.

3.2. Magnetic Properties

On account of the estimations of the band structures and the density of states, both the zigzag and armchair CuO nanoribbons are either half or full metallic. Hence, it is interesting to analyze the magnetic properties of these one-dimensional nanomaterials. The total magnetic moments at different chiralities have been computed through the measurements of DoS at Fermi level. The experimentally reported magnetic moments of bulk CuO, isolated Cu atom, and isolated O atom are 0.86, 0.68 and 0.18μ_B, respectively [25]. In magnetization, the relationship expressed as $\mu_{total} = [\rho\uparrow(E_F) - \rho\downarrow(E_F)]\mu_B$/atom has been applied for the calculation of total dipole moment per unit volume per atom for the different morphologies of CuO nanoribbon, where $\rho\uparrow(E_F)$, $\rho\downarrow(E_F)$, and μ_B are electronic energy densities of spin up and spin down at Fermi level, and Bohr's magneton, respectively. The variation in computed magnetic moment per atom as a function of widths of the zigzag and armchair CuO nanoribbons is shown in Fig. 5.

The computed magnetic moment as a function of width of the zigzag CuO nanoribbon varies between 0.19–0.61μ_B, while for armchair CuO nanoribbon, between 0.24–0.97μ_B at Fermi level. The net magnetic moments of both the types of the nanoribbons have to be produced by the exchange splitting of Cu-3d and O-2p states. As per Hund's rule of magnetism [26, 27], the total magnetic moment of such nanoribbons depends on the magnetic moment of individual atoms, which is in present case the Cu and O atoms. The resultant magnetic moment of Cu and O atoms decreases with decrease in bond length because of the increment in interaction between them. Hence, the fluctuation in magnetic moment on increasing the width are produced in accordance with the variation of bond length between Cu and O. Comparatively, the computed magnitude of magnetic moment of armchair nanoribbon is higher than that of zigzag nanoribbon of CuO.

In the same way, the magnetic nature of metal can be found on the basis of spin-polarization. The spin polarization P is the ratio of the difference of the electron density up spin and down spin to their sum at Fermi level. It is analytically expressed as below, reported elsewhere [28, 29]:

$$P = \frac{\rho\uparrow(E_F) - \rho\downarrow(E_F)}{\rho\uparrow(E_F) + \rho\downarrow(E_F)}, \quad (2)$$

where $\rho\uparrow(E_F)$ is electronic energy density of spin up, $\rho\downarrow(E_F)$ is electronic energy density of spin down, and E_F is Fermi energy.

By using Eq. (2), the spin polarizations of both the zigzag and armchair CuO nanoribbon has been computed and is greater than 0 and equal to or less than 1, tabulated in Tables 1 and 2, respectively, and also depicted in Fig. 6.

The spin polarization distinguishes the half- and full-metal ferromagnetism in zigzag and armchair CuO nanoribbons. The observation confirms that the half-metal (P = 1) and full-metal ($0 < P \leq 1$) ferromagnetic natures of the computed zigzag and armchair CuO nanoribbons.

CONCLUSIONS

The present computational analysis, made through (DFT + U)-based ab initio approach, includes the computation of binding energy per atom varies between –3.16 and –2.18 eV as a function of width of CuO nanoribbon, defends the stabilities of selected nanostructures. The metallic and ferromagnetic behaviors are confirmed through the calculated magnetic moments ranging between 0.19–0.61μ_B in zigzag and 0.24–0.97μ_B in armchair forms of CuO nanoribbon. Comparative analysis confirms that the magnetic moment of armchair CuO nanoribbon is higher than

that of zigzag CuO nanoribbon. The spin polarization, in both the cases, is greater than 0 and equal to or less than 1, confirms the half- or full-metallic ferromagnetic nature of nanoribbons. These peculiar magnetic behaviors in comparison to their bulk counterpart can be well exploited in high-frequency devices, memory devices, sensors, etc. As these findings may cover large areas of the developing fields of science, medicine, and technology, many researchers would get interested in further exploring the other properties of these nanostructures, through computational as well as experimental researches.

ACKNOWLEDGMENTS

TPY is thankful to Midwestern University, Surkhet, Nepal and Central Department of Physics, Tribhuvan University, Nepal for providing the permission for higher study, also grateful to Nepal Academy of Science and Technology (NAST), Nepal for providing the doctoral fellowship. Authors would also like to thank the ABV-IIITM, Gwalior, India for providing the computational resources for carrying out this research work at CNT lab.

CONFLICTS OF INTERESTS

The authors declare that they have no conflict of interest.

REFERENCES

1. H. C. Zeng, Int. J. Nanotechnol. **4**, 329 (2007).
2. Q. Zhang, K. Zhang, D. Xu, G. Yang, H. Huang, F. Nie, C. Liu, and S. Yang, Prog. Mater. Sci. **60**, 208 (2014).
3. H. M. Xiao, S. Y. Fu, L. P. Zhu, Y. Q. Li, and G. Yang, Eur. J. Inorg. Chem. **2007**, 1966 (2007).
4. M. R. Quirino, G. L. Lucena, J. A. Medeiros, I. M. G. D. Santos, and M. J. C. D. Oliveira, Mater. Res. **21**, e20180227 (2018).
5. M. A. Dar, Q. Ahsanulhaq, Y. S. Kim, J. M. Sohn, W. B. Kim, and H. S. Shin, Appl. Surf. Sci. **255**, 6279 (2009).
6. T. H. Tran and V. T. Nguyen, Int. Scholar. Res. Notes **2014**, 856592 (2014).
7. A. Bello, D. D. Arhin, K. Makgopa, M. Fabiane, and N. Manyala, Am. J. Mater. Sci. **4**, 64 (2014).
8. C. Lu, L. Qi, J. Yang, D. Zhang, N. Wu, and J. Ma, J. Phys. Chem. B **108**, 17825 (2004).
9. J. B. Torrance, Y. Tokura, S. J. Laplaca, T. C. Huang, R. J. Savoy, and A. I. Nazzal, Solid State Comun. **66**, 703 (1988).
10. J. G. Bednorz and K. A. Müller, Z. Phys. B **64**, 189 (1986).
11. Y. Wang, S. Lany, J. Ghanbaja, Y. Fagot-Revurat, Y. P. Chen, F. Soldera, D. Horwat, F. Mucklich, and J. F. Pierson, Phys. Rev. B **94**, 245418 (2016).
12. M. Heinemann, B. Eifert, and C. Heiliger, Phys. Rev. B **87**, 115111 (2013).
13. R. K. Sahoo, A. Das, K. Samantaray, S. K. Singh, R. S. Mane, H. C. Shin, J. M. Yun, and K. H. Kim, Cryst. Eng. Comm. **21**, 1607 (2019).
14. Y. X. Zhang, M. Huang, M. Kuang, C. P. Liu, J. L. Tan, M. Dong, Y. Yuan, X. L. Zhao, and Z. Wen, Int. J. Electrochem. Sci. **8**, 1366 (2013).
15. Q. Yu, H. Huang, R. Chen, P. Wang, H. Yang, M. Gao, X. Peng, and Z. Ye, Nanoscale **4**, 2613 (2012).
16. B. Liu and H. C. Zeng, J. Am. Chem. Soc. **126**, 8124 (2004).
17. K. J. Lo, H. Y. Liao, H. W. Cheng, W. C. Lin, B. Y. Yu, J. J. Shyue, and C. C. Chang, J. Nanopart. Res. **13**, 669 (2011).
18. Z. Wang, F. Li, H. Wang, A. Wang, and S. Wu, J. Mater. Sci. **29**, 16654 (2018).
19. W. Kohn and L. J. Sham, Phys. Rev. **140**, A1133 (1965).
20. J. P. Perdew, K. Burke, and M. Ernzerhof, Phys. Rev. Lett. **77**, 3865 (1996).
21. J. M. Soler, E. Artacho, J. D. Gale, A. García, J. Junquera, P. Ordejón, and D. S. A. Portal, J. Phys.: Condens. Matter **14**, 2745 (2002).
22. Atomistix ToolKit, Version 11.8. 2 and 2014.2 QuantumWise A/S. www.quantumwise.com.
23. R. D. Parra and H. H. Farrell, J. Phys. Chem. C **113**, 4786 (2009).
24. A. Fathalian, J. Jalilian, and S. Shahidi, Solid State Commun. **151**, 1635 (2011).
25. S. Paudel, T. P. Yadav, A. Srivastav, and G. C. Kaphle, J. Mater. Sci. Nanotechol. **6**, 1021 (2018).
26. V. M. Medel, J. U. Reveles, S. N. Khannaa, V. Chauhan, P. Sen, and A. W. Castleman, Proc. Natl. Acad. Sci. U. S. A. **108**, 10062 (2011).
27. L. Miao, R. Basak, S. Ran, Y. Xu, E. Kotta, H. He, J. D. Denlinger, Y. D. Chuang, Y. Zhao, Z. Xu, J. W. Lynn, J. R. Jeffries, S. R. Saha, I. Giannakis, P. Aynajian, C. J. Kang, Y. Wang, G. Kotliar, N. P. Butch, and L. A. Wray, Nat. Commun. **10**, 644 (2019).
28. N. A. Cherepkov, J. Phys. B **14**, 2165 (1981).
29. X. Han, W. Mi, and X. Wang, J. Mater. Chem. C **7**, 8325 (2019).

SPELL: OK

Available online at www.sciencedirect.com

ScienceDirect

Materials Today: Proceedings 47 (2021) 6526–6535

materialstoday: PROCEEDINGS

www.materialstoday.com/proceedings

IWCCMP 2016

Half-Metallic and Magnetic Properties for Cu_2O Nanowire: Ab-initio Study

Om Prakash Upadhyay[a,b], Puspa Raj Adhikari[b], Tarani Prasad Yadav[c], Gopi Chandra Kaphle[c,1*], Anurag Srivastava[a]

[a] Advanced Materials Research Group, Computational Nanoscience and Technology Laboratory, ABV-Indian Institute of Information Technology and Management, Gwalior, Madhya Pradesh, India.

[b] Department of Physics, Patan Multiple Campus (T.U.), PatanDhoka, Lalitpur, Nepal.

[c] Central Department of Physics, Tribhuvan University,Kirtipur, Kathmandu, Nepal.

Abstract

The investigation of structural stability, electronic and magnetic properties of Cu_2O nanowire, in the direction of growth (100) and (111) having square: Cu_2O-S(m,n) and hexagonal: Cu_2O-H(m,n) cross-section respectively and diameter ranging from ~(7-15)Å, has been done by using standard Density Functional Theory based on ab-initio self-consistent approach with generalized gradient approximation employing spin polarized case parameterized by revised Perdew Burke Ernzerhoff functional. Here, the binding energy calculation shows that as the cross-section of both the nanowires increases, the binding energy also increases which indicates that the nanowire having smallest cross-section is the least stable and vice-versa. Interestingly, from the analysis of electronic properties it can be concluded that the considered Cu_2O nanowire exhibit half metallic nature showing the 100% of spin polarization at Fermi energy E_f. The asymmetric nature of spin up and spin down density of states shown by total DOS plot suggests us that all the Cu_2O nanowire structures are magnetic in nature. Here, we found that there is decrease in total calculated magnetic moment per atom with increase in cross-sectional diameter but the total magnetic moment per unit cell gives the integer value with increased status. Also, the analysis of spin orientation of Cu and O atoms shows that both atoms are Ferro magnetically spin polarized with each other indicating the Cu_2O nanowire is half-metallic ferromagnetic semiconductor.

© 2019 Elsevier Ltd. All rights reserved.

Peer-review under responsibility of the scientific committee of the International Workshop/Conference on Computational Condensed Matter Physics and Materials Science: Materials of Energy and Environment, IWCCMP-2016, 18–20 Nov 2016, ABV-Indian Institute of Information Technology and Management, Gwalior.

*Keywords:*DFT, Binding energy, Magnetic moment, ferromagnetism, Half-metal, Cu_2O, Spin polarization.

1. Introduction

A dramatic increase in research activities on nanostructured semiconductor materials due to their unique physical properties [1-5] has created a great demand for a reference source that summarizes the current state-of-the-art nanotechnology. Among them, Nanowires, which are one of the most common 1-D nanostructures, that exhibit high aspect ratio and quantum confinement effect, are attractive candidates since they present variety of applications [6-8] in the field of Nano devices. From past decades, the transition metal oxide semiconductor nanostructure

E-mail: gck223@gmail.com

© 2019 Elsevier Ltd. All rights reserved.

Peer-review under responsibility of the scientific committee of the International Workshop/Conference on Computational Condensed Matter Physics and Materials Science: Materials of Energy and Environment, IWCCMP-2016, 18–20 Nov 2016, ABV-Indian Institute of Information Technology and Management, Gwalior.

attracted a steadfast attention to the researcher in the experimental as well as theoretical research as they offer new opportunities both for fundamental research & technological applications [9-11].

Being relatively nontoxic, low cost & high natural abundance, the nanostructured Cu_2O act as a versatile candidate as it possesses unique electronic, magnetic & optical properties [12-14]. It is well known p-type direct band gap (2.17eV) transition metal oxide semiconductor and crystallizes in its cuprite structure with lattice constant 4.2696Å where Cu cations can be viewed in a fcc sub lattice and O anions in a bcc sub lattice [15,16]. It is diamagnetic in its ground state [17]. The nanostructured Cu_2O with various morphologies have been successfully synthesized using various methods [18-22] which have variety of applications in the field of Nano devices such as optoelectronic [23], thermoelectric device [24], sensing [25], solar cells[26], photocatalysis [27], spintronic [28] etc. Experimentally it has been reported that there is induction of anomalous weak ferromagnetism [29] in Cu_2O nanowire having diameter (50-100)Å. Also, doping of transition metal on bulk Cu_2O induces stable integer magnetic moment resulting either insulating or half metallic ground state [28]has already been reported. These literatures suggest us that the confinement of material from bulk to Nano size or changing their internal configuration may lead to unique as well as unexpected results. Half metals, first postulated by de Groot, are those magnetic materials who's one spin direction exhibit metallic character and the other spin direction shows semiconducting or insulating character leading to 100% spin polarization [30]. The materials which exhibit half metallic ferromagnetism, uses electron spin in place of electron charge, have attracted precise attention in the spintronic applications [31, 32]. From the past few years, the researchers were much more exercising to create those spintronic devices which exhibit high curie temperature (T_c) and high magnetic moment and of course numerous types of detailed studies on different materials [33] has been done.

In this article, firstly we report the stability of the considered Cu_2O nanowire on the basis of binding energy. Secondly, by analyzing band structure and DOS profile we investigate the half metallic nature on which, to our knowledge, no such data has been reported yet. And, lastly we examine the magnetic moment and orientation of spin direction by means of Mullikan population analysis. The following section contains the computational details, which is followed by the section "Result and Discussion" and "Conclusion".

2. Computational Details

In this paper, the first principal computation has been performed in the framework of density functional theory (DFT) [34, 35] followed by non-equilibrium green function (NEGF) [36] which is supported by ab-initio coded Atomistix Toolkit Virtual Nano lab (ATK-VNL) [37]. This ATK-VNL is developed in academic code Tran SIESTA [38] employing localized basis set developed in SIESTA [39]. The entire calculation of this work has been done through generalized gradient approximation [40] with spin polarized case whose functional is parameterized by revised Perdew Burke Ernzerhoff (rPBE) [41]. The description of valance electrons of copper and oxygen was made by localized pseudo atomic orbital's (PAOs) [42]. For Cu valance electrons, double zeta double polarize (DZDP) basis set and for O valance electrons, double zeta polarize (DZP) [37] basis set was chosen. In order to minimize the total energy, all the nanowire structures were optimized before performing calculations. The calculations were run by taking k-point sampling 1x1x30, mesh cut off energy 75 Hartree and maximum force of tolerance 0.05 eV/A.

3. Results and Discussions

3.1 Structural Stability

In the present work, the investigation of structural stability, electronic and magnetic properties of Cu_2O-S(m,n) and Cu_2O-H(m,n) nanowire [S, H, m & n represents square cross-sectional, hexagonal cross-sectional, number of copper atom and number of oxygen atom respectively] are made by using standard Density Functional Theory with SGGA-

rPBE functional. Before taking the calculations, all the nanowire structures are relaxed in order to achieve them in their minimum energy state (stable) configuration. Also we take (110) surface energy equals to 0.1 as it lowers the surface energy by ten times for energy minimization. The optimized structures of both Cu2O-S(m,n) and Cu2O-H(m,n) are as shown in figure (1-2) as below. In order to find binding energy first we calculate the total energy of isolated copper atom and oxygen atom which are found to be -1228.4282eV and -429.9342eV respectively. Now the binding energy calculations are done by using the standard formula as given in equation [43]:

$$E_b = \frac{\{nE_T(Cu_{iso})+mE_T(O_{iso})-E_T(Cu_2O)\}}{n+m} \quad (2)$$

Where, E_T represents the total energy of isolated copper, oxygen atom and Cu_2O nanowire, and n, m represents the number of Cu-atom and O-atom respectively.

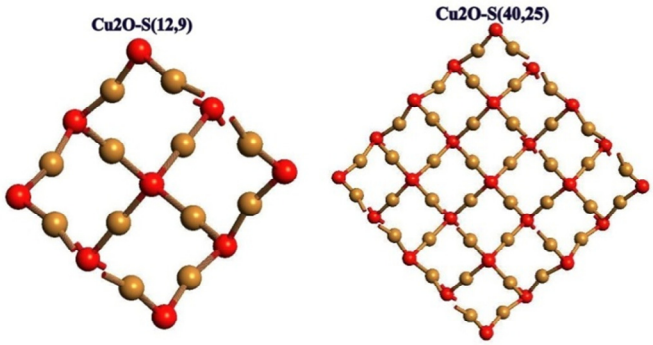

Fig: 1 Optimized geometry of Cu_2O-S(12,9) (left) and Cu_2O-S(40,25) (right) NWs.

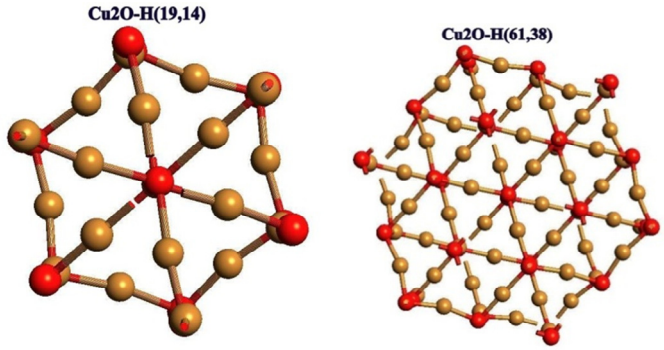

Fig: 2 Optimized geometry of Cu_2O-H(12,9) (left) and Cu_2O-H(40,25) (right) NWs.

Table 1: The calculated half-metallic band gap, binding energy, calculated total & partial magnetic moments and spin polarization for Cu_2O-S(m,n) & Cu_2O-H(m,n) nanowire.

The calculated binding energies of each structure are tabulated in table 1. The comparative study focuses on the fact that the binding energy of smallest diameter nanowire for both cross-section is least and goes on increasing as the cross-sectional diameter increases from which we can conclude that the stability of both the nanowire increases as the cross-sectional diameter increases. Also we calculate the binding energy of bulk 2x2x2 Cu_2O relaxed structure and was found to be 4.25eV which is about to that of considered nanowire structure. From this we can say that the stability of our considered nanowire structure is about the same as bulk Cu_2O structure.

3.2 Electronic Properties

The calculated spin polarized band structure for considered relaxed nanowire with spin up (majority) and spin down (minority) electron state are illustrated as in figure (3-6), where red lines indicates the minority spin and black lines indicates the majority spin. The band structure plot for each nanowire of different diameter shows that the minority spin state crosses the Fermi level, which indicates metallic nature due to spin down electrons whereas the majority spin state has remarkable energy gap around Fermi level. This confirms the present system as a half-metal. The half metallic energy gap (E_{HM}) for majority carriers is calculated from the energies of valance band maximum (VBM) and conduction band minimum (CBM) and is illustrated in table 1. Here, the dispersed bands in band structure around Fermi level are mostly because of strong hybridization between Cu-3d and O-2p electrons. The comparative study of band structure tells us that as the cross-sectional diameter increases, the half metallic band gap goes on decreasing from wide band gap semiconductor to small band gap semiconductor. Also we found that half metallic band gap of hexagonal cross-sectional nanowire is somewhat greater than that of square cross-sectional nanowire as compared with comparative diameter.

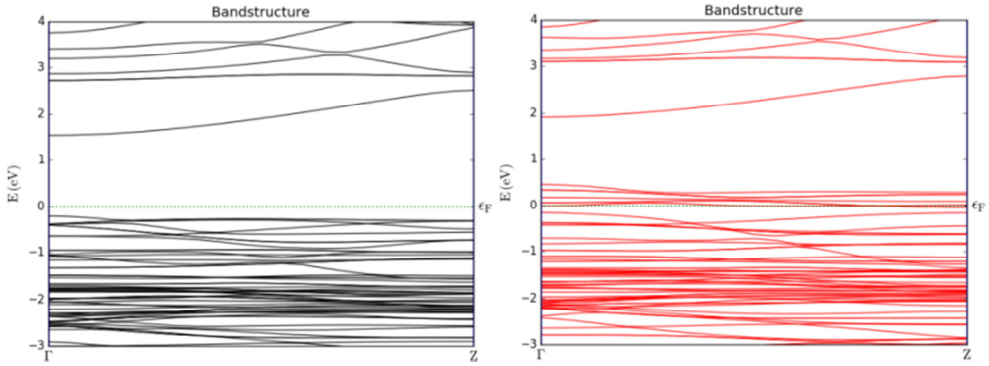

Fig: 3 Band structure of spin-up state (left) and spin-down state (right) of Cu_2O-S(12,9) Nws.

Table-1. Energy Bandgap, binding energy and magnetic moment of different configurations.

S.N.	Structures	Diameter (Å)	Bandgap (eV)	B.E. (eV)	m_{cu} (μ_B)	m_o (μ_B)	m_t/unit cell (μ_B)	m_t/atom (μ_B)	Polarization (%)
1.	Cu_2O-S(12,9)	7.37	1.74	4.04	3.136	2.867	6.003	0.286	100
2.	Cu_2O S(40,25)	14.52	0.83	4.16	5.918	4.060	9.978	0.154	100
3.	Cu_2O-H(19,14)	7.20	1.79	4.04	4.710	4.298	9.008	0.273	100
4.	Cu_2O-H(61,38)	14.16	0.96	4.16	9.020	5.906	14.926	0.151	100

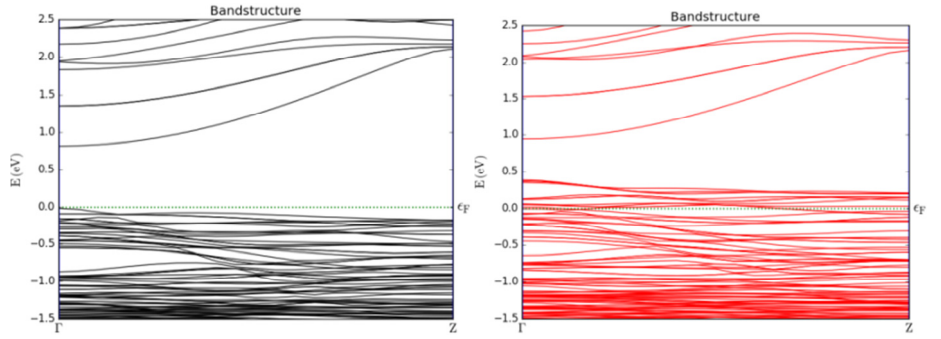

Fig: 4 Band structure of spin-up state (left) and spin-down state (right) of Cu_2O-S(40,25) Nws.

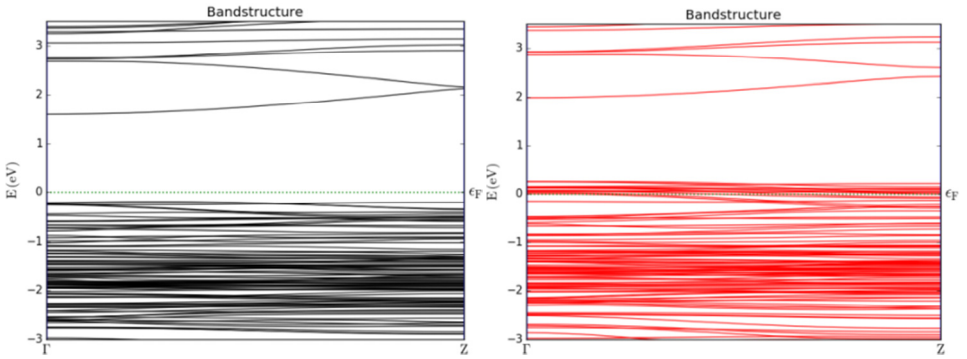

Fig: 5 Band structure of spin-up state (left) and spin-down state (right) of Cu_2O-H(19,14) Nws.

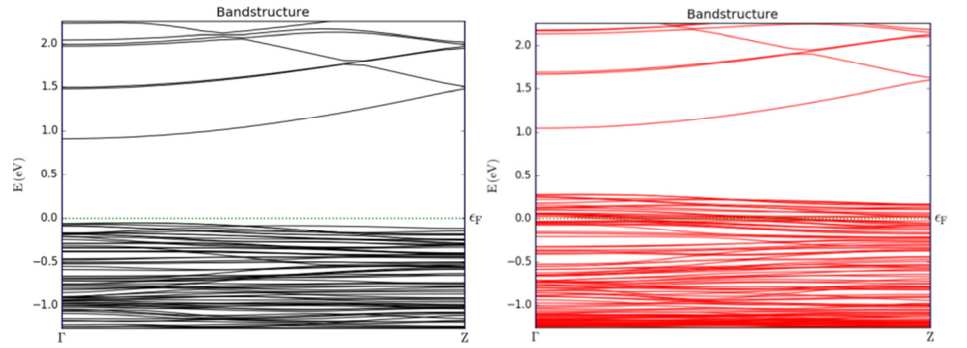

Fig: 6 Band structure of spin-up state (left) and spin-down state (right) of Cu_2O-H(61,38) Nws.

Similarly, the calculated spin polarized total DOS and partial DOS plot of all the considered nanowire structures with majority spin and minority spin are depicted as in figure (7-10) respectively, where black lines indicates the majority spin state and red lines indicates the minority spin state. From the analysis of DOS we observe that, for all structures, there is a finite gap in the majority spin state at the Fermi level while in the minority spin state, the density of state has some value different from zero which also confirms the considered system as half metal. Also, the asymmetric nature of spin up and spin down density of states shown by total DOS plot suggests us that all the Cu_2O nanowire structures are magnetic in nature. Here, for both square as well as hexagonal cross-sectional nanowire, the 2-D plot of DOS shows that there is high concentration of charge carriers in valance band where as the carrier concentration in conduction band is negligible. The total contribution to majority spin and minority spin channel form total DOS is mainly due to copper 3d and somewhat due to oxygen 2p electrons.Also, PDOS analysis shows that in both valance band and conduction band thepeaks around the Fermi energy is majorly composed of 3d

states of copper andsomewhat due to 2p states of oxygen. The peaks around the Fermi level due to 4sstate shows the negligible contribution for both square and hexagonal cross-sectional nanowire as compared to Cu-3d and O-2p states.

This energy gap in the majority spin state leads to 100% spin polarization, which mathematically can be defined by the equation [44]:

$$P = \frac{N\downarrow(E_f) - N\uparrow(E_f)}{N\downarrow(E_f) + N\uparrow(E_f)} \text{ x } 100\% \qquad (2)$$

Where, $N\downarrow(E_f)$and $N\uparrow(E_f)$represents the density of states of spin down and spin up states respectively at Fermi level.

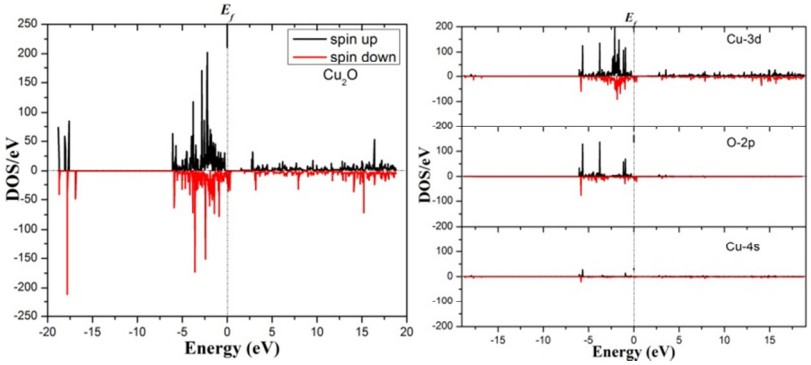

Fig:7 Total (left) and partial (right) DOS of Cu_2O-S(12,9) Nws.

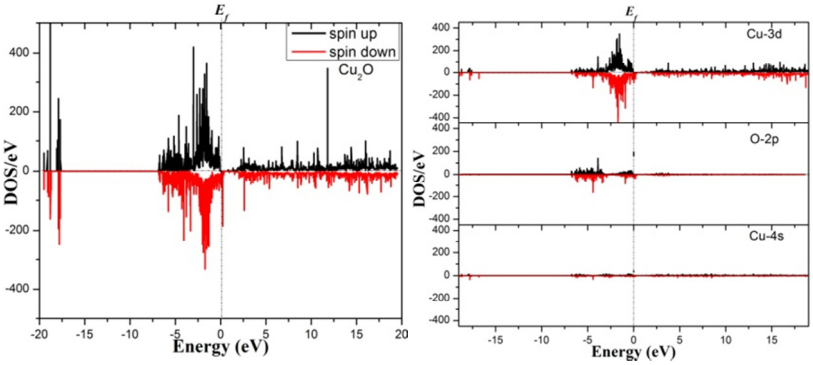

Fig:8 Total (left) and partial (right) DOS of Cu_2O-S(40,25) Nws.

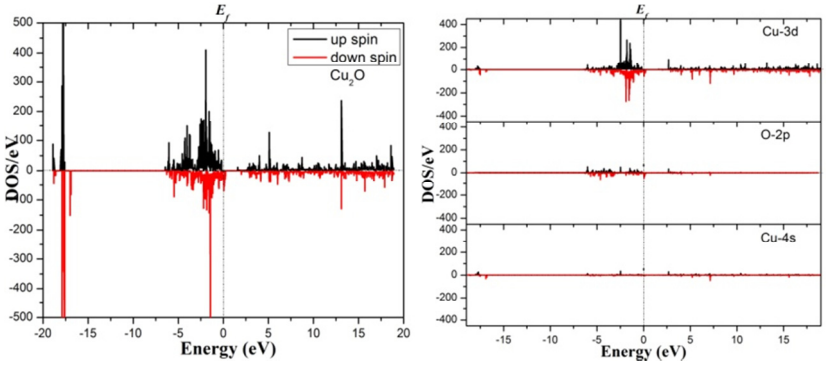

Fig:9 Total (left) and partial (right) DOS of Cu_2O-H(19,14) Nws.

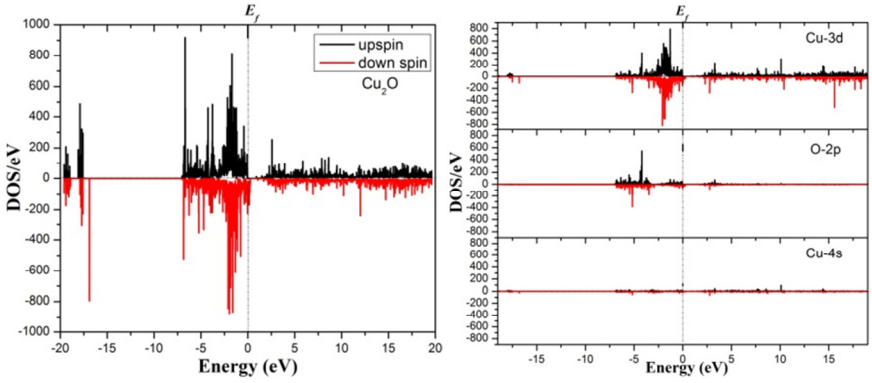

Fig:10 Total (left) and partial (right) DOS of Cu_2O-H(61,38) Nws.

3.3 Magnetic Properties

As the band structure along with DOS of Cu_2O nanowire exhibits half metallic nature, it becomes an interesting task to summarize the magnetic properties too. To calculate magnetic moment we use Mullikan population analysis method. The calculated total and partial magnetic moments per unit cell of Cu_2O nanowire of respective diameter are listed as in table1. From this result we came to know that the local magnetic moment per atom at both Cu and O cites goes on decreasing if we increase cross-sectional diameter of both nanowire. This fact may be the result of increase in number of atoms with increase in diameter that causes strong hybridization and hence made the local magnetic moment at both Cu and O cite to decreases. But the total as well as partial magnetic moment per unit cell of all structure goes on increasing resulting almost integer value which again confirms the half metallic nature as integer magnetic moment is the property of half metal. Also we found that the magnetic spin of both copper and oxygen atoms has the same spin direction as shown in table1 which confirms the ferromagnetic nature. From this we can conclude that Cu_2O nanowire is a half metallic ferromagnetic. In general, the exchange splitting of majority and minority states generates the magnetic moment. In Cu_2O nanowire, the majority as well as minority states are mainly due to copper 3d and oxygen 2p states and hence the exchange splitting between these major two states may be the main cause for generation of total magnetic moment. Here, we analyse that, for the comparative diameter, the magnetic moment per unit cell of Cu_2O nanowire with hexagonal cross-section is higher than that of rectangular cross-sectional diameter.

4. Conclusions

In conclusion, we have studied the Cu_2O nanowire with their structural, electronic and magnetic properties in the framework of DFT within SGGA approximation as a function of diameter. From the detailed analysis, we found that all these properties of nanowire are strongly influenced due to quantum confinement effect as the bulk Cu_2O is well known p-type direct band gap semiconductor and is nonmagnetic in its ground state. Stability analysis confirms that stability of nanowire increases with increase in diameter. Further, band structure and DOS analysis surprises us that all the considered nanowire exhibit half metallic nature leading to 100% spin polarization at Fermi energy. We found the remarkable integer magnetic moment per unit cell which is also sign of half metallicity. Also, magnetic moment of both copper and oxygen atom shows the same spin direction indicating ferromagnetic nature. Thus, we can conclude that our considered system of Cu_2O nanowires exhibit half-metallic ferromagnetic semiconducting nature which makes it as a promising material for spintronic applications such as non-volatile magnetic memories,

magnetic sensors, spin injectors etc. So far we know, no refinement data has been published yet on Cu_2O nanowire of half metallic ferromagnetic semiconducting nature with diameter ranging from ~(7-15)Å. So, we hope that this literature, for both experimental as well as theoretical researcher, may certainly be of great interest to explore other properties of this nanowire.

Acknowledgements

The authors are grateful to ABV-IIITM Gwalior for providing Computational Nanoscience and Technology Laboratory (CNTL) for the computational work. Also I would like to express my gratitude to AMR group for technical support for carrying out the present research work.

References

[1] L. S. Li, J. Walda, L. Manna and A. P. Alivisatos. Semiconductor nanorod liquid crystals. Nano Letters, 2(6), (2002) 557.
[2] N. Gorjizadeh, and Y. Kawazoe. Chemical functionalization of grapheme nanoribbons. Journal of Nanomaterials, 2010(13), (2010). (2010) 513501.
[3] S. M. Lee, Y. H. Lee, Y. G. Hwang, J. Elsner, D. Porezag and T. Frauenheim. Stability and electronic structure of GaN nanotubes from density-functional calculations. Physical Review B, 60(11), (1999) 7788.
[4] S. G. Rejitha and C. Krishnanb. Optical characterizations of Zn-doped CuO nanoparticles. Science Acta Xaver, 4(1), (2013) 91.
[5] C. Li, D. Zhang, S. Han, X. Liu, T. Tang, B. Lei, Z. Liu and C. Zhou. Synthesis, electronic properties, and applications of indium oxide nanowires. Annals of the New York Academy of Sciences, 1006(1), (2003) 104.
[6] Y. Li, F. Qian, J. Xiang and C. M. Lieber. Nanowire electronic and optoelectronic devices. Materials Today, 9(10), (2006) 18.
[7] W. Lu, P. Xie and C. M. Lieber. Nanowire transistor performance limits and applications. IEEE transactions on Electron Devices, 55(11), (2008) 2859.
[8] T. Mikolajick and W. M. Weber. Silicon nanowires: fabrication and applications. Anisotropic Nanomaterials, Springer International Publishing, (2015) 1.
[9] Z. Szoteka, W. M. Temmermana, A. Svaneb, L. Petitb , G. M. Stocksc and H. Winterd. Half-metallic transition metal oxides. Journal of Magnetism and Magnetic Materials, 272(11), (2004) 1816.
[10] M. H. Park, J. H. Li, A. Kumar, G. Li and Y. Yang. Doping of the metal oxide nanostructure and its inuence in organic electronics. Advanced Functional Materials, 19(8), 1241 (2009). M. H. Park, J. H. Li, A. Kumar, G. Li and Y. Yang. Doping of the metal oxide nanostructure and its inuence in organic electronics. Advanced Functional Materials, 19(8), (2009) 1241.
[11] Y. N. Chang, M. Zhang, L. Xia, J. Zhang and G. Xing. The toxic effects and mechanisms of CuO and ZnO nanoparticles. Materials, 5(12), (2012) 2850.
[12] J. Ghijsen, L. H. Tjeng, J. van Elp, H. Eskes, J. Westerink and G. A. Sawatzky. Electronic structure of Cu_2O and CuO. Physical Review B, 38(16), (1988) 11322.
[13] E. Ruiz, S. Alvarez, P. Alemany and R. A. Evarestov. Electronic structure and properties of Cu_2O. Physical Review B, 56 (12), (1997) 7189.
[14] I. S. Brandt, A. D. C. Viaegas, J. H. D. D. Silva and A. A. Pasa. Structural and optical properties of Cu_2O crystalline electrodeposited films. Thin Solid Films, 562(3), (2014) 144.
[15] P. A. Korzhavyi and B. Johansson. Literature review on the properties of cuprous oxide Cu_2O and the process of copper oxidation. Swedish nuclear fuel and waste management company, (2011) 1.
[16] W. Y. Ching, Y. N. Xu and K. W. Wong. Ground-state and optical properties of Cu2O and CuO crystals. Physical Review B, 40(11), (1989) 7684.
[17] C. Chen, L. He, L. Lai, H. Zhang, J. Lu, L. Guo and Y. Li. Magnetic properties of undoped Cu_2O _ne powders with magnetic impurities and/or cation vacancies. Journal of Physics: Condensed Matter, 21(14), (2009) 14560.

[18] X. M. Liu and Y. C. Zhou. Electrochemical deposition and characterization of Cu2O nanowires. Applied Physics A, 81(4), (2005) 685.
[19] J. Shi, J. Li, X. Huang and Y. Tan. Synthesis and enhanced photocatalytic activity of regularly shaped Cu_2O nanowire polyhedra. Nano Research, 4(5), (2011) 448.
[20] M. A Khan, M. Ullah, T. Iqbal, H. Mahmood,A. A. Khan and et al. Surfactant Assisted Synthesis of Cuprous Oxide (Cu_2O) Nanoparticles via Solvothermal Process. Nanoscience and Nanotechnology Research. 3(1), (2015) 16.
[21] C. H. Kuo and M. H. Huang. Morphologically controlled synthesis of Cu_2O nanocrystals and their properties. Nano Today, 5(2), (2010) 106.
[22] S. Bugarinovic, M. R. Vujasinovic, Z. Stevic and V. Grekulovic. Cuprous oxide as an active material for solar cells. Solar Cells New Aspects and Solutions, 17(8), (2011) 167.
[23] P. W. Baumeister. Optical absorption of cuprous oxide. Physical Review, 121(2), (1961) 359.
[24] X. Chen, D. Parker, M. H. Du and D. J. Singh. Potential thermoelectric performance of hole-doped Cu_2O. New Journal of Physics, 15(4), (2013) 043029.
[25] M. Kevin, W. L. Ong, G. H. Lee and G. W. Ho. Formation of hybrid structures: copper oxide nanocrystals templated on ultralong copper nanowires for open network sensing at room temperature. Nanotechnology, 22(23), (2011) 235701.
[26] . Mittiga, E. Salza, F. Sarto, M. Tucci and R. Vasanthi. Heterojunction solar cell with 2% efficiency based on a Cu2O substrate. Applied Physics Letters. 88(16), (2006) 163502.
[27] J. Shi, J. Li, X. Huang and Y. Tan. Synthesis and enhanced photocatalytic activity of regularly shaped Cu_2O nanowire polyhedra. Nano Research. 4(5), (2011) 448.
[28] M. Sieberer, J. Redinger and P. Mohn. Electronic and magnetic structure of cuprous oxide Cu_2O doped with Mn, Fe, Co and Ni: A density-functional theory study. Physical Review B, 75(3), (2007) 035203.
[29] L. Liao, B. Yan, Y. F. Hao, G. Z. Xing, J. P. Liu and et al. P-type electrical, photoconductive, and anomalous ferromagnetic properties Cu_2O nanowires. Applied Physics Letters, 94(11), (2009) 113106.
[30] R. A. de Groot, F. M. Mueller, P. G. Van Engen and K. H. J. Buschow. New class of materials: half-metallic ferromagnets. Physical Review Letters, 50(25), (1983) 2024.
[31] M. I. Katsnelson, V. Y. Irkhin, L. Chioncel, A. I. Lichtenstein and R. A. de Groot. Half-metallic ferromagnets: From band structure to many-body effects. Reviews of Modern Physics, 80(2), (2008) 315.
[32] S. Picozzi, A. Continenza and A. J. Freeman. Co_2MnX (X= Si, Ge, Sn) Heusler compounds: An ab-initio study of their structural, electronic, and magnetic properties at zero and elevated pressure. Physical Review B, 66(9), (2002) 094421.
[33] H. Kato, T. Okuda, Y. Okimoto, Y. Tomioka, K. Oikawa and T. Kamiyama. Structural and electronic properties of the ordered double perovskites A_2MReO_6 (A= Sr, Ca; M= Mg, Sc, Cr, Mn, Fe, Co, Ni, Zn). Physical Review B, 69(18), (2004) 184412.
[34] H. Eschrig. The fundamentals of density functional theory. Stuttgart: Teubner, 32(12), (1996) 76.
[35] M. Brandbyge, J. L. Mozos, P. Ordejon, J. Taylor and K. Stokbro. Density functional method for nonequilibrium electron transport. Physical Review B, 65(16), (2002) 165401.
[36] F. D. Novaes, A. J. R. da Silva and A. Fazzio. Density functional theory method for non-equilibrium charge transport calculations: TRANSAMPA. Brazilian Journal of Physics, 36(3A), (2006) 799.
[37] Atomistix Tool Kit Version 11.8.2 and 2014.2 ,Quantumwise A/S .(www.quantumwise.com).
[38] K. Stokbro, J. Taylor, M. Brandbyge and P. Ordejon. TranSIESTA: a spice for molecular electronics. Annals of the New York Academy of Sciences, 1006(1), (2003) 212.
[39] J. M. Soler, E. Artacho, J. D. Gale, A. Garcia, J. Junquera, P. Ordejon and D. S. Portal. The SIESTA method for ab-initio order-N materials simulation. Journal of Physics: Condensed Matter, 14(11), (2002) 2745.
[40] J. P. Perdew, K. Burke and M. Ernzerhof. Generalized gradient approximation made simple. Physical Review Letters. 77(18), (1996) 3865.

[41] B. Hammer, L. B. Hansen and J. K. Norskov. Improved adsorption energetic within density-functional theory using revised Perdew-Burke-Ernzerhof functionals. Physical Review B, 59(11), (1999) 7413.
[42] G. B. Bachelet, D. R. Hamann and M. Schlter. Pseudopotentials that work: from H to Pu. Physical Review B, 26(8), (1982) 4199.
[43] A. Srivastava, S. K. Jain and P. S. Khare. Ab-initio study of structural, electronic, and transport properties of zigzag GaP nanotubes. Journal of Molecular Modeling, 20(3), (2014) 1.
[44] S. Paudel, S. Dandeliya, R. Chaurasiya, A. Srivastava and G. C. Kaphle. Magnetism in zigzag and armchair CuO nanotubes: Ab-initio study. Journal of Magnetism and Magnetic Materials, 406(9), (2016) 8.

ISSN 1063-7834, Physics of the Solid State, 2020, Vol. 62, No. 8, pp. 1361–1369. © Pleiades Publishing, Ltd., 2020.

MAGNETISM

DFT Analysis of Ferromagnetism in Zigzag and Armchair CuO Nanosheets

T. P. Yadav[a, b, c], A. Srivastava[b, *], and G. C. Kaphle[a]

[a] *Central Department of Physics, Tribhuvan University, Kirtipur, Kathmandu, Nepal*

[b] *Advanced Materials Research Group, CNT Lab, Atal Bihari Vajpayee Indian Institute of Information Technology and Management, Gwalior (M.P.), 474010 India*

[c] *Central Campus of Science and Technology, Mid-Western University, Surkhet, Nepal*

** e-mail: profanurag@gmail.com*

Received March 23, 2020; revised March 23, 2020; accepted March 23, 2020

Abstract—We report the structural, electronic, and magnetic properties of "zigzag" and "armchair" CuO nanosheets. The density function theory (DFT)-based ab initio approach has been applied through revised Perdew, Burke, and Ernzerhof (rPBE) parameterized spin generalized-gradient approximation (SGGA) + mean-field Hubbard correction (U) exchange-correlation functional. In comparison to the semiconducting bulk CuO, the other forms of CuO nanosheets show metallic behavior and their structural stabilities have been analyzed through binding energy estimation. Using SGGA, the computed magnetic moment per atom of zigzag CuO nanosheet varies irregularly between 0.66 and 1.19 μ_B, whereas for armchair CuO, between 0.59 and 1.53 μ_B. The addition of U changes this variation from 0.68 to 0.76 μ_B in zigzag and from 0.62 to 1.29 μ_B in armchair nanosheets, respectively. The computed spin polarization as unity or less than unity identifies the ferromagnetism in these materials. Obtained results of CuO nanosheets defend them as a potential candidate for a variety of electronic devices like gas sensors, electrodes, energy storage devices, etc.

Keywords: CuO, nanosheet, DFT, electronic properties, magnetic moment, SGGA

DOI: 10.1134/S1063783420080314

1. INTRODUCTION

Since the discovery of graphene by Geim and Novoselov through their innovative experiments [1] performed in 2004 and received the Nobel Prize in 2010, various efforts have been made on the possible applications of this material. The graphene consists of a monolayer of carbon atoms wrapped up into zero, one, two, and three-dimensional forms as a cluster, tube, sheet, and graphite (bulk), etc. The discovery of different morphologies of carbon and its applications has made a revolutionary vs. evolutionary impact in the field of electronics, engineering, and medical science. In the same series, the oxides have also been impacted a lot the various industries. This has opened the door of new research for many researchers, to look for the morphologies of different metal oxides, including CuO and others. The bulk form of CuO is semiconducting with a band gap of 1.4 ± 0.3 eV [2–5], whereas its one-dimensional forms show unique physical and chemical properties due to large specific surface area [6], excellent solar light absorbance [7], and a narrow band gap as p-type semiconductor. The CuO cluster, nanotube, nanowire, and nanosheet have been reported with their attractive properties such as the increment in the relative surface area and new quantum effects [8–11]. This enhancement in the properties of reduced dimensional CuO has motivated us to look at its two-dimensional nanosheets in zigzag and armchair morphologies as a potential candidate in gas sensing of various flammable gases like ethanol, gasoline, acetone, and other gases as H_2S [12, 13], batteries [14, 15], novel energy storage devices, photo catalysts [16], non-enzymatic glucose sensor [17], etc. Due to novel electronic, magnetic, and recently reported the high-temperature superconductivity in copper oxide perovskites [18], the structural stability of nanowire, nanoribbon, and a metal-doped nanotube of CuO are of great interest to the scientific community. In a few earlier DFT-based reports, the local density approximation (LDA)-based analysis couldn't explain the semiconducting behavior of bulk CuO, whereas the addition of Hubbard correction with LDA has made this analysis possible. However, various DFT analysis have confirmed that the band structure prediction is much easier through GGA-, rather than LDA-based analysis.

In the present report, the optimized zigzag ($1 \le n \le 8$, $m = 0$) and armchair ($1 \le n \le 8$, $m = n$) CuO nanosheets have been analyzed for its structural stability and electronic and magnetic properties, discussed

Table 1. The width, binding energy, magnetic moment per atom, and spin polarization of zigzag CuO nanosheets with different chirality

S.N.	Zigzag nanosheet of CuO	Width, Å	Binding energy per atom, eV		Magnetic moment per atom, μ_B		Spin polarization	
			SGGA	SGGA+U	SGGA	SGGA+U	SGGA	SGGA+U
1	(1, 0)	1.97	–3.89	–2.57	0.71	0.76	0.61	1
2	(2, 0)	5.18	–3.88	–2.57	0.93	0.72	0.70	1
3	(3, 0)	8.52	–3.89	–2.56	0.66	0.69	0.58	1
4	(4, 0)	11.88	–3.88	–2.56	0.97	0.70	0.63	1
5	(5, 0)	15.25	–3.88	–2.56	0.93	0.76	0.61	1
6	(6, 0)	18.62	–25.81	–2.56	1.19	0.73	0.69	1
7	(7, 0)	21.99	–22.42	–2.55	0.72	0.76	0.58	1
8	(8, 0)	25.37	–29.28	–2.52	0.90	0.68	0.64	1

Table 2. The width, binding energy, magnetic moment per atom, and spin polarization of armchair CuO nanosheets with different chirality

S.N.	Armchair nanosheet of CuO	Width, Å	Binding energy per atom, eV		Magnetic moment per atom, μ_B		Spin polarization	
			SGGA	SGGA+U	SGGA	SGGA+U	SGGA	SGGA+U
1	(1, 1)	5.15	–3.04	–2.58	0.71	0.62	0.61	1
2	(2, 2)	10.84	–3.08	–2.50	0.59	0.71	0.59	1
3	(3, 3)	16.63	–3.16	–2.50	0.63	0.71	0.58	0.62
4	(4, 4)	22.46	–3.11	–2.50	1.53	0.69	0.75	1
5	(5, 5)	28.29	–3.14	–3.20	0.69	0.72	0.61	0.74
6	(6, 6)	34.14	–3.09	–2.50	0.70	0.65	0.61	1
7	(7, 7)	39.98	–3.10	–3.20	0.63	1.29	0.58	1
8	(8, 8)	45.83	–3.09	–3.20	1.21	0.74	0.72	1

in terms of their binding energy, the magnetic moment per atom, and spin polarization, where integers n and m denote the numbers of unit vector along two directions in the crystal lattice of nanosheet. The remaining sections of this paper are orderly arranged as computational details, results and conclusion.

2. COMPUTATIONAL DETAILS

To analyze the structural stability, electronic and magnetic properties of CuO nanosheet in its zigzag and armchair morphologies, the Density Functional Theory-based ab initio approach has been applied through, Atomistix Toolkit–Virtual Nanolab (ATK–VNL) material modeling code which is a further development of TransSIESTA-C. It is in part McDCal employing localized basis sets as developed in SIESTA.

The spin generalized gradient approximation (SGGA), also with Hubbard correction (SGGA+U), have been used as an exchange-correlation function for the optimization of CuO nanosheets through total energy minimization approach, employed before proceeding further for magnetic property analysis, using SGGA as well as SGGA+U with revised Perdew, Burke, and Ernzerhof parameterization type. The valence electrons are described by linear combination of atomic orbitals (LCAOs) with double-ζ-polarized (DZP) basis sets. The mesh cutoff of 75 Hartree has been found suitable for the entire calculations with the k-point sampling of $1 \times 7 \times 7$ for Brillouin zone integration, having maximum force tolerance as 0.05 eV/A and maximum stress tolerance as 0.05 eV/A [19–22]. The computed binding energy per atom, the magnetic moment per atom, and spin polarization for both morphologies of CuO nanosheets are reported in Tables 1 and 2.

3. RESULTS AND DISCUSSION

To analyze the structural stability and electronic and magnetic properties of zigzag and armchair CuO nanosheets, the binding energy, band structure and density of states, and spin polarization have been com-

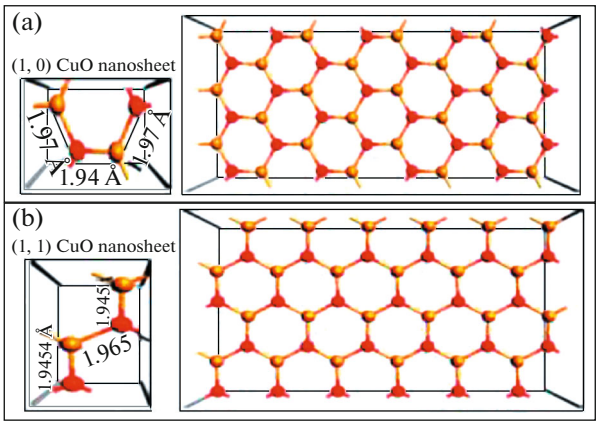

Fig. 1. Super cells with (a) (1, 0) zigzag and (b) (1, 1) armchair CuO nanosheets.

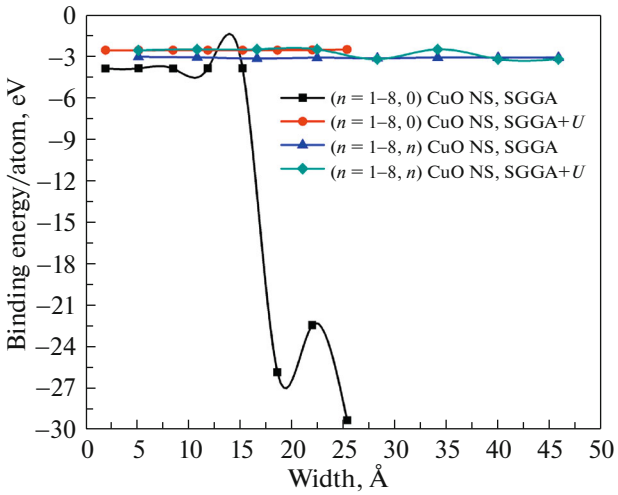

Fig. 2. Binding energy per atom of zigzag and armchair CuO nanosheet as a function of nanosheet width.

puted and compared with its bulk counterpart. The challenge of simple LDA scheme that failed to explain the semiconducting behavior of bulk CuO can be overcome by adding Hubbard (U) correction in LDA and HSE06 hybrid functional, where, the prediction of semiconducting behavior of bulk CuO as p-type semiconductor with narrow band gap of 1.39 eV and direct band gap of 1.91 eV become possible. Attempting with SGGA, to look at the semiconducting as well as magnetic behavior of these oxides, has been a challenge, and here, too, with the addition of Hubbard potential U to SGGA, the semiconducting behavior has easily been predicted with an approximate value of 2.2 eV for bulk CuO. Figures 1a and 1b illustrates the demonstration of super cells of orders (1 × 3 × 4) and (1 × 2 × 6) of the zigzag (1, 0) and armchair (1, 1) CuO nanosheets in the bulk forms, respectively.

3.1. Energetic Analysis

The binding energy denotes the structural stability of both the zigzag and armchair nanosheets have been computed using Eq. (1) and reported in Tables 1 and 2, respectively. The size of the super cell in both the nanosheets increases in B and C directions concerning the variation of area. The widths of both the nanosheets are directly proportional to their chiralities, while the number of molecules is proportional to the area. The equation of binding energy is expressed as

$$E_b = \frac{[E_T - (NE_{Cu}) - ME_O]}{N + M}, \quad (1)$$

where E_b, E_T, E_{Cu}, and E_O are binding energy per atom, total energy of CuO nanosheet, and energy of isolated Cu and O atoms, respectively. N and M are number of copper and oxygen atoms, respectively [23].

Table 1 shows the variation of binding energy from −2.57 to −2.52 eV in SGGA+U and from −29.28 to −3.88 eV in SGGA due to the variation of Cu–O bond length. Similarly, Table 2 shows the variation of binding energy from −3.20 to −2.50 eV in SGGA+U and from −3.16 to −3.04 eV in SGGA. The variation of binding energy with width is also depicted in Fig. 2.

Our observations show that the zigzag CuO nanosheet is more stable at higher indices (9, 0) in comparison to that at lower indices (n = 1–5, 0), whereas the armchair CuO nanosheet is also stable at indices (3, 3) than at indices (1, 1) using SGGA; the binding energy per atom remains fixed around −3 eV for both the zigzag and armchair CuO nanosheet in SGGA+U-based analysis. The comparative analysis through SGGA+U confirms that the armchairs (7, 7) and (8, 8) CuO nanosheet has relatively higher stability than their zigzags counterpart.

3.2. Electronic Properties

The computed band structures with density of states (DOS) profiles of the (n = 1–8, 0) zigzag CuO nanosheets through SGGA and SGGA+U are shown in Figs. 3 and 4, respectively.

Similarly, the computed band structures and DOS profiles of the (n = 1–8, n) armchair CuO nanosheets are shown in Figs. 5 and 6, respectively, where the black and the red lines indicate the majority spin and the minority spin, respectively.

It has been observed that both the CuO nanosheets in the zigzag and armchair forms show the metallic behavior, while CuO bulk is semiconducting and antiferromagnetic. The possible reason of the metallic nature of these nanosheets is due to the hybridization between Cu3d and O2p states at the Fermi level, reported earlier. However, only the band structure information is not enough to analyze the electronic properties; hence, the DOS profiles have also been analyzed for these nanosheets. The computed DOS of

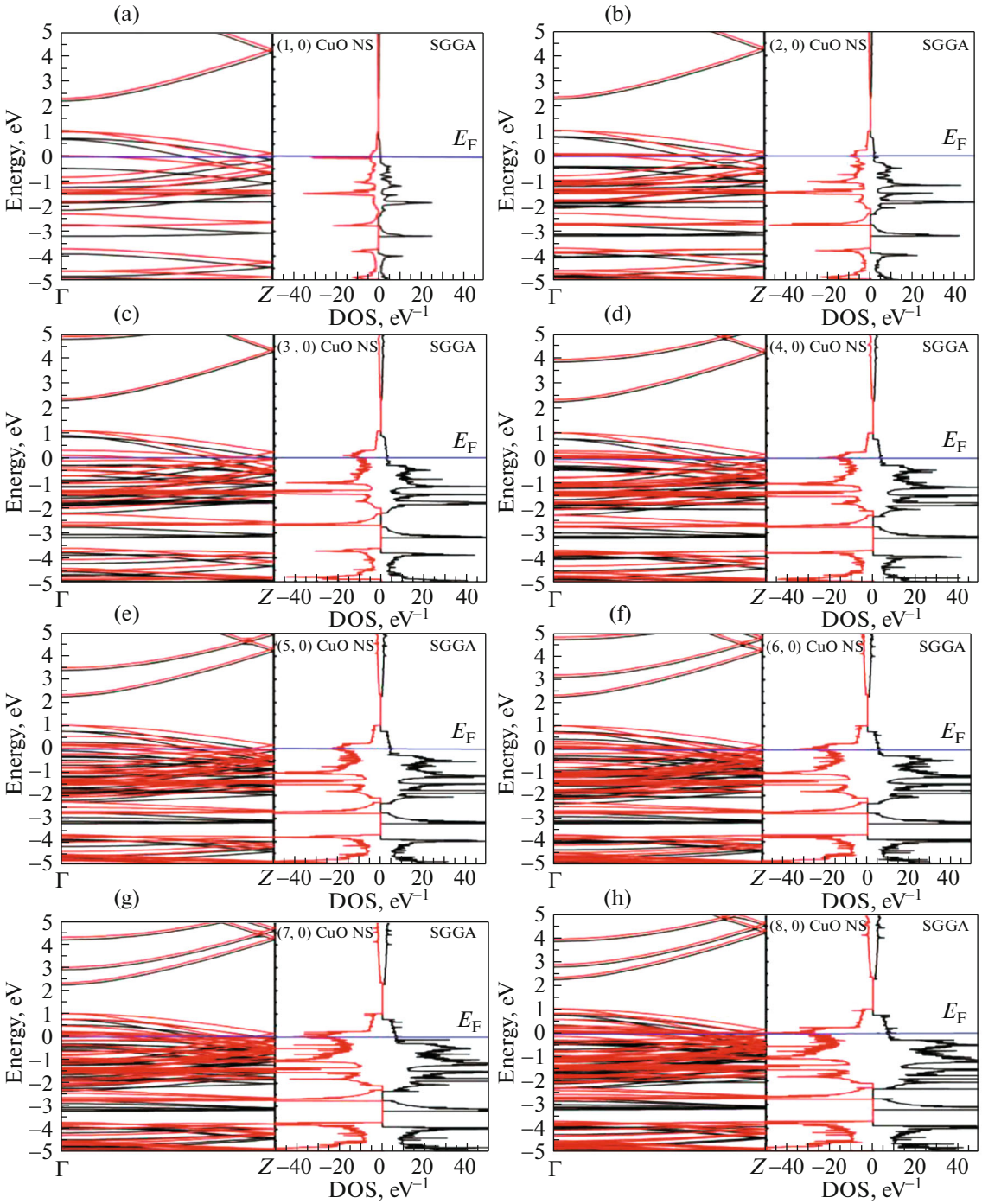

Fig. 3. Band structures of the (n = 1–8, 0) zigzag CuO nanosheets with DOS profile, using SGGA.

both the CuO nanosheets of the different chiralities near the Fermi level, the peaks in the valence band and conduction band are observed due to the combined effect of Cu3*d* and O2*p* and Cu4*s* states. The metallic behaviors of both the CuO nanosheets may be the effect of not only the hybridization of Cu3*d* and O2*p* states but also the finite contribution of O atom to the density of states at Fermi level [24].

3.3. Magnetic Properties

The computed electronic properties of CuO nanosheets, discussed in the earlier section in terms of band structures and the density of states, predict the metallic nature of the zigzag and the armchair CuO nanosheets. With an objective to utilize these nanosheets for a variety of applications, where its magnetic properties can be exploited, the efforts have been

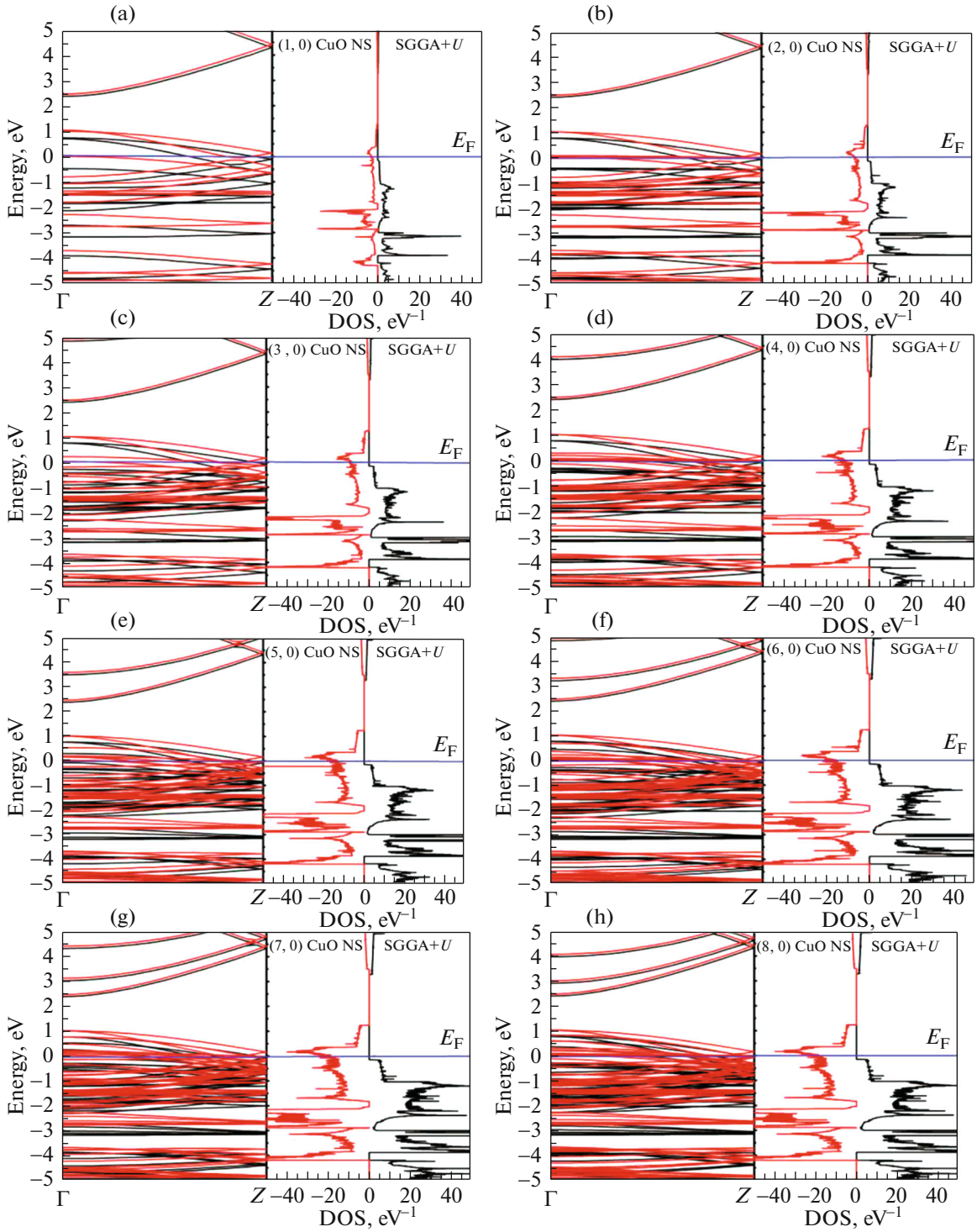

Fig. 4. Band structures of the (n = 1–8, 0) zigzag CuO nanosheets with DOS profile, using SGGA+U.

made to analyze the magnetism in terms of the magnetic moment for different chiralities, computed through spin polarization, reported in Tables 1 and 2. The magnetic moments of bulk CuO, isolated Cu, and isolated O are 0.68, 0.7, and 0.14 μ_B, respectively, and have already been reported by our group [24]. Where, the spin dipole moment (μ_B), known as Bohr's magneton, the fundamental unit of magnetic dipole moment, calculated using the formula $\mu_{total} = [n\uparrow(E_F) - n\downarrow(E_F)]\mu_B$/atom, for calculating the total dipole moment per unit volume per atom of CuO nanosheet at different morphologies. The spin polar-

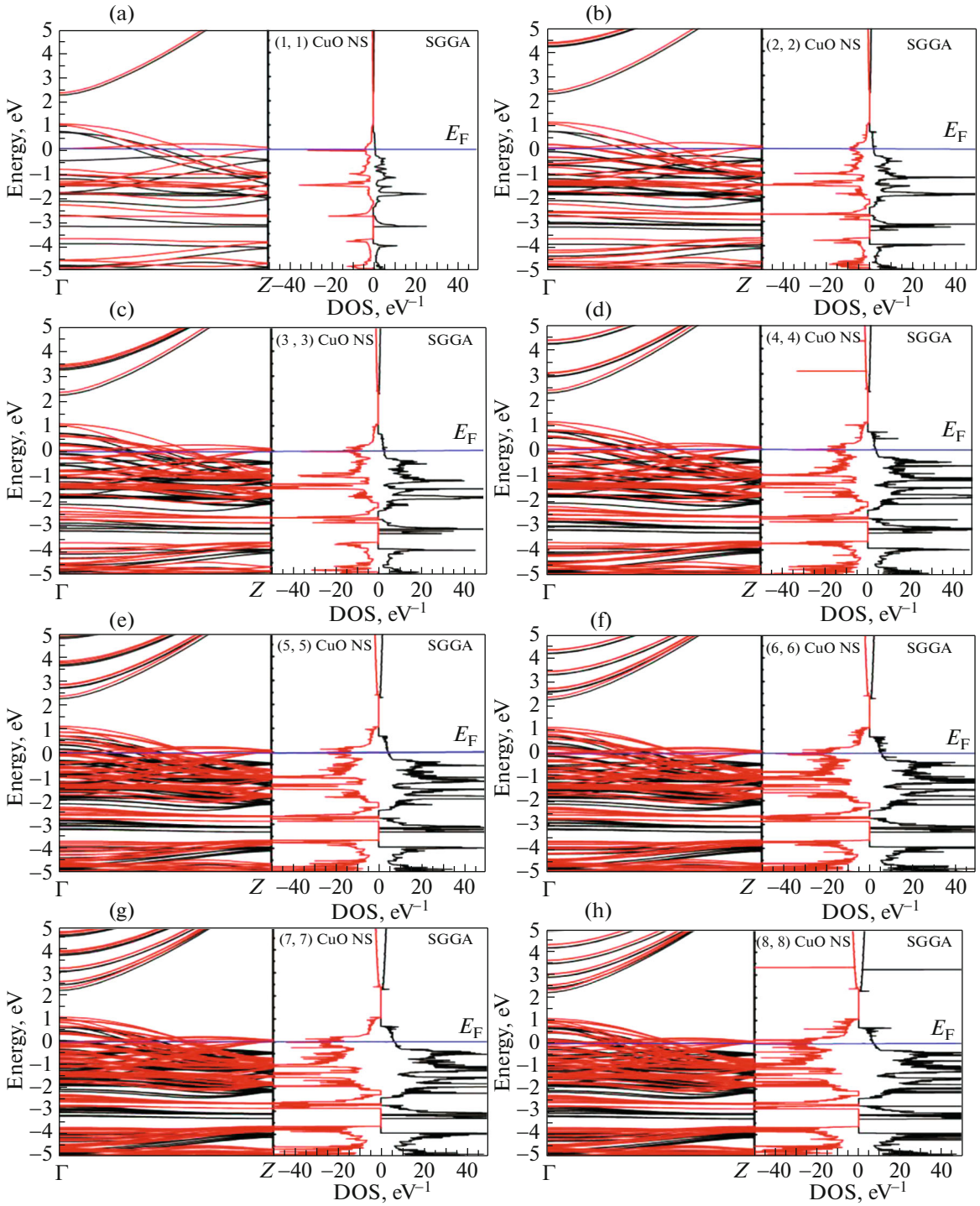

Fig. 5. Band structures of the (n = 1–8, n) armchair CuO nanosheets with DOS profile, using SGGA.

ization (P) is the ratio of the difference of electron density of up-spin and electron density of down-spin to their sum at a Fermi level and analytically expressed below, reported elsewhere,

$$P = \frac{n_{\uparrow}(E_F) - n_{\downarrow}(E_F)}{n_{\uparrow}(E_F) + n_{\downarrow}(E_F)}, \quad (2)$$

where $n_{\uparrow}$ and $n_{\downarrow}$ are electron density up-spin and electron density down-spin, respectively, at Fermi level [25].

The change in magnitude of total magnetic moments, concerning to the increment in widths of the zigzag and armchair CuO nanosheets, is reported in Tables 1 and 2 and also through graphs in Fig. 7.

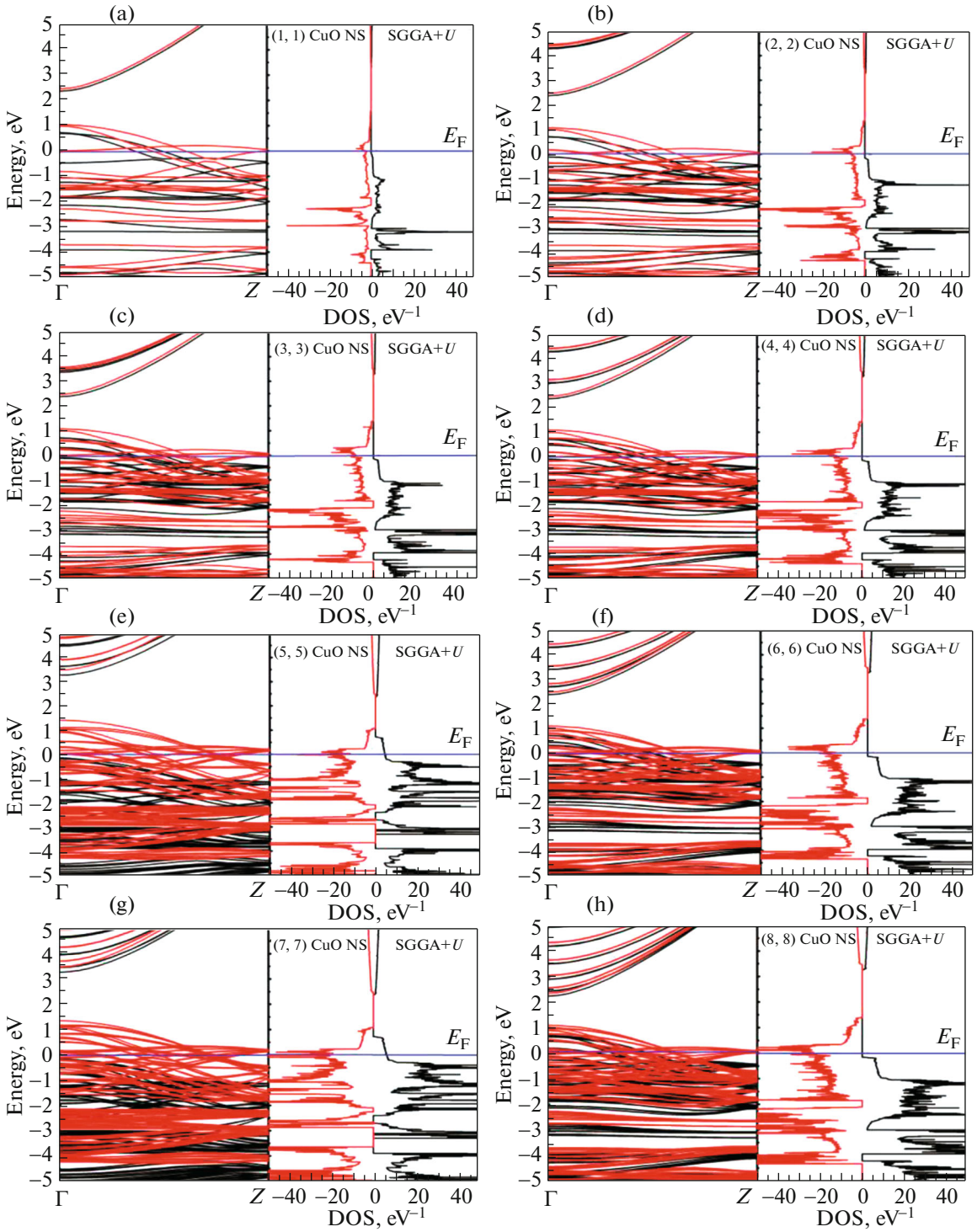

Fig. 6. Band structures of the (n = 1–8, n) armchair CuO nanosheets with DOS profile, using SGGA+U.

The computed magnetic moments using SGGA are 1.19 and 1.53 μ_B for zigzag (6, 0) and armchair (4, 4) CuO nanosheets, respectively, whereas, with Hubbard correction (SGGA+U), it is 0.76 and 1.29 μ_B for the zigzag (5, 0) and armchair (7, 7) of CuO nanosheets, respectively. Similarly, the spin polarization for both the zigzag (n = 1–8, 0) and armchair (n = 1–8, n) CuO nanosheets are reported in Tables 1 and 2, respectively and their variation with widths are depicted in Fig. 8.

Both these parameters confirm the ferromagnetic nature of CuO nanosheets, where the splitting states of

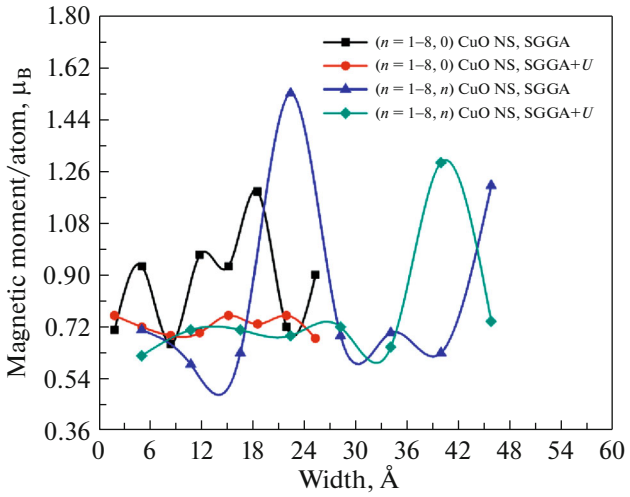

Fig. 7. Magnetic moment of zigzag and armchair CuO nanosheet as a function of nanosheet width.

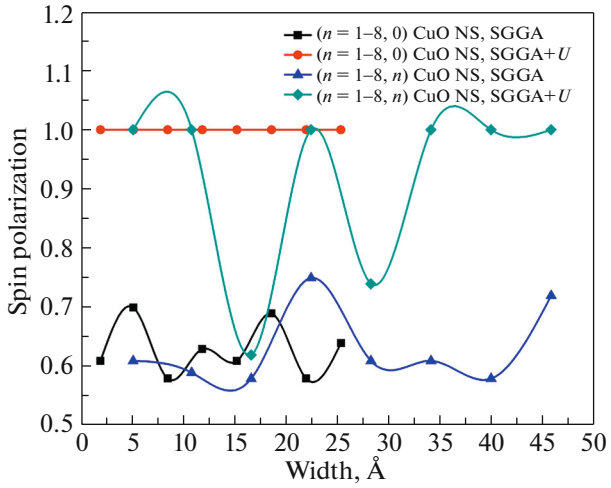

Fig. 8. Spin polarization of zigzag and armchair CuO nanosheet as a function of nanosheet width.

Cu3*d* and O2*p* exchange themselves and produce magnetic moment.

The Hund's rule for the magnetism states that when the atoms come closer to each other, the interaction between them increases, and the resultant magnetic moment decreases, and vice versa. In the same way, the net magnetic moment of individual CuO nanosheet depends on their individual magnetic moment of Cu and O atoms [26, 27]. The variation in magnetic moment with respect to width of zigzag and armchair CuO nanosheets is produced due to the variation in the Cu–O bond length, reported in Tables 1 and 2, respectively.

4. CONCLUSIONS

The optimized zigzag and armchair CuO nanosheets have been analyzed to understand their structural, electronic, and magnetic properties, using SGGA and SGGA+*U* exchange-correlation functional under DFT-based ab initio regime. The electronic and magnetic properties of proposed nanosheets have been analyzed in terms of the band structures and density of states with spin-up and spin-down. In reference to the antiferromagnetic and semiconducting bulk CuO, both the forms of CuO nanosheets show metallic ferromagnetic nature and their energetic have been discussed through their binding energies. Interesting electronic properties of CuO nanosheets can be exploited for applications like in gas sensors and batteries, and at particular chirality, both the zigzag and armchair CuO nanosheets show outstanding magnetic moment and spin polarization, hence making them a suitable candidate for energy storage device as well as magnetic storage media.

ACKNOWLEDGMENTS

Authors are thankful to Computational Nanoscience and Technology Lab of Atal Bihari Vajpayee Indian Institute of Information Technology and Management, Gwalior, India for providing the computational infrastructural for carrying out the present research work and Nepal Academy of Science and Technology, (NAST), Nepal for the doctoral fellowship. TPY and GCK are thankful to Mid-Western University, Surkhet, Nepal and Tribhuvan University, Kirtipur, Nepal for providing the research facilities.

CONFLICTS OF INTERESTS

The authors declare that they have no conflicts of interest.

REFERENCES

1. A. K. Geim and K. S. Novoselov, Nat. Mater. **6**, 183 (2007).
2. M. Heineman, B. Eifert, and C. Heiliger, Phys. Rev. B **87**, 115111 (2013).
3. Y. Wang, S. Lany, J. Ghanbaja, Y. Fagot-Revurat, Y. P. Chen, F. Soldera, D. Horwat, F. Mucklich, and J. F. Pierson, Phys. Rev. B **94**, 245418 (2016).
4. C. Batchelor-McAuley, Y. Du, G. G. Wildgoose, and R. G. Compton, Sens. Actuators, B **135**, 230 (2008).
5. J. Ghijsen, L.-H. Tjeng, J. van Elp, H. Eskes, J. Westerink, G. A. Sawatzky, and M. T. Czyzyk, Phys. Rev. B **38**, 11322 (1988).
6. G. Xiao, P. Gao, L. Wang, Y. Chen, Y. Wang, and G. Zhang, J. Nanomater. **2011**, 439162 (2011).
7. Y.-N. Chang, M. Zhang, L. Xia, J. Zhang, and G. Xing, Materials (Basel) **5**, 2850 (2012).
8. M. A. Latif, J. W. J. Wu, R. Moriyama, M. Nakano, K. Ohshimo, and F. Misaizu, ACS Omega **3**, 18705 (2018).

9. L. Xu, Q. Yang, X. Liu, J. Liu, and X. Sun, RSC Adv. **4**, 1449 (2014).
10. B. J. Hansen, G. Lu, and J. Chen, J. Nanomater. **2008**, 830474 (2008).
11. J. Zhi-Ang, C. Jiang-Tao, W. Jun, Z. Ren-Fu, Y. De, Z. Fei, and Y. Peng-Xun, Chin. Phys. Lett. **26**, 086202 (2009).
12. X. Jia, H. Fan, and W. Yang, J. Dispers. Sci. Technol. **31**, 866 (2010).
13. F. Zhang, A. Zhu, Y. Luo, Y. Tian, J. Yang, and Y. Qin, J. Phys. Chem. C **114**, 19214 (2010).
14. Z. Deng, Z. Ma, Y. Li, L. Chen, X. Yang, H.-E. Wang, and B.-L. Su, Front. Chem. **6**, 428 (2018).
15. M. Fan, H. Yu, and Y. Chen, Mater. Technol. **32**, 598 (2017).
16. J. Demel, A. Zhigunov, I. Jirka, M. Klementova, and K. Lang, J. Colloid Interface Sci. **452**, 174 (2015).
17. Z. Ibupoto, K. Khun, V. Beni, X. Liu, and M. Willander, Sensors **13**, 7926 (2013).
18. J. B. Torrance, Y. Tokura, S. J. la Placa, T. C. Huang, R. J. Savoy, and A. I. Nazzal, Solid State Commun. **66**, 703 (1988).
19. W. Kohn and L. J. Sham, Phys. Rev. A **140**, 1133 (1965).
20. J. P. Perdew, K. Burke, and M. Ernzerhof, Phys. Rev. Lett. **77**, 3865 (1996).
21. J. M. Soler, E. Artacho, J. D. Gale, A. Garcia, J. Junquera, P. Ordejon, and D. Sanchez-Portal, J. Phys.: Condens. Matter **14**, 2745 (2002).
22. QuantumATK Atomic-Scale Modeling for Semiconductor and Materials. https://www.synopsys.com/silicon/quantumatk.html. Accessed Dec. 18, 2019.
23. R. D. Parra and H. H. Farrell, J. Phys. Chem. C **113**, 4786 (2009).
24. S. Paudel, T. P. Yadav, A. Srivastava, and G. C. Kaphle, J. Mater. Sci. Nanotechol. **6**, 102 (2017).
25. X. Han, W. Mi, and X. Wang, J. Mater. Chem. C **7** (27), 8325 (2019).
26. L. Miao, R. Basak, S. Ran, Y. Xu, E. Kotta, H. He, J. D. Denlinger, Y.-D. Chuang, Y. Zhao, Z. Xu, J. W. Lynn, J. R. Jeffries, S. R. Saha, I. Giannakis, P. Aynajian, C. J. Kang, Y. Wang, G. Kotliar, N. P. Butch, and L. A. Wray, Nature Commun. **10** (1), 644 (2019)
27. B. L. Frankamp, A. K. Boal, M. T. Tuominen, and V. M. Rotello, J. Am. Chem. Soc. **127**, 9731 (2005).

Computational Study of the Structural, Electronic and Magnetic Properties of Nanoclusters of Cu2O and CuO: Ab-Initio Approach

T. P. Yadav, G. C. Kaphle and A. Srivastava

Journal of Nepal Physical Society

Volume 6, Issue 1, June 2020

ISSN: 2392-473X (Print), 2738-9537 (Online)

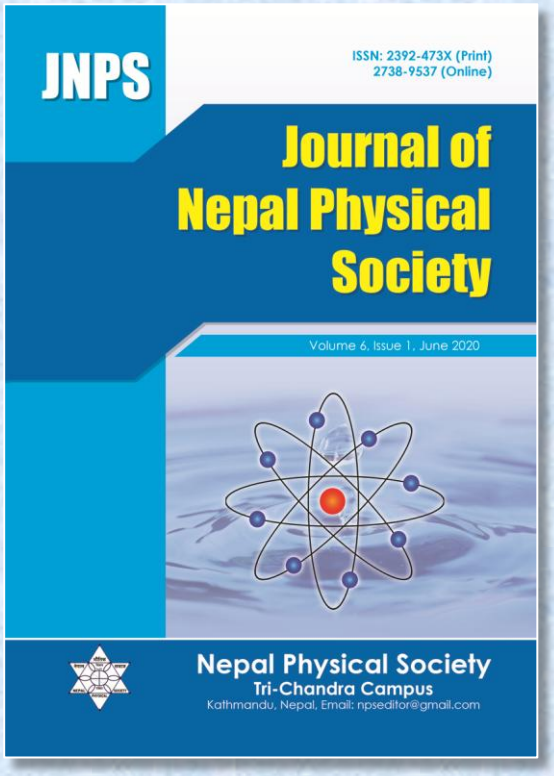

JNPS, **6** (1), 68-72 (2020)

DOI: http://doi.org/10.3126/jnphyssoc.v6i1.30523

Editors:

Dr. Binod Adhikari

Dr. Manoj Kumar Yadav

Mr. Kiran Pudasainee

Published by:

Nepal Physical Society

P.O. Box: 2934

Tri-Chandra Campus

Kathmandu, Nepal

Email: npseditor@gmail.com

JNPS ***6*** *(1), 68-72 (2020)* ***Research Article*** *© Nepal Physical Society*
ISSN: 2392-473X (Print), 2738-9537 (Online) *DOI: http://doi.org/10.3126/jnphyssoc.v6i1.30523*

Computational Study of the Structural, Electronic and Magnetic Properties of Nanoclusters of Cu_2O and CuO: Ab-Initio Approach

T. P. Yadav[1,2,3], G. C. Kaphle[2 *] and A. Srivastava[3]
[1]Central Campus of Science and Technology, Mid-Western University, Surkhet, Nepal
[2]Central Department of Physics, Tribhuvan University, Kirtipur, Kathmandu, Nepal
[3]Advanced Materials Research Group, CNT Lab, Atal Bihari Vajpayee Indian Institute of Information Technology and Management, Gwalior (M.P.) 474010 India
[*]Corresponding Author: gck223@gmail.com, gopi.kaphle@cdp.tu.edu.np

Received: *11 Apr., 2020;* ***Revised:*** *15 May, 2020;* ***Accepted:*** *26 Jun., 2020*

Abstract

The structural, electronic and magnetic properties of the nanoclusters of (Cu_2O) n= 1, 2, 3 and (CuO) m = 2, 4, 6 have computationally studied. Density Functional Theory incorporated in Atomistic tool kit (ATK-DFT) calculators with exchange-correlation functional (SGGA+U) based ab-initio approach is applied for simulation and calculation of these nanoclusters. In the computational study, the nanoclusters $(Cu_2O)_1$, $(Cu_2O)_3$, $(CuO)_2$ and $(CuO)_6$ show semiconducting behavior whereas $(Cu_2O)_2$ and $(CuO)_4$ show semi-metallic behaviors. The nanoclusters $(Cu_2O)_1$ and $(Cu_2O)_3$ show diamagnetic, $(Cu_2O)_2$ and $(CuO)_4$ show ferromagnetic, $(CuO)_2$ and $(CuO)_6$ show antiferromagnetic behaviors. The magnetic moments $0.28\mu_B$ and $0.03\ \mu_B$ are observed in the nanoclusters $(Cu_2O)_2$ and $(CuO)_4$ while others are found to be as nonmagnetic . The total energy of nanoclusters have found to be decreasing towards total minimum energy with increasing number of atoms of copper oxides. The nanoclusters (Cu_2O) n = 1, 2, 3 and (CuO) m = 2, 4, 6 are used in various applications as in the synthesis of technological materials. The analysis of the effects of bond length and binding energy with the size of nanoclsters have been presented.

Keywords: Density of States, Magnetic moments, Nanoclusters, Semi-metals, Binding energy.

1. INTRODUCTION

The copper oxides Cu_2O and CuO exist as stable in the bulk phase. They are transition-metal compound in general and the high-T, superconductors in particular [1]. Cu_2O and CuO are expected to have the essentially full Cu-3d shell ($3d^{10}4s^1$) and open Cu-3d shell ($3d^9 4s^2$) respectively. The shape-sizes and dimensions of both copper oxides play very important role on their structural, electronic and magnetic properties in nanosystem. As experimentally and theoretically, the bulk Cu_2O is found to be diamagnetic and p-semiconductor with a band gap 2.17 eV where as the bulk CuO be the antiferromagnetic and p-semiconductor with a band gap 1.2-1.9 eV [2, 3]. They are widely used in various catalytic reactions, semiconducting materials, environmental protection, and energy storage and conversion systems [4]. In comparison to bulk, nano-sized clusters (NCs) are more active and selective due to their large specific surface area and quantum-confinement effects. The nanoclusters (0-dimenson) of Cu_2O and CuO are applied to examine the remarkable physical and chemical properties of atomic or molecular species in the condensed phases. They can play a key role in various environmental processes and contribute to health hazards associated with airborne fine particles [5, 6]. They play an important role in the synthesis of technological materials [7]. The nanoclusters of both copper oxides Cu_2O and CuO can be formed by proper synthesis of copper and oxygen in the plane oriented substrates or other process [8]. An extensive experimental investigation is powerful probe to study their structural, electronic and magnetic properties and are given invaluable insight on the changes of their properties with shape-size [9]. Their physical and chemical properties are closely related to the crystalline quality, structure and stoichiometry [10]. In electrochemical reaction, the measurement reports that surface CuO clusters acts as a promoter for the

reduction of O_2 [11]. The CuO nanoclusters coated with mesoporous SiO_2 also are highly active and stable catalysts for olefin epoxidation [12]. That is why we are interested to study the various properties of clusters $(Cu_2O)_{n = 1, 2, 3}$ and $(CuO)_{m = 2, 4, 6}$. The SGGA+U exchange correlation with hubbard parametrization based on ab-initio approach is employed for their optimization and analyzing perpose.

Our present paper is organized as follows: The method and computational details are described in section-2 after completion of the introduction in section-1. The results and discussion are written in section-3 before the conclusive remarks explained in section-4. Acknowledgments and references are listed at the end of the sections.

2. METHOD AND COMPUTATIONAL DETAILS

A powerful set of modeling tools Atomistix ToolKit (ATK) is used for investigating a variety of nanoscale systems as molecules, bulk and two-probe systems. We have applied the ATK-DFT calculator with exchange-correlation functional SGGA+U (U=7.5eV) with review-Perdew-Burke-Ernzerhof (rPBE) parameterization based on density-functional theory through first-principle approach for simulation of the nanoclusters (NCs) of both $(Cu_2O)_{n = 1, 2, 3}$ and $(CuO)_{m = 2, 4, 6}$. The structures of all nanoclusters have been optimized and analyzed before the estimation of our calculations. In the present calculation, we have calculated the physical properties like total energy, the bond length of Cu-O, the molecular energy spectrums (MES), the density of states (DOS), magnetic moment, spin polarization, etc using ATK toolKit. We have chosen the basic settings such as electron temperature 300K, grid mesh cut off 75, exchange correlation SGGA+U and spin polarized through ATK-DFT [13-16] toolkits. The computational structures of nanoclusters, calculated values of various parameters, total energy/bond length vs total atoms and the molecular energy spectrums (MES) with density of states (DOS) are reported in Fig. 1(1-f), Table 1, Fig. 2, 3 and, Fig. 4 (a-c) and 5(a-c), respectively.

3. RESULTS AND DISCUSSION

The structures, electronic and magnetic properties of the nanoclusters (NCs) of the both $(Cu_2O)_{n = 1, 2, 3}$ and $(CuO)_{m = 2, 4, 6}$ are described in following sub-sections .

3.1 Nanocluster Structures

In computational method, the molecular structures of copper oxide nanoclusters $(Cu_2O)_{n = 1, 2, 3}$ and $(CuO)_{m = 2, 4, 6}$ have been found as shown in Fig. 1 (a-f), where the yellow and the red colors spheres represent copper and oxygen atoms respectively.

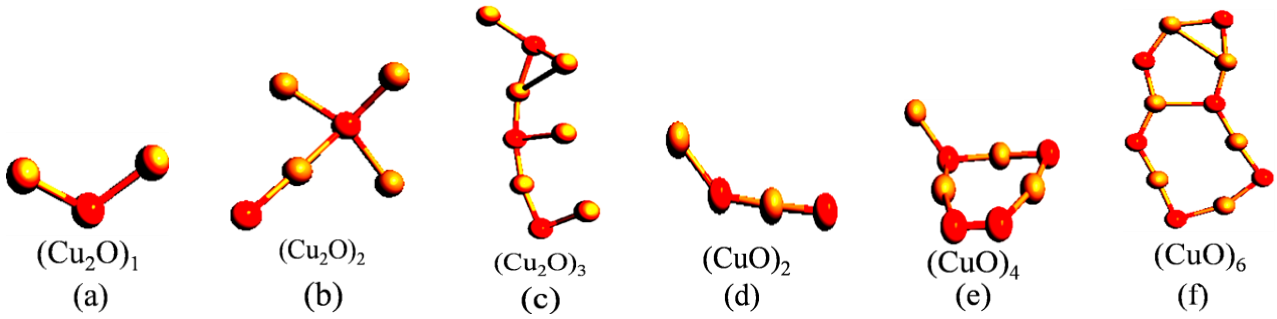

Fig. 1 (a-f): *The molecular structures of the nanoclusters* $(Cu_2O)_{n = 1, 2, 3}$ *and* $(CuO)_{m = 2, 4, 6}$

In the present calculation, the nanoclusters $(Cu_2O)_{n = 1, 2, 3}$ and $(CuO)_{m = 2, 4, 6}$ have been used as samples contain 3, 6, 9 and 4, 8, 12 atoms respectively as in Table 1. The binding energy and total energy of both type of nanoclusters have found to be increasing with the increasing number of atoms indicating that the nanoclusters (NCs) of more molecules are more stable than that of less atoms as in Table 1 and Fig. 2 respectively and approaches towards the bulk behavior. Similarly, the bond length between Cu and O have found to be increasing with the increasing number of atoms in the nanoclusters of both types of copper oxides as in figure 3. All parameters are comparable with previously calculated available data [17-19].

Table 1: The calculated parameters of the nanoclusters $(Cu_2O)_{n = 1, 2, 3}$ and $(CuO)_{m = 2, 4, 6}$

Nano-Clusters (NCs)	Total No. of Atoms	Total Energy (eV)	Binding Energy/ Atom (eV)	Bond Lengths (Cu-O)	Band Gap (eV)	HUMO - LUMO (eV)	Magnetic Moment (μ_B)	Spin Polarization	Natures
$(Cu_2O)_1$	3	2892.65	1.38	1.79	1.00	1.40	0	indefinable	Dia, Semi-conductor
$(Cu_2O)_2$	6	5785.94	1.58	1.82	0	0.28	0.28	1	Ferro, Half-metal
$(Cu_2O)_3$	9	8682.47	1.82	1.88	0.20	0.56	0	indefinable	Dia, Semi-conductor
$(CuO)_2$	4	3325.89	1.30	1.81	0.80	2.00	0	indefinable	Antiferro Semi-conductor
$(CuO)_4$	8	6656.35	1.55	1.85	0	0.40	0.03	1	Ferro Half-metal
$(CuO)_6$	12	9985.65	1.57	1.90	0.1	0.60	0	indefinable	Antiferro Semi-conductor

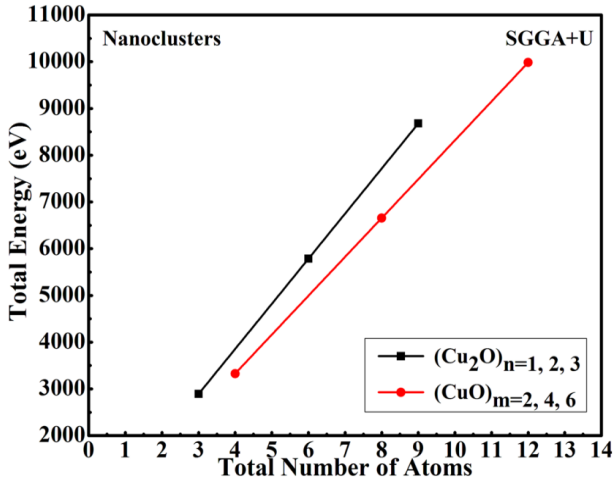

Fig. 2: *The total energy vs total number of atoms in nanoclusters $(Cu_2O)_{n = 1, 2, 3}$ and $(CuO)_{m = 2, 4, 6}$*

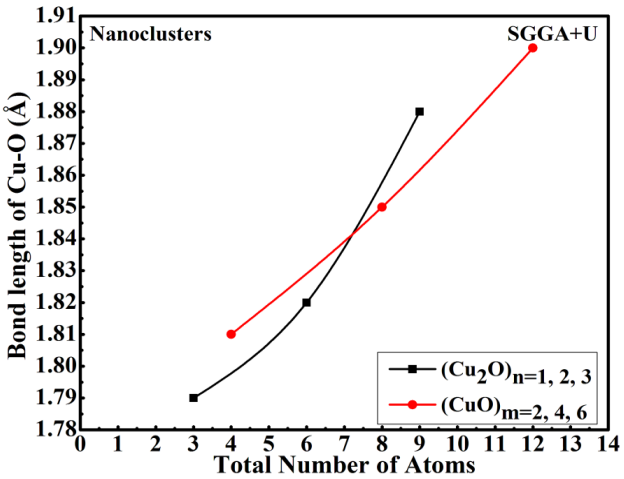

Fig. 3: *The bond length vs total number of atoms in nanoclusters $(Cu_2O)_{n = 1, 2, 3}$ and $(CuO)_{m = 2, 4, 6}$*

3.2 Electronic Properties

We have investigated the molecular energy spectrum (MES) with density of states (DOS) of both the nanoclusters $(Cu_2O)_{n = 1, 2, 3}$ and $(CuO)_{m = 2, 4, 6}$ for the study of their electronic properties as depicted in Fig. 4 (a-c) and Fig. 5 (a-c) respectively. In this calculation $(Cu_2O)_1$, $(Cu_2O)_3$, $(CuO)_2$ and $(CuO)_6$ are showing semi-conducting properties whereas $(Cu_2O)_2$ and $(CuO)_4$ found to be as half-metals. The nanoclusters $(Cu_2O)_2$ and $(CuO)_4$ have found as same molecular structures of unit cells of the bulks copper (I) and copper (II) oxides respectively. But both bulk forms of copper oxide are P-type semiconductors of band gaps 2.17eV and 1.2-1.9 eV experimentally [1-3].

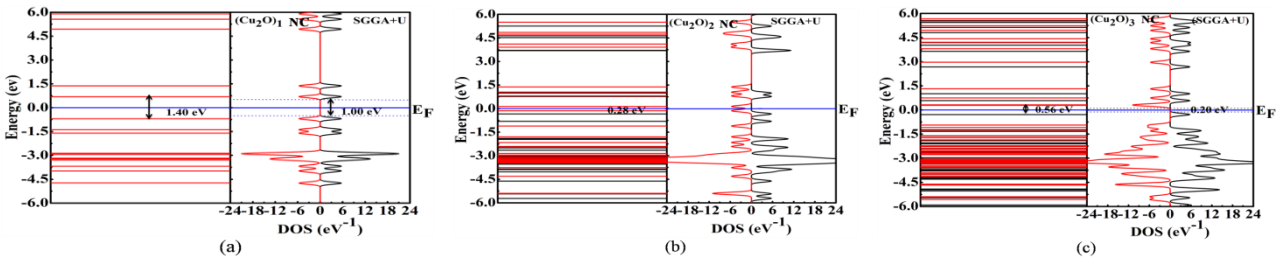

Fig. 4 (a-c): *The molecular energy spectrums of the nanoclusters* $(Cu_2O)_{n=1,2,3}$ *with DOS profiles*

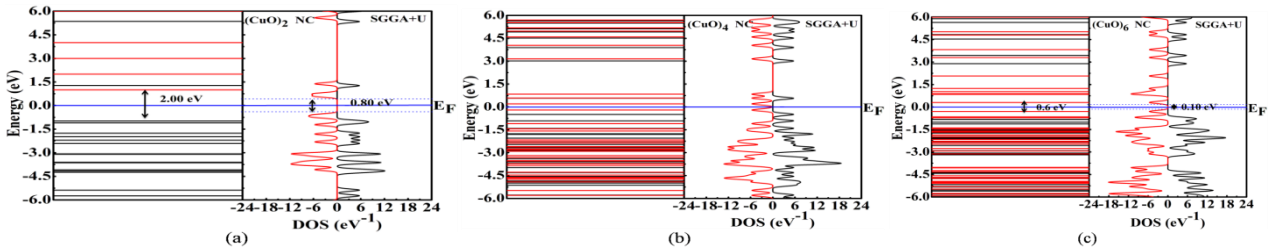

Fig. 5 (a-c): *The molecular energy spectrums of the nanoclusters* $(CuO)_{m=2,4,6}$ *with DOS profiles*

3.3 Magnetic Properties

In our observation, the clusters $(Cu_2O)_1$ and $(Cu_2O)_3$ show diamagnetic behaviors because each individual atomic moment for both cases are found separately to be zero where cluster $(Cu_2O)_2$ as ferromagnetic. The clusters $(CuO)_2$ and $(CuO)_6$ behave as antiferromagnetic being magnetic moments of unit cell is zero but individual atoms have some polarization. Similarly $(CuO)_4$ has found to be as ferromagnetic. But the bulk forms of Cu_2O and CuO are diamagnetic and anti ferromagnetic materials respectively. The magnetic moments of nanoclusters $(Cu_2O)_2$ and $(CuO)_4$ are $0.28\mu_B$ and $0.03\mu_B$, and their matching spin polarization unity. The useful physical equations to calculate the magnetic moment per atom and spin polarization expressed as equations (1) and (2) which explains the magnetic properties [20-25].

$$\mu_{total} = \frac{m_B}{atom} = [n\uparrow(E_F) - n\downarrow(E_F)]\,\mu_B/atom \quad \text{..... (1)}$$

and

$$P = \frac{[n\uparrow(E_F) - n\downarrow(E_F)]}{[n\uparrow(E_F) + n\downarrow(E_F)]} \quad \text{..... (2)}$$

where, μ_{total} = magnetic moment per atom, m_B = magnetic moment, μ_B = magnetic moment per electron, P = spin polarization, $n\uparrow(E_F)$ = spin up and $n\downarrow(E_F)$ = spin down electrons density at Fermi level.

4. CONCLUSION

The bulks of copper oxides Cu_2O and CuO are transition-metal p-type semiconductors in general and the high-T_C, superconductors in particular. They show dia-magnetic and anti ferromagnetic behaviors as experimentally and theoretically. In the present calculations using ATK-DFT have found that nanoclusters of bulks Cu_2O and CuO found as half-metal ferromagnetic nano- materials, the clusters $(Cu_2O)_1$, $(Cu_2O)_3$ and $(CuO)_2(CuO)_6$ as semiconductors behave as diamagnetic and anti ferromagnetic nano-materials respectively. The magnetic moments of clusters $(Cu_2O)_2$ and $(CuO)_4$ have found to be $0.28\mu_B$ and $0.03\mu_B$ respectively with spin polarization unity. The total maximum energy and also binding energy increase with increasing number of atoms or molecules in these nano-clusters. Similarly, the bond length between Cu-O is found to be directly proportional to the number of atoms / molecules . It clarifies the stability of nanoclustor depends on its number of atoms tend towards bulk properties. They can be used in various environmental processes, health hazards and synthesis of technological materials gas sensors etc..

ACKNOWLEDGEMENT

One of the Author, Tarani Prasad Yadav, is thankful to Nepal Academy of Science and Technology (NAST), Nepal for partial support and

ABV-IIITM, Gwalior, MP, India for computational facilities.

REFERENCES

[1] Ghijsen J, Tjeng LH, Elp JV, Eskes H, Westerink J, Sawatzky GA, Czyzyk MT. Electronic structure of Cu_2O and CuO, *Phys. Rev. B*, **38** (16),11322 (1988).

[2] Wang Y, Lany S, Ghanbaja J, Fagot-Revurat Y, Chen YP, Soldera F, Horwat D, M¨ucklich F, Pierson JF , Electronic structures of Cu_2O, Cu_4O_3, and CuO: A joint experimental and theoretical study, Phys. Rev. B **94**, 245418 (2016).

[3] Heinemann M, Eifert B, Heiliger C , Band structure and phase stability of the copper oxides Cu_2O, CuO, and Cu_4O_3, *Phys. Rev. B* **87**, 115111 (2013).

[4] Wang LS, Wu H, Desai SR, Electronic structure of small copper oxide clusters: From Cu_2O to Cu_2O_4, *Phys. Rev. B* **53** (12), 15 (1996).

[5] Bae GT, Dellinger B, Hall RW , Density Functional Calculation of the Structure and Electronic Properties of Cu_nO_n (n = 1-8) Clusters, *J. Phys. Chem. A*, **115**, 2087 (2011).

[6] Jadraque M, Martin M, DFT calculations of $Cu_nO_m0/+$ clusters: Evidence for Cu_2O building blocks, Chem. Phy. Lett. **456**(1-3), 51–54 (2008).

[7] Latif MA, Wu JWJ, Moriyama R, Nakano M, Ohshimo K, Misaizu F, Stable Compositions and Structures of Copper Oxide Cluster Cations Cu_nO_m (n = 2−8) Studied by Ion Mobility Mass Spectrometry, *ACS Omega*, **3**, 18705 (2018).

[8] Subramanian S, Valantina R, Ramanathan C, Structural and Electronic Properties of CuO, CuO2 and Cu2O Nanoclusters –a DFT Approach, *Mat. Sci.,* **21**(2), 1292 (2015).

[9] Massobrio C, Pouillon Y Structural properties of CuO 4 and CuO 5 clusters: A density functional study, *J. Chem. Phy.* **119 ,** 16 (2003).

[10] Lyubinetsky I, Thevuthasan S, McCready DE, Baer DR, Formation of single-phase oxide nanoclusters: Cu_2O on $SrTiO_3$ (100), J. Applied Phy. **94** ,7926 (2003).

[11] Jin Q, Fujishima M, Iwaszuk A, Nolan M, Tada H, Loading Effect in Copper (II) Oxide Cluster-Surface-Modified Titanium (IV) Oxide on Visible- and UV-Light Activities, J. Phys. Chem. C, **117**, 23848 (2013).

[12] Chen C, Qu J, Cao C, Niuab F, Song W, CuO nanoclusters coated with mesoporous SiO2 as highly active and stable catalysts for olefin epoxidation†, *J. Mater. Chem*, **21**, 5774 (2011).

[13] Kohn W, Sham LJ , Self-consistent equations including exchange and correlation effects. *Phys. Rev.* **140**, A1133 (1965).

[14] Perdew JP, Burke K, Ernzerhof M, Generalized gradient approximation made simple. *Phys. Rev. Lett.* **77,** 3865 (1996).

[15] Soler JM, Artacho E, Gale JD, Garc A, Junquera J, Ordej´on P, S´anchez-Portal D The SIESTA method for ab initio order-N materials simulation. *J. Phys. Condens Matter*, **14,** 2745 (2002).

[16] Quantum ATK Atomic-Scale Modeling for Semiconductor & Materials. https://www.synopsys.com/silicon/quantumatk.html. Accessed 18 Dec (2019).

[17] Rao GN, Yao YD, Chen JW , Evolution of size, morphology, and magnetic properties of CuO nanoparticles by thermal annealing, *J. Appl. Phys.*, **105**, 093901 (2009).

[18] Parra RD, Farrell HH, Binding energy of metal oxide nanoparticles. *J. Phys. Chem. C*, **113,** 4786 (2009).

[19] Paudel S, Yadav TP, Srivastava A, Kaphle GC, Magnetic Moment of Zigzag CuO Nanotubes at Different Temperature and Size: Ab-Initio Study, *J. Mat. Sci. Nanotechol.* **,** (1), 102 (2018).

[20] Datta S, Kaphle GC, Baral S, Mookerjee A . Study of morphology effects on magnetic interactions and band gap variations for 3d late transition metal bi-doped ZnO nanostructures by hybrid DFT calculations. *J. Chem. Phys.***143** (8), 084309 (2015).

[21] Paudel S, Dandeliya S, Chaurasiya R, Srivastava A, Kaphle GC ,Magnetism in zigzag and armchair CuO nanotubes: Ab-initio study. *J. Mag. Mag. Matt.* **406**, 4(2016).

[22] Mørup S, Hansen MF, Frandsen C, Magnetic interactions between nanoparticles, *Beilstein J. Nanotechnol*., **1**, 182(2010).

[23] Chalsani P, Upadhyay SK, Ozatay O, Buhrman RA , Andreev reflection measurements of spin polarization, *Phys. Rev. B* **75**, 094417 (2007).

[24] Miao L, Basak R, Ran S, Xu Y, Kotta E, He E, Denlinger JD, Chuang YD, Zhao Y, Xu Z, Lynn JW, Jeffries JR, Saha SR, Giannakis I, Aynajian P, Kang CJ, Wang Y, Kotliar G, Butch NP, L. A. Wray LA, High temperature singlet-based magnetism from Hund's rule correlations, *Nat. Comm.*, **10,** 644 (2019).

[25] Han X, Mi W, Wang X, Spin polarization and magnetic properties at the $C_{60}/Fe_4N(001)$ sp interface, *J. Mater. Chem. C*, **7**, 8325 (2019).

Journal of Materials Science & Nanotechnology
Volume 6 | Issue 1
ISSN: 2348-9812

Research Article Open Access

Magnetic Moment of Zigzag CuO Nanotubes at Different Temperature and Size: Ab-Initio Study

Paudel S[1,2], Yadav TP[3,4], Srivastava A[1] and Kaphle GC[*3,4,5]

[1]Advanced Materials Research Group, Computational Nanoscience and Technology Laboratory, ABV-Indian Institute of Information Technology and Management, Gwalior, M.P, India
[2]Department of Physics, Tribhuvan University, Patan Multiple Campus, Patandhoka, Lalitpur, Nepal
[3]Central Department of Physics, Tribhuvan University, Kirtipur, Kathmandu, Nepal
[4]Hydra Research and Policy Center Kathamndu, Nepal
[5]Condensed Matter Physics Research Center, Butwal, Rupandehi, Nepal

[*]**Corresponding author:** Kaphle GC, Central Department of Physics, Tribhuvan University, Kirtipur, Kathmandu, Nepal, Tel: +9779849000975, E-mail: gck223@gmail.com

Citation: Paudel S, Yadav TP, Srivastava A, Kaphle GC (2017) Magnetic Moment of Zigzag CuO Nanotubes at Different Temperature and Size: Ab-initio study. J Mat Sci Nanotechol 6(1): 102

Received Date: October 09, 2017 **Accepted Date:** January 02, 2018 **Published Date:** January 05, 2018

Abstract

Temperature and size dependence magnetic moment of zigzag (n, 0) (n= 4, 6, 8, 10) copper oxide nanotubes (CuO NTs) have been computed by using a standard density functional theory. The computational work carried out by employing spin polarized generalized gradient approximation with revised Perdew Burke Ernzerhoff type parameterization along ab-initio approach. Bond length, binding energy and total magnetic moment have been analyzed and found that the bond length decreases at first and become saturated with increasing size of the nanotube. Highest binding energy of (10, 0) confirms this as the most stable amongst all the NTs taken into consideration. The observed electronic properties of considered CuO NTs, confirms the metallic nature. The size dependence magnetic moment at room temperature is decreases around up to (8,0) beyond that magnetic moments found to be increased with the diameter of the nanotubes. The computed temperature dependence's magnetic moment of NTs first increase up to room temperature (300K) and then decreases for all NTs except (8, 0).

Keywords: Density Functional Theory (DFT); Bond length, Binding energy; Magnetic moment; CuO Nanotube

Introduction

In the past few years' investigation in the magnetic properties with different aspect in nano structure have been increased rapidly because of their technological importance, lots of attractive properties like, high surface-volume ratio, electronic, optical and magnetic properties as well as for understanding the physics involved in their many unusual properties comparing with the bulk [1-5]. Since, the discovery of the high temperature superconductor in copper oxide peroviskit and its unique electric and magnetic properties, Copper oxide (CuO) got more attention and made more interesting candidate for research [6-8]. Our recent ab-intio investigation on magnetism in zigzag and armchair CuO nanotubes shows remarkable magnetic properties at different diameter [9]. So, it is wrathful to investigate the temperature and size dependent magnetic properties in zigzag CuO nano tubes as a function of temperature.

As a bulk CuO is a p-type semiconductor with band gap of 1.1-1.9 eV, unlike other transition metal oxide semiconductor, it have monoclinic structure and possess versatile band structure, optical and magnetic properties [8,10,11].

Our work focuses on the stability analysis of zigzag CuO nanotube in terms of its binding energy, diameter along with temperature dependence of magnetic properties. Organization of this article is as follows, next section discusses the method and computational details followed by result and discussion section and conclusion of the work is presented before the references.

Method and Computational Detail

Computational calculation has been done by Density Functional Theory (DFT), based on ab-initio code named Atomisitix Toolkit (ATK-VNL) with non-equilibrium Green Function (NEGF) [12-15]. ATK-VNL is a further development of TransSIESTA-C and is based on the methodology, models, algorithms developed in academic code TransSIESTA and in part McDCal employing localized

in SIESTA [16-18]. Spin Generalized Gradient Approximation with revised Perdew Burke Eenzerhoff used for exchange correlation energy [19,20]. Valence electrons were described by localized pseudo atomic orbital's (PAOs), with double ζ double polarized basis set. Mesh cut-off 75 Hartee is applied in entire calculation, with K-point sampling of 1x1x20 and maximum force tolerance set at 0.05eV/Å [21]. Calculation was began by minimization energy, optimized geometry and further. Minimization of energy gives us stable bond length between Cu and O. The stable bond length is used to creates the CuO zigzag nanotubes using ATK-VNL tool.

Results and Discussion

Stability and Structural Analysis

The current work carries the analysis of diameter dependence of structural stability and electronic properties. The diameter and temperature dependence magnetic properties of zigzag CuO nanotubes also studied shown in Figure 1.The calculated magnetic properties and structure parameter have been listed in Table 1. From Table 1 for the larger diameter nanotubes, the number of atom and Binding energy (E_b) increases, whereas bond length between Cu-O is first increased and then become saturated. The nanotube of chirality (4, 0) is found to be stable at bond length (Cu-O) of 1.95 Å, where chirality (10, 0) is stable at 1.90 Å. The buckle appeared on the optimized structure of nanotube decreases with increasing the diameter as shown in Figure 1. This is mainly due to well known effect of reduction of bond strain on the curvature surface with increase in the diameter of nanotube [9].

Binding energy of the NTs are calculated through following relation;

$$E_b = \frac{[N * E_T(Cu_{iso} + M * E_T(O_{iso}) - E_T(CuONT)]}{N + M} \quad (1)$$

Where N= number of copper atoms present in SWNT
M= number of Oxygen atoms present in SWNT
E_T= Total energy of Cu, O and CuO SWNTs respectively

Similarly, the binding energy is calculated through equation 1 and listed in Table 1, which concludes that the binding energy increases significantly with diameter of zigzag nano tubes for small value of diameter and after certain increase in the diameter it increase very slowly: this character of binding energy arise due to reduction in the strain.

Chirality (n,0)	No. of atom N	Bond length (Cu-O) Å	Diameter Å	E_B (eV)	μtotal (μB/ atom)
(4,0)	16	1.95	4.30	4.73	0.453
(6,0)	24	1.90	6.29	4.81	0.314
(8,0)	32	1.90	8.39	4.84	0.191
(10,0)	40	1.90	10.46	4.85	0.230

Table 1: Bond length, Binding energy, Diameter and Total Magnetic Moment at room temperature of CuO SWNTs

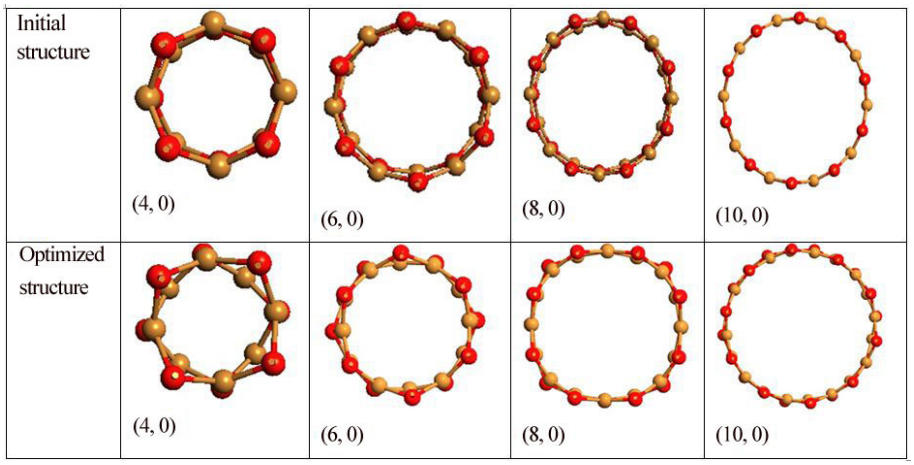

Figure 1: (color online) Initial and optimized geometries of CuO NTs

Electronic Property

Band structure of CuO zigzag nanotubes with majority and minority spin at room temperature are plotted in Figure 2. Where black lines indicate the majority spin and red lines indicates the minority spin. Our work shows that zigzag CuO nanotubes are metallic in nature, but the bulk CuO is a p-type semiconductor. This is responsible due to hybridization between O-2p and Cu-3d states near the Fermi level. This nature observed here in our case is in line with that reported earlier [22,23].

At different diameter, and at room temperature, the density of state (DOS) of zigzag CuO nanotubes have also been observed using spin polarization DFT calculation and plotted at Figure 3. The peaks appear near the Fermi levels in valance band are because of Cu-3d and O-2p states, while the peak in conduction band is due to 4s state of Cu. The finite contribution of O atom to the density of state at Fermi level might be a reason for the metallic nature of nanotube, besides the hybridization on of Cu-3d and O-2p states.

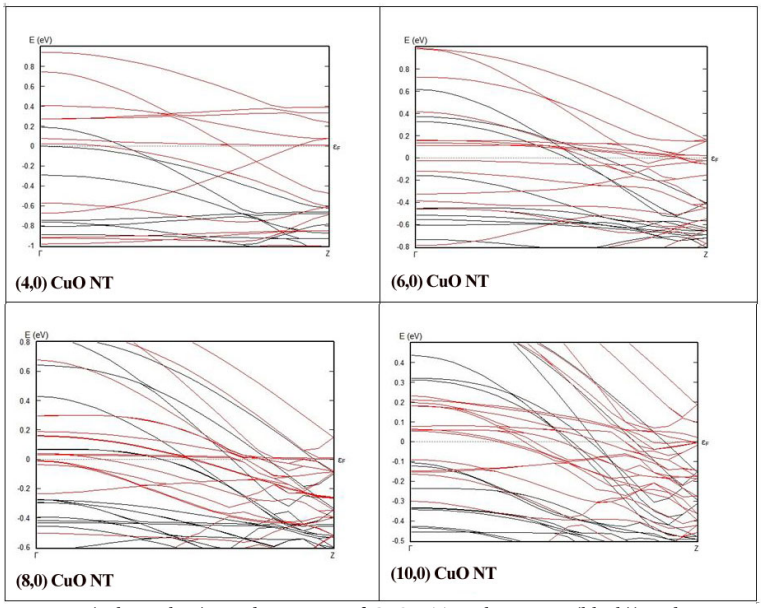

Figure 2: (color online) Band structure of CuO NTs with majority(black)) and minority (red)Spin

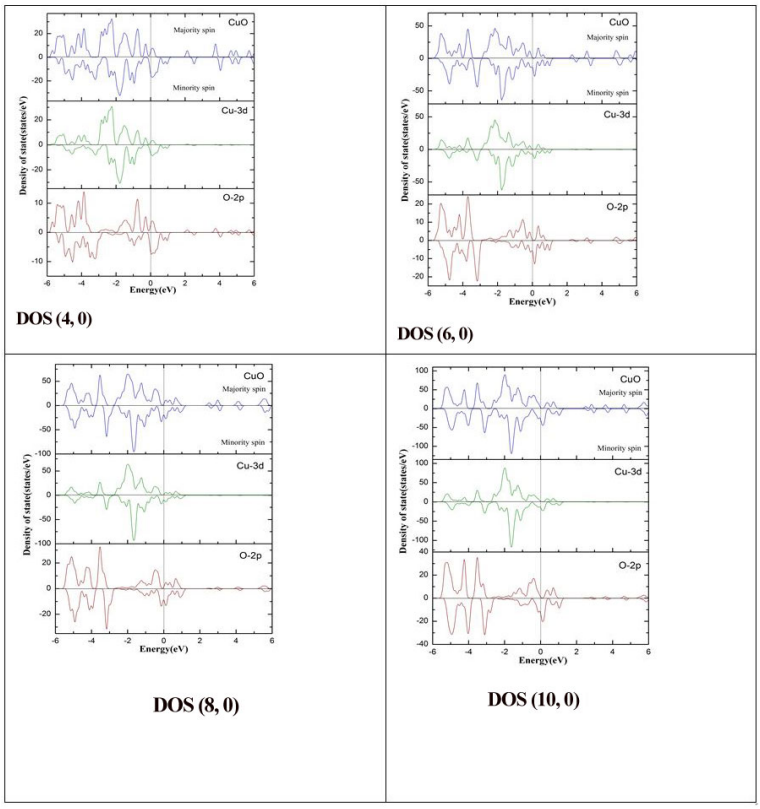

Figure 3: (color online) Spin Polarized DOS of CuO NTs at room temperature

Magnetic moment

It would be exciting to analyze the magnetic properties because of the metallic nature of CuO nanotubes. Magnetic moment of zigzag CuO nanotube at room temperature listed in Table 1 on which we observe that the magnetic moment is high for (4, 0) (1.95 Å), after increasing in diameter magnetic moment is decreases but at for (10, 0) (1.90 Å) structure, it starts increases (Figure 4). The

magnetic moment of bulk CuO is 0.86 μB/atom and individual Cu, O atoms values are 0.68 μB/atom and 0.18 μB/atom respectively [8]. Magnetic moment is induced due to the exchange-splitting between states, here exchange splitting of the Cu-3d and O-2p states provide magnetic moment to CuO NTs. The fluctuation on magnetic moment on increasing diameter are due to increase in number and decrease in bond length between Cu and O atom. According to Hund's rule of magnetism if the bond length is decrease and number of atom increased that means the atom coming together and interaction between them increases, here this is responsible for decreasing magnetic moment [24]. The total magnetic moment μ_{total} (μB/atom) of CuO nanotubes are linked directly to the individual magnetic moment of Cu and O atoms, strong interaction decrease their individual magnetic moment and affect the total magnetic moment of CuO nanotubes.

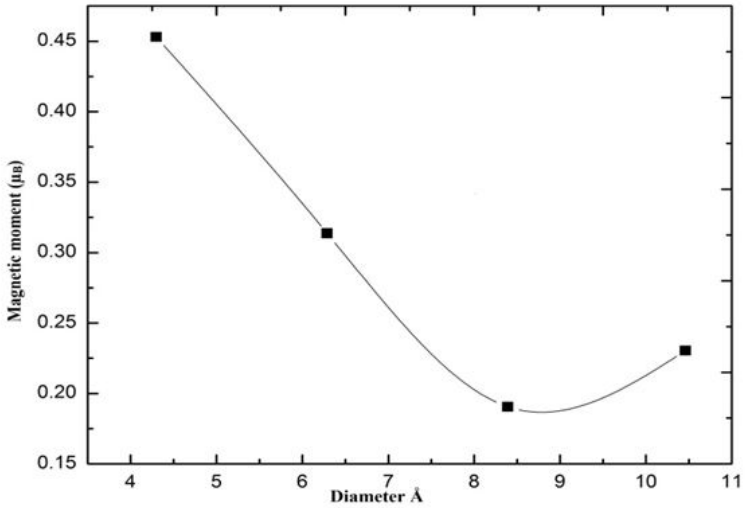

Figure 4: (color online) Magnetic moment as a function of diameter at room temperature.

Further we analyzed magnetic moment with different temperature. The temperature variation of the nano tubes is performed manually; it actually represents the temperature under which calculations are performed. We found that magnetic moment have high value at room temperature (300K) then decrease with increasing temperature which is shown at Figure 5. But for (8, 0) NT magnetic moment is increasing with increasing temperature. In our result maximum magnetic moment is observed at 4.30Å [(4,0) NT] and minimum at 8.39Å [(8,0)NT].

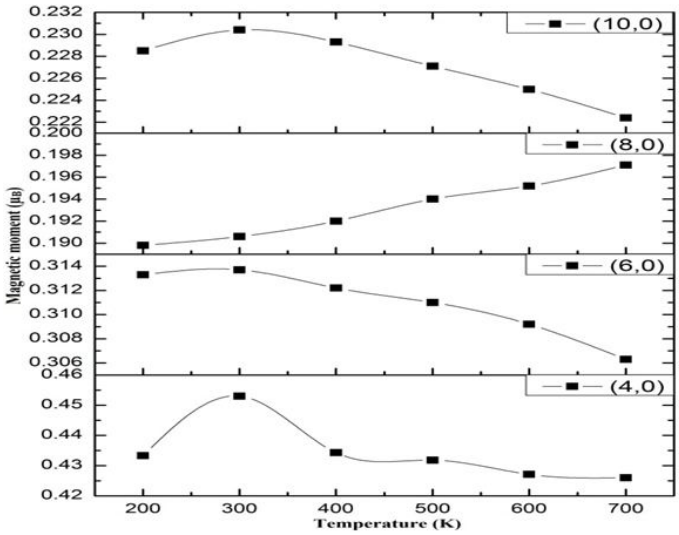

Figure 5: (color online) Magnetic moment as function of Temperature (K).

Conclusion

Structural, electronic and magnetic properties of zigzag nano tube of (4, 0), (6, 0), (8, 0) and (10, 0) NT were analyzed by density function theory based on ab-initio code ATK-VNL. Buckling has been occurred on optimized geometry structure. The magnitude of buckling is decreases on increasing diameter of tube. Furthermore as diameter increases the number of atoms are also increases, however binding energy of CuO nano tube increases at first and tends towards the saturation with increasing number of atoms. The hybridization of Cu 3p state and O 2p state make CuO nanotube metallic. Magnetic moments were calculated through Mulliken population analysis of CuO nanotube. Magnetic moments with respect to different diameter and different temperature were investigated. Highest value of magnetic moment 0.453μB was observed for (4, 0) at 300 K, which continuously decreases for higher

diameter nanotubes which attains minimum value at (10, 0) beyond that it is found to be increased. We were also analyzed relation of temperature and magnetic moment. All study show peak value at room temperature except (8, 0). In (8, 0) nanotube magnetic moment is increase with temperature. As our findings are first in series, it would certainly be of great importance to the theoretical as well as experimental workers of this area. CuO show remarkable magnetic moment indicating that we can use it in spintronics devices, memory devices and magnetic sensors. We are seeking the experimental verification of these data. If verified CuO can be used as binary analog to other CNT with novel magnetic properties.

Acknowledgment

We are thankful to ABV-IIITM, Gwalior for providing the computational nano-Science and Technology lab for entire computational work. HRPC, Nepal is also acknowledged for partial support for this project.

References

1. Batlle X, Labarta AL (2002) Finite-size effects in fine particles: magnetic and transport properties. J Phys D Appl Phys 35: R15-42.

2. Miao J, Hu W, Guo N, Lu Z, Zou X, et al. (2014) Single InAs Nanowire Room-Temperature Near-Infrared Photodetectors. ACS Nano 8: 3628-35.

3. Mattheiss LF (1972) Electronic Structure of the 3 d Transition-Metal Monoxides. I. Energy-Band Results. Phys Rev B 5: 290-306.

4. Harrison WA (2007) Heisenberg exchange in the magnetic monoxides. Phys Rev B 76: 10.1103/PhysRevB.76.054417.

5. Anisimov VI, Zaanen J, Andersen OK (1991) Band theory and Mott insulators: Hubbard U instead of Stoner I. Phys Rev B Condens Matter 44: 943-54.

6. Bednorz JG, Müller KA (1988) Perovskite-Type Oxides—the New Approach to High-Tc Superconductivity. Nobel Lecture. Angewandte Chemie 27: 735-48.

7. Bednorz JG, Müller KA (1986) Possible high Tc superconductivity in the Ba– La– Cu– O system. Z Phys Rev B Condens Matter 64: 189-93.

8. Ekuma CE, Anisimov VI, Moreno J, Jarrell M (2014) Electronic structure and spectra of CuO. Eur Phys J B 87: 10.1140/epjb/e2013-40949-5.

9. Paudel S, Dandeliya S, Chaurasiya R, Srivastava A, Kaphle GC (2016). Magnetism in zigzag and armchair CuO nanotubes: Ab-initio study. J Magn Magn Mater 406: 8-14.

10. Wu D, Zhang Q, Tao M (2006) LSDA+ U study of cupric oxide: Electronic structure and native point defects. Phys Rev B 73: 10.1103/PhysRevB.73.235206.

11.Wang W, Liu Z, Liu Y, Xu C, Zheng C, et al. (2003) A simple wet-chemical synthesis and characterization of CuO nanorods. Appl Phys A 76: 417-20.

12. Kohn W, Sham LJ (1965) Self-consistent equations including exchange and correlation effects. Phys Rev B 140: A1133-8.

13. Dreizler RM, Gross EKU (1990) Density Functional Theory: An Approach to the Quantum Many-Body Problem, Springer Science & Business Media, Germany.

14. Quantum Wise (2014) Atomistix ToolKit version 11.8.2 and 2014.2 QuantumWise, Denmark.

15. Brandbyge M, Mozos JL, Ordejón P, Taylor J, Stokbro K (2002) Density-functional method for nonequilibrium electron transport. Phys Rev B Condens Matter 65: 10.1103/PhysRevB.65.165401.

16. Stokbro K, Taylor J, Brandbyge M, Ordejón P (2003) TranSIESTA: a spice for molecular electronics. Ann N Y Acad Sci 1006: 212-26.

17. Taylor J, Guo H, Wang J (2001) Ab initio modeling of quantum transport properties of molecular electronic devices. Physical Review B 63: 10.1103/PhysRevB.63.245407.

18. Soler J M, Artacho E, Gale JD, García A, Junquera J, et al. (2002) The SIESTA method for ab initio order-N materials simulation. Phys Rev B Condens Matter 14: 2745-79.

19. Wu Y, Lai Y, Zhang ZQ (2011) Elastic metamaterials with simultaneously negative effective shear modulus and mass density. Phys Rev Lett 107: 105506.

20. Perdew JP, Burke K, Ernzerhof M (1996) Generalized gradient approximation made simple. Phys Rev Lett 77: 3865-8.

21. Bachelet GB, Hamann DR, Schlüter M (1982) Pseudopotentials that work: From H to Pu. Phys Rev B 26: 4199-228.

22. Farrell HH, Parra RD (2011) Oxide nanotube analogues: CuO nanobarrels. J Vac Sci Technol B Nanotechnol Microelectron 29: 10.1116/1.3661990.

23. Luo LB, Wang XH, Xie C, Li ZJ, Lu R, et al. (2014) One-dimensional CuO nanowire: synthesis, electrical, and optoelectronic devices application. Nanoscale Res Lett 9: 1-8.

24. Bachelet GB, Hamann DR, Schlüter M (1982) Pseudopotentials that work: From H to Pu. Phys Rev B 26: 4199-228.

Submit your next manuscript to Annex Publishers and benefit from:

- Easy online submission process
- Rapid peer review process
- Online article availability soon after acceptance for Publication
- Open access: articles available free online
- More accessibility of the articles to the readers/researchers within the field
- Better discount on subsequent article submission

Submit your manuscript at
http://www.annexpublishers.com/paper-submission.php

LIST OF CONFERENCE PRESENTATIONS

[1] Certificate of appreciation for Oral Presentation at Association of Nepali Physicists in America Conference (ANPA) 2020

July 17 - 19, 2020

[2] Workshop on Materials for Smarter Community 2019

Advanced Materials Research Group, Atal Bihari Vajpayee - Indian Institute of Information Technology and Management, Gwalior, MP, India.

September 11, 2019

[3] International Conference on Nanosciences and High Energy Physics (ICNHEP - 2019)Central Department of Physics, Tribhuvan University, Kirtipur, Kathmandu, Nepal

February 4 - 6, 2019

[4] International Conference on Advances in Nanomaterials and Devices for Energy and Environment (ICAN-2019), Advanced Materials Research Group, CNTLab, Atal Bihari Vajpayee Indian Institute of Information Technology and Management, Gwalior, MP, India

January 27 - 29, 2019

[5] National Conference on Advanced Nanomaterials and their Applications (NAN - 2018) Department of Physics, Motilal Nehru National Institute of Technology Allahabad, Prayagraj, UP, India

December 21 - 23, 2018

[6] 23rdInternational Conference of International Academy of Physical Sciences (CONIAPS XXIII) on Advances in Physical Sciences to Achieve Sustainable Development Goals (2018), Nepal Academy of Science and Technology, Kathmandu, Nepal (NAST)

November 16 - 18, 2018

[7] National Conference on Recent Trends in Condensed Matter Physics& Materials Science Centre of Advanced Studies, Department of Physics, Institute of Science Banaras Hindu University Varanasi.

September 15 - 16, 2018

[8] National Conference on Materials and Devices (NCMD - 2018), School of Basic Sciences & Research Sharda University, Greater Noida, UP (India)

July 31st - August 1st, 2018

[9] International Conference on Nanomaterials: Initiatives & Applications (ICNIA - 2018) School of Studies in Environmental Chemistry & Institute of Engineering, Jiwaji University, Gwalior, India

09 - 11 March 2018

[10] Lecture Series on Research Methodology 2017, Central Department of Physics, Tribhuvan University, Kirtipur, Nepal

November 6th - December 22th, 2017

[11] International Conference on Nano-Materials and Computational Physics,(ICNMCP-2017), Central Department of Physics, Tribhuvan University, Kirtipur, Kathmandu, Nepal

27-29 December 2017

[12] International Conference on Physics of Space and Materials (ICPSM - 2017), St. Xavier's College Kathmandu, Nepal

2 - 3, September 2017

[13] 4th International Workshop / Conference on Computational Condensed Matter Physics and Materials Science (IWCCMP-2016), Atal Bihari Vajpayee - Indian Institute of Information Technology & Management, Gwalior(MP), India.

18-20 November 2016

[14] International Conference on New Scintillations on Materials Horizon (ICNSMH - 2016), Mahatma Jyotiba Phule Rohilkhand University, Bareilly(UP), India.

21 - 23 October 2016

[15] National Conference on Science and Technology (NCST - 2016), Mid-Western University. Surkhet, Nepal.

24 - 25 September 2016

Association of Nepali Physicists in America-ANPA

Certificate of Appreciation

THIS CERTIFICATE IS PRESENTED TO

MR. TARANI P. YADAV

Tribhuvan University, Nepal

FOR YOUR PRESENTATION DURING THE ANPA CONFERENCE 2020

DR. CHET R. BHATT
CHAIR, ANPA CONFERENCE 2020

DR. SHREE K. BHATTARAI
PRESIDENT, ANPA

Workshop

On Materials for Smarter Community

11 September, 2019

Advanced Materials Research Group
Atal Bihari Vajpayee-
Indian Institute of Information Technology and Management, Gwalior

Certificate of Participation

This is to certify that Prof./Dr./Mr./Ms. Tarani Prasad Yadav has participated in "Workshop on Materials for Smarter Community" and presented his/her current research findings.

Prof. Anurag Srivastava
Chief Mentor, AMRG

ICAN 2019

I[st] International Conference on Advances in Nanomaterials and Devices for Energy and Environment

ABV-IIITM Gwalior | 27-29 Jan. 2019

Certificate of Participation

This is to certify that Prof./Dr./Mr./Ms. Tarani Prasad Yadav

From Tribhuvan University, Nepal

has participated in "ICAN-2019" and presented a Research paper.

Title of Talk / Paper. Electronic and Magnetic Behaviors of Zigzag and Armchair Forms of Zn-Dopped CuO Nanotube : First Principles Study.

Dr. Anurag Srivastava
Convener

National Conference on Advanced Nanomaterials and their Applications (ANA-2018)

ANA 2018

December 21-23, 2018

CERTIFICATE

This is to certify that Prof. / Dr. / Mr. / Ms. Tarani Prasad Yadav of Tribhuvan University, Kirtipur, Kathamandu, Nepal has delivered an Invited Talk/ Oral / Poster Presentation /attended in the National Conference on "Advanced Nanomaterials and their Applications (ANA-2018)" organized by Department of Physics at Motilal Nehru National Institute of Technology Allahabad, Prayagraj-211004, India during December 21-23, 2018.

Prof. Arvind Agarwal	Dr. Rohit R. Shahi	Dr. Arun Kumar Singh	Dr. Animesh K. Ojha
Chairperson	Convener	Convener	Head of the Department

23RD INTERNATIONAL CONFERENCE OF INTERNATIONAL ACADEMY OF PHYSICAL SCIENCES
(CONIAPS XXIII)

On

Advances in Physical Sciences to Achieve Sustainable Development Goals

November 18, 2018

Organized by

NEPAL ACADEMY OF SCIENCE AND TECHNOLOGY, KATHMANDU, NEPAL

Certificate

This is to certify that Prof. /Dr./ Mr./Ms. Tarani Prasad Yadav, central Department of Physics, T.U., Nepal has participated in the **23rd International Conference of International Academy of Physical Sciences** on **Advances in Physical Sciences to Achieve Sustainable Development Goals** held at **Nepal Academy of Science and Technology** during November 16-18, 2018 and delivered Invited Lecture/Chaired a Session/ Presented a paper /Presented a paper in Young Scientist Award Category.

Title of the Invited Lecture/Paper magnetic moment in S-doped and undoped Ce Onanowires at different ... first-principle study

Prof. P. N. Pandey General Secretary IAPS	Dr. Buddhi Ratna Khadge Convenor CONIAPS XXIII	Ramila Raut Ms. Ramila Raut Organizing Secretary CONIAPS XXIII

National Conference

on

Recent Trends in Condensed Matter Physics and Materials Science (CMPMS-2018)

(September15-16, 2018)

CMPMS 2018

CERTIFICATE

Abstract Ref. No.....

This is to certify that Dr./Mr./Ms **Tarani Prasad Yadav** of **IIITM, Gwalior** participated/Presented a Research paper (Poster) in the National Conference on Recent Trends in Condensed Matter Physics and Materials Science (CMPMS-2018) organized by the Centre of Advanced Study, Department of Physics, Institute of Science, Banaras Hindu University, Varanasi-221005 during the period of September 15-16, 2018.

Dr. M.A. Shaz Convener	Prof. R.P. Malik Head, Department of Physics	Prof. Sanjay Kumar Coordinator Centre of Advanced Study

SHARDA UNIVERSITY
Beyond Boundaries

SCHOOL OF
BASIC SCIENCES & RESEARCH
DEPARTMENT OF PHYSICS

"NATIONAL CONFERENCE ON
MATERIALS & DEVICES"
JULY 31ST - AUGUST 1ST, 2018

Certificate of Participation

This is to certify that

Dr/Mr/Mrs Tarani Prasad Yadav of IIT-M Gwalior
(Oral-033) attended **National Conference on Materials & Devices (NCMD-2018)**
held from **July 31st - August 1st, 2018** at **Sharda University, Greater Noida.**

Meenal Gupta
Dr. Meenal Gupta
Convener

Prof. R. C. Singh
Chairman

INTERNATIONAL CONFERENCE
ON
NANOMATERIALS: INITIATIVES & APPLICATIONS
March, 9 - 11, 2018
Jiwaji University, Gwalior
School of Studies in Environmental Chemistry & Institute of Engineering

This is certify that Prof./Dr./Mr./Ms. Tarani Prasad Yadav *of* IITTM, Gwalior and Far Western University, Surkhet, Nepal
Participated/Delivered lecture/Chaired Technical Session/ Presented paper(Oral/Poster) on the topic entitled
Dimensional Effects on Electronic and Magnetic Properties of Copper (I) oxide (Cu_2O) *in the*
"International conference on "Nanomaterials: Initiatives & Applications", March 9 - 11, 2018.

Prof. Rajeev Jain
(Convenor)

Prof. A.K. Halve
(Organizing Secretary)

Dr. Nimisha Jadon
(Incharge Technical Sessions)

International conference on
Nano-Materials and Computational Physics
27-28 December 2017
Central Department of Physics
Tribhuvan University, Kirtipur, Nepal

Participation Certificate

Tarani prasad yadav
Central Department of physics, T.U

participated the conference during 27-28 December 2017 and contributed oral/poster presentation entitled

Structural, Electronic and Magnetic properties of Cuprite (Cu_2O) at different Morphologies : First Principles study.

Prof. Dr. Ram Pd Khatiwada
Dean
IoST, Tribhuvan University, Kirtipur

Dr. Gopi Chandra Kaphle
Secretary
Organizing Committee

Prof. Dr. Binil Aryal
Head
CDP, TU, Kirtipur

Lecture Series on
Research Methodology
6 November – 22 December 2017
Central Department of Physics
Tribhuvan University, Kirtipur, Nepal

Participation Certificate

Tarani prasad yadav
Central Department of physics & Midwestern University, Surkhet

participated in 21 hours lecture series on Research Methodology delivered by Prof. Dr. Subodh R. Shenoy, TIFR, India during 6 November to 22 December 2017.

Prof. Dr. Subodh R. Shenoy
Guest Speaker
Tata Institute of Fundamental Research, India

Prof. Dr. Binil Aryal
Head
CDP, TU, Kirtipur

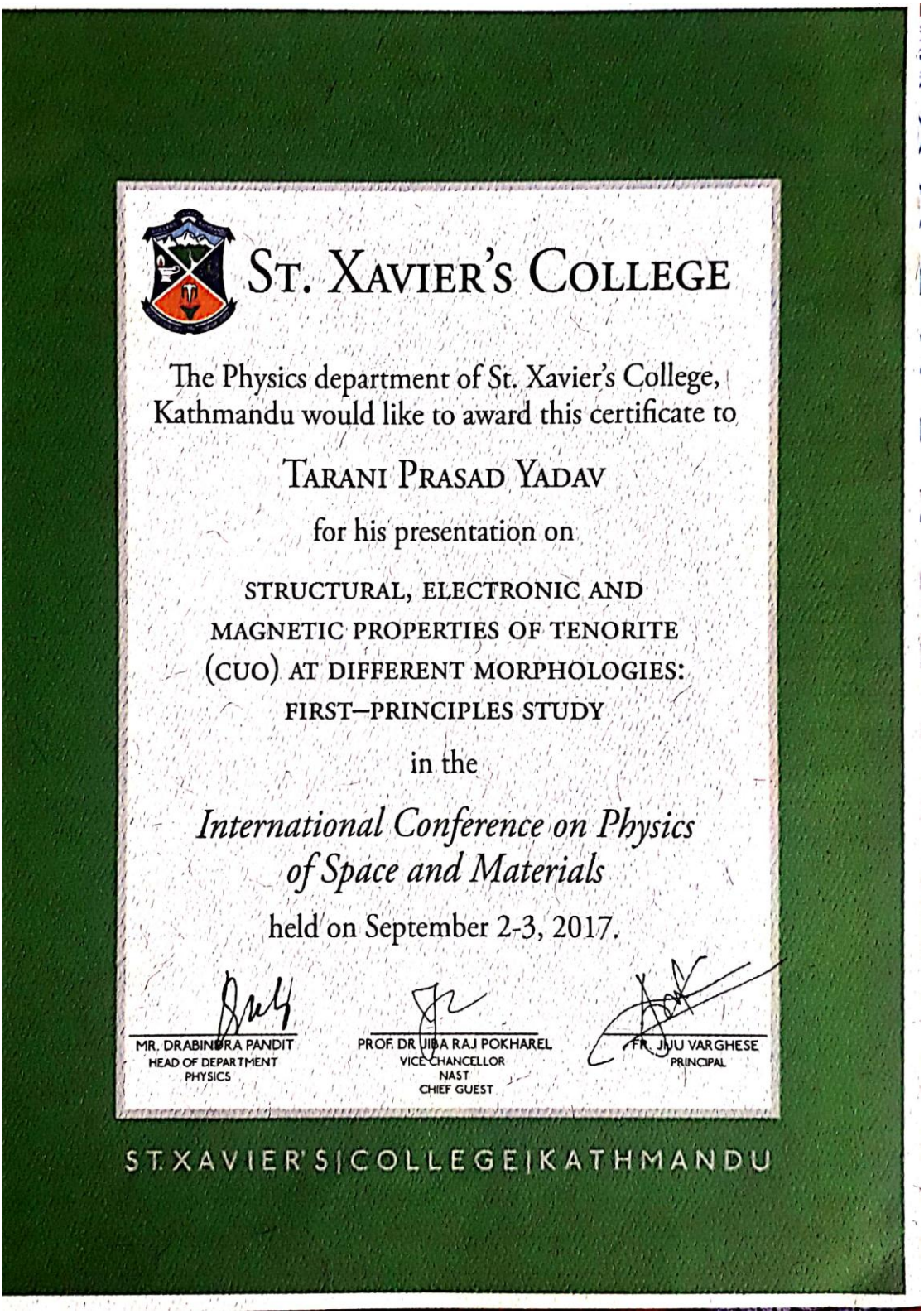

ST. XAVIER'S COLLEGE

The Physics department of St. Xavier's College, Kathmandu would like to award this certificate to

TARANI PRASAD YADAV

for his presentation on

STRUCTURAL, ELECTRONIC AND MAGNETIC PROPERTIES OF TENORITE (CUO) AT DIFFERENT MORPHOLOGIES: FIRST–PRINCIPLES STUDY

in the

International Conference on Physics of Space and Materials

held on September 2-3, 2017.

MR. DRABINDRA PANDIT
HEAD OF DEPARTMENT
PHYSICS

PROF. DR. JIBA RAJ POKHAREL
VICE-CHANCELLOR
NAST
CHIEF GUEST

FR. JIJU VARGHESE
PRINCIPAL

ST.XAVIER'S|COLLEGE|KATHMANDU

4th International Workshop/Conference on Computational Condensed Matter Physics and Materials Science
(IWCCMP-2016)

Materials For Energy and Environment
18-20 November, 2016

Organised by
Advanced Materials Research Group, CNT Laboratory
Atal Bihari Vajpayee- Indian Institute of Information Technology & Management, Gwalior (M.P.) 474015 India

Certificate of Participation

conferred to
Tarani Prasad Yadav
of Tribhuvan University, Kathmandu, Nepal
for the paper
Electronic and Magnetic properties of CuO Bulk and Nanotubes : Ab-initio study

Dr. Anurag Srivastava
Convener, IWCCMP-2016

Prof. S. G. Deshmukh
Director, ABV-IIITM,Gwl

International Conference on New Scintillations on Materials Horizon (ICNSMH-2016)

21-23 OCTOBER, 2016

Organised by : Department of Applied Physics, Faculty of Engineering and Technology
Mahatma Jyotiba Phule Rohilkhand University, Bareilly, INDIA

Certificate

Certified that Prof./Dr./Mr./Ms. Tarani Prasad Yadav
from Tribhuvan University, Nepal
participated as Chairperson of a Session/Plenary Speaker/ Invited Speaker/Contributor of a Research Paper for Oral/Poster Presentation/volunteer.
Title of the Talk/Paper Electronic and Magnetic properties of CuO Bulk and Nanotubes : Ab-initio Study

Dr. M. Saleem Khan
Co-ordinator

Dr. Archana Gupta
Convener

Prof. A.K. Gupta
Chairman

CERTIFICATE OF AWARD

This Certificate is awarded to

Tarani Prasad Yadav

As

Oral Presentation

in

The National Conference on Science and Technology

(NCST - 2016)

Birendranagar, Surkhet

(24-25 September, 2016)

Prof. Dr. Upendra Kumar Koirala
Chief Guest
Vice Chancellor
Mid- Western University

Prof. Dr. Kedar Nath Bhimire
Special Guest
Member, Tribhuvan University
Service Commission

Prof. Dr. Deba Bahadur Khadka
Convener
Dean Faculty of Science & Technology
Mid-Western University